Cyclic loading design of offshore wind turbine foundations

vorgelegt von
M. Sc.
Gianluca Zorzi

an der Fakultät VI - Planen Bauen Umwelt
der Technischen Universität Berlin
zur Erlangung des akademischen Grades

Doktor der Ingenieurwissenschaften
- Dr.-Ing. -

genehmigte Dissertation

Promotionsausschuss:

Vorsitzender: Prof. Dr.-Ing. Yuri Petryna

Gutachter: Prof. Dr.-Ing. Frank Rackwitz

Gutachter: Prof. Gudmund Reidar Eiksund

Tag der wissenschaftlichen Aussprache: 30. November 2021

Berlin, 2022

"Energy research and innovation have an essential role to play in … satisfying security of energy supply, competitiveness of EU industry and ensuring affordable prices for the citizens, whilst at the same time combating climate change"

Horizon 2020 – EU's research and innovation programme

Eidesstattliche Erklärung/Affidavit

Hiermit erkläre ich an Eides statt, dass ich die vorliegende Arbeit selbstständig und eigenhändig sowie ausschließlich unter Verwendung der aufgeführten Quellen und Hilfsmittel angefertigt habe.

I hereby confirm that I prepared this thesis independently and by exclusive reliance on literature or tools indicated herein.

_____

Gianluca Zorzi

Berlin, 22.11.2022

Preface

I started my early stage research (ESR) position in the INFRASTAR project in October 2016, together with 11 other ESR fellows. The aim of the INFRASTAR project was to explore the effects of repeated loads on structures covering a wide range of subjects, such as crack detection, applying non-destructive testing, improving the standards and knowledge of structural design, and development of reliability-based design methods. We were spread across Europe, based in various universities working in research groups or with industrial partners. During this project, I had the chance to enrich my background by means of several weeks of training and "implementation days", in which I was provided with an opportunity to discuss and share my research both internally within the project group and externally.

For the entire duration of my PhD I was based at GuD Geotechnik und Dynamik Consult GmbH in Berlin under the industrial supervision of Dr.-Ing. Fabian Kirsch and Prof. Dr.-Ing Thomas Richter. Being a part of the offshore geotechnical team helped me focus my research immediately on current challenges faced by the offshore wind sector during the process of designing the foundations. The cyclic loading design of offshore foundations is still a complex, fascinating, and frustrating task that has to be dealt with in day-to-day projects. Pursuing my goal to provide a method (introduced later in the thesis by the name "soil cluster degradation method") for cyclic loading design, I had the opportunity to develop a multidisciplinary research

approach dealing with finite element methods, laboratory tests, discrete element methods, and aeroelastic simulations.

For my PhD degree, I was enrolled at the Technical University of Berlin. My academic supervisor was Prof. Frank Rackwitz, head of the geotechnical department at the School VI-Planning-Building-Environment. The department has years of experience in cyclic/dynamic soil–structure interaction problems and in conducting cyclic laboratory testing. The cyclic laboratory data provided by his department were fundamental for the validation of the methods proposed in this thesis. In the three years of my successful collaboration with Prof. Rackwitz and his team, I was able to adopt a numerical model based on the discrete element method (DEM) as a substitute for the cyclic laboratory testing.

During the first year of my PhD programme, I spent two months at COWI-Aalborg, Denmark in the department of offshore wind. I worked under the supervision of Dr. Ing. Anders Hust Augustesen, Martin Underlin Østergaard and Dr.-Ing. Søren Hyldal Sørensen. During these two months, I developed the core of the soil cluster degradation method. This fruitful collaboration with COWI continued after the secondment by further validating the proposed method for designing cyclic loaded offshore structures.

A part of my research focused on improving the cyclic laboratory testing campaign and specifically, on substituting the cyclic laboratory tests with numerical simulations adopting the DEM. Dr.-Ing. Fabio

Gabrieli from the department of Civil Environmental and Architectural Engineering (ICEA), University of Padova supervised my work and actively collaborated on programming and validating the DEM codes.

In the final year of my PhD programme, I spent two months at Aalborg University (AAU; Denmark) under the supervision of Prof. John Dalsgaard Sørensen, head of the Reliability and Risk Analysis research group. In these two months, I achieved the closure of my research by implementing the soil cluster degradation method in a probabilistic based design framework. This approach is a crucial part of my research because it assists geotechnical engineers to quantify the probability that a foundation would fail when subjected to cyclic loads considering the variability in the input design parameters.

Acknowledgements

This thesis concludes three stressful, challenging, and yet beautiful years of my research. I had the opportunity to travel the world, meet many interesting people, develop a network for my career, and most importantly become a father.

I cannot describe how thankful I am to my family—Melina and Benjamin, for constantly supporting me throughout this time, reading all my papers, and listening to me blabber about wind turbine foundations all day; and to my parents who, during these years were always there to support me.

I would like to say grazie mille...

...to my industrial supervisors Dr.-Ing. Fabian Kirsch and Prof. Thomas Richter, who always gave me the time they could to enrich my research with new ideas;

…to my colleagues, Dr.-Ing. Bert Schädlich, Dr.-Ing. Patrick Arnold and Simon Wiesener, who would listen to my problems when I got stuck and try to help me find solutions;

...to everyone involved in the INFRASTAR project, especially the project manager Dr. Hakim Ferria and the project coordinator Dr. Odile Abraham, for wonderfully orchestrating the project, and for being very patient with us (the ESR fellows), listening to our problems and concerns and finding the best solutions for them;

…to my work package leader, Prof. Eugen Brühwiler, whose insightful questions made me always reflect on the core elements and novelties of my research;

...to COWI that hosted me for two months and made me feel comfortable to carry on my research, with special mention going to Dr. Ing. Anders Hust Augustesen, Martin Underlin Østergaard, and Dr.-Ing. Søren Hyldal Sørensen, who always dedicated their time for weekly meetings during my stay, and were very enthusiastic about my research; Martin and Søren kept on mentoring me until the end of my PhD thesis, providing me crucial advice and critical comments to improve my research;

...to my academic supervisor Prof. Frank Rackwitz from TU Berlin who guided me in these three years, offering his invaluable advice and innovative ideas and

to Dr.-Ing. Viet Hung Le, who helped me gain an insight on laboratory testing and assisted me with the data;

...to Dr.-Ing. Fabio Gabrieli from UNIPD, who followed and shaped my career since my bachelor's thesis, introducing me to the fantastic world of cyclic loads of granular materials; I am very grateful that he was always patient to discuss my research, especially regarding the DEM modelling;

...to Aalborg university, which hosted me as a PhD guest and provided all the support for my research, with special thanks going to Prof. John D. Sørensen, who organised it; I am very happy that thanks to his supervision, I left Aalborg with a new understanding of reliability analysis in geotechnical engineering;

...to Amol Mankar who was my desk neighbour during my stay at AAU. I really enjoyed my daily discussions with him on statistics and probabilistic modelling, during which he persistently tried to explain the incredible but sometimes very abstract world of probabilistic analysis to me.

...to Joey Velarde, who I collaborated with on different topics during these three years and with whom I exchanged a lot of interesting ideas and methods related to the modelling of offshore foundations.

The thesis was written within the framework of the European project INFRASTAR (infrastar.eu), which has received funding from the European Union's Horizon 2020 research and innovation programme under the Marie Skłodowska–Curie grant agreement No 676139. The grant is gratefully acknowledged.

Thanks to all of you for making it possible.

Sincerely,

Gianluca

Abstract

Deutsch

Offshore-Windenergieanlagen sind in der Regel schlanke, flexible Strukturen, die aufgrund der rauen Offshore-Bedingungen kontinuierlich schwingen. Während der Lebensdauer der Gründung können verschiedene Formen von zyklischen und dynamischen Belastungen infolge von Wind, Wellen, Strömungen, Taifune und Erdbeben den Betrieb der Anlage beeinträchtigen und möglicherweise zu einer Abschaltung führen. In gesättigten, zyklisch belasteten Böden kann es zu einer Akkumulation permanenter Verformungen und einem Anstieg des Porenwasserdrucks kommen, was zu einer Schiefstellung der Gründung führen kann. In Bezug auf den Grenzzustand der Gebrauchstauglichkeit (serviceability limit state, SLS) muss sichergestellt sein, dass das Fundament die vom Windturbinenhersteller vorgeschriebene Betriebstoleranz von typischerweise 0,25 % Schiefstellung während seiner gesamten Lebensdauer nicht überschreitet. In den einschlägigen Regelwerken gibt es jedoch keine validierten und allgemein anerkannten Methoden zur Ermittlung der Verformungsakkumulation.

Im Rahmen dieses Forschungsprojekts wird eine genaue, vielseitig einsetzbare und benutzerfreundliche Methode entwickelt, um die akkumulierte Verformung des Bodens und die Schiefstellung der Gründung für zyklisch belastete Offshore-Windenergieanlagen zu prognostizieren. Diese Methode, die im Folgenden als „soil cluster degradation method“ bezeichnet wird, basiert auf einer Reihe von zyklischen Labortests und einer dreidimensionalen Finite-Element-Modellierung, die eine genaue Ermittlung der Spannungsumverteilung um die Gründung ermöglicht. Darüber hinaus soll diese Arbeit Vertrauen in die Anwendung dieser Methode in praktischen Projekten schaffen. Zur Optimierung der zyklischen Labortests werden verschiedene numerische Tools vorgeschlagen. Die Validierung der Methode erfolgt mit einem umfangreichen Test an einem Schwerkraftfundament, das hunderttausenden regelmäßigen Belastungszyklen ausgesetzt war. Schließlich wird eine probabilistische Entwurfsmethodik vorgeschlagen, um die Hauptursache für die Ungenauigkeit bei der

Überprüfung der SLS-Kriterien und bei der Gründungsbemessung für ein bestimmtes Zuverlässigkeitszielniveau zu beseitigen. Diese Forschungsarbeit bietet ein zuverlässiges Werkzeug zur kostengünstigen und risikoarmen Dimensionierung von Offshore-Windturbinengründungen, wenn die Schiefstellung der Gründung im Laufe der Lebensdauer bestimmend für den Entwurf ist.

Schlüsselwörter: *zyklische lasten; schiefstellung der gründung; grenzzustand der gebrauchstauglichkeit; degradation der bodensteifigkeit; zyklische zonturdiagramme; 3D-Finite-Elemente-Modell; probabilistischen entwurfsmethodik.*

English

Offshore wind turbines (OWT) are slender flexible structures that continuously swing owing to the harsh offshore conditions. During the lifetime of a wind turbine's foundation, various forms of cyclic and dynamic loads, such as wind, waves, currents, typhoons, and earthquakes can interfere with the operation of its structure and potentially cause a premature shutdown. It can be observed from the soil–structure interaction that cyclic loads cause the saturated soil to experience an accumulation of permanent deformation and an increase in the pore water pressure, which eventually, leads to the tilting of the foundation. In terms of serviceability limit state (SLS), geotechnical engineers have to ensure that the foundation does not exceed the operational tolerance prescribed by the wind turbine manufacturer, e.g., 0.25°, throughout its lifetime. However, upon reviewing the relevant code of practice, it would be evident there are no validated and generally accepted methodologies that are recommended to assess the SLS.

In this research project, an accurate, versatile, and user-friendly method, called the soil cluster degradation method (SCM), is developed. This method can predict the lifelong deformation due to soil–structure-interaction for offshore wind turbines, which are subjected to a series of regular cyclic loads. This method bases its prediction on (i) three-dimensional (3D) finite element modelling (FEM), which enables an accurate computation of stress redistribution around the foundation and (ii) a series of cyclic laboratory tests. Moreover, this thesis aims to provide confidence to geotechnical engineers on implementing this method in day-to-day projects. Different numerical tools were proposed for

improving the cyclic laboratory test campaign and the proposed method was validated with a full-scale test on a gravity-based foundation, which was subjected to hundreds of thousands of load cycles. Finally, a reliability-based-design (RBD) methodology was proposed to address the main source of uncertainty involved in verifying the SLS criteria and designing the foundation to an annual reliability target level. The outcome of this research provides a reliable tool to the foundation designers to deliver cost-effective and low-risk offshore wind turbine foundations, where the foundation tilting has to be predicted during the structure lifetime.

Keywords: *cyclic loads; foundation tilting; serviceability limit state; soil stiffness degradation; cyclic contour diagrams; 3D finite element model; probabilistic foundation design.*

List of papers

This PhD thesis is a collection of papers, which are attached in the Appendices. Publications included in this thesis:

Appendix A Zorzi, G., Richter, T., Kirsch, F., Augustesen, A. H., Østergaard, M. U., & Sørensen, S. P. (2018). Explicit method to account for cyclic degradation of offshore wind turbine foundations using cyclic interaction diagrams. The 28th International Ocean and Polar Engineering Conference. Sapporo, Japan: International Society of Offshore and Polar Engineers. **(Published)**

Appendix B Zorzi, G., Kirsch, F., Richter, T., Østergaard, M. U., & Sørensen, S. H. (2018). Lifetime tilting prediction of offshore wind turbine foundations due to soil strain accumulation. 14th EAWE PhD Seminar on Wind Energy. Vrije Universiteit Brussel, Belgium. **(Published)**

Appendix C Zorzi, G., Kirsch, F., Gabrieli, F., & Rackwitz, F. (2017). Long-term cyclic triaxial tests with DEM simulations. PARTICLES 2017, V International Conference on Particle-based Methods – Fundamentals and Applications. Hannover, Germany. **(Published)**

Appendix D Zorzi, G., Gabrieli, F., Le, H., Rackwitz, F., & Kirsch, F. (2019). DEM modelling of high cyclic loading: calibration, sensitivity analysis and practical application. **(Draft paper).**

Appendix E Zorzi, G., Kirsch, F., Richter, T., Østergaard, M., & Sørensen, S. (2019). Comparison of cyclic simple shear tests for different types of sands. 2nd International Conference on Natural Hazards & Infrastructure (ICONHIC2019). **(Published)**

Appendix F Zorzi, G., Kirsch, F., Richter, T., Østergaard, M., & Sørensen, S. (2019). Validation of explicit method to predict accumulation of

strain during single and multistage cyclic loading. ECSMGE 2019 - The XVII European Conference on Soil Mechanics and Geotechnical Engineering. **(Published)**

Appendix G Zorzi, G., Kirsch, F., Richter, T., Østergaard, M., & Sørensen, S. (2019). Application of the Soil-Cluster-Degradation method to a full-scale gravity-based foundation test. **(Draft paper)**

Appendix H Zorzi, G., Mankar, A., Velarde, J., Sørensen, J. D., Arnold, P., & Kirsch, F. (2019). Reliability analysis of offshore wind turbine foundations under lateral cyclic loading. Wind Energ. Sci., 5, 1521–1535, 2020. **(Published)**

Contents

1. INTRODUCTION 1

1.1. MOTIVATION 1
1.1. RESEARCH AIM 3
1.2. OVERVIEW OF THE THESIS 4

2. LITERATURE REVIEW ON CYCLIC LOADING DESIGN OF OWT FOUNDATIONS 5

2.1. DESIGN OF OWT FOUNDATIONS 5
2.2. SOLUTIONS FOR OFFSHORE WIND TURBINE FOUNDATIONS 9
2.3. ENVIRONMENTAL AND ACCIDENTAL LOADS IN OFFSHORE CONDITIONS 11
2.4. LOAD INPUTS FOR CYCLIC LOADING DESIGN 14
2.5. PLANNING THE LABORATORY TESTS 17
2.6. EXISTING METHOD TO PREDICT THE ROTATION OF FOUNDATIONS 22
2.7. SLS VERIFICATION 24
2.8. SUMMARY 25

3. OVERVIEW OF RESEARCH METHODOLOGY 27

3.1. PART I: DEVELOPMENT OF THE SCD METHOD (APPENDICES A AND B) 29
3.2. PART II: IMPROVEMENT OF CYCLIC LABORATORY TEST CAMPAIGN (APPENDICES C, D, AND E) 30
3.3. PART III: VALIDATION OF THE SCD METHOD (APPENDIX F AND G) 31
3.4. PART IV: RELIABILITY ANALYSIS OF OFFSHORE STRUCTURES UNDER CYCLIC LATERAL LOADING (APPENDIX H) 32

4. CONCLUSIONS AND FUTURE DEVELOPMENTS 35

4.1. DISCUSSIONS AND CONCLUSIONS 35
4.2. FURTHER RESEARCH 37

REFERENCES 39

APPENDICES: PUBLICATIONS 53

APPENDIX A 55
APPENDIX B 77
APPENDIX C 91
APPENDIX D 111
APPENDIX E 163
APPENDIX F 181
APPENDIX G 199
APPENDIX H 233

Abbreviations

ASR	Average stress ratio
CPT	Cone penetration test
CSR	Cyclic stress ratio
FE	Finite element
FLS	Fatigue limit state
HAWC2	Horizontal Axis Wind turbine simulation Code 2nd generation
HCA	High cycle accumulation
LCOE	Levelised cost of energy
LS	Limit state
OWT	Offshore wind turbine
PM	Palmgren Miner
RBD	Reliability based design
REV	Representative elementary volume
SCD	Soil cluster degradation
SDM	Stiffness degradation method
SLS	Serviceability limit state
SSI	Soil–structure interaction
UDCAM	Undrained cyclic accumulation model
ULS	Ultimate limit state
3D	Three-dimensional

Symbols and units

$\boldsymbol{F_y}$	Horizontal force at mudline
$\boldsymbol{H_s}$	Wave height
Hz	Hertz
$\boldsymbol{M_x}$	Overturning moment at mudline

MW	Megawatt
$\boldsymbol{U_w}$	Mean wind speed
$\boldsymbol{\theta_{calc}}$	Predicted foundation tilting
$\boldsymbol{\theta_{max}}$	Allowed foundation tilting

1. Introduction

1.1. Motivation

Record temperatures, devastating floods, and destructive storms are just a few consequences of climate change. To mitigate these effects there has to be a transformation in our sources of energy production, such as minimising the use of fossil fuels and nuclear energy, and adopting "greener energies". To incentivise this transition, the cost of producing the renewable energies has to be the lowest, thus attracting new investments. In this regard, the levelised cost of energy (LCOE) is an important concept, which economically assesses the feasibility of different modes of electricity generation (IREA, 2019). Its calculation is based on the initial capital investment, expected electricity production, and operational, as well as maintenance costs. The advances made in the technologies, the competitiveness, and the gaining of experience are the key factors for lowering the cost of energy.

In the past decades, the commitment of the European Union to higher green energy consumption has led to a remarkable investment in offshore wind energy, leading to an on-going decline of the LCOE for offshore wind projects. Generally, installing wind turbines in open seas allows harvesting much higher and consistent wind speeds and at the same time, helps reduce the noise and visual pollution on land. On the other hand, building and installing offshore wind turbines (OWTs) requires an intensive initial capital investment (almost 75% of the total lifetime cost (Morthorst & Kitzing, 2016)). Furthermore, operation and maintenance in offshore conditions is often more expensive than on land. As for the overall cost of a wind turbine, the foundation makes up for a large component, i.e., 30%–40% of the total cost. This is mainly due to the installation equipment costs and the vessel costs, which are related to the dimensions of the foundation. The current trend in the wind industry is to use larger wind turbines (in terms of hub height and rotor diameter) in deeper waters, aiming to unlock more wind resources, and increase the output of electricity. At the same time, this requires even larger foundations owing to the higher

loads. For these reasons, it is of vital importance to keep the projects financeable and viable by designing cost-effective and reliable offshore structures, improving the state-of-the-art design methods, and reducing the level of conservatism.

OWTs are slender and flexible structures and during their lifetime, they have to withstand a harsh environment, in which diverse sources of cyclic loads (e.g., winds, waves, and typhoons) make them swing back and forth continuously. The foundation has to resist this repeated structural movement by minimising the deformations. The continuous swing of the structure transfers the cyclic stresses to the soil. A saturated soil subjected to cyclic loads experiences an accumulation of permanent deformation, which leads to the tilting of the foundation. The prediction of the accumulation of rotation at the design stage is fundamental because OWTs are subject to a strict operational tolerance (serviceability criterion) prescribed by wind turbine manufacturers, certification bodies, or insurance companies. This operational restriction ensures that the maximum tilting of the structure θ_{max} is typically < 1° (e.g., 0.25° (DNV-GL, 2017)).

The maximum allowed rotation of the foundation is supposed to guarantee that the wind turbines are operating as designed without the development of second order effect (P-δ effect), which can potentially increase the fatigue load on the structural elements and reduce the lifetime of the structure and hence an earlier shutdown. Moreover, an excessing tilting can have detrimental effects on the rotor-nacelle-assembly components and lead to a reduced energy production.

To comply with this serviceability requirement and design a cost-effective and reliable foundation, an accurate prediction of the foundation tilting is essential. Therefore, to obtain a certification for the design of an offshore foundation, a geotechnical report is needed to predict the foundation rotation during the lifetime of the OWT.

Upon reviewing the relevant code of practice, there appears to be no validated cyclic load method that is recommended to be used for soils (BSH, 2015; DNV-GL, 2017). To address this lack of a generally accepted method, various empirical formulations based on model testing (Cuéllar, et al., 2012; Hettler, 1981 ; LeBlanc, et al., 2009). However, these formulations are not accurate because it is challenging to extrapolate prediction of the foundation behaviour from small

laboratory tests to prototypes. On the other side, numerical soil models have been proposed to replicate as accurate as possible the behaviour of soil at a high number of cycles (Niemunis, et al., 2005; Jostad, et al., 2014). However, they are too complex and not practical for a day-to-day use. As a result, the serviceability criterion is often not thoroughly investigated in offshore projects.

Thus, this gap in the standard for an accurate and practical method to predict the behaviour of cyclic loaded soil and to be used for checking if the serviceability criterion is respected has motivated this thesis.

1.1. Research aim

The aim of this PhD project is to develop an accurate, versatile and user-friendly numerical method, which is capable of predicting the lifelong deformation of the soil-structure-interaction for offshore wind turbines when are subjected to a series of regular cyclic loads.

The scientific research objectives are:

- To develop a numerical method based on 3D Finite Element (FE) method and a cyclic laboratory test campaign. Specifically, the method has to deliver an explicit prediction of the permanent accumulation of deformation at a high number of cycles and effectively linking the cyclic contour diagram framework with the 3D FE environment.
- To substitute the cyclic laboratory tests with cyclic numerical tests adopting Discrete Element Method or mathematical formulations in order to improve the accuracy of the cyclic contour diagrams.
- To validate the numerical method with single and multistage cyclic laboratory tests and a full-scale cyclic test.
- To establish a reliability-based design framework to assess from a probabilistic point of view the lifelong deformation of the soil-structure-interaction taking into account the relevant sources of uncertainties involved in the numerical method.

These scientific objectives contribute to step further towards a validated general accepted method and are expected to provide guidance to the designers when checking if the serviceability criterion is respected.

1.2. Overview of the thesis

This thesis is a collection of eight papers, which can be found in the appendix section. Before introducing the research methodology, i.e., how the papers are linked together, a literature review on the topic of verifying the serviceability criterion (i.e., foundation tilting) is explained (Chapter 2). A general overview is given first on different geotechnical design steps necessary for dimensioning the foundation, namely preliminary data collection, static load design, and cyclic load design. This chapter then focuses on the cyclic load design phase, and especially the different aspects that need to be considered when the serviceability criterion is verified. These aspects include the transferring mechanism of the cyclic loads for different types of offshore foundations, environmental and accidental loads in offshore conditions, definition of the design event, planning the cyclic laboratory testing, existing methods to predict the foundation rotation, and final serviceability verification against maximum allowed tilting.

The third chapter provides an overview of the research methodology; specifically it explains how the papers in the appendices are linked together to fulfil the research aim. The research methodology is divided in four different parts named (i) development of the soil cluster degradation method, (ii) improvement of cyclic laboratory test campaign, (iii) validation of the soil cluster degradation method and (iv) reliability analysis of offshore structures under cyclic lateral loading. The contribution of each part to the overall picture is explained. Then, different key points are summarised, which reflect the original contributions in terms of methodology and outcomes.

The last chapter focuses on the overall findings of this thesis and possible research lines that should be investigated in future.

2. Literature review on cyclic loading design of OWT foundations

2.1. Design of OWT foundations

From a geotechnical point of view, the design of foundations for an OWT has to follow three main steps (Figure 1): preliminary data collection, static load design, and cyclic load design. The project often starts with the collection of relevant wind turbine data from the manufacturer, metocean data from in situ measurements, results from site investigations, such as geological and geotechnical profiles across the wind farm, and finally, site and laboratory testing (Arany, et al., 2017). The next step is the optimisation of the design of the foundation, which is divided into static and cyclic loading designs. Adopting the limit state design philosophy, for each design step (static or cyclic) the foundation is considered safe if it meets specific criterion called "limit state" (LS). When a structure goes beyond a "limit state", it is considered as suffering from a failure and the foundation dimensions have to be modified.

In the static load design step, the preliminary dimension (pre-design) of the foundation is determined by satisfying the ultimate limit state (ULS). This limit state is related to the ultimate static capacity of the soil, which means that the structure does not collapse when subjected to an extreme static load event. In this phase, the dimensions of the foundation are chosen on a preliminary basis. A very time-consuming iteration process between the geotechnical engineer and the substructure designer is required to optimise the dimensions. In this loop, several design load cases and updated soil stiffness values are exchanged back and forth until an optimal solution is achieved. In this loop, the geotechnical engineer has to verify that the foundation has enough bearing capacity under the analysed extreme load and only deforms within an allowable margin.

The preliminarily chosen dimensions are then checked in the cyclic load design phase. This design phase aims to verify if the dimensions are large enough for

the soil to resist the cyclic load design events, such as extreme storms, typhoons or earthquakes, without affecting the operation of the wind turbine.

The application of cyclic stresses in a saturated soil may potentially lead to three effects, namely generation of pore water pressure, accumulation of permanent deformation, and change in soil stiffness. These three effects take place simultaneously. However, with the purpose to simplify the design, these are divided into three different limit states — the ULS, the serviceability limit state (SLS) and the fatigue limit state (FLS), respectively. When the cyclic load action generates pore water pressure in the soil, it causes a reduction in the effective stresses, which leads to a degradation of the foundation capacity. Therefore, the ULS criterion should be re-verified for the cyclic load design event. The SLS criterion is related to the prediction of the maximum rotation that the foundation experiences during the lifetime, which has to be less than the allowed rotation. Therefore, the accumulation of permanent deformation in the soil and its relative consequence on the foundation has to be calculated. The FLS is related to the possible variation in the soil stiffness (e.g. softening or stiffening) that can harm the dynamic behaviour of the wind turbine, causing a possible resonance. It should be noted that these limit criteria are very challenging to assess owing to a lack of guidelines in the common standards (BSH, 2015; DNV-GL, 2017) and knowledge from field monitoring. If one of these LSs is not within the prescribed limits, the foundation dimensions should be increased and the design should again start from the static load design phase.

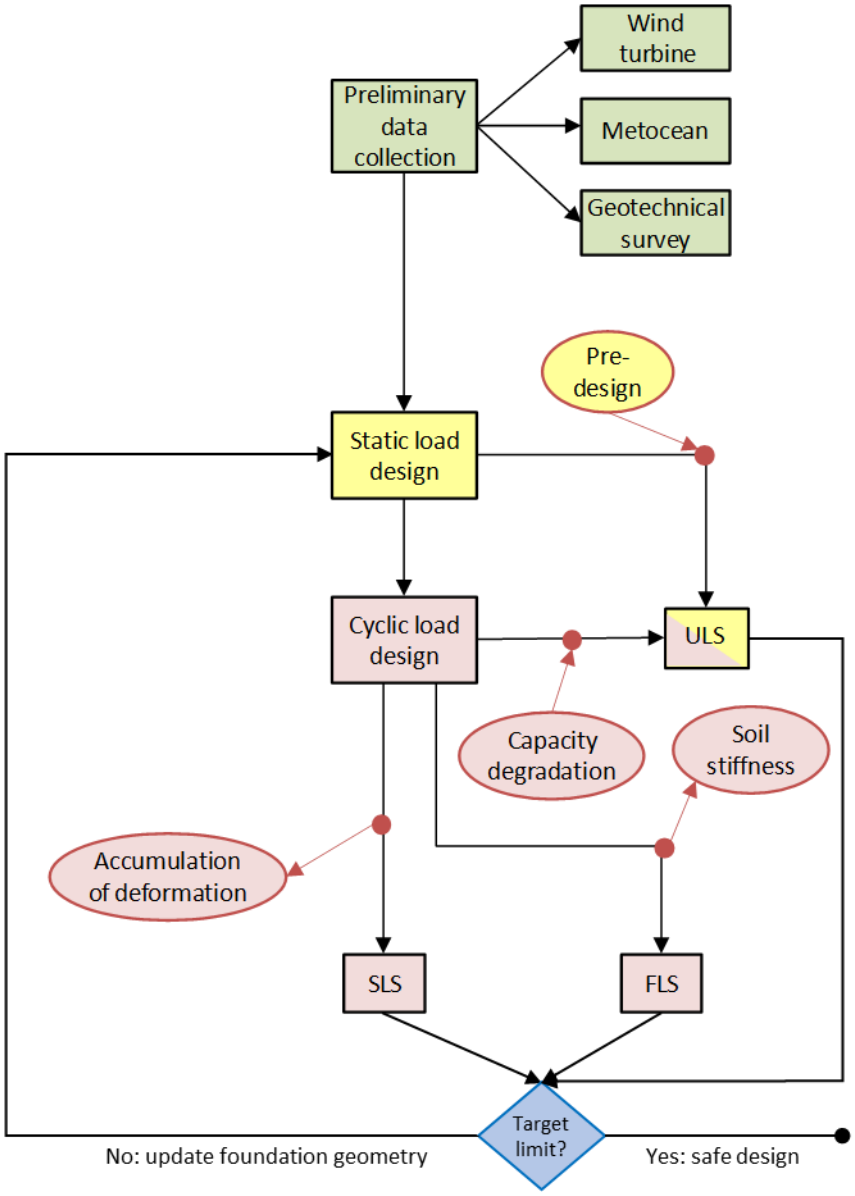

Figure 1. Foundation design steps

This thesis focuses on developing a method for verifying the SLS criterion, i.e., predicting the long-term tilting of the foundation. Figure 2 shows a workflow of the necessary steps to carry out the cyclic loading design for SLS verification.

All the steps involved in the SLS verification, as illustrated in Figure 2, are explained briefly shortly. The workflow starts with the analysis of the type of

support structure (*section 2.2*). Different types of foundations transfer the external cyclic actions to the soil through different mechanisms and an overview of the types of foundations is presented here.

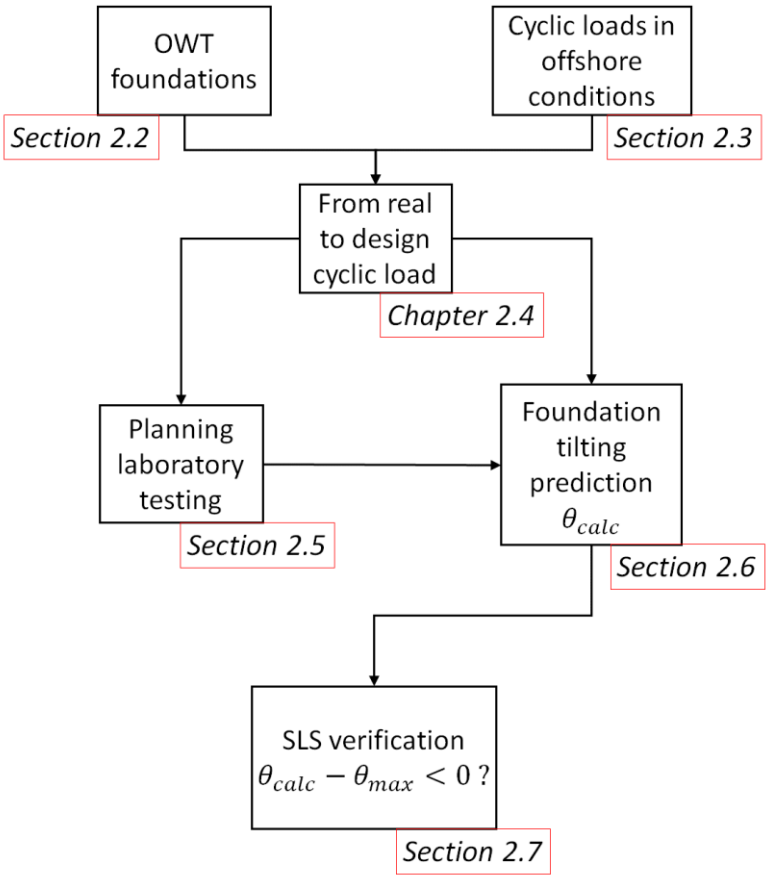

Figure 2. Cyclic loading design (SLS verification)

The second step (*section 2.3*) is to choose a cyclic load design event to analyse the external cyclic forces that are likely to act on the structure, such as hurricanes, typhoons, or seismic forces. Based on the type of the foundation and the external loads acting on it, the next phase involves defining the loads transferred to the foundation using aeroelastic simulations (*section 2.4*). In this phase, a simplification of the real irregular cyclic load to a regular cyclic load, which leads to the same damage in the soil, has to be implemented. Cyclic laboratory testing to analyse the accumulation of permanent deformation of the investigated soil is a fundamental input for predicting the tilting of the foundation. In

this phase (*section 2.5*), the soil samples extracted from the field have to be tested in conditions that represent the in situ conditions and in relation to the stresses transferred from the foundation to the soil. Based on the design loads and the results from the cyclic laboratory test campaign, the prediction of the long-term tilting of the foundation is calculated. In *section 2.6*, the existing methods are presented. Finally (*section 2.7*), the predicted tilting is verified with the allowed foundation rotation.

2.2. Solutions for offshore wind turbine foundations

OWTs are designed to be slender and flexible structures characterised by very long columns with a very heavy mass mounted on the top (rotor nacelle assembly). Cyclic loads in offshore conditions continuously swing the structure back and forth. The foundation, which is the component of the structure in contact with the soil, receives a significant cyclic overturning moment and cyclic horizontal load from the upper structure.

Figure 3 shows different solutions for a bottom fixed foundation. The choice of foundation type is mainly driven by factors, such as water depth, soil stratigraphy, and experience gained from past projects. During the early assessment of the project feasibility, a cost-optimal choice among several types of foundations is prepared, keeping in mind that lowering the LCOE is of high importance.

Gravity based foundations (GBFs) (Figure 3.a) withstand cyclic overturning moment by utilising their weight and size of the footprint on the seabed (vertical load) (Randolph & Gourvenec, 2011). A GBF is made of an outer concrete structure that is constructed onshore and floated offshore to the installation location, where it is sunk to the seabed with the help of a filling material. This type of structure is chosen for shallow waters since it is not feasible to design them for deeper water. Furthermore, the structure becomes too large and expensive to resist higher hydrodynamic loads.

Monopiles (Figure 3.b) are large hollow cylinders usually up to 10 m in diameter. Contrary to the gravity-based foundation, they resist the cyclic overturning moment by means of the lateral resistance provided by the soil, which is a function of the embedded pile length, pile thickness, and pile diameter. Renting

vessels and equipment to carry out the installation of these monopiles is the most expensive part of the foundation (Byrne & Houlsby, 2006). The structure can be drilled, vibrated, or hammered into the soil. In deeper waters, where higher loads are expected, installing larger monopiles can negatively impact the feasibility of the project.

In deeper waters, from approximately 40 to 80 m, using a tripod or jacket foundation is more cost effective than using a large monopile. This type of foundation is composed of multiple individual pods, which are connected by a steel substructure (lattice-frame jacket). The reduction of the free length of the tower by the substructure leads to an overall stiffer structure (Byrne & Houlsby, 2006). Piles or suction buckets may function as pods and the transferring mechanism of the cyclic overturning moment is decomposed to an axial cyclic loading.

For even deeper waters, floating turbines are the most economic choice. These floating structures are anchored to the seabed by mooring lines (Stevens & Rahim, 2014). The seabed anchors can be embedded (for example through piles, suction buckets, or embedded plates) or installed using small gravity based foundations (Stevens & Rahim, 2014).

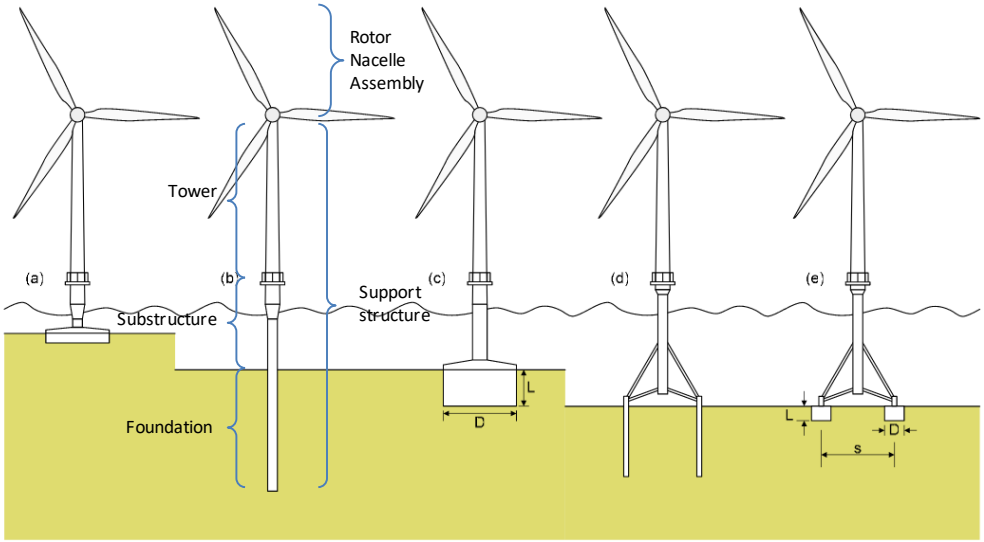

Figure 3. Different types of wind turbine foundations (Byrne & Houlsby, 2006)

2.3. Environmental and accidental loads in offshore conditions

Cyclic loads in offshore conditions have different origins and vary significantly in amplitude, period, duration, and direction (Andersen, 2015). Figure 4 shows the range of cyclic loads, varying in the number of cycles and period that can endanger the structure. It is interesting to see that an OWT potentially experiences up to 10^8 load cycles during its lifetime with a relatively large range of different loading frequencies compared to other structures.

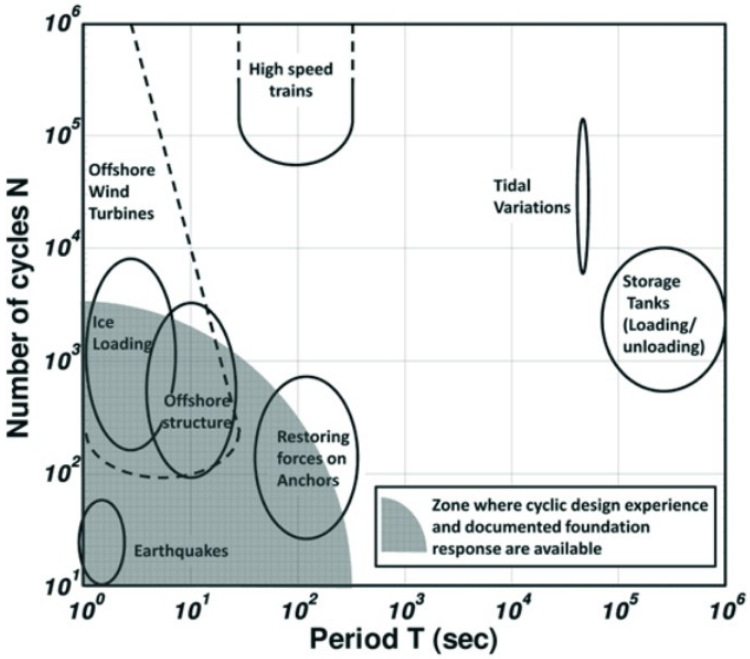

Figure 4. Periods and number of cycles for typical cyclic loading events (Andersen, et al., 2013)

Loads on OWTs are classified into static loads resulting from self-weight of the structure and cyclic/dynamic loads (Arany, et al., 2017). The latter, which is highly challenging for the design of foundations, is divided into environmental loads, operational loads, and accidental loads.

The environmental loads, generally caused by winds and waves, are random in both space and time and they are described accurately by statistical methods (Bhattacharya, 2019). Waves crash against the substructure applying a lateral

load. The magnitude of this load depends on the water depth, wave height, and period. Waves feature a frequency range of 0.05–0.2 Hz. The wind produces a thrust on the tower and the blades. The wind speed can be approximated by the mean wind speed, which pushes the tower in one direction, and its fluctuation, which is the local variation of the wind along the mean. The wind spectrum is characterised by very low cyclic loading frequencies. The directions of the wind and the waves are also an important aspect. These two loads may act in different directions (wind–wave misalignment) (Bhattacharya, 2019). In theory, a blowing wind creates the waves and the dominant wind direction is generally, the same as that of the waves. However, to keep a steady power production, the rotor could yaw out the dominant wind direction, thus creating a wind–wave misalignment (Bhattacharya, et al., 2017). During the design of the foundation, the assumption that the wind and the waves move collinearly could lead to an overestimation of the forces acting on the foundation, but it serves as a conservative choice (Bhattacharya, 2019).

The operational loads are (i) due to the rotation frequency of the rotor, usually referred to as 1P which ranges from 0.1 to 0.25 Hz and (ii) the shadowing effect of the tower blades, usually referred to as 3P for a three-blade turbine, which is in the range of 0.3–0.6 Hz (Kaynia, 2019; Bhattacharya, 2019). These ranges are typical for an eight MW Vestas wind turbine (Arany, et al., 2016). The 1P and 3P frequency ranges depend on the wind turbine capacity.

Earthquakes, typhoons, and tsunamis are considered as accidental loads. Nowadays, offshore wind farms are planned and installed in several countries that are in high seismic regions, such as the USA, China, India, and South East Asia (De Risi, et al., 2018). Installing offshore wind farms in a seismically sensitive zone creates an extra degree of challenge during the design of the foundation. A seismic wave in offshore areas gives rise to secondary effects, such as surface rupture, ground shaking, soil settlement, and soil instability, leading to liquefaction and induced tsunamis. An earthquake is characterised by a loading frequency of 1–10 Hz for a duration of a few seconds. Guidelines for an earthquake design of OWTs are scarce compared to those for onshore buildings (Kaynia, 2019). Typhoons are considered extreme weather conditions with a large-scale rotation system around the so-called eye area. In the outer part of the eye region,

there are extreme gusts, turbulent fluctuations, and sudden changes of wind direction causing serious hazards to large OWTs (Han, et al., 2019). The characteristics of typhoons are different from normal storms in terms of mean wind speed, and can be up to 200 Km/h in extreme events and with significant wave heights of more than 10 m.

To summarise, Figure 5 shows the frequency contents for various excitation sources acting on an OWT. It should be kept in mind that these cyclic loads can be design-driving loads as described in appendix H . For instance, designing an offshore wind farm meant to withstand an extreme earthquake or typhoon could result in exceptionally large foundation dimensions, which will make the project unfeasible. Alternatively, it may be acceptable that some wind turbines fail (e.g., an excessive tilting from an SLS point of view) under extreme accidental load events and in lieu of them, new ones may be installed in other positions.

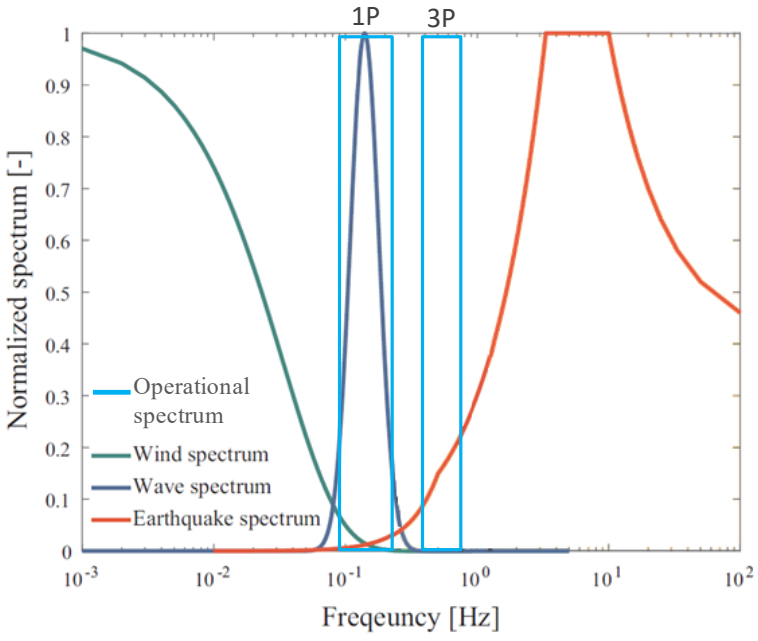

Figure 5. Frequency contents of various sources of excitation. Modified from (De Risi, et al., 2018)

2.4. Load inputs for cyclic loading design

For the cyclic load design verification, a "design event" that stands out from millions of cyclic loads during the wind turbine's lifetime is chosen. The magnitude of the design event depends on the return period, i.e., how often the event occurs. The larger the return period, the higher is the magnitude of the event.

The design event, which can be an environmental or accidental load, is supposed to cause the most severe impact on the foundation during the planned lifetime, while other events will have a smaller contribution on the final deformation. This approach is based on Miner's rule (Miner, 1945). This rule states that the sequence of several blocks of cycles with constant amplitude is not pivotal for the final accumulation of deformation. This theory is validated through laboratory testing for a relatively large number of cycles, on quartz sand and proved to yield good results (Wichtmann, et al., 2010).

Once the design event is chosen, the representation of the loads transmitted to the soil as realistic as possible is an important ingredient for the cyclic load design phase. Fully coupled aero-hydro-servo-elastic models are used to perform time-domain wind turbine load simulations. These models were developed to capture the complex dynamic behaviour of OWTs by simultaneously modelling the influence of the structure, soil stiffness, wind, and wave loads and different operation conditions (Velarde, et al., 2019). Figure 6 shows a schematic layout of an offshore wind turbine OWT with a monopile foundation implemented in an aero-elastic wind turbine simulation tool subjected to a storm design event with mean wind speed U_w and wave height H_s (Velarde, et al., 2019). The interaction between the foundation and the soil is modelled using nonlinear soil springs. The substructure designers use these models to extract at the mudline section (e.g., the red point in Figure 6), and the 10-min irregular load history for the horizontal force and the bending moment ("real-world loads").

Figure 6.b–c shows the 10-min irregular load at the mudline (red point in Figure 6.a) for different return periods, i.e., magnitudes. Figure 6.b presents the loads for a storm event with return period of 1 year and Figure 6.c presents the loads for a return period of 100 years. The overturning moment M_x and horizontal

force F_y transmitted to the foundation increase proportionately upon reducing the frequency of occurrence (i.e., by increasing return period).

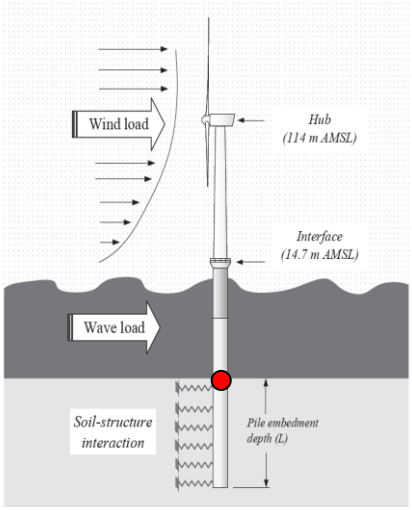

a)

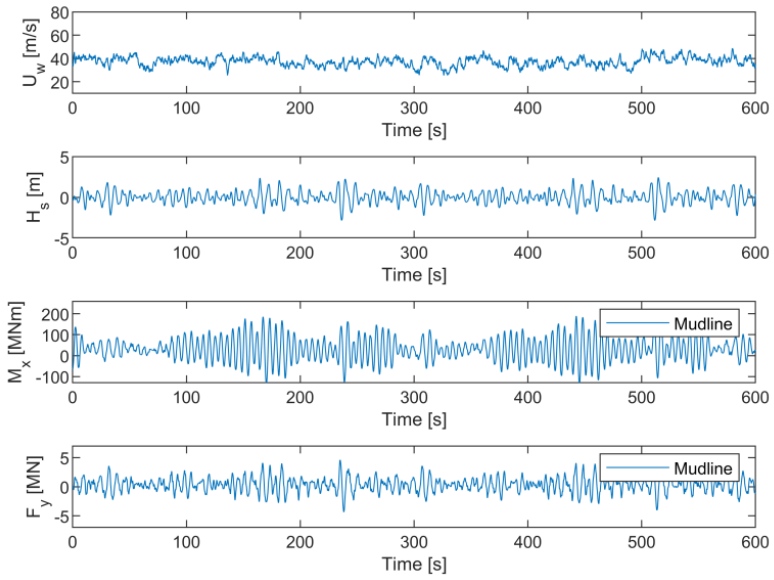

b)

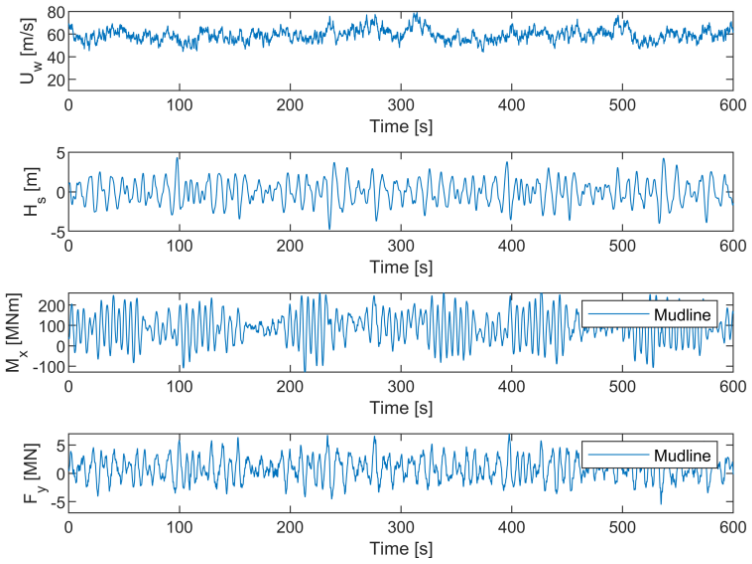

c)

Figure 6. (a) Monopile-supported offshore wind turbine as modelled in an aeroelastic simulation (Velarde, et al., 2019); (b) one-year return period loads; (c) 100-year return period loads

This complex irregular load history is composed of several cycles with different average and cyclic components and frequencies. The irregular loads are complicated to deal with from a laboratory testing and design method point of view. For this reason, the irregular loading is decomposed and approximated to an equivalent uniform sinusoidal loading parcel (or package) with a constant average, cyclic amplitude, and period (regular cyclic load).

The decomposition procedure is an important step for designing the foundation and it should be executed based on the engineering judgment and experience. The procedure is based on the cumulative damage hypothesis and equivalent number of cycles, which is known as Palmgren-Miner rule (PM) (Palmgren, 1924; Miner, 1945), and was first applied to study fatigue in metals. Seed et al. carried out the first application of this rule for sand material for liquefaction analysis during earthquake loadings (Seed, et al., 1975). The PM rule generally states that the damage caused by an irregular load history can be approximated with uniform sinusoidal loads applied for an equivalent number of loading cycles. A decomposition procedure is explained in Andersen (Andersen, 2015). This procedure is based on rainflow counting and a series of cyclic laboratory tests and it is presented in the attached paper (see appendix H).

2.5. Planning the laboratory tests

Usually, the long-term prediction of the foundation tilting is based on the results of an advanced laboratory test campaign in which the soil is subjected to regular cyclic loads. The soil used for the laboratory testing is obtained from a geotechnical investigation by sampling boreholes in the area where the wind park is located. The cyclic laboratory test campaign has to be planned to accurately represent the in situ soil condition when the foundation is cyclically loaded. The choice of the test device, stress magnitude of the regular loading, sample preparation technique, and drainage condition are key parameters that should be carefully planned (Andersen, 2015). Planning the cyclic laboratory tests requires experience and engineering judgement because these factors highly influence the accumulation of permanent deformation experience by the soil sample and consequently the prediction of the foundation tilting.

The stress condition in the soil surrounding an offshore foundation subjected to cyclic loads is highly complex. Depending on the type of foundation and hence, the transferring mechanism, different soil volumes are subjected to different stress path conditions, i.e., different cyclic shearing mechanisms. From an analysis of the stress path, for instance, the failure mechanism provides the geotechnical engineer an idea about the orientation of the principal stress direction of different soil elements (Hight, et al., 1983). Figure 7 shows an approximation of the orientation of the principal stresses along a hypothetical failure line beneath a shallow foundation. It can be seen that some soil elements might be better represented by compression tests and others by simple shear tests. A precise prediction of the accumulation of permanent deformation beneath a foundation would require testing the soil samples in the laboratory by replicating the same stress path (orientation of principal stresses) of different soil elements. Although a hollow cylindrical apparatus has a possibility to replicate different inclinations of the principal stresses (Hight, et al., 1983), it is not widely used in practical applications. Therefore, the stress path under a foundation is rather approximated by means of a classical laboratory testing, such as cyclic simple shear tests or cyclic triaxial tests (Andersen, 2015).

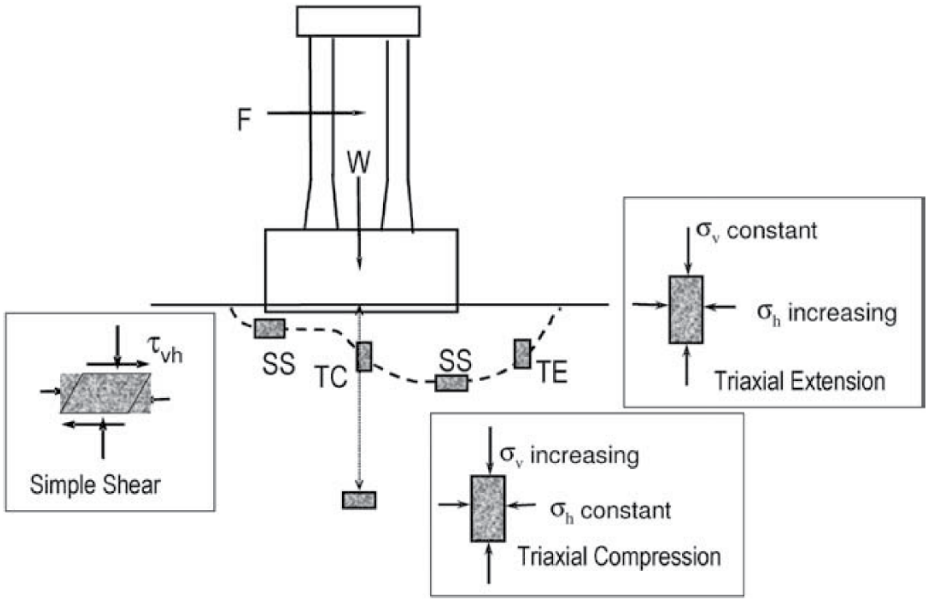

Figure 7. Stress path under a gravity based foundation (Randolph & Gourvenec, 2011)

Generally, the cyclic loads in the tests are applied stress-controlled loads, which are assumed to be the best representation of a cyclic event (Andersen, 2015). For cohesion-less soils, the reconstituted sample should be tested with the same static and cyclic combination as the one theoretically experienced in the field. Figure 8 shows that different soil elements are subjected to several combinations of average shear stresses and cyclic shear stresses. Certain soil elements experiences higher static components τ_{avr} (one-way loading), while the others experience higher cyclic amplitude stresses τ_{cly} (two-way loading).

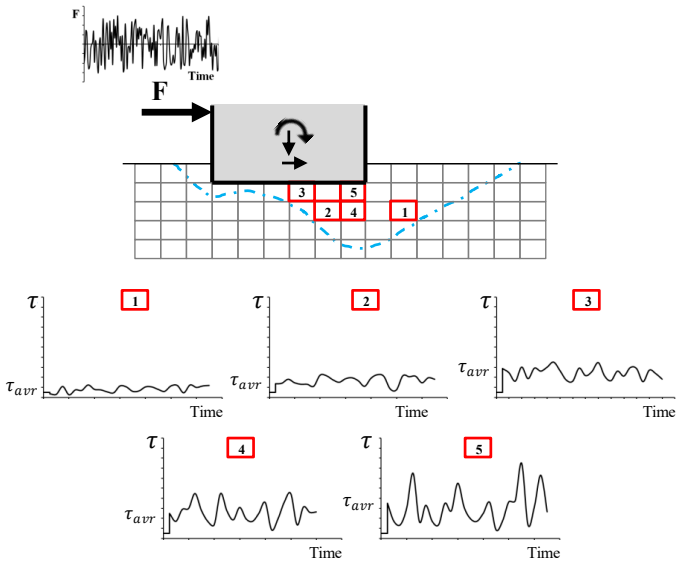

Figure 8. Stress variation for a specific soil volume under a gravity based foundation. Redesign from (Ibsen & Lade, 1998)

However, it is not feasible to perform large number of laboratory tests under all possible combinations of stresses that the foundation may experience. Therefore, the prediction of deformation of the soil for other stress combinations has to be extrapolated from a limited number of laboratory tests. Generally, there are two different options to utilise the obtained data: calibrating a numerical model with the available tests and using it to predict the soil behaviour for other stress combinations (see appendix D); or interpolating the limited data in design graphs called cyclic interaction or cyclic contour diagrams (Andersen, 2015). The different soil volumes at different depths (e.g., Figure 8) in a soil domain have different vertical and horizontal pressures. Therefore, the soil is solicited at different combinations of the cyclic load magnitude and the confining pressure. To reduce the amount of laboratory testing, it is useful to deal with 'average stress ratio' (ASR) and 'cyclic stress ratio' (CSR), which are the ratio of average stress to the consolidation stress, and the ratio of the cyclic stress amplitude to the consolidation stress, respectively. It is assumed that the behaviour of the soil tested under different stress conditions, but the same ASR and CSR provides the same accumulation of permanent deformation. This assumption is partially verified in the paper presented in Appendix E. The FE modelling can

be very useful to plan the laboratory test campaign. After the decomposition of the irregular stress history into a uniform load parcel, the average components and the cyclic components can be applied as a static load to the FE model of the investigated foundation. The soil domain can be divided into different soil volumes, and the ASR and CSR can be calculated and plotted as contour plots. In this way, the variation of magnitude of the stresses becomes visible and therefore, this combination should be investigated in the lab. For example, Figure 9 shows the variation of the ASR under a gravity based foundation subjected to a static peak load.

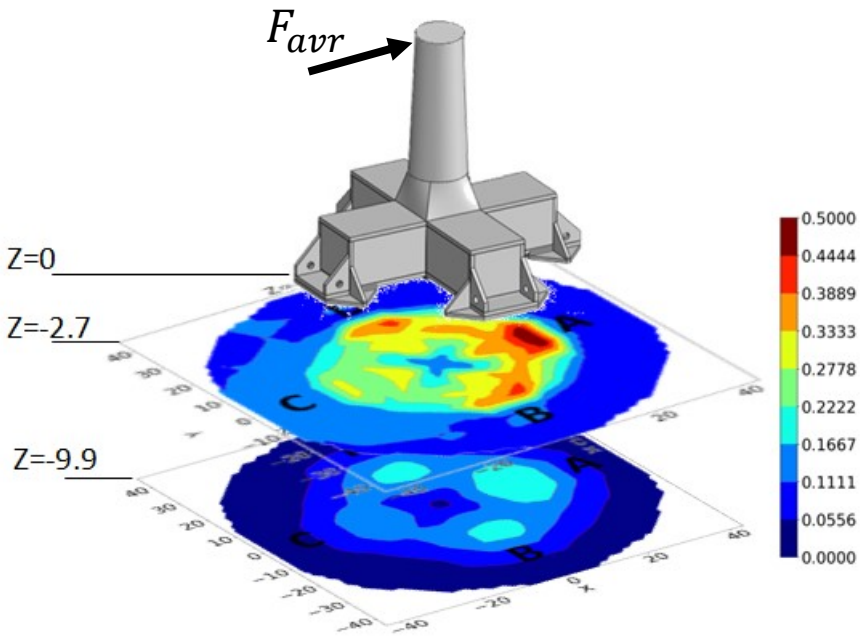

Figure 9. 3D Variation of ASR under a gravity based foundation

Extracting samples in a cohesion-less soil from the probe of the boreholes leads to an alteration of the soil structure. The method of sample preparation (e.g., moist tamping vs. dry deposition) plays an important role on the sand response to cyclic loads (Sze & Yang, 2014). For sand samples, it is recommended to reconstitute the sand by wet tamping or water deposition (Andersen, 2015). The sample should be reconstituted to a relative density value. This value is generally obtained from empirical formulation from the tip resistance of the cone

penetration tests. It can be argued that the level of uncertainty of the relative density values can be significant.

The hypothesis of considering one design event can lead to an overestimation of the deformation. Before the design event, the in situ soil is subjected to small cyclic loads that change the soil fabric by improving the interlocking between the particles and increasing the relative density of the soil. These small loads are characteristic of smaller storms, the built-up phase of a design storm (Andersen, 2015), or low intensity earthquakes. In the laboratory tests, after the consolidation to the desired stresses, a pre-loading phase can be executed which involves the application of small cyclic amplitudes to improve the soil conditions. If the pre-loading is in undrained conditions, a consolidation phase to dissipate the generated pore water pressure should be allowed before starting the main cyclic loading phase. The effect of small pre-loading causes a strengthening of subsequent cyclic loads (Porcino, et al., 2009; Vaid, et al., 1989; Ishihara & Okada, 1978). The pre-loading cycles are generally of small magnitude and last for a few hundred cycles. In a cohesion-less soil, the pre-loading causes a slight reduction of the relative density after consolidation. It is however not clearly understood how such a slight reduction can cause such a beneficial effect (Andersen, 2015), and the investigation from a micromechanical point of view may be helpful to have an insight into the change of the soil fabric. It should be noted that pre-loading might have a detrimental effect on over consolidated sand. The value of the pre-loading is however difficult to determine.

The drainage condition (i.e., drained, partially drained, or undrained) depends on the in situ situations, such as magnitude and period of the loads, soil layering, soil properties and degree of drainage. The drainage condition is an important choice in the design process because it can be a design-driving factor. When the soil experiences an accumulation of pore water pressure after each cycle, the grain particles lose contact with each other. Therefore, the soil is subjected to a decrease in the inter-particle forces (i.e., effective stresses), which carry the external load leading to a softening of the soil structure and a high accumulation of soil deformation. A drained condition develops when the pore water is able to escape the grain particles during a cyclic load event. As for the soil fabric, this condition leads to a soil stiffening, i.e., a better interlocking of

the soil grain. At the same time, the sand accumulates permanent deformation, which is smaller in magnitude than in that partially drained or undrained conditions. Generally, undrained behaviour is assumed in the design stage, which is a conservative assumption owing to the higher amount of permanent deformation experienced by the soil. For cyclic laboratory testing, the undrained and drained conditions are routinely tested. On the other hand, the partially drained condition is not used for the design because of the difficulties in carrying out cyclic laboratory tests with partial drainage. Owing to the uncertainty in the in situ drainage behaviour, it may be useful to predict the foundation tilting in undrained and drained conditions. Nonetheless, this verification requires double the amount of testing and is therefore, unfeasible. The paper in Appendix E provides a formula titled 'Undrained2drained', which theoretically converts the permanent shear strain developed with undrained tests into a drained permanent shear strain. This formulation potentially saves time and money.

2.6. Existing method to predict the rotation of foundations

Currently, the geotechnical engineers have to use a method to predict the foundation tilting based on simplified regular load and results from cyclic laboratory tests. In practice, the prediction of the behaviour of a soil subjected to cyclic loads is based on two strategies (Wichtmann, 2005): implicit and explicit predictions. The first strategy derives the accumulation of permanent deformation by modelling each cycle in the time domain adopting the common soil constitutive models. Theoretically speaking, this would be the best strategy because it can be done by accounting for the holistic behaviour of the soil. While, adopting the common constitutive models in the FE modelling, the applicability is restricted to a very low number of cycles owing to the accumulation of excessive numerical errors (Niemunis, et al., 2005; Wichtmann, 2005). An innovative alternative for modelling a large number of cycles in time domain is to employ the discrete element method as shown in the appendix D. The explicit strategy is the preferred choice when a large number of cycles are considered. The prediction of the accumulation of permanent deformation is directly based on the number of cycles employing empirical formulations or contour diagrams derived from the laboratory cyclic test campaign.

In the literature, there are two explicit strategies to predict the foundation tilting, global level and local level. The first category involves the application of mathematical formulations that link the global rotation of the foundation directly based on the number of cycles N. These formulations are derived from small-scale model tests (Cuéllar, et al., 2012; LeBlanc, et al., 2009; Yu, et al., 2015; Hettler, 1981). Generally, it is challenging to extrapolate the results or trend from small laboratory tests to a prototype. This is because the model scale tests are executed under the natural gravity force (1g), while in reality higher stresses are expected in the field (Nadim, 2001). One way to overcome this problem is to use a centrifuged system to increase the gravitational field and overcome the stress dependency problem. An example of a monopile test is as described by Klinkvort and Hededal (Klinkvort & Hededal, 2013). On the other hand, the model tests are valid benchmarks to validate the numerical models, which are used for designing full-scale foundations (Nadim, 2001). In addition, the proposed formulae are quite simple as they do not consider the local stress distribution in the soil and may not lead to accurate predictions when used for more general problems, e.g., different soil stratigraphy or foundation geometry than the one tested in the laboratory.

The prediction of the foundation tilting at the local level is based on a combination of 3D finite element models and cyclic laboratory tests. Examples for such advanced numerical models include the high cycle accumulation model (Niemunis, et al., 2005), the undrained cyclic accumulation model (UDCAM) (Jostad, et al., 2014), and the stiffness degradation method (SDM) (Achmus, et al., 2007). The first and second models are very complex, which make them less attractive for use in day-to-day geotechnical design projects. The first is the most advanced model for high cycle loading design and it was originally developed in Abaqus 3D. The explicit prediction of the accumulation of strain in the soil is based on a sophisticate mathematical formulation, which aims to take into account the change in the void ratio, stress history, polarisation of the cyclic loading loop, cyclic amplitude, and the ASR. A large number of phenomenological parameters need to be calibrated with an extensive laboratory test campaign. The UDCAM model is applied in PLAXIS 3D and the explicit prediction of the strain is based on the cyclic contour diagrams developed from a

laboratory test campaign. This model is then degrading the parameters of the NGI-ADP constitutive model in order to account for the cyclic degradation. The last method, the stiffness degradation method (SDM) (Achmus, et al., 2007), has a lower degree of complexity, but potentially higher practicability. This method is applied in a 3D FE model and the accumulation of deformation is based on the degradation of the soil stiffness. The degradation is based on the development of plastic strain derived from an empirical formulation, which is related to the number of cycles, a stress dependent variable, and two regression parameters calibrated with cyclic laboratory testing.

2.7. SLS verification

The final step is the SLS check, which consists of comparing the predicted tilting θ_{calc} with the allowed θ_{max}. The wind turbine manufacturers provide a tilting restriction for operational reasons. The recommended practice DNV-GL-RP-C212 (DNV-GL, 2017) gives an example of $\theta_{max} = 0.25°$ of allowed tilting throughout the planned lifetime. This strict verticality requirement may have originated from different design criteria, which however, are mainly rooted within the OWT sector (Bhattacharya, 2019): (1) blade-tower collision, (2) reduced energy production, (3) yaw motors and yaw breaks, (4) nacelle bearing, (5) variation in the fluid levels and the cooling fluid movement, (6) P–δ effect and (7) aesthetic reasons.

This strict tilting requirement, i.e. $\theta_{max} = 0.25°$, in conjunction with extreme loads can increase the foundation dimension and significantly increase the cost of the project. For example, typhoon–tsunami–earthquake proofing of OWTs can lead to a significant foundation dimension making the project unfeasible and the final cost of energy very high. On the other hand, a less strict verticality requirement (which could be a function of the dimension and type of the installed wind turbine), for example an angle of rotation of 1–3°, could lead to a smaller foundation size and still meet the safety requirements. Therefore, it is fundamental to calculate a reliable prediction of the foundation tilting to avoid an early shutdown of the wind turbine and obtained a cost-effective foundation.

2.8. Summary

This chapter provides an overview of the different steps that a geotechnical engineer should follow when designing a foundation. As this thesis provides a method for predicting the foundation tilting, emphasis is put on the workflow needed for validating the SLS criterion: (i) the selection of the design event, (i) the simplification of the irregular real-world loads into regular cyclic loads, (iii) planning of the laboratory test campaign and (iv) the existing method to predict the tilting of the foundation.

To date, explicit methods are most commonly used in engineering practice to predict the foundation behaviour under cyclic loads. Even though different methods exist at the global or local level prediction of the permanent rotation, these are not reliable and validated or too complex to be implemented in day-to-day projects. Planning the cyclic laboratory test campaign require different assumptions regarding the test device to be used, the stress magnitude of the regular loading, the sample preparation technique and drainage condition. In addition, a large number of cyclic laboratory tests are usually required at different stress levels, relative densities and drainage conditions, which affect the project cost and time. With this in mind, the design involves several sources of uncertainty regarding the laboratory testing, the loads and the design methods. Contrary to the deterministic design commonly used for verifying the SLS criterion, adopting a probabilistic design philosophy a cost effective foundation can be designed by quantifying the main uncertainties.

These open issues are addressed by this Ph.D. thesis as explained in the next chapter.

3. Overview of research methodology

The research methodology is divided in four interconnected parts (core project objectives). Figure 10 depicts the four parts and their interconnections. The development of each part is thoroughly investigated by means of one or more papers, which are attached in the appendices.

The methodology starts with *Part I (appendices A and B),* which focuses on the theoretical development of the soil cluster degradation (SCD) method. This method provides an explicit prediction of the foundation tilting when subjected to a regular cyclic load design event and it is based on cyclic laboratory tests and 3D FE model. *Part II (appendices C, D, and E)* aims to substitute the cyclic laboratory tests by means of numerical tools. The validation of the SCD method in *Part III (appendices F and G)* is needed to verify the quality and explore the performance of the SCD method with the laboratory tests, and a full-scale test, and implement the proposed improvements in Part II. The last *Part IV (appendix H)* closes the research loop and focuses on implementing the SCD method in a reliability-based design (RBD) framework to address the main source of uncertainty involved in verifying the SLS criterion and designing the foundation to an annual reliability target.

In the following subsections, a description of the novelty of each part, which can be found in the papers, is explained.

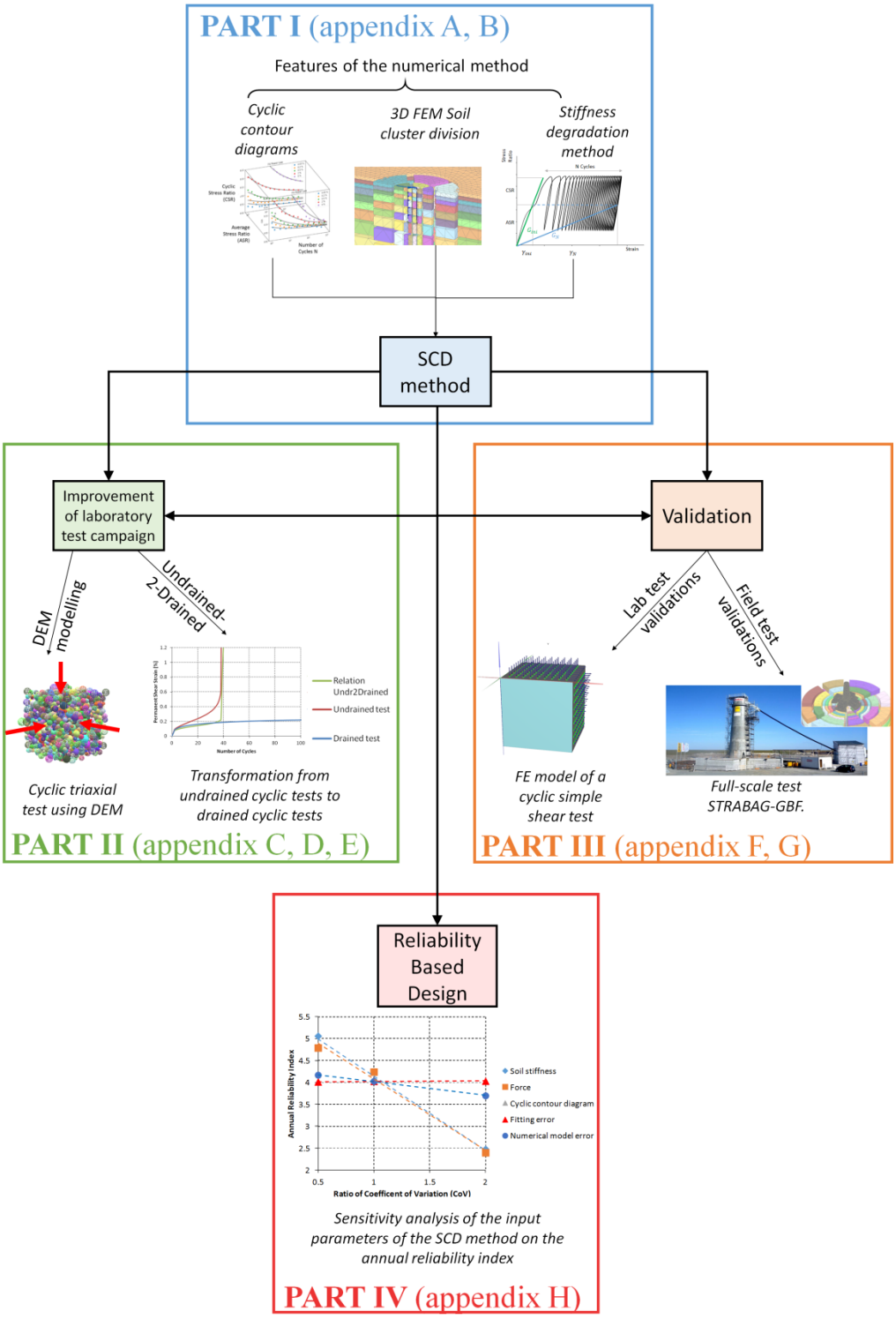

Figure 10. Overview of the methodology for cyclic loading design

3.1. Part I: Development of the SCD method (Appendices A and B)

This part encompass the conceptual and practical development of the SCD method. The first paper in Appendix A provides the theory behind the developed explicit method, its working principles, and a practical application. In the same manner, the second paper in Appendix B shows the flexibility of the application of the SCD method on different types of foundation.

The key points of the two papers can be summarised as follows:

- **The SCD method in a nutshell:** the SCD method explicitly predicts the long-term response of an offshore foundation accounting for the cyclic accumulation of permanent strain in the soil. It is based on 3D finite element (FE) simulations in order to account for a precise local distribution of the cyclic stresses around the foundation. The final accumulation of permanent strain in the soil due to a regular cyclic load event is taken into account explicitly by degrading a fictional elastic shear modulus (which is based on the work of Achmus and co-authors (Achmus, et al., 2007)) in a 3D cluster-wise division of the soil domain. Based on the local stress level in each soil cluster, the reduction of the soil modulus is related to the accumulated permanent strain interpolated in a cyclic contour diagram (Andersen, 2015). This diagram has to be previously developed from cyclic laboratory tests. The method of equivalent number of cycles is adopted to take into account the strain history, if the cyclic design event made of different regular cyclic loads, i.e., parcels (damage accumulation between parcels). A simple Mohr–Coulomb soil model is necessary for implementing the soil stiffness degradation.
- **Automation of the offshore design:** The present method has been implemented in the commercial finite element code PLAXIS 3D, which allows for the design of an automated model by means of a remote scripting interface based on the Python programming language (PLAXIS, 2017). For each type of foundation, a Python script is programmed and the cyclic loading design is done automatically in terms of the cluster division, extrapolation of the local stresses,

interfacing with the cyclic contour diagrams, and the final extraction of the foundation tilting.
This automated design minimises the amount of manual work and the related risk.

- **General applicability:** The SCD method is suited for different types of structures, such as monopile and gravity based foundations, and suction buckets.

This part provides the theoretical basis for the development of the SCD method. Parts II, III, and IV further develops this method in different aspects to improve its trustworthiness.

3.2. Part II: Improvement of cyclic laboratory test campaign (Appendices C, D, and E)

Owing to the time and budget constraints of the project, it might not be feasible to plan a large laboratory test campaign to construct different cyclic contour diagrams for different drainage conditions, relative density and different cyclic stresses. Therefore, this part aims to substitute a part or the entirety of the laboratory test campaign with numerical tools.

One innovative improvement developed in this part is centred on adopting the discrete element method (DEM) to ultimately substitute the cyclic laboratory tests. Then, the DEM simulations of the soil sample can be run quickly and easily to extract the accumulated permanent strain at different cyclic stress conditions and relative density. In this way, it is possible to increase the amount of data to construct more reliable cyclic contour diagrams. The papers in appendices C and D describe the application of the DEM to simulate the cyclic laboratory tests first qualitatively and then, quantitatively.

The main key findings can be summarised as follows:

- **Modelling the laboratory tests:** A representative elementary volume (REV) with periodic boundary conditions and only 3000 particles is found to be enough to successfully replicate the monotonic and cyclic behaviour obtained from the triaxial test device.

- **Calibration of the REV for high cyclic loading:** the approach of using the DEM-REV to simulate a high number of cycles is validated with drained cyclic triaxial tests on Berliner sand up to 10,000 cycles.
- **Practical application of the DEM in offshore foundation design:** the drained permanent shear strain extracted from a large amount of DEM simulation of the drained cyclic triaxial tests are used to create the cyclic contour diagram. This DEM-based cyclic contour diagram is used in the SCD method for a practical application in which the tilting of a gravity-based foundation is predicted in the event of a storm design event.

Another improvement of the cyclic laboratory test campaign is related to the drainage test condition. The papers in appendices E and F focus on developing and validating an innovative mathematical formula, which links the accumulation of permanent deformation of cyclic loaded soils under different drainage conditions.

The main key points can be summarised as follows:

- **Transformation formula Undrained2Drained:** a formula is proposed to transform the permanent shear strains developed with cyclic undrained tests into permanent drained strains, which are theoretically obtained with the same cyclic stress configuration, but in drained conditions. This formula is developed for simple shear tests,
- **Validation:** The formula is validated with a few cyclic simple shear tests under different stress levels and different drainage conditions.

This transformation formula is applied to obtain the cyclic drained contour diagrams, which are implemented for the validation with the full-scale gravity based foundation test (Part III).

3.3. Part III: Validation of the SCD method (Appendix F and G)

The aim of this part is to provide confidence to the geotechnical engineers to apply the SCD method in offshore projects. The SCD method is validated with cyclic laboratory tests as explained in appendix F, and with a full-scale cyclic loading test of a gravity based foundation (appendix G).

The key points can be summarised as follows:

- **Cyclic laboratory tests:** The link between the fictitious stiffness degradation and the cyclic contour diagram is validated with single stage and multistage cyclic simple shear tests. The validation is carried out by modelling the cyclic simple shear test using 3D finite element models. Moreover, a mathematical framework for constructing the design cyclic contour diagrams is introduced, in which the permanent shear strain surfaces are assumed to follow a power law in the plain N-CSR.
- **Full-scale test:** the SCD method is validated by simulating a full-scale cyclic loading test of a gravity-based foundation. The prototypes were subjected to more than one million cycles and the soil and structure were extensively monitored during the test. This validation shows the complete application of the method, which includes (i) the investigation of the in-situ soil condition and the derivation of the soil stiffness necessary for the SCD method, (ii) the development of the cyclic contour diagram, (iii) the choice of the modelling assumptions, and (iv) a final comparison with the in situ monitoring.

3.4. Part IV: Reliability analysis of offshore structures under cyclic lateral loading (Appendix H)

The cyclic load design flowchart for the verification of the SLS criterion is currently carried out deterministically, i.e., excluding various sources of uncertainties. The aim of this part is to check the serviceability criterion using a probabilistic approach based on the RBD framework. Following this approach, the foundation can be designed to meet a specific target reliability level accounting for significant uncertainties. The paper in appendix H focuses on developing such a framework.

The key points can be summarised as follows:

- **RBD framework:** The framework starts with the uncertainty quantification from the available data (cone penetration test (CPT), cyclic

laboratory tests of the soil, and metocean and aero-hydro-servo-elastic model) and the derivation of the stochastic input variables, such as soil stiffness, cyclic contour diagram, and storm event, necessary for the SCD model. Based on the stochastic input variables, a response surface is then trained to yield the same output in terms of structural tilting as the SCD method. Next, the response surface is used to calculate the probability of failure (via Monte Carlo simulation). If the calculated probability of failure does not meet the target probability, the foundation geometry has to be adjusted accordingly and the methodology is repeated to check whether the new design is safe.

- **Practical application:** In this study, the RBD framework is applied to the cyclic loading design (SLS criterion) of a large diameter monopile supporting a 10 MW offshore wind turbine. A sensitivity analysis of the main input uncertainties found in the annual reliability index is carried out.

4. Conclusions and future developments

4.1. Discussions and conclusions

The prediction of the lifelong foundation tilting of structures subjected to cyclic loads is still a challenge for geotechnical engineers owing to a lack of a generally accepted method. Consequently, this aspect is often missing a thorough investigation in OWT projects even though the wind turbine manufacturers impose strict serviceability criterion. For this reason, this thesis delivers an advanced numerical method called the SCD method to assist geotechnical engineers to design cyclic loaded structures verifying the SLS criteria, i.e., the foundation rotation, when subjected to a design event. To provide confidence and boost the use of this method in offshore projects, this thesis went through different parts explaining the general applicability of the SCD method, providing new numerical tools for improving the cyclic laboratory test campaign, validating the method, and proving an RBD methodology for carrying out a cost-effective design. The following findings are summarised:

- Explicitly calculating the accumulation of permanent deformation combining the stiffness degradation method (Achmus, et al., 2007) and the cyclic contour diagram framework (Andersen, 2015) in a clustered soil domain is shown to be a simple and numerically stable method, which can be easily implemented in day-to-day projects. This method is a simplification of the more complex behaviour developed during cyclic loaded saturated soil. At the present, phenomena such as densification and change in soil stiffness are not predicted from the SCD model. Another critical point is when the prediction of the rotation is assess over different parcels. The equivalent number of cycle method is taking into account the history regarding the accumulation of permanent deformation but not the change in the fabric and its effect on the following parcels.
- The SCD method is implemented in the 3D FE PLAXIS tool, which is widely used for geotechnical projects and allows to control the FE

environment by means of a remote scripting interface. Owing to its automatic modelling concept by using the Python interface in PLAXIS it is suitable for testing designs with complex soil stratigraphy, as well as different types of foundation, and simply develop sensitivity analysis. On the other side, the simulations are time consuming due to post-processing reasons: the tensors in each stress point of the FE has to be one-by-one read it. This takes time event thought it is done automatically and especially when (i) the soil domain is divided in a high amount of 3D clusters, (ii) different load parcels have to be simulated and (iii) a fine mesh is chosen.

- It has been shown that the SCD method can deliver an accurate and reliable prediction of permanent deformations and stress redistributions at the SSI level. This is based on comparing the deformation behaviour with cyclic laboratory testing and the accumulation of tilting measured on a cyclic loading full-scale gravity based foundation subjected to approximately 300,000 regular cycles. In these validation phases, different assumptions were involved. For instance, the uncertainties in the cyclic contour diagrams and soil cluster division have not been investigated on the final prediction.
- Verifying the SLS criteria, the assumption of the drainage condition can be a design-driving factor. If pure undrained conditions are assumed during a design event, an upper bound of rotation of the foundation is expected (pore water pressure leads to a high accumulation of permanent deformation). The SCD method can predict the rotation of the foundation under the assumption of fully undrained or drained conditions. This is achieved by interpolating the undrained or drained permanent strain in the cyclic contour diagrams.
- To facilitate the final user in planning an optimal laboratory test campaign and developing reliable cyclic contour diagrams, different methods were investigated: (i) using the FE model to plan the applied stress range for cyclic loads, (ii) fitting a mathematical framework to construct the cyclic contour diagrams, (iii) theoretically converting the undrained shear strain to the drained shear strain

(Undrained2Drained formula), and (iv) proposing an innovative concept of using the DEM model to integrate or substitute the cyclic laboratory tests. All of these proposed improvements are based on a limited series of test validations. Engineering judgment should be used when these methods are implemented in different soil conditions, relative densities, stress levels or type of soil.

- When a probabilistic analysis has to be employed for verifying the SLS criteria, a reliability based design framework is proposed and applied for a typical monopile foundation. Therefore, the end user will be able to implement the SCD method in such a framework accounting for the main uncertainties involved and verify that the dimension of the foundation respects the annual reliability target specified by the standards.

4.2. Further research

The developed method also opened different possible research lines that should be investigated in the future. In summary, further development steps are

- At its present form, the SCD method is a simplified method to predict only the accumulation of permanent deformation experienced by the soil when subjected to cyclic loads. Currently, the effects, such as soil stiffening or softening and change in the soil density are not directly predicted. Hence, it should be investigated if the SCD method can be adapted to predict such behaviour.
- The degradation of the stiffness in each cluster is linked to a plastic strain (based on the local stress level) obtained from the contour diagram. After the degradation phase in the FEM, a control function should be used to check if the cluster has the wanted plastic strain (the one extracted from the contour diagram) and effective stresses.
- If the SCD method has to be applied with drained condition, engineering judgment should be given on which strain in the contour diagram should be used: axial, radial or volumetric.
- The proposed method is based on the division of the soil volume into clusters. The cluster division has to follow the shape of the

foundation and a sensitivity analysis should be done to understand the influence of the cluster dimension on the final structural tilting.

- As highlighted in chapter 2, the in situ 3D orientation of the principal stresses may be different from the laboratory testing conditions. Currently, it is not clearly understood as to what effect this assumption has on the structural tilting prediction.
- An interesting development of the SCD method, when undrained conditions are assumed, involves predicting the structural tilting using the permanent pore water pressure cyclic contour diagrams. Based on the local stress level in each cluster, the extracted accumulated pore water pressure can be into the soil clusters. In this way, the FE model is able to calculate the foundation tilting based on the consequent reduction of the effective stresses, which is in relation to the water pressure. This procedure will also allow running a consolidation analysis.
- A helpful future development would be to implement the SCD method for predicting the foundation tilting when subjected to earthquakes.
- This thesis dealt with cohesion-less soil. However, different cyclic contour diagrams for different materials such as clay and silt can be constructed (Andersen, 2015) and easily used using the SCD method.
- The theoretical formula Undrained2drained is developed for simple shear tests.
- The prediction of the accumulated permanent deformation is derived from the cyclic contour diagrams. They are based on an extensive cyclic laboratory test campaign. The proposed improvements using the DEM model and the theoretical formula Undrained2drained have been verified based on only a few cyclic tests. Future developments for understanding the limitations of these methods and developing guidelines by verifying them with different cyclic testing devices, different relative densities, and stress conditions are anticipated.

References

Aboul Hosn, R., Sibille, L., Benahmed, N. & Chareyre, B., 2017. Discrete numerical modeling of loose soil with spherical particles and interparticle rolling friction. *Granular Matter, Springer Verlag,19 (1), pp.4. 10.1007/s10035-016-0687-0.*

Achmus, M., Abdel-Rahman, K. & Kuo, Y., 2007. *Behavior of large diameter monopiles under cyclic horizontal loading.* s.l., s.n.

Achmus, M., ABDEL-RAHMAN, K. & KUO, Y., 2007. BEHAVIOR OF LARGE DIAMETER MONOPILES UNDER CYCLIC HORIZONTAL LOADING. *Twelfth International Colloquium on Structural and Geotechnical Engineering.*

Achmus, M., Abdel-Rahman, K. & Peralta, P., 2005. *On the design of monopile foundations with respect to static and quasi-static cyclic loading.* Copenhagen Offshore Wind 2005: s.n.

Allotey, N. & El Naggar, M., 2005. *Cyclic soil degradation/hardening models: a critique.* Rotterdam, MillPress Science Publishers, pp. 785-790.

Andersen, K., 2015. *Cyclic soil parameters for offshore foundation design.* s.l., s.n., pp. 5-82.

Andersen, K., 2015. *Cyclic soil parameters for offshore foundation design.* London, Taylor & Francis Group, pp. 5-82.

Andersen, K. H., 2015. Cyclic soil parameters for offshore foundation design. *The 3rd McClelland Lecture, Frontiers in Offshore Geotechnics III, ISFOG'2015,* Volume 1, pp. 5-82.

Andersen, K. H., 2015. Cyclic soil parameters for offshore foundation design. *The 3rd McClelland Lecture, Frontiers in Offshore Geotechnics III, ISFOG'2015*, pp. 5-82.

Andersen, K. H., Puech, A. A. & Jardine, R., 2013. Cyclic Resistant Geotechnical Design And Parameter Selection For Offshore Engineering And Other Applications. *Proceedings of the ISSMGE conference – TC 209 Workshop – Design for cyclic loading: piles and other foundations,* pp. 9-44.

Arany, L., Bhattacharya, S. M. ,. J. & Hogan, S., 2017. Design of monopiles for offshore wind turbines in 10 steps. *Journal of Soil Dynamics and Earthquake Engineering,* Volume 92, pp. 126-152.

Arany, L., Bhattacharya, S., Macdonald, J. H. & Hogan, S. J., 2016. Closed form solution of Eigen frequency of monopile supported offshore wind turbines in deeper waters incorporating stiffness of substructure and SSI. *Soil Dynamics and Earthquake Engineering,* Volume 83, pp. 18-32.

Atkinson G.M. , D. Wald, C.B. Worden, V. Quitoriano, 2018. The Intensity Signature of Induced Seismicity. *Bulletin of the Seismological Society of America*, 108(3a), pp. pp. 1080-1086.

Baldi, G. et al., 1986. Interpretation of CPTs and CPTUs; 2nd part: drained penetration of sands. *Proc. 4th Int. Geotech. Seminar*, pp. 143-156.

Bellotti, R., Ghionna, V., Jamiolkowski, M. & Robertson, P., 1989. Design parameters of cohesionless soils from in situ tests. *Transportation Research Record.*

Bhattacharya, S., 2019. *Design of foundations for offshore wind turbines.* s.l.:Wiley.

Bhattacharya, S., 2019. *Design of foundations for offshore wind turbines.* s.l.:Wiley.

Bhattacharya, S., Nikitas, G., Arany, L. & Nikitas, N., 2017. Soil-Structure Interactions (SSI) for Offshore Wind Turbines. *IET Engineering and Technology Reference,* p. 23.

BSH, 2015. Standard Design: Minimum requirements concerning the constructive design of offshore structures within the Exclusive Economic Zone (EEZ). *Federal Maritime and Hydrographic Agency (BSH).*

Byrne, B. W. & Houlsby, G. T., 2006. Novel foundations for offshore wind farms. *World Maritime Technology Conference.*

Casagrande, A., 1971. On Liquefaction Phenomena. *Géotechnique*, p. 21(3):197–202.

Castro, G., 1975. Liquefaction and Cyclic Mobility of Saturated Sands. *Journal of the Geotechnical Engineering Division*, p. 101(6):551–569.

Cheng, H., Shuku, T., Thoeni, K. & Yamamoto, H., 2017. Calibration of micromechanical parameters for DEM simulations by using the particle filter. *EPJ Web of Conferences 140:12011.*

Cuéllar, P., Georgi, S., Baeßler, M. & Rücker, W., 2012. On the quasi-static granular convective flow and sand densification around pile foundations under cyclic lateral loading. *Granular Matter,* Volume 141, pp. 11-25.

Cui , L. & Bhattacharya, S., 2016. *Soil–monopile interactions for offshore wind turbines.* s.l., s.n., pp. 171-182.

Cundall, P. & Strack, O., 1979. A discrete numerical model for granular assemblies. *Géotechnique 29(1),* pp. 47-65.

De Risi, R., Bhattacharya, S. & Goda, K., 2018. Seismic performance assessment of monopile-supported offshore wind turbines using unscaled natural earthquake records. *Soil Dynamics and Earthquake Engineering,* Volume 109, pp. 154-172.

DNV-GL, 2017. DNVGL-RP-C212 - Offshore soil mechanics and geotechnical engineering.

DNV-GL, 2017. DNVGL-RP-C212: Offshore soil mechanics and geotechnical engineering.

Ed. Züblin AG, 2013. Final Report of the Research Project ”Beschreibung des Bodenverhaltens bei zyklisch belasteten Flachgründungen für Offshore-Windenergieanlagen durch Versuche im Originalmaßstab (FKZ 0325175). *Technische Informationsbibliothek Hannover*.

Ed. Züblin AG, 2013. Final Report of the Research Project ”Beschreibung des Bodenverhaltens bei zyklisch belasteten Flachgründungen für Offshore-Windenergieanlagen durch Versuche im Originalmaßstab (FKZ 0325175). *Technische Informationsbibliothek Hannover*.

García-Rojo, R. & Herrmann, H., 2005. Shakedown of unbound granular material. *Granular Matter 7(2-3),* pp. 109-118.

Glasenapp, R., 2016, http://dx.doi.org/10.14279/depositonce-5402 (in German). *Das Verhalten von Sand unter zyklischer irregulärer Belastung.* s.l.:PhD Thesis, Technische Universität Berlin.

Glasenapp, R., 2016. Das Verhalten von Sand unter zyklischer irregulärer Belastung. *Ph.D thesis, Technical University of Berlin.*

Guo, N., 2014. *Multiscale characterization of the shear behavior of granular media.* Hong Kong: The Hong Kong University of Science and Technology.

Hadda, N. & Wan, R., 2020. Micromechanical analysis of cyclic and asymptotic behaviors of a granular backfill. *Acta Geotechica,* Volume 15, p. 715–734.

Han, R. et al., 2019. Study of Dynamic Response Characteristics of the Wind Turbine Based on Measured Power Spectrum in the Eyewall Region of Typhoons. *Appl. Sci.,* 9(12).

Hettler, A., 1981 . Verschiebungen starrer und elastischer Gründungskörper in Sand bei monotoner und zyklischer Belastung. *Institut für Bodenmechanik und Felsmechanik der Universität Fridericiana,* p. 127.

Hight, D. W., Gens, A. & Symes, M. J., 1983. The development of a new hollow cylinder apparatus for investigating the effects of principal stress rotation in soils. *Géotechnique,* 33(4), pp. 355-383.

Hu , M., O'Sullivan, C., Jardine, R. & Jiang, M., 2010. Stress-induced anisotropy in sand under cyclic loading. *Granular Matter 12(5),* pp. 469-476.

Ibsen, L. B. & Lade, P. V., 1998. The Strength and Deformation Characteristics of Sand Beneath Vertical Breakwaters Subjected to Wave Loading. *Geotechnical Engineering Group. AAU Geotechnical Engineering Papers: Soil Mechanics Paper,* R 9805(23).

IREA, 2019. Renewable Power Generation Costs in 2018. *International Renewable Energy Agency.*

Ishihara, K. & Okada, S., 1978. Effects of stress history on cyclic behaviour of sand. *Soils and Foundations,* 18(4), pp. 31-45.

Jamiolkowski, M., Ghionna, V., Lancellotta, R. & Pasqualini, E., 1988. New correlations of penetration tests for design practice. *International Journal Of Rock Mechanics And Mining Sciences & Geomechanics.*

Jiang, M., Zhang , A. & Li, T., 2019. Distinct element analysis of the microstructure evolution in granular soils under cyclic loading.. *Granular Matter (2019), 21: 39, https://doi.org/10.1007/s10035-019-0892-8.*

Jostad, H. et al., 2014. A FE Procedure for Foundation Design of Offshore Structures – Applied to Study a Potential OWT Monopile Foundation in the Korean Western Sea. *Geotechnical Engineering Journal of the SEAGS & AGSSEA*, p. 45(4).

Jostad, H. et al., 2014. FE Procedure for Foundation Design of Offshore Structures – Applied to Study a Potential OWT Monopile Foundation in the Korean Western Sea. *Geotechnical Engineering Journal of the SEAGS & AGSSEA ,* 45(4).

Jostad, H. P. et al., 2014. FE Procedure for Foundation Design of Offshore Structures – Applied to Study a Potential OWT Monopile Foundation in the Korean Western Sea. *Geotechnical Engineering Journal of the SEAGS & AGSSEA,* p. 45(4).

Kammerer, A. M. et al., 2001. *Use of Cyclic Simple Shear Testing in Evaluation of the Deformation Potential of Liquefiable Soils.* s.l., s.n., p. 16.

Kaynia, A. M., 2019. Seismic considerations in design of offshore wind turbines. *Soil Dynamics and Earthquake Engineering,* Volume 124, pp. 399-407.

Klinkvort, R. & Hededal, O., 2013. Lateral response of monopile supporting an offshore wind turbine. *Proceedings of the ICE-Geotechnical Engineering ,* Volume 1662, pp. 147-158.

Kozicki, J., Tejchman, J. & Mühlhaus, H. B., 2014. Discrete simulations of a triaxial compression test for sand by DEM. *Numerical und Analytical Methods in Geotechnics,* 38(18), pp. 1923-1952.

LeBlanc, C., Houlsby, G. & Byrne, B., 2009. Response of stiff piles in sand to long-term cyclic lateral loading. *Geotechnique,* Volume 602, pp. 79-90.

Le, V. H., 2015 (in German). *Zum Verhalten von Sand unter zyklischer Beanspruchung mit Polarisationswechsel im Einfachscherversuch, PhD Thesis, Volume 66 of Publication of Soil Mechanics and Geotechnical Division, Technische Universität Berlin.* s.l.:Shaker Aachen.

Lombardi, D., Bhattacharya, S., Hyodo, M. & Kaneko, T., 2014. Undrained behaviour of two silica sands and practical implications for modelling SSI in liquefiable soils. *Soil Dynamics and Earthquake Engineering*, pp. 293-304.

Lunne, T., Robertson, P. & Powell, J., 1997. Cone Penetration Testing in Geotechnical Practice. *CRC Press, London.*

Martin, G., Finn, W. & Seed, H., 1975. Foundamentals of liquefaction under cyclic loading. *Journal of the Geotechnical engineering division*, pp. 101(5):423-438.

Mayne, P. W. et al., 2009. State-of-the-art paper (SOA-1): geomaterial behavior and testing. *17th International Conference on Soil Mechanics and Geotechnical Engineering.*

Miner, M., 1945. Cumulative damage fatigue. *Transaction of the American Society of Mechanical Engineering,* Volume 67, pp. 159-164.

Modenese, C., Utili, S. & Houlsby, G., 2012. *A Numerical Investigation of Quasi-static Conditions for Granular Media.* s.l., s.n., pp. 187-195.

Morthorst, P. E. & Kitzing, L., 2016. Economics of building and operating offshore wind farms. *Offshore wind farms : Technologies, Design and Operation,* Volume 92, pp. 9-28.

Nadim, F., 2001. Marine Geotechnics. *International Conferences on Recent Advances in Geotechnical Earthquake Engineering andSoil Dynamics,* Volume 7.

Niemunis, A., Wichtmann, T. & Triantafyllidis, T., 2005. A high-cycle accumulation model for sand. *Computers and Geotechnics,* 32(4), pp. 245-263.

Niemunis, A., Wichtmann, T. & Triantafyllidis, T., 2005. A high-cycle accumulation model for sand. *Computers and Geotechnics,* 32(4), pp. 245-263.

Niemunis, A. W. T. a. T. T., 2005. A high cycle accumulation model for sand. *Computers and Geotechnics,* p. 245–263.

O'Sullivan, C., Cui, L. & O'Neil, S., 2008. Discrete element analysis of the response of granular materials during cyclic loading. *Soils and Foundations, 48(4),* pp. 511-530.

Palmgren, A., 1924. Life length of rollerbearing. *Zeitschrift des Vereins Deutscher Ingenieure,* 68(14), pp. 339-341.

Pecker A. & Pender MJ, 2000. *Earthquake Resistant Deisgn of Foundations: NEW Construction.* Melbourne, s.n., pp. 313-332.

Plassiard, J., Belheine, N. & Donze, F., 2007. Calibration procedure for spherical discrete elements using a local moment law. *University Grenoble.*

PLAXIS, 2017. Plaxis 3D Reference Manual. *Edited by Brinkgreve, R.B.J., Kumarswamy, S., Swolfs, W.M., and Foria F., .*

Porcino, D., Marcianò, V. & Ghionna, V. N., 2009. Influence of cyclic pre-shearing on undrained behaviour of carbonate sand in simple shear tests. *Geomechanics and Geoengineering ,* 4(2), pp. 151-161.

Quinteros, V. et al., 2018. Shallow depth characterisation and stress history assessment. of an over-consolidated sand in Cuxhaven, Germany. *Proceedings of the 4th International Symposium on Cone Penetration Testing (CPT'18).*

Radjai, F. & Dubois, F., 2011. *Discrete-element modeling of granular materials.* s.l.:Wiley-Iste, 425 p..

Randolph, M. & Gourvenec, S., 2011. *Offshore Geotechnical Engineering.* 1st Edition ed. s.l.:CRC Press.

Roux, J. & Combeb, G., 2010. *How granular materials deform in quasistatic conditions.* s.l., s.n.

Schanz, T. & Vermeer, P. A., 1996. Angles of friction and dilatancy of sand. *Géotechnique,* 46(1), pp. 145-151.

Schmertmann, J. H., 1978. Guidlines for cone penetration test, performance and design. *US Federal Highway Administration, Washington DC, Report FHWA-TS-78-209.*

Sedlacek, G., Miehe, A., Libreros, A. & Heider, Y., 2012. Geotechnical Stability of Gravity Base Foundations for Offshore Wind Turbines on Granular Soils. *ASME 2012 31st International Conference on Ocean, Offshore and Arctic Engineering*.

Sedlacek, G., Miehe, A., Libreros, A. & Heider, Y., 2012. Geotechnical Stability of Gravity Base Foundations for Offshore Wind Turbines on Granular Soils. *ASME 2012 31st International Conference on Ocean, Offshore and Arctic Engineering*.

Seed, H. B., Idriss, I. M., Makdisi, F. I. & Banerjee, N. G., 1975. Representation of irregular stress time histories by equivalent uniform stress

series in liquefaction analyses. *UCB Report. Earthquake Engineering Research Center,* Volume EERC 75-29.

Shajarati, A., Sørensen, K. W., Nielsen, S. K. & Ibsen, L. B., 2012. *Behaviour of Cohesionless Soils During Cyclic Loading,* s.l.: Aalborg: Department of Civil Engineering, Aalborg University. DCE Technical Memorandum, No. 14.

Skempton, A., 1954. *The Pore-Pressure Coefficients A and B.* s.l.:ICE Publishing. doi: 10.1680/geot.1954.4.4.143.

Šmilauer, V., 2015. *Yade Documentation.* s.l.:2nd ed. The Yade Project. doi: 10.5281/zenodo.34073.

Stevens, R. F. & Rahim, A., 2014. Mooring Anchors for Marine Renewable Energy Foundations. *Marine Energy Technology Symposium.*

Sze, H. Y. & Yang, J., 2014. Failure Modes of Sand in Undrained Cyclic Loading: Impact of Sample Preparation. *JOURNAL OF GEOTECHNICAL AND GEOENVIRONMENTAL ENGINEERING*, pp. 152-169.

Sørensen, J. D. & Toft, H. S., 2010. Probabilistic Design of Wind Turbines. *Energies,* pp. 241-257.

Vaid, Y. P., Chung, E. K. F. & Kuerbis, R. H., 1989. Pre-shearing and undrained response of sand. *Soils and Foundations,* 29(4), pp. 49-61.

Vanden Bergen, J., 2001. Sand Strength Degradation within the Framework of Vibratory Pile Driving. *PhD thesis, University Catholique de Louvain, Faculty of Applied Science Civil and Environmental Engineering Division.*

Velarde, J., Kramhøft, C. & Sørensen, J. D., 2019. Global sensitivity analysis of offshore wind turbine foundation fatigue loads. *Renewable Energy,* Volume 140, pp. 177-189.

Velarde, J., Kramhøft, C., Sørensen, J. D. & Zorzi, G., 2019. Fatigue reliability of large monopiles for offshore wind turbines. *Submitted to International Journal of Fatigue.*

Velarde, J., Sørensen, J. D., Kramhøft, C. & Zorzi, G., 2019. Fatigue reliability of large monopiles for offshore wind turbines. *Submitted to International Journal of Fatigue.*

Wichtmann, t., 2005. Explicit accumulation model for non-cohesive soils under cyclic loading. *Publications of the Institute of Soil Mechanics and Foundation Engineering, Ruhr-University Bochum,* Issue 38.

Wichtmann, T., 2016. Soil behaviour under cyclic loading - experimental observations, constitutive description and applications. In: *Habilitation thesis.* s.l.:s.n.

Wichtmann, T., Niemunis, A. & Triantafyllidis, T., 2010. Strain accumulation in sand due to drained cyclic loading: On the effect of monotonic and cyclic preloading (Miner's rule). *Soil Dynamics and Earthquake Engineering,* 30(8), pp. 736-745.

Widuliński, L., Kozicki, J. & Tejchman, J., 2009. Numerical Simulations of Triaxial Test with Sand Using DEM. *Archives of Hydro-Engineering and Environmental Mechanics 56, nr. 3-4,* pp. 149-172.

Yu, L.-Q.et al., 2015. Long-term dynamic behavior of monopile supported offshore wind turbines in sand. *Theoretical and Applied Mechanics Letters,* Volume 52, pp. 80-84.

Zachert, H. et al., 2014. Validation of a high cycle accumulation model via FE-simulations of a full-scale test on a gravity base foundation for offshore wind turbines. *International Wind Engineering Conference, IWEC 2014.*

Zachert, H. et al., 2014. Validation of a high cycle accumulation model via FE-simulations of a full-scale test on a gravity base foundation for offshore wind turbines. *International Wind Engineering Conference, IWEC.*

Zachert, H., Wichtmann, T. & Triantafyllidis, T., 2016. Soil Structure Interaction of Foundations for Offshore Wind Turbines. *International Society of Offshore and Polar Engineers ISOPE*.

Zhang, L. et al., 2016. The role of force chains in granular materials: from statics to dynamics. *European Journal of Environmental and Civil Engineering 21(7-8),* pp. 874-895.

Zorzi, G., Baeßler, M. & Gabrieli, F., 2017. *Influence of Structural Stiffness on Ratcheting Convection Cells of Granular Soil under Cyclic Lateral Loading.* s.l., s.n.

Zorzi, G., Kirsch, F., Gabrieli, F. & Rackwitz, F., 2017. *Long-term cyclic triaxial tests with DEM simulations.* s.l., s.n., p. 273–284.

Zorzi, G. et al., 2019. Reliability analysis of offshore wind turbine foundations under lateral cyclic loading. *Submitted to Wind Energ. Sci. Discuss.* .

Zorzi, G. et al., 2018. *Explicit Method to Account for Cyclic Degradation of Offshore Wind Turbine Foundations Using Cyclic Interaction Diagrams.* Sapporo, Japan, s.n.

Zorzi, G. et al., 2018. *Explicit Method to Account for Cyclic Degradation of Offshore Wind Turbine Foundations Using Cyclic Inter-action Diagrams.* Sapporo, Japan, s.n.

Zorzi, G. et al., 2018. Explicit Method to Account for Cyclic Degradation of Offshore Wind Turbine Foundations Using Cyclic Inter-action Diagrams. *International Society of Offshore and Polar Engineers,* pp. ISOPE-I-18-271.

Zorzi, G. et al., 2019. *Validation of explicit method to predict accumulation of strain during single and multistage cyclic loading.* s.l., s.n.

Zorzi, G., submitted, 2020. *Cyclic loading design of offshore wind turbine foundations.* Berlin: PhD Thesis, Technische Universität Berlin.

Appendices: Publications

Appendix A

Explicit method to account for cyclic degradation of offshore wind turbine foundation using cyclic interaction diagrams

This paper was presented at the Annual International Offshore and Polar Engineering Conference (ISOPE) held in Sapporo 2018 (http://legacy.isope.org/conferences/conferencesINT.htm).

This is the post-print of the accepted manuscript of the article published by the International Society of Offshore and Polar Engineers in ISOPE - International Society of Offshore and Polar Engineers (https://www.onepetro.org/conference-paper/ISOPE-I-18-271).

Original version: Zorzi, G., Richter, T., Kirsch, F., Augustesen, A. H., Østergaard, M. U., & Sørensen, S. P. H. (2018, July 30). Explicit Method to Account for Cyclic Degradation of Offshore Wind Turbine Foundations Using Cyclic Interaction Diagrams. International Society of Offshore and Polar Engineers. ISBN: 978-1-880653-87-6 Copyright: 2018. International Society of Offshore and Polar Engineers.

Explicit Method to Account for Cyclic Degradation of Offshore Wind Turbine Foundations Using Cyclic Interaction Diagrams

Gianluca Zorzi[1], Thomas Richter[1], Fabian Kirsch[1],

Anders Hust Augustesen[2], Martin Underlin Østergaard [2], Søren Peder Hyldal Sørensen [2]

[1] GuD Geotechnik und Dynamik Consult GmbH, Berlin, Germany

[2] COWI A/S, Aalborg, Denmark

ABSTRACT

Cyclic loading could lead to progressive degradation of soil in terms of plastic strain accumulation, pore pressure build up and changes in soil strength and stiffness. The present paper outlines an explicit method to predict the accumulated foundation displacement under cyclic loading. Cyclic contour diagrams, derived from cyclic laboratory tests, are linked to the finite element software PLAXIS by means of a Python interface. The effects of cyclic loading on the accumulation of strain is taken into account by the modification of the elastic shear modulus of the soil in a cluster-wise division in the finite element mesh.

Key words: PLAXIS; cyclic loading; cyclic contour diagrams; explicit method; stiffness degradation; gravity based foundation; monopiles.

INTRODUCTION

The design of wind turbines relies on knowledge of different engineering disciplines with multiple interfaces. For the design of the foundation structure, iterative loops between the wind turbine manufacturer and the foundation designer (incl. the geotechnical design team) are needed to update the load calculations at the interface level (bottom of tower). Wind turbine manufacturers provide the irregular variation of fatigue and extreme loads by means of aeroelastic and hydrodynamic analyses, which in turn provide the basis for the foundation design.

In each loop the geotechnical designers have to ensure that the foundation obeys a series of criteria such as foundation capacity, when experiencing the

maximum load (ULS), and the prediction of the foundation response during the lifetime of the structure (SLS). The analysis of the foundation capacity can be done by applying simplified approaches such as a Winkler model approach using p-y curves or by use of finite element modeling, cf. DNV GL AS (2016). The prediction of the foundation response over the lifetime of the structure remains challenging.

During a lifetime of 25 years, offshore structures undergo millions of irregular loading cycles distributed randomly over time and direction (Andersen et al. 2013). These cyclic loads are likely to cause relevant changes in the behavior of the soil-structure interaction with time. In this regard, different requirements should be addressed, such as: ensuring bearing capacity following cyclic loading, which may differ from the capacity under monotonic loading; assuring that the cyclic displacement of the structure obeys the requirements provided by the wind turbines manufacturer; assessing the change in the foundation stiffness and damping; and ensuring stability against the pore pressure build up during a cyclic storm event.

During the geotechnical design process, a simplification of the irregular loading from the wind turbine manufacturer is needed. Soil models cannot implicitly predict the soil behavior under irregular cyclic loading with sufficient accuracy. Therefore, the explicit representation of the response of cyclically loaded soil is based on laboratory test campaigns, for which sequences of irregular cycles are not suitable.

The irregular load history for a design storm event condition is divided into a number of constant cyclic load amplitudes around a constant average load. In this case, a counting method, e.g. Rainflow-Counting, is used to reduce this irregular load-time histories to a number of load spectra. The result is a description of the function in terms of the number of the load cycles inherent in the time history. Each load package consists of an average value, a load amplitude and a number of cycles. The load collective is then converted into the form of a so-called Markov matrix. For monopiles, the Markov matrices of the relevant storm at the level of the seabed can be reduced to an equivalent load collective and an equivalent number of cycles as described in EA-Pfähle (2012).

The lack of a generally accepted unified method to account for cyclic loading has led to the development of different approaches. Some of them are focused on specific types of structures. For monopiles it is current practice to use the "softened" static p-y curves. Alternatively, the permanent pile head rotation can be estimated according to the Hettler approach, cf. EA-Pfähle (2012). Others methods are developed aiming to predict the strain accumulation (Achmus et al, 2009) or pore pressure build up. Several more advanced methods, such as PDCAM and UDCAM (Jostad et al, 2014) or the High Cycle Accumulation method (Niemunis et al, 2005), which can be applied for different types of offshore foundation have been developed for similar purposes.

The paper aims to contribute to diminishing the existing lack of an accepted generic method, which addresses the foundation design when cyclic loading conditions are considered. Hereafter, a methodology is defined to evaluate the tilt of a foundation under cyclic loading. The developed method is an extension of the one presented in Kirsch et al. (2016). The effects of cyclic degradation are taken into account by the modification of a fictional elastic shear modulus of the soil in a cluster-wise division in the finite element domain. The modification of the soil modulus is based on the cyclic interaction diagrams framework, cf. Andersen (2015). This is achieved through the use of a Python interface, which allows for a fast communication between the finite element model and the cyclic contour diagram. The concept of the cyclic contour diagrams is to provide a way of establishing a generalized relation between shear stresses (average and cyclic), shear strains (average and cyclic), excess pore water pressures and number of cycles. Fig. 1 shows an example of a 3D cyclic contour diagram for cyclic and average shear strain variation based on cyclic and average shear stresses and number of cycles (cf. Andersen, 2015).

They can be established based on laboratory test campaigns and they have been applied successfully for decades for the design of different offshore foundations, however careful engineering judgment shall be used for the construction and interpretation. A suitable laboratory testing strategy to develop the cyclic contour diagrams is explained in Andersen (2015). For determination of cyclic contour diagrams it will, according to Andersen (2015), require minimum five tests to validate if the soil behaves similar to typical cyclic contour diagrams. In

case the tests do not match literature published diagrams further laboratory testing would be required. Published cyclic contour diagrams for similar soil and test conditions could help to improve the testing strategy.

As it is the case for the cyclic contour diagrams, the proposed methodology is flexible, and it can be used for different types of foundations, such as monopiles or gravity based foundations.

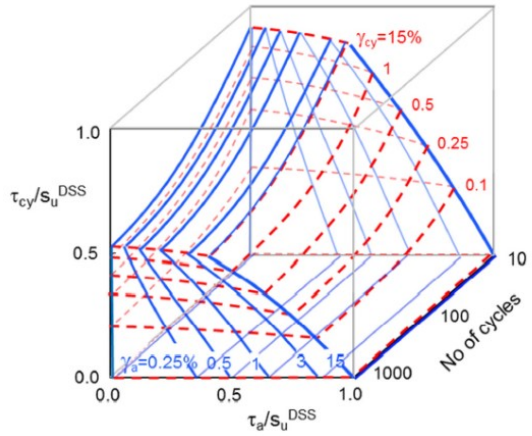

Fig. 1 3D example of cyclic contour diagram (cf. Andersen, 2015).

DEGRADATION CONCEPT OF THE EXPLICIT METHOD

A central part when dealing with cyclic loading is to link degradation of stiffness and strength with the number of load cycles, stress level, strain and pore water pressure build up. In this paper, focus is paid to the accumulation of strains with respect to load level, number of cycles and the strains in the soil.

The stiffness can be defined in different ways as shown in the idealized cyclic test sketched in Fig. 2. G_{ini} is the secant shear modulus of the monotonic part of the stress-strain curve, if the average shear stress is different from zero, i.e. the inclination of a line through origo and the shear stress τ_a and shear strain γ_{ini} at which the first cycle is commenced. If the average shear stress equals zero then G_{ini} is the tangent stiffness for the first quarter of a cycle. G_N is the shear modulus corresponding to the average shear strain for cycle number N, i.e. the inclination of a line through origo and the average shear stress τ_a and shear strain

($\gamma_{ini}+\gamma_n$) for cycle N. Last, the secant stiffness of cycle N is defined as the inclination of a line through the stress extrema for cycle number N. In this study, G_{ini} and G_N are important in the evaluation of the stiffness changes since the effects of cyclic loading is not evaluated cycle-by-cycle but merely by a "global approach". Hence, the modification of the shear modulus is done in an explicit way based on the number of cycles, load average and load amplitude for a given irregular load history.

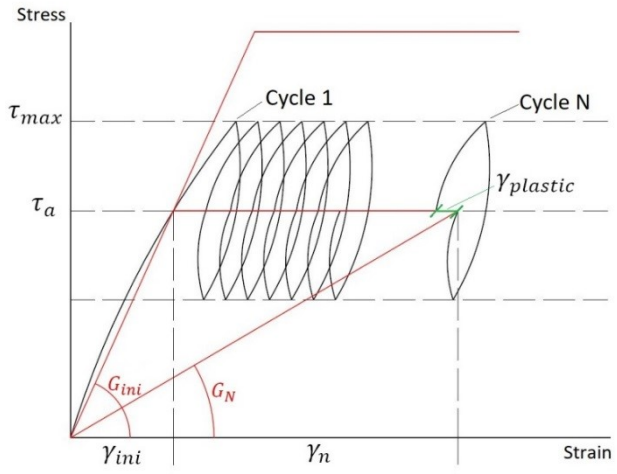

Fig. 2 Stiffness degradation concept.

G_{ini} is assumed related to elastic deformations. This is not entirely correct for high average shear stresses, but it is a conservative assumption, since it leads to higher degradation of the shear modulus. The average shear strain γ_n developed during the cyclic loading consists of contributions from both elastic and plastic deformations. The changes in stiffness for a cyclic event is thus related to the difference between G_{ini} and G_N. With reference to Fig. 2 the stiffness at the end of cycle N will thus be:

$$G_N = G_{ini} \frac{1}{1+\frac{\gamma_n}{\gamma_{ini}}} \quad (1)$$

γ_{ini} is the average shear strain at the average shear stress before cyclic loading, while γ_n is the average shear strain developed during the cyclic loading (from cycle 1 to cycle N). This relation is based on triangle similitude at the average

component level. Other definitions of the shear strains can be assumed with a corresponding modification to the calculation procedure. The chosen type of shear strain shall be consistent with an appropriate cyclic interaction diagram.

The above change in shear modulus and hence accumulated deformations during cyclic loading is handled in the finite element code with the help of the Python interface and the procedure described in the following section. In the finite element model, the soil domain is divided into clusters, i.e. volumes of soil. A unique material is assigned to each cluster, and this allows for the modification of the material parameters in different soil volumes based on the development of the local stress conditions. The average shear strains γ_{ini} are calculated from the finite element program, and the development of the shear strains, γ_n are directly extracted from the cyclic contour diagrams.

The present explicit method can potentially be extended to include other design verifications. In order to also consider the pore pressure build-up, different procedures will be analyzed in the future. The first is a linear variation between pore pressure and bulk modulus. The second is to insert the pore pressure from the cyclic contour diagram directly in the soil cluster. This analysis may be relevant for certain type of soil conditions in which the change in pore water pressure may lead to soil liquefaction and a subsequent loss of bearing capacity.

CALCULATION PROCEDURE: DRAINED ANALYSIS

Two distinct methods are proposed for the calculation of the foundation displacement when exposed to cyclic loading. These two methods (denoted Method 1 and Method 2) are sketched in Fig. 3 and Fig 4.

Method 1 consists of the following phases:

- Phase 0.1: Initial K0-phase.
- Phase 0.2: Installation of foundation (including self-weight of all structures).
- Phase 1: Application of load parcel 1

    - Phase 1.1: Average loads from load parcel 1 are applied. For all clusters the undegraded shear modulus is applied.
    - Phase 1.2: Maximum loads from load parcel one are applied. For all clusters, the undegraded shear modulus is applied. Phase initiates from Phase 1.1.
    - Phase 1.3: The shear modulus is degraded (Eq. 1) utilizing the cyclic contour diagrams based on the soil stresses calculated for phase 1.1 and 1.2 and the number of load cycles within load parcel 1. Average loads from load parcel 1 are applied. Phase initiates from phase 0.2.
- Phase k: Application of load parcel k
    - Phase k.1: Average loads from load parcel k are applied. For all clusters, a shear modulus representative for post-cyclic behavior is applied. Phase initiates from phase (k-1).3.
    - Phase k.2: Maximum loads from load parcel k are applied. For all clusters, a shear modulus representative for post-cyclic behavior is applied. Phase initiates from Phase k.1.
    - Phase k.3: The shear modulus is degraded (Eq. 1) utilizing the cyclic contour diagrams based on the soil stresses in phase k.1 and k.2 and the number of load cycles within load parcel k. Average loads from load parcel k are applied. Phase initiates from phase (k-1).2.

For Method 1, a post-cyclic shear modulus is required for phases k.1 and k.2. This shear modulus can be obtained from post-cyclic load phases from laboratory testing. As an alternative, the post-cyclic shear modulus can be set equal to either the undegraded or the degraded shear modulus. For most cases, the post-cyclic shear modulus will likely be in between these values. Hereafter, the term "Method 1.a" (Fig. 3.a) indicates that the post-cyclic shear modulus is equal to

the degraded shear modulus, while the term "Method 1.b" (Fig. 3.b) indicates that the post-cyclic shear modulus is equal to the initial undegraded shear modulus.

Method 2 consists of the following phases:

- Phase 0.1, Phase 0.2 and Phase 1 are the same as in Method 1.
- Phase k: Application of load parcel k
    - Phase k.1: Average loads from load parcel k are applied. For all clusters, the undegraded shear modulus is applied. Phase initiates from phase 0.2.
    - Phase k.2: Maximum loads from load parcel k are applied. For all clusters, the undegraded shear modulus is applied. Phase initiates from Phase k.1.
    - Phase k.3: The shear modulus is degraded (Eq. 1) (1) utilizing the cyclic contour diagrams based on the soil stresses in phase k.1 and k.2 and the number of load cycles within load parcel k added with the equivalent no. of load cycles, N_{eq}, k corresponding to the previous load parcels. Average loads from load parcel k are applied.

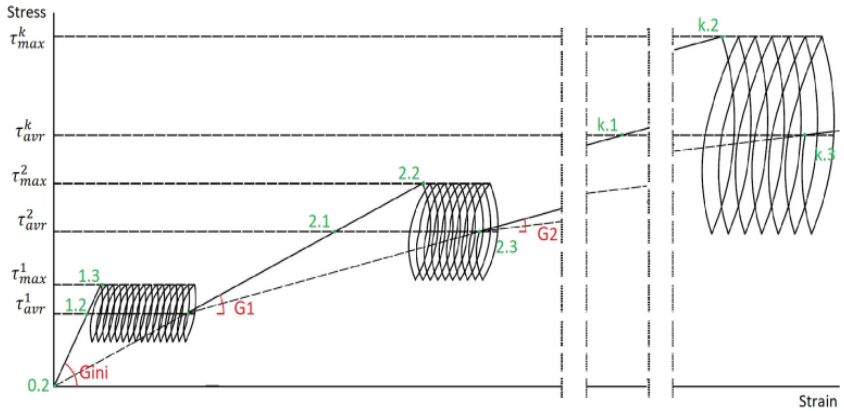

(a)

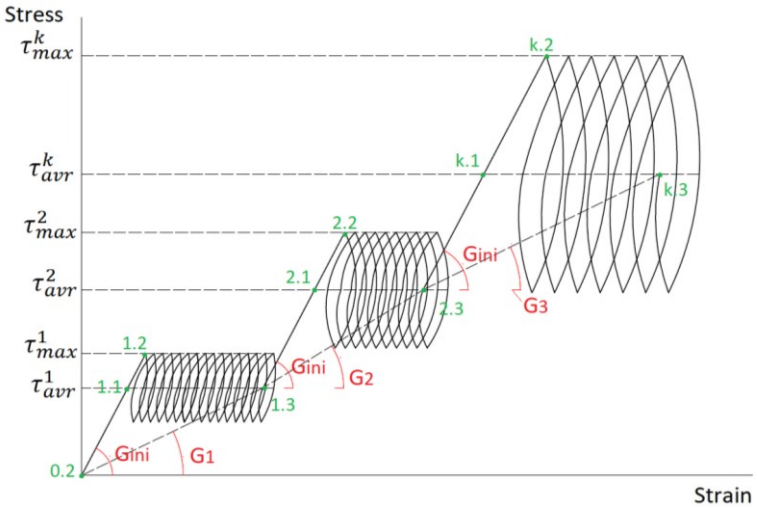

(b)

Fig. 3 Method 1: Drained analysis. (a) Method 1.a; (b) Method 1.b.

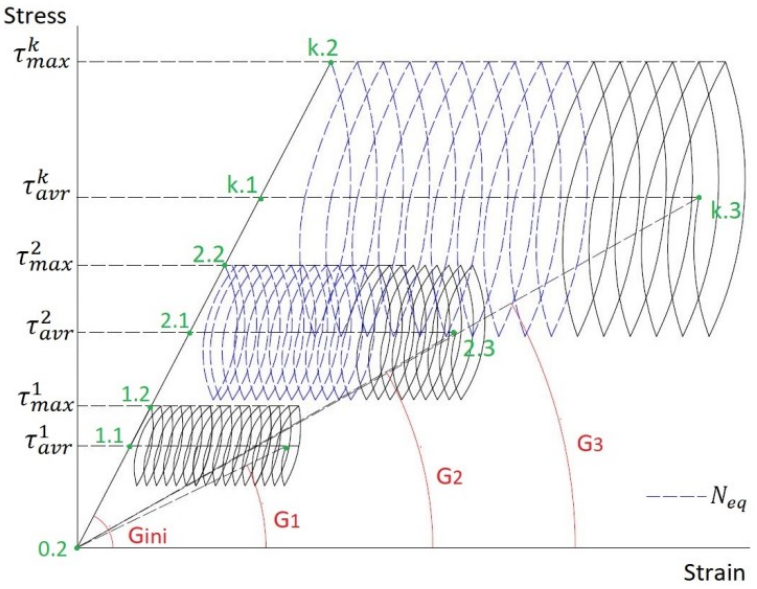

Fig. 4 Method 2: Drained analysis.

For both Method 1 and Method 2, the degraded shear moduli are calculated from Eq. 1 which is based on the soil stresses (in each cluster) from phases k.1 and k.2 and the number of load cycles for the given load parcel. Within each cluster, the average principle soil stresses are calculated and based on these, the maximum shear stress is calculated. The permanent strain due to cyclic loading

is then extrapolated based on the shear stresses from phase k.1 (average shear stress) and k.2 (cyclic shear stress) and the number of load cycles by means of the cyclic contour diagram. The initial average strain γ_{ini} for each cluster is the maximum shear strain obtained from the principal strain transformation from phase k.1. Note that the cyclic shear stresses are based on the stress differences between phase k.2 and phase k.1, while the average shear strains are based on the strain difference between phase k.1 and phase (k-1).3 for Method 1 and between phase k.1 and phase 0.2 for Method 2.

For Method 2, the number of equivalent load cycles is required. This value is extracted independently from the cyclic contour diagram for each soil cluster, and the equivalent number of load cycles for load parcel k shall be determined such that the permanent strains for $N_{eq,k}$ load cycles of load parcel k equals the permanent strains from all the previous load parcels.

One of the advantages of Method 1 is that the stresses applied to determine the permanent shear strains from load parcel 2 to the last load parcel are dependent on the previous load cycles. That is not the case for Method 2. The major disadvantages of Method 1 is that the way the cyclic loads are divided into load parcels will affect the end result. For instance, modelling 100 identical load cycles as 100 load parcels each with one cycle will provide a different result than modelling the 100 load cycles in one parcel. Using Method 2 would result in the same end result for the two scenarios.

AUTOMATIC DESIGN CALCUTATION

An automating design procedure for the prediction of the effects of cyclic loading is a key factor for foundation design in offshore wind due to the tight time constraints of projects, as it can drastically reduce the workload that would be required. Moreover, sensitivity studies on the reliability of the foundation structure can be done faster, which helps optimize the design for site-specific soil conditions.

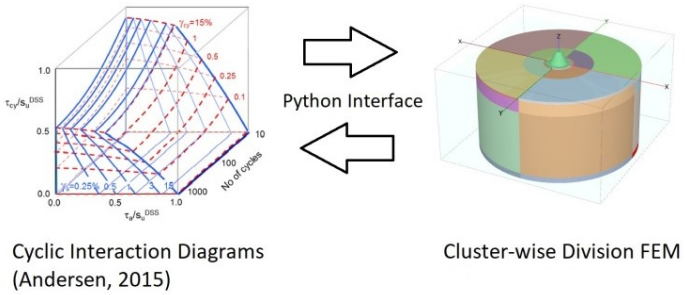

Fig. 5 Explicit method communication

The presented framework requires an extensive communication between the finite element program and the cyclic contour diagrams (Fig. 5). The present method has been implemented in the commercial finite element code PLAXIS 3D, which allows for the creation of an automated model by means of a remote scripting interface based on Python language (PLAXIS, 2017). In this way, the automated model can create the soil, cluster division and structure domain, as well as store, control and process the output data from the different simulations phases and change the input for the next calculation step.

The cyclic contour diagrams are created and stored in Python as 3D matrices in which the data volume is the plastic strain accumulation, and the three indices are the cyclic stress ratio, the average stress ratio and the number of cycles.

The Python code for the presented explicit method can be written for different types of foundations, e.g. gravity based foundations and monopiles. Generally, the automatic explicit method can be used for different projects and foundations by modifying the relevant input parameters such as the foundation dimension, site-specific soil conditions and the loading parcel values.

A specific function has been build and integrated in the Python code to automatize the creation of soil clusters. For each cluster, a soil material (which is specific for that cluster) is created to allow for modification of the stiffness parameters in dependency of the stress condition of the cluster. Given three input parameters (depth, radial and circular discretization) the Python interface divides the soil domain automatically according to the discretization parameters. For a gravity based foundation, an exponential division is considered along the depth

and on the circular division. In this way, smaller clusters are created near the foundation where a large stress variation is present and bigger clusters are created further from the foundation. This division is also efficient in terms of computational time. Fig. 6 shows two examples of cluster division for two typical offshore wind turbine foundations.

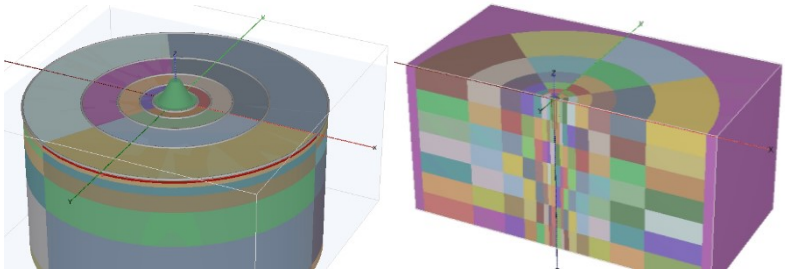

Fig. 6 Cluster division for gravity based foundation and monopile foundation.

APPLICATION EXAMPLE

An application example of the presented methods for a gravity based foundation (GBF) for a storm design condition is presented. The accumulated tilting of the GBF through the simulated storm event will be plotted to compare the practical implication of the assumption made for Method 1.a, Method 1.b and Method 2.

Numerical Model Set-Up

The dimensions of the GBF are depicted in Fig. 7. The concrete substructure consists of a base plate, a conical section and a cylindrical section. The mean water level (MSL) is assumed to be 30 meters. In PLAXIS, the GBF is modelled from foundation level to the lower ring beam. The GBF is founded on a uniform dense sand layer. The Mohr-Coulomb constitutive model is used and a set of typical soil parameters for North Sea dense sand are applied, cf. Table 1.

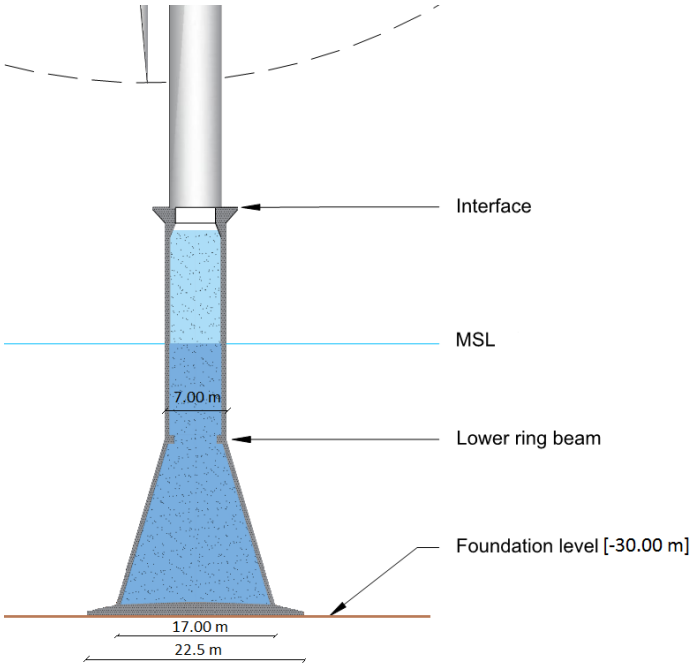

Fig. 7 Typical GBF dimensions.

Soil Parameters	Values
E [MN/m^2]	130
ν [-]	0.3
φ [°]	35
c' [kN/m^2]	0
γ_{Sat} [kN/m^3]	18
γ_{UnSat} [kN/m^3]	9

Table 1 Soil parameters.

In Table 2, load values at the mudline for a design storm event are given. The load series consist of three load parcels each with an average and maximum shear force and overturning moment and a number of load cycles. A constant vertical force of 15 MN is applied to account for the weight of the superstructure.

Load Parcel	H_{avr} [kN]	H_{max} [kN]	M_{avr} [kNm]	M_{max} [kNm]	Number of cycles
1	1000	5000	50000	200000	500
2	2000	7000	70000	270000	100
3	3000	11000	90000	340000	20

Table 2 Load values at the mudline.

The soil domain is divided into clusters as presented in Fig. 8. For a real application, a sensitivity analysis on the number of clusters must be carried out. However, for demonstrating the method, the applied cluster division is considered sufficiently fine.

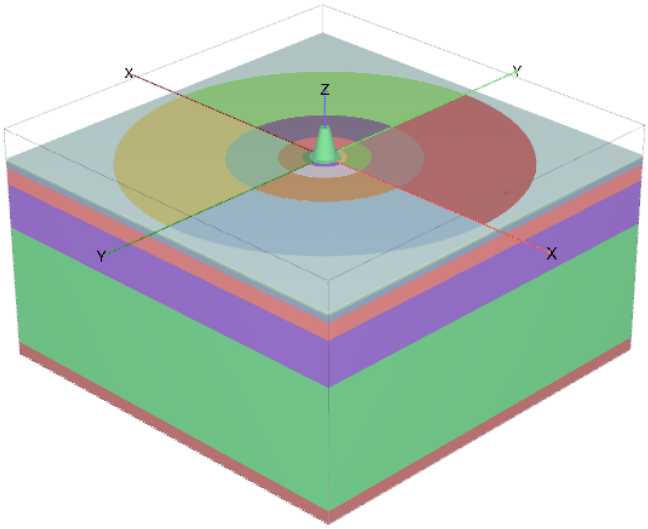

Fig. 8. Cluster division of the soil domain

The cyclic contour diagram in Fig. 9 has been digitalized from Andersen (2015). It represents the contour of cyclic shear strain as a function of number of cycles and cyclic shear ratio for the average shear stress equal to zero on normally consolidated sand and silt.

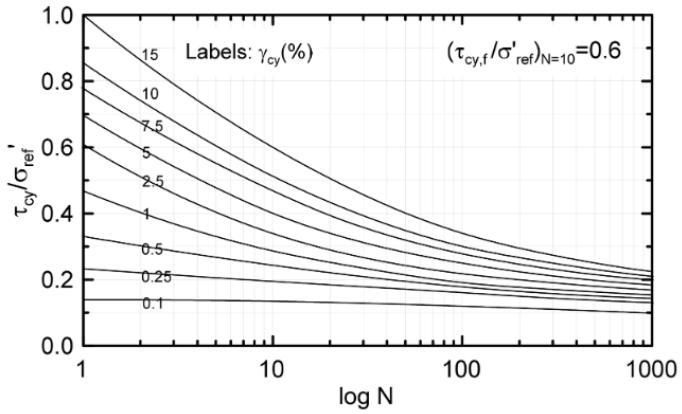

Fig. 9 Applied cyclic contour diagram for normally consolidated sand and silt, after Andersen (2015).

For this application example, the same diagram is considered for different average stress ratios and independently from the effective reference stress. For each cluster, the effective reference stresses in Fig. 9 are assumed equal to the vertical effective stresses calculated after the foundation installation (Phase 0.2).

Horizontal Displacement Accumulation

The horizontal displacements along the loading direction at the lower ring beam (Fig. 7) were extracted after the application of each loading parcel and normalized with the initial displacement from the first loading parcel. Note that this displacement is the same for all the three methods. Fig. 10 shows the relative accumulated horizontal displacement for the three methods at the end of each loading parcel. In Fig. 10, the grey dots represent the accumulation of displacement due to the application of the single load parcel from the initial conditions without considering any contribution from the other load parcels.

For all three methods, the accumulated horizontal displacement increases exponentially with the cyclic amplitude. Method 1.a gives the larger accumulation of displacement, which represents an upper bound method. This result is expected since the post-cyclic shear modulus is set equal to the degraded shear modulus, cf. Fig. 3.a, which is a very conservative assumption. The grey dots represent a lower bound. Therefore, the actual cyclic degradation curve should be enclosed between the upper and lower bound limits. Method 2 shows the lowest cyclic degradation through the simulated storm event. The advantage of this method is that for each parcel, an equivalent number of cycles is calculated

and added to the number of cycles of the new load parcel in order to account for the previous cyclic load parcels. In contrary, the accumulated strain for each parcel in Method 1.b is independent from the previous load parcels, which lead to an overestimation of the degradation.

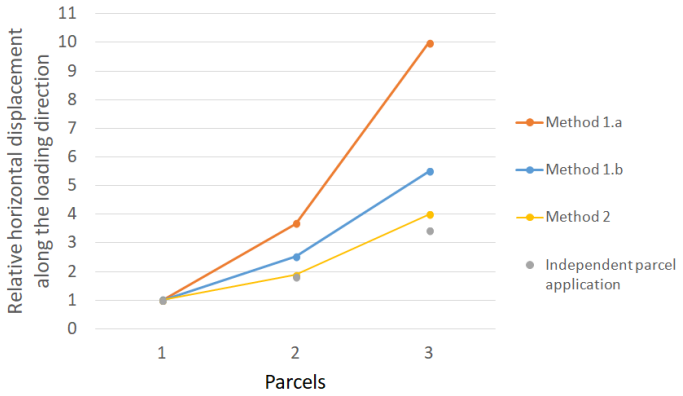

Fig. 10 Relative horizontal displacement along the loading direction

Soil Stiffness Variation

In order to account for the accumulation of the strain in the soil clusters, a fictive degradation of the secant shear stiffness has been used (Eq. 1). The following figure shows an example of the variation of the Young's modulus in each cluster of the soil domain at the end of load parcel 3 for Method 2 (Phase 3.3). Fig. 11 is a slice of the soil domain along the loading direction. A lower Young's modulus in a cluster means a larger accumulation of strains, i.e. a larger foundation settlement. Overall, a higher degradation is shown closer to the foundation, where there are larger shear stresses. Fig. 12 shows the total displacement contour of the GBF for the same phase as considered for Fig. 11.

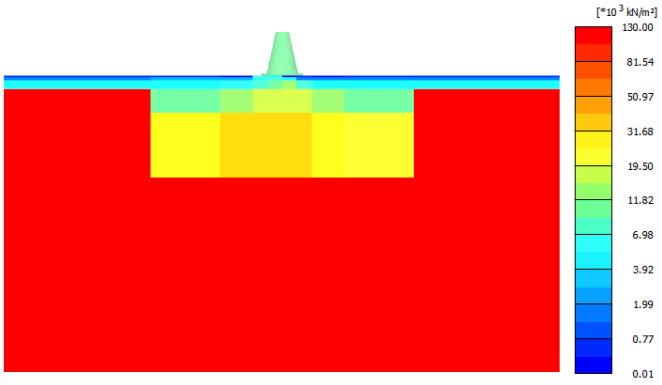

Fig. 11 Young's modulus degradation contour plot for each cluster at the end of load parcel 3 using Method 2.

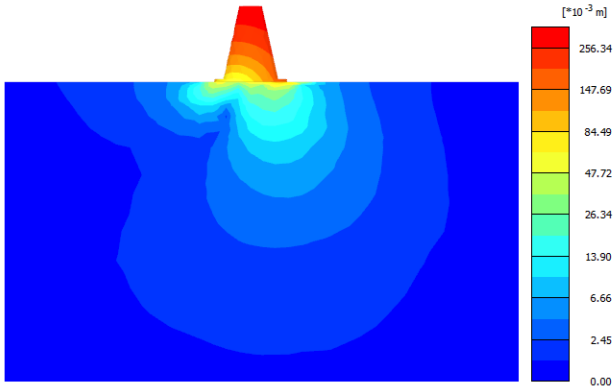

Fig. 12 Total displacement contour plot at the end of parcel 3 using Method 2.

CONCLUSIONS AND FUTURE DEVELOPMENT

This paper presents an explicit method to account for the accumulation of strain (foundation tilting) under cyclic loading. This framework will be extended in the future to account for changes in pore water pressure and soil damping. Moreover, the influence on the cluster dimension to the sensitivity of the present explicit method will be analyzed further.

The main advantage of this framework is that it is an automatized procedure taking into account the 3D behavior of the soil surrounding the foundation. The procedure cannot only be applied for gravity based foundation, but it is also suitable for monopile foundations and suction buckets.

ACKNOWLEDGEMENTS

This research is part of the Innovation and Networking for Fatigue and Reliability Analysis of Structures - Training for Assessment of Risk (INFRASTAR) project. This project has received funding from the European Union's Horizon 2020 research and innovation program under the Marie Skłodowska-Curie grant agreement No. 676139.

REFERENCES

Achmus, M., Abdel-Rahman K. , Kuo, Y.–S. (2009). "Behavior Of Monopile Foundations Under Cyclic Lateral Load", Computers And Geotechnics, 36(5), 725-735. Elsevier BV.

Andersen, K.H., Puech, A.A., and Jardine, R.J. (2013), "Cyclic resistant geotechnical design and parameter selection for offshore engineering and other applications", Proceedings of TC 209 Workshop - 18th ICSMGE, Paris 4 September 2013.

Andersen, K.H. (2015), "Cyclic soil parameters for offshore foundation design". The 3rd McClelland Lecture. Frontiers in Offshore Geotechnics III, ISFOG'2015, 1, 5-82.

DNV GL AS (2016). "Support structures for wind turbines", Offshore Standard DNVGL-ST-0126, Edition April 2016.

EA-Pfähle (2012). "Deutsche Gesellschaft für Geotechnik, Empfehlungen des Arbeitskreises 2.1", Pfähle2. Auflage 2012

Jostad, H.P., Grimstad, G., Andersen, K.H., Saue M., Shin, Y., and You D. (2014). "A FE Procedure for Foundation Design of Offshore Structures – Applied to Study a Potential OWT Monopile Foundation in the Korean Western Sea", Geotechnical Engineering Journal of the SEAGS & AGSSEA, 45(4).

Kirsch, F., Richter, T., Schädlich, B., Wiesener, S. (2016)."Ansatz zur Erfassung der Porenwasserdruckakkumulation bei Offshore-Monopilegründungen", Der Bauingenieur, 91(1), 26-33.

Niemunis A, Wichtmann T, Triantafyllidis T. (2005). "A high-cycle accumulation model for sand", Computers and Geotechnics, 32(4), 245-263.

PLAXIS (2017). "Plaxis 3D, Reference Manual", Edited by Brinkgreve, R.B.J., Kumarswamy, S., Swolfs, W.M., and Foria F.

Appendix B

Lifetime tilting prediction of offshore wind turbine foundations due to soil strain accumulation

This paper was presented at 14th European academy of wind energy (EAWE) PhD Seminar held at Vrije Universiteit Brussels 2018 (https://phd2018.eawe.eu/).

This is the post-print of the accepted manuscript of the article.

Original version: Zorzi, G., Kirsch, F., Richter, T., Østergaard, M. U., & Sørensen, S. H. (2018). Lifetime tilting prediction of offshore wind turbine foundations due to soil strain accumulation. 14th EAWE PhD Seminar on Wind Energy. Vrije Universiteit Brussel, Belgium.

The additional remarks in red to the original paper have been made for this thesis.

Lifetime tilting prediction of offshore wind turbine foundations due to soil strain accumulation

G Zorzi[a], F. Kirsch[a], T. Richter[a]

M.U. Østergaard[b], S.P.H. Sørensen[b]

[a] GuD Geotechnik und Dynamik Consult GmbH, Berlin, Germany
[b] COWI A/S, Aalborg, Denmark

E-mail: zorzi@gudconsult.de

ABSTRACT.

Cyclic loading can lead to progressive degradation of soil in terms of plastic strain accumulation, pore pressure build-up, and changes in soil strength, soil stiffness and stress redistribution, which may significantly influence the behaviour of offshore wind turbine foundation structures throughout their lifetime. The prediction of these effects is of vital importance for the design of offshore wind turbine foundations, yet there is a lack of a generally accepted method to account for cyclic loading conditions. The present paper introduces the application of an innovative explicit method to predict the accumulated foundation displacement under cyclic loading for different foundation types. The explicit method integrates cyclic contour diagrams derived from cyclic laboratory tests into the finite element software PLAXIS by means of a remote scripting interface. The effect of cyclic degradation is taken into account by reducing the elastic shear modulus of the soil in a cluster-wise division in the finite element mesh. The interface automates the model creation in terms of meshing, cluster division, load parcel application and soil parameter degradation, which is optimal as it minimizes the amount of manual work and the risk related hereto. Application examples of the method for different offshore wind turbine foundations (such as gravity based foundations, monopiles and suction buckets) under a design storm condition are presented. This paper demonstrates the advantages of the developed method in terms of automatized design while taking into account the 3D behaviour of soil surrounding the foundations.

Keywords: Offshore foundations, Cyclic loading, Accumulation of displacements, Numerical modelling.

INTRODUCTION

During the detailed design phase of offshore wind turbine (OWT) foundations, the structures have to be evaluated for fatigue to ensure that they will withstand the variable and cyclic environmental loads maintaining the operational and safety level throughout their intended design life (typically 25 years) [1]. The prediction of the fatigue life of the foundation embedded in the soil is generally not easily included. This needs to be based on an accurate modelling of the soil-structure interaction under cyclic loading conditions.

Occasionally, soil fatigue models [2] are used in geotechnical engineering projects. These types of models explicitly predict the behaviour of cyclic loaded soil by using empirical formulations based on the number of cycles and calibrated against constant stress amplitude tests. One of them is the Fatigue (or Cyclic) Contour Diagram Model [3]. The concept of the contour diagrams is to provide a relation for the chosen response of the material (fatigue variable) subjected to N number of cycles and certain stress conditions (mean and amplitude stress). This fatigue model is interpolated from laboratory test campaigns. Different "fatigue" variables (i.e. different sets of contour diagrams) can be derived such as average and cyclic pore pressure, average and cyclic shear strain, damping and stiffness. These diagrams can be used independently for predicting the soil-structure interaction under cyclic loading (i.e. earthquakes or storm events): accumulation of deformation (serviceability problems), liquefaction evaluation (stability problems), and change in damping and stiffness (useful for dynamic analysis).

One of the operational restrictions for wind turbine manufacturers is to ensure that the maximum tilting of the structure during its lifetime is less than e.g. 0.25°. In order to make use of the previous soil fatigue models, assumptions need to be made about the loading conditions. Offshore wind turbines experience more than 10^8 cycles during their lifetime. The nature of these cyclic loadings is random over time and regarding the direction. Therefore, it is common practice for wind turbine manufacturers to provide the irregular variation of

extreme loads of an *n*-year return period storm events, which is assumed to have the most significant impact on the foundation during its lifetime. The irregular load series of the selected storm event is then broken down to a series of ascending parcels with constant mean and amplitude loads and number of cycles.

The cyclic explicit method explained in [4,5] is considered in the present paper for different case studies. The methodology is defined to evaluate the tilting of a foundation due to the application of an ascending series of regular load packages. The fatigue variable used is the average shear strain. The effects of cyclic degradation in terms of plastic strain accumulation are considered by the modification of a fictional elastic shear modulus of the soil in a cluster-wise division in the finite element domain. The reduction of the soil modulus is based on the Fatigue (or Cyclic) Contour Diagram framework, which is embedded in the Finite Element domain. This is achieved through the use of a Python interface, which allows for a fast communication between the finite element model and the cyclic contour diagram (figure 1). The method is implemented in the commercial code PLAXIS 3D, which consent to develop automatic model by means of a remote scripting interface based on Python language [6].

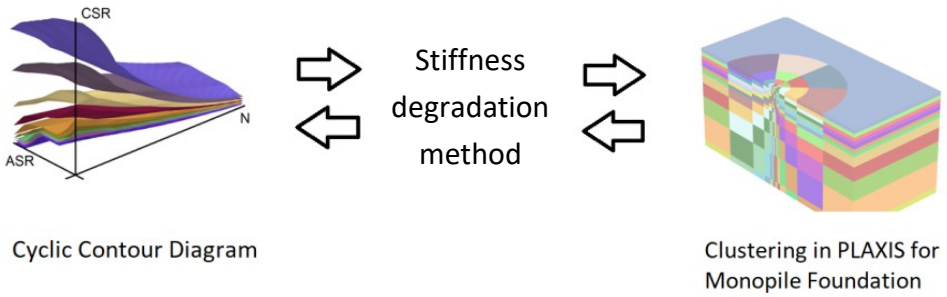

Figure 1 Framework of the method

The paper will briefly show the cyclic contour diagrams, typically for North Sea sand, which will be used for the case studies. Then the explanation of the methodology, from the load application to the reduction of the shear modulus, and the final application for different wind turbines foundations, will be presented.

FATIGUE CONTOUR DIAGRAM MODEL

In the present method a basic ingredient for the prediction of the behavior of the foundations under the design storm event is the development of fatigue contour diagrams representative of the soil condition, stress distribution and stress path under the considered foundation. In [3], an exhaustive explanation of the basic concepts is given.

The soil considered in the following case studies is typical for North Sea sand with a relative density of 90%. The contour diagrams have been extrapolated from stress-control two-way and one-way cyclic simple shear tests performed at the Soil Mechanics laboratories of the Technical University of Berlin. The tests were carried out undrained (constant volume) with different mean and amplitude stresses. The Average Stress Ratio (ASR), which is defined as the ratio between the average shear stress and the vertical effective stress in the tests, ranges from 0.00 to 0.26, while the Cyclic Stress Ratio (CSR), which is the ratio between the cyclic shear stress and vertical effective stress in the tests, ranges from 0.02 to 0.26. The present methodology is focused on the prediction of the strain accumulation. Therefore, the fatigue variable extracted from the tests was the average plastic shear strain γ_p at the end of each cycle. Figure 2 shows two contour plot slices (log(N)-CRS, where N is the number of cycles) of the 3D data at different ASR. The different surfaces represent the average plastic shear strain γ_p.

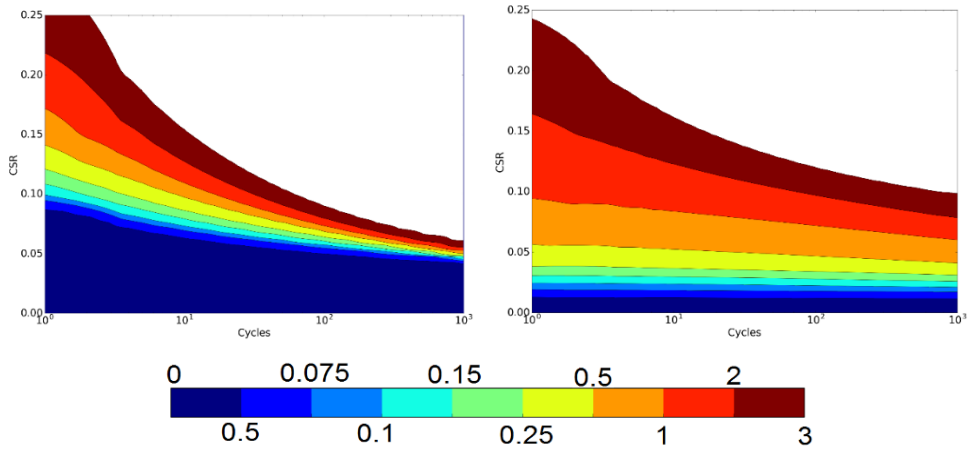

Figure 2 Cyclic contour diagrams of average plastic shear strain, γ_p, shown in percentage. Left figure – ASR equals 0.02. Right figure – ASR equals 0.20.

METHOD EXPLANATION:

Of the methods explained in [4], "*method 2*" is the preferable one in which the equivalent number of cycles is used to take into account the strain history between the parcels (damage accumulation). Figure 3 [4] shows the procedure in which three independent parcels are applied and in each parcel an equivalent number of cycles is used to take into account the previous accumulation of strain (dashed blue lines).

The present method requires an extensive exchange of information between the cyclic contour diagram framework and the Finite Element Method. Table 1 describes the steps taken in the python script. The [i] denotes input steps in PLAXIS Input, while [o] denotes the steps after the phase calculation in which PLAXIS Output is open in order to retrieve the stress and strain values from the stress points. The explicit method is presented thoroughly in [4].

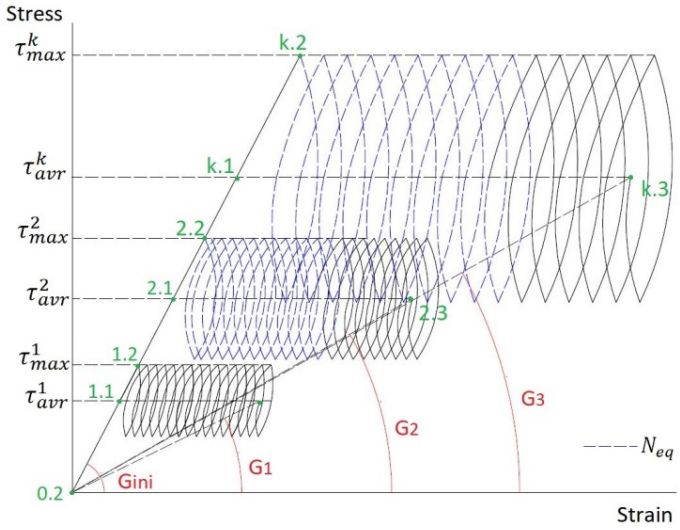

Figure 3. Accumulation procedure [4]

Table 1 Steps in the Finite Element Method

Phases	**Description**
0.1	[i] Cluster division of the soil domain a. A function has been developed in order to automatize the cluster division. [i] Assign a material set with the initial shear modulus G_{ini} to each cluster

	a. A very fine cluster division required the creation of a high amount of Material Set, hence increasing the computational time [i] K0 procedure
0.2	[i] Installation of the foundation (wished into place) [o] Extraction of cartesian strain and stress tensors for each Stress point Average of the stress tensors for each Cluster: $\boldsymbol{\epsilon}^{ini}, \boldsymbol{\sigma}^{ini}$
1.1	[i] Application of Average Loads [o] Extraction of cartesian strain and stress tensors for each Stress point Average of the stress tensors for each Cluster: $\boldsymbol{\epsilon}^{avr}, \boldsymbol{\sigma}^{avr}$ Calculation of the Average Stress Ratio ASR and the initial shear strain γ_{ini}
1.2	[i] Application of Maximum Loads [o] Extraction of cartesian stress tensors for each Stress point Average of the stress tensors for each Cluster: $\boldsymbol{\sigma}^{cly}$ Calculation of the Cyclic Stress Ratio CSR Extrapolation of $\gamma_n(ASR, CSR, \gamma_{ini}, N, N_{eq})$ from the 3D Cyclic contour diagram for each cluster Calculation of G_n for each cluster (Eq. 1)
1.3	[i] Assign new material properties G_n for each cluster Application of Average Loads

The present scripts based on few inputs (foundation dimension, cluster division and load conditions) can give a fast evaluation of the predicted tilting of the foundation for the considered design storm event. Moreover, the use the automatic design procedure allows to run more simulations in order to take into account the uncertainty on the cyclic contour diagram on the final tilting of the foundation.

CASE STUDIES

In order to illustrate the applicability of the presented explicit method, three different types of offshore wind turbine foundations are modelled. Hence, the applied loading, the soil profile and the foundation dimensions are fictious. A uniform soil profile of dense sand typical of the North Sea is employed in all analyses (chapter 2). The soil parameters for the Mohr-Coulomb constitutive

model are shown in Table 2. The 3D matrix of the cyclic contour diagrams is attached to the scripts. Table 3 shows load values at the mudline for a design storm event. To simplify, the same load series are applied for all the case studies. The load series consist of four load parcels each with an average and maximum horizontal force and overturning moment and a number of load cycles. Regarding the cluster division, a large stress variation is expected to occur in the vicinity of the foundations and therefore smaller clusters are used. The soil is then divided in larger clusters further away from the structure in order to reduce the computational time. A mean water level of 30 m is assumed in all the case studies.

Table 2 Load Parcels

Load Parcel	H_{avr} $[kN]$	H_{max} $[kN]$	M_{avr} $[kNm]$	M_{max} $[kNm]$	Number of Cycle
1	1000	1500	30000	50000	700
2	2000	3000	50000	85000	500
3	3000	5000	70000	115000	100
4	4000	7000	80000	150000	20

Table 3 Soil model parameters

Soil Parameters	Values
E [MN/m^2]	76
ν [-]	0.2
φ [°]	36
ψ [°]	0
γ_{sat}[kN/m^3]	18
γ_{Unsat}[kN/m^3]	9

Gravity Based Foundation (gbf)

The dimensions of the gravity based foundation and the cluster dimension of the soil domain are presented in figure 4. To each cluster a soil material is assigned, hence the clusters are represented with different colours (figure 4). The substructure consists of a base plate, a conical and a cylindrical section. A constant vertical force of 15 MN is applied to account for the weight of the superstructure. The interface element is used for the reduced shear strength at the GBF surface. The reference point for the load application is the mudline. The "fictious degradation phase", i.e. the reduction of the stiffness modulus, from

the last parcel is shown in figure 5. The figure is a slice of the soil domain along the loading direction and shows the variation of the Young's modulus in each cluster. The accumulation of deformations are extending up to 21 m below the foundation base.

Monopile

The pile dimension are shown in figure 6. The pile is modelled as a hollow rigid body cylinder and interface elements are used for the reduced shear strength at the pile surface. The monopile is modelled until 2 meters above the mudline. The reference point for the load application is the mudline. The clusters division has been chosen as in figure 7. Finer clusters are chosen close to the pile. A vertical load of 20 MN is applied to account for the entire load of the structure. Figure 7 shows the stiffness degradation of the Young's modulus for each clusters due to the application of the last parcel. The soil is accumulating deformations up to 55 meters below the mudline.

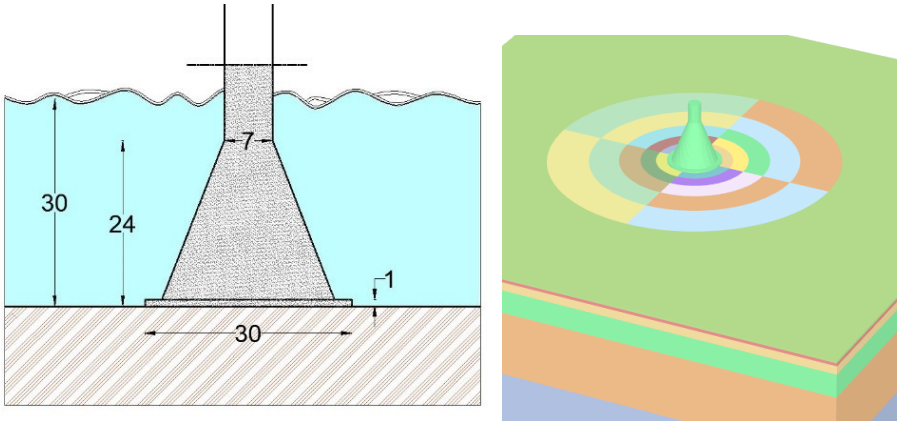

Figure 4 GBF dimension and cluster division of the soil domain

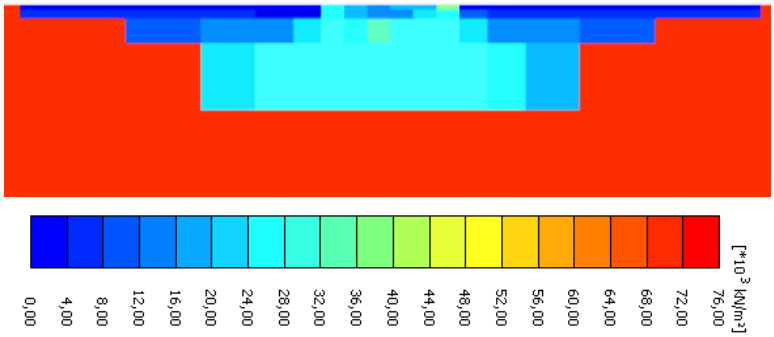

Figure 5 Young's modulus degradation at the last loading parcel over the clusters for the GBF

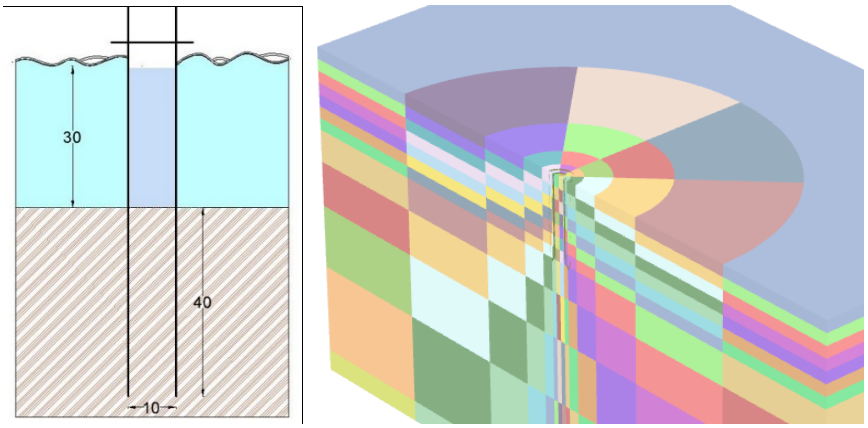

Figure 6 Monopile dimension and cluster division of the soil domain

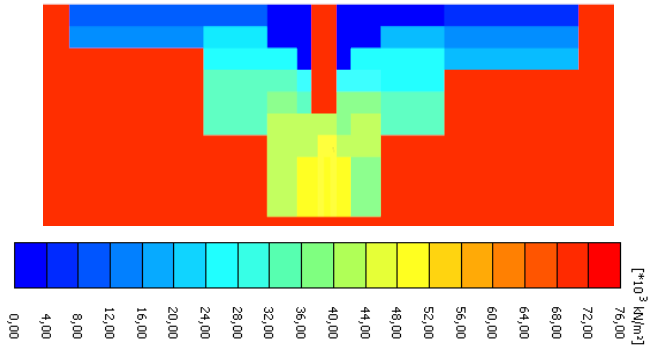

Figure 7 Young's modulus degradation at the last loading parcel over the clusters for the monopole

Suction bucket foundation

The dimension of the suction bucket is shown is figure 8. The bucket is modelled as a hollow rigid body cylinder with a rigid cap and interface elements are used to account for the reduced shear strength at the pile surface. The cluster division of the soil domain is chosen as in figure 8. Finer clusters are present close to the foundation. The soil deformation are developing until a depth of minus 40 m from the mudline (figure 9).

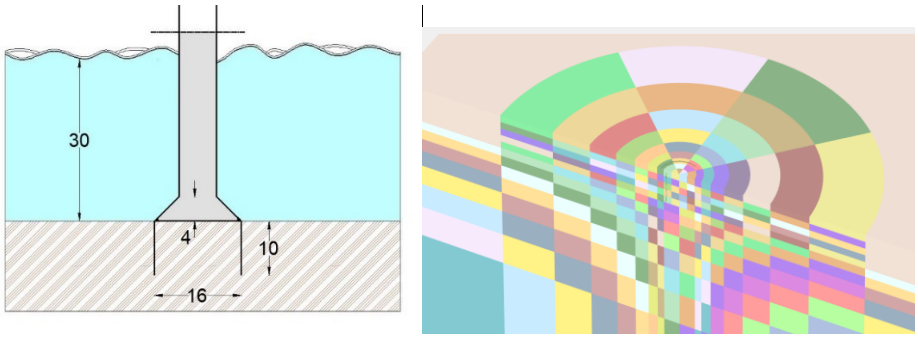

Figure 8 Suction bucket dimension and cluster division of the soil domain

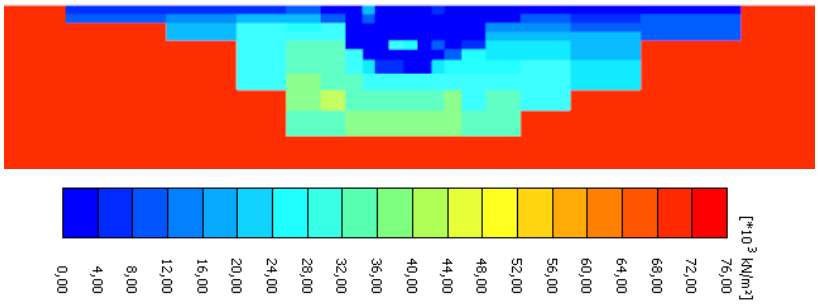

Figure 9 Young's modulus degradation at the last loading parcel over the clusters for the suction bucket

OUTPUT OF THE METHOD AND FUTURE DEVELOPMENT

The output of the presented analysis is the accumulated foundation tilting during the storm event. Figure 10 shows the comparison of the relative inclination along the loading direction of the three foundations subjected to the same design storm. For each foundation, the rotations are normalized with the initial rotation (parcel 1). The automatic modeling of the tilting makes it suitable for a design optimization of the foundation against the maximum allowed tilting.

The link between the cyclic contour diagrams and the stiffness degradation method seems promising. The python script developed for the above case studies can easily be adapted with different structural geometries and different soil layers by changing few inputs. Even though the calculation and creation of the model have been automatized with the python interface, some effort to create the cyclic contour diagrams is required.

Different improvements and method validations are under way:

1. Validation of the fictious stiffness phase against laboratory tests and validation against full scale tests.
2. The possibility of integrating a convergence criterion between the expected strain from the contour diagrams and the strain developed by the FEM model after the "fictious degradation phase".
3. The sensitivity of different cluster divisions of the soil domain to the final foundation tilting will be analysed
4. Effect of uncertainty of the cyclic contour diagram on the predictions of accumulated tilt.

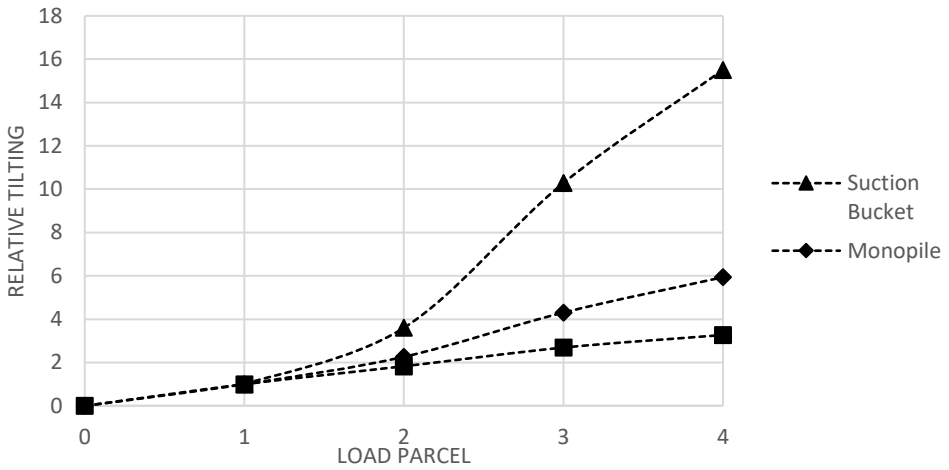

Figure 9 Relative accumulated tilting

ACKNOWLEDGEMENTS

This research is part of the Innovation and Networking for Fatigue and Reliability Analysis of Structures - Training for Assessment of Risk (INFRASTAR) project. This project has received funding from the European Union's Horizon 2020 research and innovation program under the Marie Skłodowska-Curie grant agreement No. 676139. The laboratory tests are provided by the Chair of Soil Mechanics and Geotechnical Engineering of the Technical University of Berlin. We are grateful for the kind permission to use those test results.

BIBLIOGRAPHY

1. Velarde, J., Kramhøft, C., & Sørensen, J. D. (2018). Uncertainty Modeling and Fatigue Reliability Assessment of Concrete Gravity Based

Foundation for Offshore Wind Turbines. International Society of Offshore and Polar Engineers.

2. Allotey, N. and El Naggar, M.H. (2005). "Cyclic soil degradation/hardening models: a critique". Proc. of 16th International Conference of Soil Mechanics and Geotechnical Engineering. MillPress Science Publishers, Rotterdam, 785-790.
3. Andersen, K.H. (2015), "Cyclic soil parameters for offshore foundation design". The 3rd McClelland Lecture. Frontiers in Offshore Geotechnics III, ISFOG'2015, 1, 5-82.
4. Zorzi, G., Richter, T., Kirsch, F., Augustesen, A. H., Østergaard, M. U., & Sørensen, S. P. H. (2018). "Explicit Method to Account for Cyclic Degradation of Offshore Wind Turbine Foundations Using Cyclic Interaction Diagrams". International Society of Offshore and Polar Engineers.
5. Kirsch, F., Richter, T., Schädlich, B., Wiesener, S. (2016)."Ansatz zur Erfassung der Porenwasserdruckakkumulation bei Offshore-Monopilegründungen", Der Bauingenieur, 91(1), 26-33
6. PLAXIS (2017). "Plaxis 3D, Reference Manual", Edited by Brinkgreve, R.B.J., Kumarswamy, S., Swolfs, W.M., and Foria F.

Appendix C

Long-term cyclic triaxial tests with DEM simulations

This paper was presented at the V International Conference on Particle-Based Methods held in Hannover 2017 (http://congress.cimne.com/particles2017/frontal/default.asp).

This is the post-print of the accepted manuscript of the article.

Original version: Zorzi, G., Kirsch, F., Gabrieli, F., & Rackwitz, F. (2017). Long-term cyclic triaxial tests with DEM simulations. PARTICLES 2017, V International Conference on Particle-based Methods – Fundamentals and Applications. Hannover, Germany.

The additional remarks in red to the original paper have been made for this thesis.

Long-term cyclic triaxial tests with DEM simulations

Gianluca Zorzi*[1], Fabian Kirsch[1], Fabio Gabrieli[2] and Frank Rackwitz[3]

[1] GuD Geotechnik und Dynamik Consult GmbH
Darwinstraße 13, 10589, Berlin
e-mail: zorzi@gudconsult.de, kirsch@gudconsult.de , web page: http://www.gudconsult.de

[2] Department of Civil Environmental and Architectural Engineering (ICEA)
University of Padova
Via Ognissanti 39, 35129 Padova, Italy
e-mail: fabio.gabrieli@unipd.it, web page: http://www.dicea.unipd.it

[3] Soil Mechanics and Geotechnical Engineering Division,
Technical University of Berlin
Gustav-Meyer-Allee 25, 13355 Berlin, Germany
e-mail: frank.rackwitz@tu-berlin.de,
web page: http://www.bau.tu-berlin.de/grundbau_und_bodenmechanik

Key words: DEM, cyclic loading, stress induced anisotropy

ABSTRACT

Modeling the long-term performance of granular materials under cyclic loading conditions is still a challenge and a better understanding could provide a large benefit for the design of foundations. One typical application example are the foundations of wind turbines, for which the evolution of the soil mechanical behavior could lead to irreversible strain accumulation (with tilting and settlement) and dynamic resonance problems [1].

In this framework the Discrete Element Method [2] can provide useful information starting from a micromechanical point of view: it may allow engineers to increase their knowledge on the evolution of the mechanical behavior and to optimize the long-term design of these structures [3].

The present paper presents the capability of DEM to simulate a long-term cyclic drained triaxial test (up to 100,000 cycles). The results regard the progressive accumulation of plastic strain as function of the number of particles and the initial particles rearrangement. The influence of densification and contact orientation (anisotropy) in the evolution of the strength of the soil during the cyclic loading history is investigated.

INTRODUCTION

Repeated loadings are some of the main design driven factor for fatigue analysis of many civil structures like transportation facilities, industrial plant as well as wind turbine foundations. Considering the latter, which are subjected to millions of dynamic loadings during their lifetime, it is important to capture any change in soil properties which could have an impact on the behavior of the structure in terms of irreversible strain accumulation (settlement and tilting) and dynamic resonance problems [1].

Modeling accurately the evolution of soil properties under low amplitude cyclic stress loading is of great interest for geotechnical engineers, especially because there is a lack of accurate constitutive models focusing on these problems. During each loading cycle the soil experiences an accumulation of plastic deformations, with a partially open strain hysteresis loop. The smaller the loading amplitude is, the smaller the gap will be. These small vibrations and cyclic solicitations can be considered silent on the short term and the load-deformation behavior is quasi-elastic. However, in the long-term, they possibly result in a low but progressive degradation/damage of the structure and foundation, impacting the behavior of structures and their maintenance costs. Capturing this long-term behavior has been done applying different approaches in Finite Element Method (FEM). One is the application of the common engineering constitutive soil models (hysteretic approach), which is still a challenge and could possibly lead to inaccurate results due to the accumulation of numerical errors when hundred or thousand of cycles are applied [4]. Another strategy is to use the so-called explicit method such as the High Cycle Accumulation (HCA) model [4] or Cyclic Interaction Diagrams developed at NGI. The accumulation of plastic strains for a series of cyclic amplitude excitations are directly related to the number of cycles. These models are based on empirical macroscopic behavior of soil under cyclic loading obtained from experimental laboratory testing. However, the explicit models are either too much sophisticated when implementing advanced mathematical formulations or required extensive laboratory effort if different loading paths and different soil layers are present and are difficult to be used to analyze the general soil behavior in other different loading conditions.

In the past decades Discrete Element Method (DEM, pioneered by Cundall et al. [2]) is becoming popular on simulating low amplitude cyclic triaxial tests, showing similarities to the overall macromechanical response of the laboratory tests and with the possibility to investigate the soil fabric evolution [6,7,8]. However, in those researches the application of rigid walls/membranes to simulate the real configuration required a large amount of particles and just few thousand of cycles were investigated. The DEM has proved to be a powerful method to study plasticity and non-linearity of granular materials which naturally arise from its intrinsic particle description without any particular mathematical hypothesis. Even though it is a good candidate for the comprehension and prediction of soil under cyclic loadings at a particles level point of view, its applicability in common geotechnical problems is still limited to the number of particles.

The present work shows the capability of DEM to simulate qualitatively a long-term cyclic drained triaxial test with low strain amplitude. The cyclic triaxial tests are simulated on a Representative Elementary Volume (REV) under stress-controlled conditions.

The trend of the accumulation of axial strains and strain amplitudes were analyzed in terms of reproducibility of the test results up to 10,000 cycles and with different number of particles (different REV sizes) up to 100,000 cycles. In the end, the analysis of the strength during different cyclic stages was linked to the evolution of the anisotropic soil fabric.

DISCRETE ELEMENT SIMULATIONS

Sample Generation

In the present analysis the DEM simulations were conducted using an open-source code YADE [9] based on a soft-particles approach. Spherical particles are considered to reduce the computational cost. The contact constitutive law is the classic elastic-plastic law with rolling and twisting stiffness at the contact to take into account for grain roughness [9, 10]. The long-term cyclic drained triaxial tests are simulated with a cube-shaped cell called REV. A REV is characterized of Periodic Boundary (PB) conditions. Figure 1 is an example of a REV packing where the blank wire spheres are the exact copy from the opposite side.

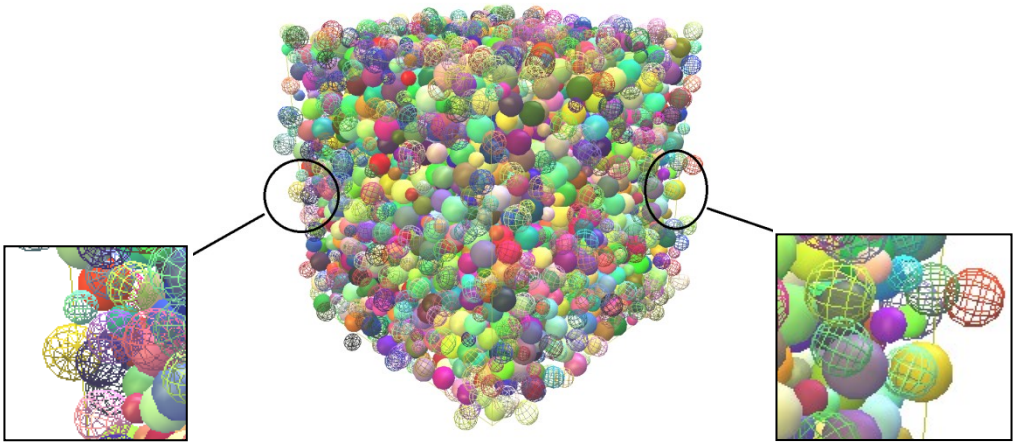

Figure 1: REV packing with periodic boundary conditions.

This configuration allows to use a smaller number of particles, which is important for computational reason and to avoid boundary effect problems arising when rigid-wall or membrane is used [11].

The aim of this paper is to show the capability of the DEM to simulate a long-term cyclic loading from a qualitative point of view and to study the initial departure of the grain assembly. Therefore, no contact law parameter calibration has been done but will be addressed in the future for a quantitative analysis of the cyclic behavior of soil. The contact parameters governing the macromechanical behavior are five and are listed in Table 1. These parameters represent an idealized cohesionless frictional material.

Table 1: Particles' contact parameters.

E_c [Pa]	4e8
v_c [-]	0.25
Phi_c [°]	32
Beta [-]	0.75
Eta [-]	0.75
Density [kg/m^3]	2535

The samples were generated in order to match two predefined global quantities: Particles Size Distribution (PSD) and target porosity. A procedure for sample preparation similar to that described in [5] was adopted. A very loose cloud of particles with random position, high porosity (non-overlapping particles) and

predefined PSD was generated in an initially large cube-shaped cell. An isotropic compression was applied with a high value of contact friction angle until a stable sample was achieved. At this stage the porosity of the sample is higher than the target one. A decrease in contact friction angle was gradually applied until the desired porosity was reached. The sample preparation was considered finished when the unbalanced force [9], which is the ratio between inertia and interaction forces, went below 10^{-3}. The contact friction angle was then set to the wanted value.

Regarding the PSD, the sample considered was a slightly uniform distribution with D_{min}=4 mm and D_{max} =8 mm. The target porosity for the sample preparation was set to be 0.50.

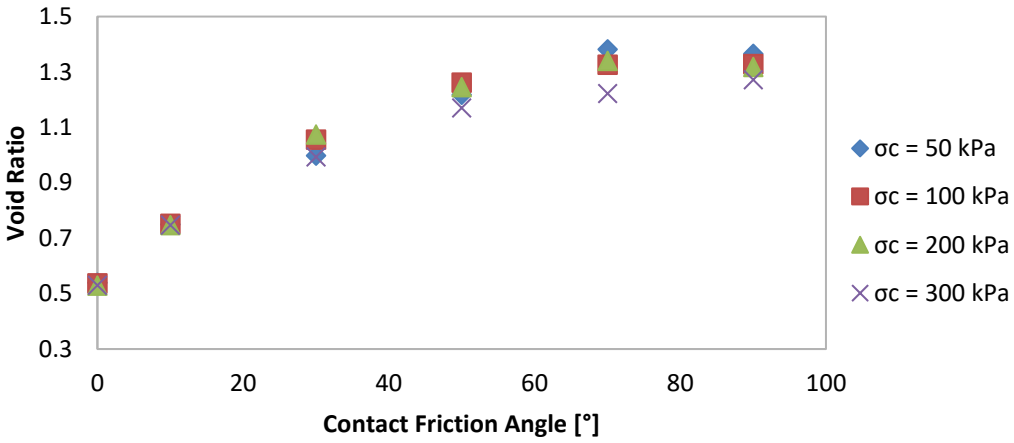

Figure 2: Void ratio of the REV for different friction angle and confining pressure.

The direct comparison in terms of porosity between laboratory and numerical samples, is not straighforward due to the difference in particles shape. Therefore, it would be more appropriate to compare relative densities and have different scales of minimum and maximum porosties between the laboratory and numerical samples. In order to have a complete overview of the relative state of density of the present sample, the minimum void ratio e_{min} and maximum void ratio e_{max} were calculated by imposing the contact friction angle to 0° and 90° respectively. The minimum and maximum void ration depend on the confining pressure being used, thus different samples were generated with different contact friction angles and 4 different confining pressures. For all the confining

pressures a low strain rate was set. It is important to underline that, during the sample preparation, the velocity of the boundaries under the isotropic confining pressure has to be as low as possible to avoid the creation of an inhomogeneous contact force distribution. As figure 2 shows, the denser state is characterized by a small variation of the minimum void ratio with different isotropic confining pressures while the loosest state is more scattered: this depends on the initial grain arrangement and chain force formation. The minimum and maximum void ratios at 100 kPa of confining pressure was adopted. e_{min} and e_{max} were equal to 0.537 and 1.32, respectively.

Triaxial Compression Test

Monotonic triaxial tests were conducted to analyze the macroscopic behavior of the sample. The lateral stress was kept constant at the confining pressure of 100kPa while the vertical boundaries were moved vertically under strain-control conditions. Two stable samples with 3000 particles and having different initial porosities were generated. The first, referred as "dense", has an initial porosity of 0.358 (I_D=0.97). The second sample, named "loose ", is characterized by an initial porosity of 0.50 (I_D=0.408). The figures 3a and 3b shows the deviatoric and volumetric behavior of the two samples.

The REV with 3,000 spheres mimics the classical drained triaxial compression test response of granular materials with different initial densities. Both samples reach the critical state with the same deviatoric shear stress and a quite constant volumetric strain. The loose state, which will be used for the cyclic loading triaxial test, shows the typical hardening behavior with shrinking.

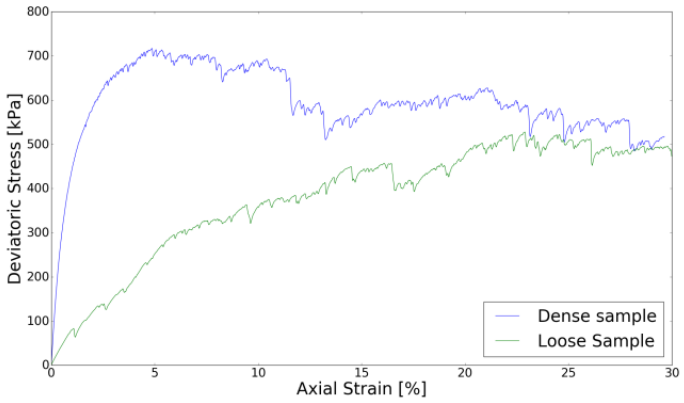

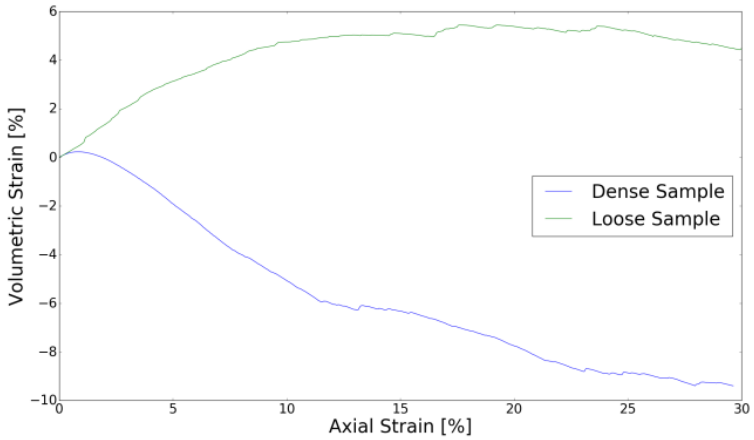

***Figure 3**: Triaxial test results of two DEM samples: (a) deviatoric and (b) volumetric behavior.*

Cyclic Triaxial Test

Also in the simulation of the cyclic triaxial tests, the lateral confining pressure σc was kept constant at 100kPa while the vertical boundaries were cyclically moved under stress-control conditions. Figure 4 shows the cyclic stress path of the simulation in the p'-q plane, where p is the mean stress and q is the deviatoric stress. The first phase (horizontal red line) represents the isotropic confining phase up to a σc of 100kPa. Then the sample is sheared with a load σs of 40 kPa until the point (qav, pav) is reached. The cyclic loading stage was then performed with a stress amplitude σamp of 30 kPa. The values of the loading stresses can be found in table 2.

Table 2: Stress loading parameters

p_{iso}	100.00 kPa
p_{av}	113.33 kPa
q_{av}	40.00 kPa
q_{amp}	±30.00 kPa

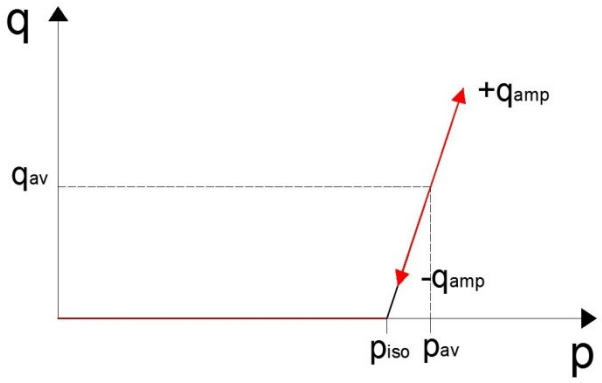

Figure 4: Cyclic Stress pat

The mass of the PBs were adjusted in order to avoid inertial forces. The aim of the paper is to investigate the capability of the DEM to simulate the effect of a small strain amplitude on the long-term cyclic loading. Therefore, the cyclic stress was chosen in order to have a low cyclic strain amplitude of the order of 10^{-3} and the static load far from failure. For small number of particles in the REV and long-term cyclic loading, the chance of having an inhomogeneous distribution of contact forces is high (again the initial sample preparation has a strong influence on the behavior of the assembly). During the cyclic test, the occurrence of a chain buckling leads to a sudden large increase of plastic strain [6].

The applied load in the granular assembly is carried by means of strong force chains passing though the contacts of the particles and propagating the stress through the sample. The strength of these chains depends on the calibrated contact parameters. Repeated loading can lead to a local failure (chain buckling) of one of these chains and can change the entire force distribution across the sample, which is accompanied by an increase in the permanent deformation.

The analyses of the results of the DEM cyclic triaxial tests were done by following the procedure and the remarks explained in [12], which are depicted in figure 5 [12] for a laboratory cyclic triaxial test.

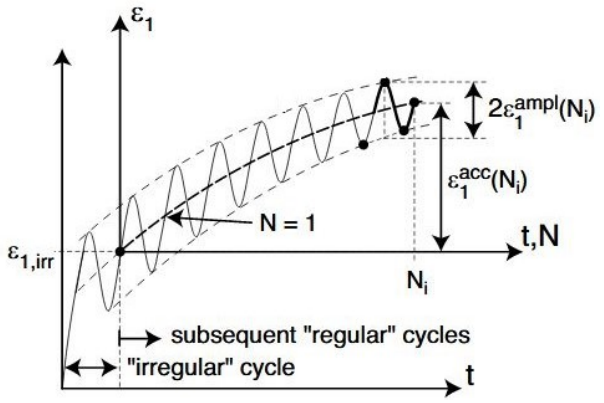

Figure 5: Cyclic Triaxial Test curve (modified from [12])

The cycles were divided in a first irregular cycle N_0 in which there is the largest deformation and in subsequent regular cycles $N_{i\ (i=1,..,n)}$.

The trend of the axial strain during the cyclic triaxial test was analyzed by calculating the axial strain accumulation (1) and the axial strain amplitude (2) from the first regular cycle N_1[12].

$$\varepsilon_{1,i}^{acc} = \frac{1}{2}[\varepsilon_1^{max}(N_{i+1}) + \varepsilon_1^{min}(N_i)] \qquad \textit{where } i=1,\ldots,n \quad (1)$$

$$\varepsilon_{1,i}^{amp} = \frac{1}{2}[\varepsilon_1^{max}(N_i) - \frac{1}{2}(\varepsilon_1^{min}(N_i) + \varepsilon_1^{min}(N_{i-1}))] \qquad \textit{where } i=1,\ldots,n \quad (2)$$

The test was conducted using 3,000 spheres in a REV packing. The total number of cycles was 100,000. Figure 6 shows the trend of the axial strain accumulation plotted with the logarithm of the number of cycles. It is clearly visible that the rate of accumulation of axial strain decreases, reaching a constant value, which means that the soil reaches a stable configuration named shakedown state [13].

The shakedown state also emerges considering the trend of porosity as shown in figure 7. The first few thousand cycles are marked with the highest adaption period to the external cyclic solicitation, with the larger accumulation of permanent deformation. Subsequently to this adaption period, the material showed a resilient response to the increasing the number of cycle stresses, typical of the shakedown behavior [13].

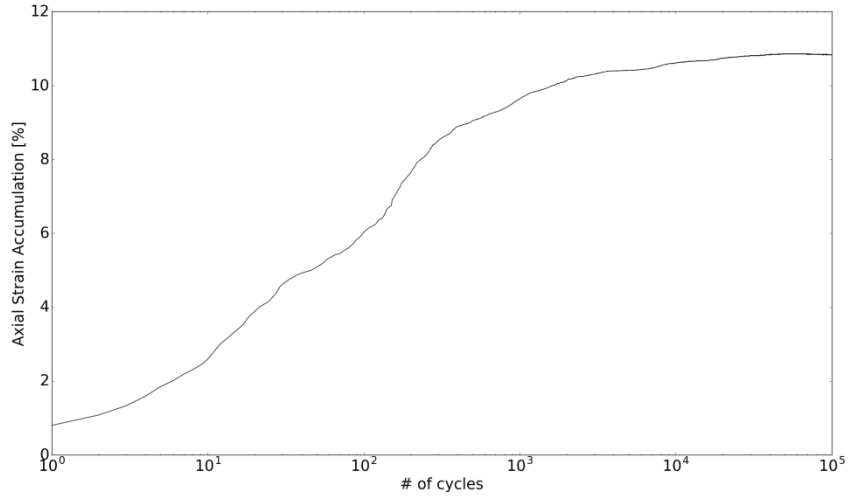

Figure 6: Axial Strain Accumulation of a REV with 3000 particles up to 100,000 cycles

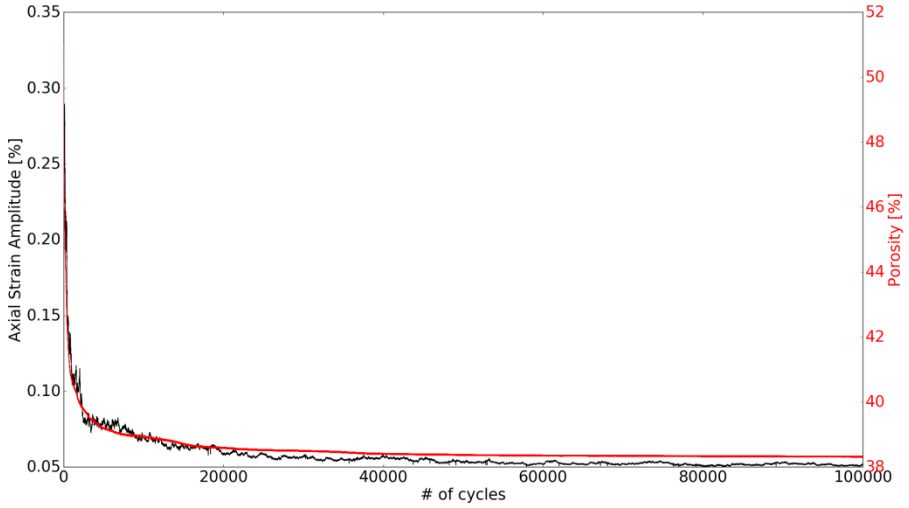

Figure 7: Trend of porosity (red line) and axial strain amplitude (black line) of a REV with 3000 particles up to 100,000 cycles

TEST REPEATABILITY OF CYCLIC TRIAXIAL TESTS

In the following, the degree of repeatability on the long-term cyclic behavior was investigated with different initial fabric and different number of particles. Different clouds of particles were prepared, with different initial random distributions and the procedure explained previously was used to create a stable packing.

Two different numbers of particles in a REV were considered: 2000 and 5000. For each number of particles, 10 samples were generated. The micromechanical parameters used in simulations are listed in table 1.

All the 20 samples were isotropically consolidated with a confining pressure of 100 kPa and cyclically loaded for 10,000 cycles. The target porosity during the sample preparation was set 0.50 and from the inspection of the 20 samples the porosity differs of 0.03%.

Figures 8 shows the same cyclic behavior described earlier. The dispersion of the curves (i.e. repeatability) resulted lower with a large number of particles. This low variability is also depicted in figure 9, where the axial strain amplitude is plotted.

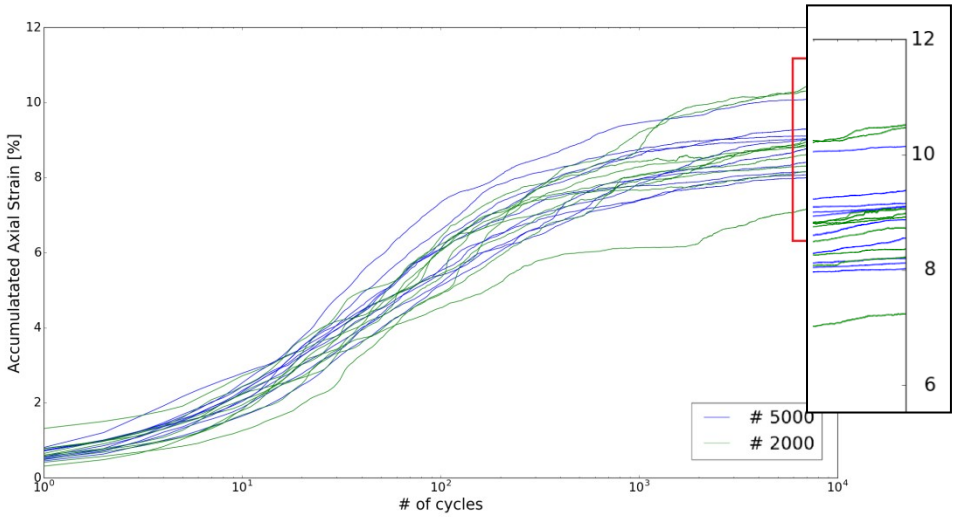

***Figure 8**: Axial Strain Accumulation for different initial packing.*

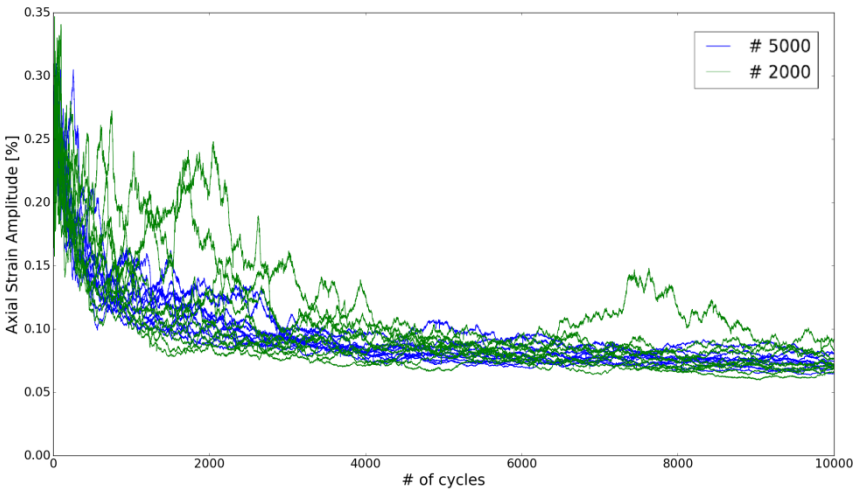

Figure 9: Axial Strain Amplitude for different initial packing.

INFLUENCE OF THE REV SIZE ON THE LONG-TERM CYCLIC BEHAVIOR

With regards to the cyclic tests, the choice of the number of particles to be used in the REV is of capital importance from a computational stand point: the larger the number of particles is, the longer the simulation will be; on the other hand a too small number of particles may lead to incorrect or unreliable results.

A minimum number of particles should be used to get reliable porosity, coordination number, stress and strain values [14]. The evaluation of the minimum amount of spherical particles for a REV can be done by looking at the orientation distribution of the contact normal which should be close to a sphere shape-like under isotropic compression [5].

Figure 10 shows the axial strain accumulation up to 100,000 cycles for different REV. The rapid increase of deformation for a small sample (with 500 particles) is due to buckling effect of large chain forces [6]. Moreover, specimens with a low number of particles can have a poor normal contact force distribution which governs the cyclic behavior. By increasing the number of particles per sample there is an increase of the axial strain accumulation.

A poor distribution of normal force or orientation of the contacts is when after an isotropic compression (i.e. during sample preparation) there is a uniform

variation of the distribution (no preferential direction). See Appendix D, Section 5.

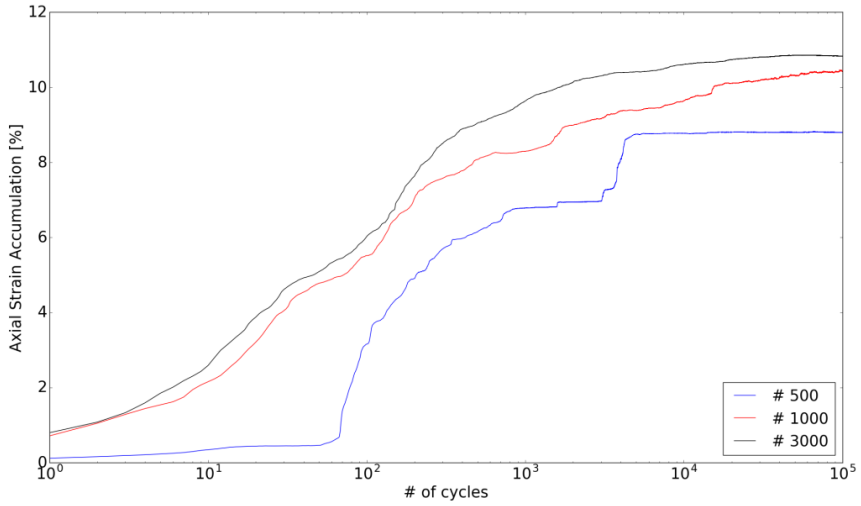

Figure 10: Axial Strain Accumulation as function of the # of particles for the sample.

STRENGTH AND STIFFNESS OF THE SAMPLE DURING CYCLIC STAGES

Cohesionless materials can benefit from low amplitude cyclic loading conditions, increasing their strength and stiffness after the cyclic loads. It is believed that this increment in stress (strength) is mainly due to the emergence of a densification process (decrease in porosity).

During the cyclic triaxial test for the REV with 3,000 spheres, the sample configuration was saved at 100/ 1,000/ 10,000/ 50,000/ 100,000 cycles, red points in figure 11. The samples were then unloaded until an isotropic confining pressure of 100kPa and the monotonic triaxial tests were conducted to analyze their strength and stiffness. The lateral stress was kept constant at the confining pressure of 100kPa while the vertical boundaries were moved vertically under strain-control conditions. In figure 12 and 13, it is clearly depicted that the sample is increasing its strength with the increasing of the number of cycles (solid lines), transforming from a typical hardening behavior with shirking (cycle 0) for loose material to a compaction-dilation behavior for dense materials.

At the same time, new samples were generated and monotonically sheared with the same exact porosity and isotropic confining pressure of 100kPa of the previously saved samples. Figure 12 and 13 show the difference between the monotonic triaxial tests of virgin samples (dashed lines) and cyclically loaded ones (solid lines) at the same porosity.

During a cyclic loading stress solicitation, the granular assembly decreases in density (behavior seen from a macroscopic point of view) but at the same time organizes its distribution of contact normal orientation in a favorable way to resist better against the external solicitation (stress induced anisotropy [6]). Figure 12 shows that the stress induced anisotropy (contact orientation) started to develop between 1,000 cycles (the red dashed and solid lines are similar) and 10,000 cycles.

This effect could be studied with the DEM by analyzing the distribution of contact orientation. During the sample generation under an isotropic confining pressure and neglecting gravity, the contact orientation should reassemble a circular shape (isotropic fabric). After 100,000 cycles, the same distribution of contact orientation should evolve to adapt to the new stress conditions. Further investigation will be done to better characterized this phenomena.

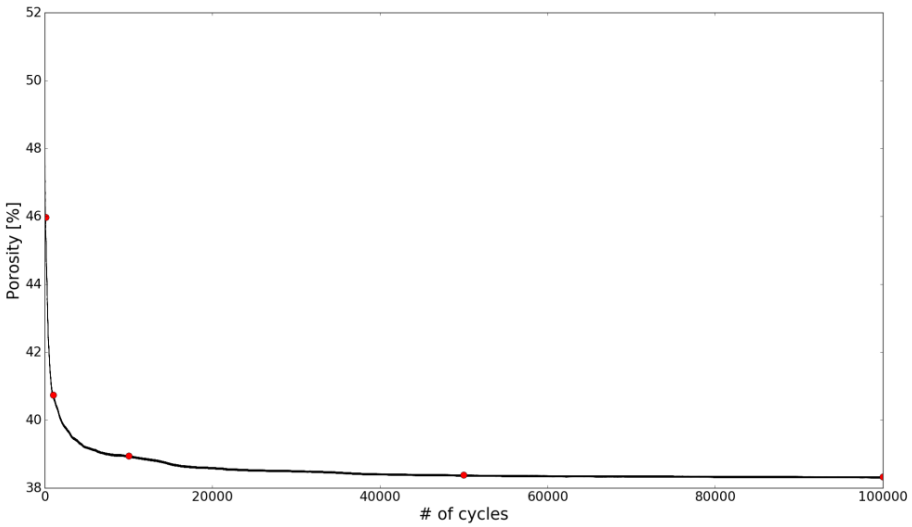

Figure 11: Porosity trend for 3,000 particles up to 100,000 cycles.

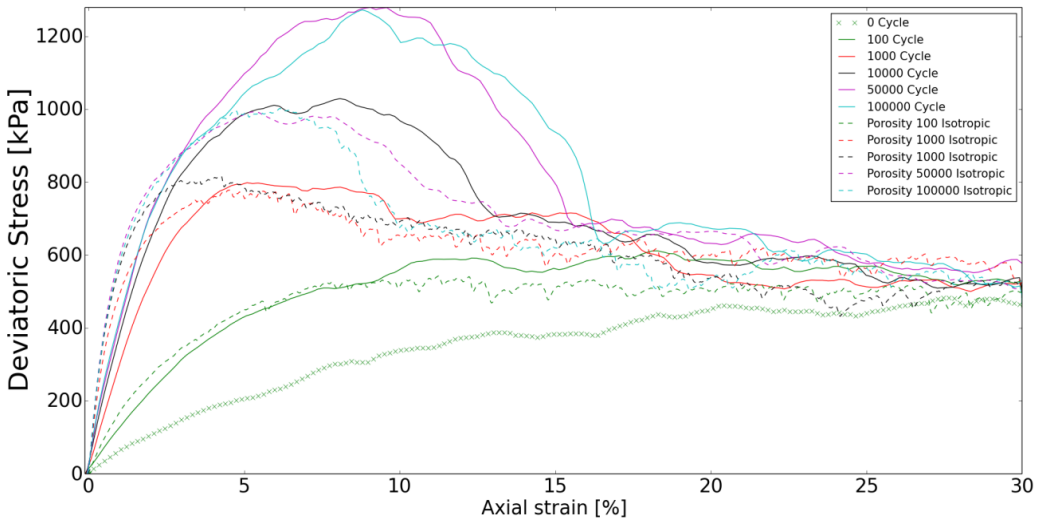

Figure 12: Triaxial tests results: deviatoric behavior. Solid line: anisotropic samples due to cyclic loading. Dashed line: isotropic samples.

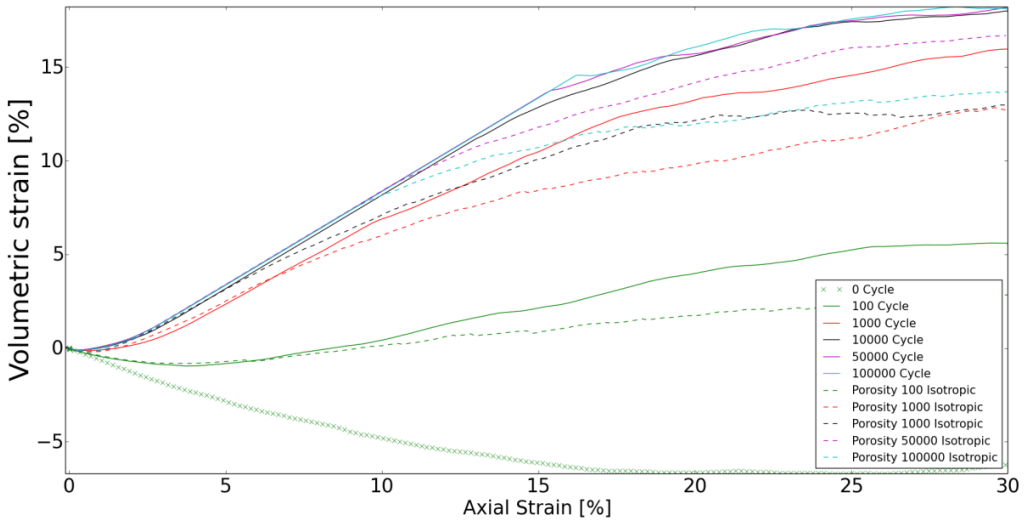

Figure 13: Triaxial tests results: volumetric behavior. Solid line: anisotropic samples due to cyclic loading. Dashed line: isotropic samples.

CONCLUSION

This paper shows the potentiality of DEM to simulate qualitatively a long-term cyclic triaxial test on a REV. The effect of different initial fabric and REV sizes have been investigated in relation to a large amount of cyclic loading. Future research will be to quantitative simulate cyclic triaxial test results of sand. It will allow a better understanding of the long-term behavior of granular materials

from a micromechanical scale, possibly resulting as a base for an accurate formulation of constitutive models for cyclic loading.

ACKNOWLEDGEMENT

This research is part of the Innovation and Networking for Fatigue and Reliability Analysis of Structures - Training for Assessment of Risk (INFRASTAR) project. This project has received funding from the European Union's Horizon 2020 research and innovation programme under the Marie Skłodowska-Curie grant agreement No 676139. The computing facilities offered by CloudVeneto (CSIA Padova and INFN) are acknowledged.

REFERENCES

[1] Bhattacharya, S. (2014). Challenges in Design of Foundations for Offshore Wind Turbines. Engineering & Technology Reference. http://dx.doi.org/10.1049/etr.2014.0041

[2] Cundall, P. & Strack, O. (1979). A discrete numerical model for granular assemblies. Géotechnique, 29(1), 47-65. http://dx.doi.org/10.1680/geot.1979.29.1.47

[3] O'Sullivan, C. & Cui, L. (2009). Fabric Evolution in Granular Materials Subject to Drained, Strain Controlled Cyclic Loading. Powsers And Grains 2009: Proceedings Of The 6Th International Conference On Micromechanics Of Granular Media, 1145, 285-288. http://dx.doi.org/10.1063/1.3179914

[4] Niemunis, A., Wichtmann, T., & Triantafyllidis, T. (2005). A high-cycle accumulation model for sand. Computers And Geotechnics, 32(4), 245-263. http://dx.doi.org/10.1016/j.compgeo.2005.03.002

[5] *Tong, A.-T., Catalano, E., Chareyre, B. (2012). Pore-scale flow simulations: model predictions compared with experiments on bi-dispersed granular assemblies, Oil & Gas Science and Technology - Rev. IFP , 67(35):743–752*

[6] Hu, M., O'Sullivan, C., Jardine, R., & Jiang, M. (2010). Stress-induced anisotropy in sand under cyclic loading. *Granular Matter*, *12*(5), 469-476. http://dx.doi.org/10.1007/s10035-010-0206-7

[7] Nguyen, N., François, S., & Degrande, G. (2014). Discrete modeling of strain accumulation in granular soils under low amplitude cyclic loading. *Computers And Geotechnics*, *62*, 232-243. http://dx.doi.org/10.1016/j.compgeo.2014.07.015

[8] O'Sullivan, C., Cui, L., & O'Neill, S. (2008). Discrete Element Analysis of the response of granular materials during cyclic loading. Soils and Foundations, *48*(4), 511-530. http://dx.doi.org/10.3208/sandf.48.511

[9] Šmilauer, V. et al. (2015), Yade Documentation 2nd ed. The Yade Project. DOI 10.5281/zenodo.34073

[10] Widuliński, L., Kozicki, J., Tejchman, J. (2009). Numerical simulations of triaxial test with sand using DEM. *Archives of Hydroengineering and Environmental Mechanics*, 56 (3-4), 149-172.

[11] Radjai, F., Dubois T. (2011). *Discrete-element modeling of granular materials*, Wiley-Iste, 181-198, 978-1-84821-260-2.

[12] Wichtmann, T., Niemunis, A., & Triantafyllidis, T. (2009). On the determination of a set of material constants for a high-cycle accumulation model for non-cohesive soils. *International Journal For Numerical And Analytical Methods In Geomechanics*, n/a-n/a. http://dx.doi.org/10.1002/nag.821

[13] García-Rojo, R., & Herrmann, H. (2005). Shakedown of unbound granular material. *Granular Matter*, *7*(2-3), 109-118. http://dx.doi.org/10.1007/s10035-004-0186-6

[14] Kawano, K, Sullivan, CO, Shire, T. (2016). Using DEM to assess the influence of stress and fabric inhomogeneity and anisotropy on susceptibility to suffusion. "Proc. 8th Int. Conf. Scour and Erosion, Harris, Whitehouse & Moxon (Eds.)", 85-94.

Appendix D

DEM modelling of high cyclic triaxial tests: calibration, sensitivity analysis and practical application

This paper is a draft ready to be submitted to a journal.

DEM modelling of high cyclic loading: calibration, sensitivity analysis and practical application

Gianluca Zorzi*■, Fabio Gabrieli ◆, Hung Viet Le▲, Frank Rackwitz▲, Fabian Kirsch■

▪ GuD Geotechnik und Dynamik Consult GmbH
Berlin, Germany
* zorzi@gudconsult.de; Tel. +49 30 789089396

◆ Department of Civil Environmental and Architectural Engineering (ICEA)
University of Padova
Padova, Italy

▲Chair of Soil Mechanics and Geotechnical Engineering,
Technische Universität Berlin
Berlin, Germany

ABSTARCT

Predicting the long-term performance of granular materials under cyclic loading conditions remains challenging. Empirical methods that are based on the results of a large and time consuming laboratory test campaign are commonly used for the prediction of soil behaviour under cyclic loads. The discrete element method (DEM) can be used in place of the cyclic laboratory tests and has potential benefits for the design stage in terms of cost and time savings. Using a representative elementary volume (REV) with periodic boundary conditions, the present work demonstrates the performance of the DEM in quantitatively and quickly simulating drained high cyclic triaxial tests for cohesionless soils. The contact parameters are calibrated by simulating monotonic triaxial tests with various confining pressures. Finally, practical applications in which the tilting of a gravity-based foundation is predicted for an offshore wind turbine that is subjected to cyclic lateral loadings (design storm events) is presented. The prediction of the foundation tilting is based on the results of many drained cyclic triaxial tests that are simulated via the DEM.

Keywords: Cyclic triaxial tests; discrete element method; cyclic loading; granular material; offshore wind turbine; representative elementary volume.

1. INTRODUCTION

The study of the long-term performance of granular materials under cyclic loading conditions is important for predicting the behaviour of soil-structure interactions under long-term serviceability conditions. Typical application examples are related to the foundations of offshore wind turbines (OWTs). These foundations are fatigue-design-driven structures, which must withstand cyclic environmental loads and maintain the required operational level throughout their intended design life of typically 25 years. Their slender design results in a high cyclic overturning moment at the mudline, which is dominant compared to horizontal and vertical forces. This is in contrast to oil and gas offshore structures, in which self-weight (vertical force) is the dominating load. There are four main cyclic loads that act on offshore wind turbines: wind and waves, which are environmental loads, and the rotor and the blade passing frequencies. Wind loads have a typical frequency of 0.01 Hz, whereas wave loads have a typical frequency of 0.1 Hz. These low-frequency cyclic loads in granular soils ensure the quasi-static conditions and likely do not allow the soil to develop significant excess pore water pressure (fully undrained condition) as in earthquake-induced liquefaction phenomena.

Wind turbine manufacturers provide to geotechnical engineers a maximum tilting operational restriction of the structure during its lifetime, and this restriction is typically < 1° (e.g., 0.25°). The maximum allowed rotation is supposed to guarantee that the wind turbines are operating as designed without the development of mass-unbalance forces, which can potentially increase the fatigue of the other elements and reduce the lifetime of the structure. During the lifetime of an offshore wind turbine, millions of cyclic loads are expected to act on the foundation element. However, in the design phase, the rotation of the foundation is analysed for design storm events, and typically, a few thousand cycles are considered for the design.

Thus, geotechnical engineers are challenged to adopt an appropriate model that accurately predicts the deformation accumulation of the soil that is due to the action of the environmental cyclic loads. Various constitutive models are used in current engineering practice to model monotonic loading for geotechnical

problems; few deal with the soil behaviour under cyclic loadings. Conventional constitutive models exhibit limited performance in predicting the accumulation of deformation during high cyclic loadings due to the inevitable accumulation of numerical errors (Niemunis, et al., 2005). The only methods that focus on the prediction of cyclic plastic strains that are far from the failure conditions are empirical methods that are based on the results of cyclic laboratory tests. These empirical methods, which are also called soil fatigue models (Allotey & El Naggar, 2005), explicitly predict the accumulation of permanent strain for a soil that is subjected to regular cyclic loads and a specified stress level. An explicit prediction can be expressed via an advanced mathematical formulation (an example is the high cycles accumulation (HCA) model (Niemunis, et al., 2005)) or 3D cyclic contour diagrams (Andersen, 2015). To obtain a realistic stress distribution under the foundation, the formulation is associated with a 3D FEM model (such as in the UDCAM (Andersen, 2015), HCA (Niemunis, et al., 2005) model, SCD method (Zorzi, et al., 2018)).

The application of those explicit methods require a large and time consuming laboratory test campaign for calibrating or deriving the empirical formulation. The laboratory tests generally consist of applying regular cyclic loads with different average and cyclic amplitude stresses for a specified number of cycles using a cyclic triaxial or simple shear apparatus. Moreover, it is typical in projects to deal with various soil layers, various relative densities and various drainage conditions, which must be tested, thereby resulting in a large laboratory campaign.

One approach that can be used to supplement the cyclic laboratory tests is to apply the discrete element method (DEM, which was pioneered by Cundall & Strack (Cundall & Strack, 1979)). Training the DEM to substitute the laboratory tests can be highly beneficial in terms of cost and time savings and to test different stress paths that cannot be explored in the laboratory testing.

In the last decades, the discrete element method has become popular for simulating the macromechanical response of granular material that is tested using laboratory devices in, e.g., conventional triaxial tests, with the possibilities of observing microscopic contact quantities and investigating the effects of the

micromechanical parameters on the overall mechanical behaviour. Monotonic triaxial tests that are simulated with DEM numerical samples are used to calibrate the micromechanical contact parameters.

Regarding the simulation of cyclic loading under drained condition, limited research has been conducted on predicting the cyclic behaviour of granular soil. For example, DEM model was used to simulate strain controlled cyclic triaxial tests of steel spheres only up to 50 cycles using mix boundary conditions (O'Sullivan, et al., 2008). Recently, several stress-controlled cyclic triaxial tests were simulated to study the macroscopic and microscopic behaviour of the granular materials at different cyclic amplitudes, static loads and void ratio and using boundary walls (Jiang, et al., 2019). In literature, DEM is also used for modelling the soil-structure inter-action under generally few cyclic loads (Hadda & Wan, 2020). Due to computational reasons the size of the grains has to be scaled up compared to the real size. However, basic macroscopic behaviour such as grain densification or ratcheting can be simulated (Cui & Bhattacharya, 2016; Zorzi, et al., 2017). Until now, the use of the DEM to model many cyclic loadings has not been considered since it is assumed to be very time-consuming. A preliminary investigation of the potential of the DEM adopting a representative elementary volume with periodic boundary conditions to reach high cyclic loadings is shown in (Zorzi, et al., 2017). This work aims at an investigation of the opportunities of employing the DEM in different applications for geotechnics. One of the main part of the study is providing and validating a framework that facilitates the substitution of drained high cyclic triaxial tests with DEM simulations. In the following, all the steps of the monotonic and cyclic triaxial laboratory tests are discussed. In the specific, calibration and sensitivity evaluation for DEM simulations, the macro- and microscopic results of the DEM cyclic triaxial tests and the effects of the simulation parameters and soil fabric are presented. At the end, a practical application in which the residual tilting of a gravity-based foundation for offshore wind turbines that are subjected to cyclic lateral loadings (design storm events) is presented. The tilting is calculated by applying an innovative explicit method (Zorzi, et al., 2018) which is based on cyclic contour diagrams and FE calculations. First the validation of the explicit method is shown with a full-scale gravity-based

foundation test. Secondly, an example showing how the cyclic loading simulations of DEM can be introduced in the explicit method is presented. Precisely, a foundation tilting of a typical gravity-based foundation is predicted based on many cyclic triaxial tests that are conducted with DEM, which will be used to construct 3D cyclic contour diagrams.

2. EXPERIEMNTAL TESTS

2.1 Testing device, material and procedures

The granular material that is considered in the following analysis is "Berlin sand". The experimental results that are presented hereafter are obtained from the Soil Mechanics Laboratories of the Technical University of Berlin and are extensively discussed in (Le, 2015 (in German)).

Berlin sand is a quartz sand that is medium-coarse graded with rounded grains (Fig. 1a). Fig. 1b shows the particle size distribution (PSD), according to which the size ratio D_{100}/D_0 is circa 67, the uniformity coefficient U is 3.3 and the mean grain size d_{50} is 0.55 mm. The minimum and maximum void ratios are 0.391 and 0.688, respectively, with a range of possible void ratios $\Delta e = \Delta e_{max} - \Delta e_{min}$ of circa 0.30. The grain density is 2.61 g/cm³.

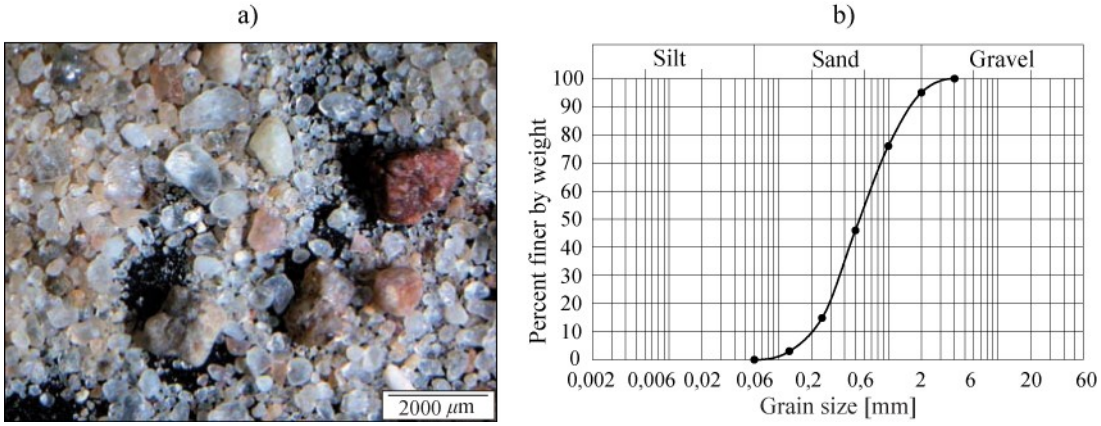

Fig. 1: Sample microscopy photo of Berlin sand (Glasenapp, 2016, http://dx.doi.org/10.14279/depositonce-5402 (in German)) (a) and its particle size distribution (b)

In the present study, the behaviour of the Berlin sand under monotonic and cyclic loading conditions is analysed using a hydraulic triaxial device. The soil sample has a diameter of 10 cm and a height of 20 cm.

The soil specimens for the cyclic and monotonic tests are prepared by pluviating dry sand out of a funnel into a rigid cylinder that is vacuum-sealed around the membrane. Various densities are realized by varying the diameter of the funnel opening and the drop height of the sand (the distance between the sand surface and the funnel). Denser samples are obtained through a smaller funnel opening and a higher drop height. During the pluviation process, the distance between the funnel opening and the sand surface is kept constant by slowly moving the funnel up. The samples are tested under water-saturated conditions. Initially, the samples are saturated with carbon dioxide (CO2) to accelerate the saturation process of passing CO2 through the sample from bottom to top at a low speed (ca. 1 h). Following a similar procedure, the sample is filled with de-aerated water. After this, the line system is freed of air bubbles and connected to the sample. Thereafter, a saturation pressure ("back pressure") of 300 kPa is applied to the sample via a volume measuring unit. After one day, the quality of the saturation is evaluated by determining the Skempton's B-value (Skempton, 1954). A B-value that exceeds 0.95 corresponds to a satisfactory sample saturation and the end of the preparation process, when the consolidation phase can be initiated. During a monotonic test the shearing was applied by moving the top cap with a constant displacement rate of 0.1 mm/min (strain-controlled) while the cell pressure was kept constant. The cyclic stress loading is sinusoidal and was applied with an external function generator.

Regarding the loading mechanism, the axial stress (static and cyclic loads) is applied with a servo hydraulic system while the radial stress is controlled by the cell pressure that surrounds the soil sample. The test and the data acquisition are controlled using a connected computer. The following quantities are recorded: the axial force, the cell pressure, the pore water pressure, the axial deformation and the volume change. The monotonic and cyclic tests in this study were performed under drained condition

2.2 Monotonic drained triaxial tests

In the following, the results that are obtained from the monotonic tests are presented as deviatoric stress plots and volumetric strain plots. Fig. 2 compares tests under three isotropic confining pressures σ_c (100, 200 and 300 kPa) and relative density I_D of 85-89%. The macroscopic behaviour of the sand is a typical stress-strain response for dense sand in which due to the interlocking and the friction between the particles, a stress peak is attained in a range of 2-4%. The interlocking between particles is intensified at a higher confining pressure, thereby yielding a higher peak strength. Once the interlocking has been overcome, a softening behaviour towards larger strain is observed. In the volumetric strain plot, the contraction-dilation behaviour for dense sand is clearly observed. Fig. 3 shows the typical monotonic behaviour of sand at various relative densities. The looser state does not form a peak but incrementally leads to the critical state (constant deviatoric stress) and to a higher volumetric contraction.

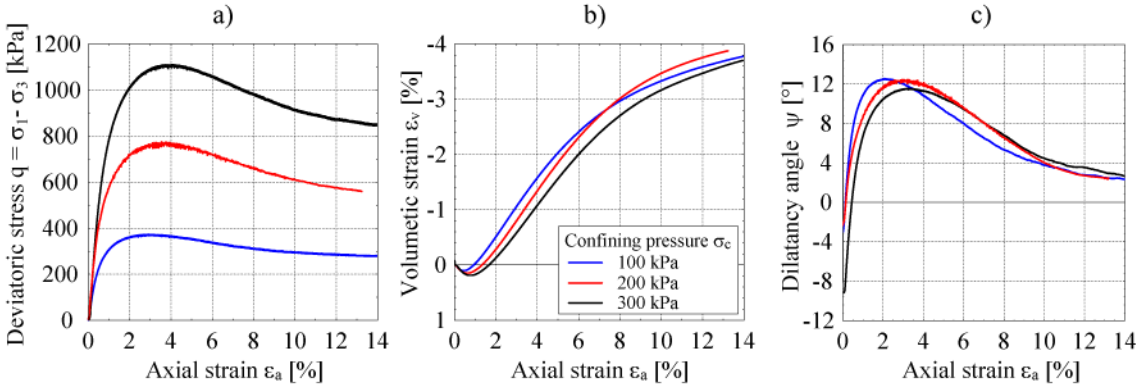

Fig. 2: Deviatoric stress (a) volumetric strain (b) and dilatancy angle (c) vs. axial strain plots for relative density $\boldsymbol{I_D = 85 - 89}$ *% and three confining pressures* $\boldsymbol{\sigma_c}$ *= 100, 200 and 300 kPa*

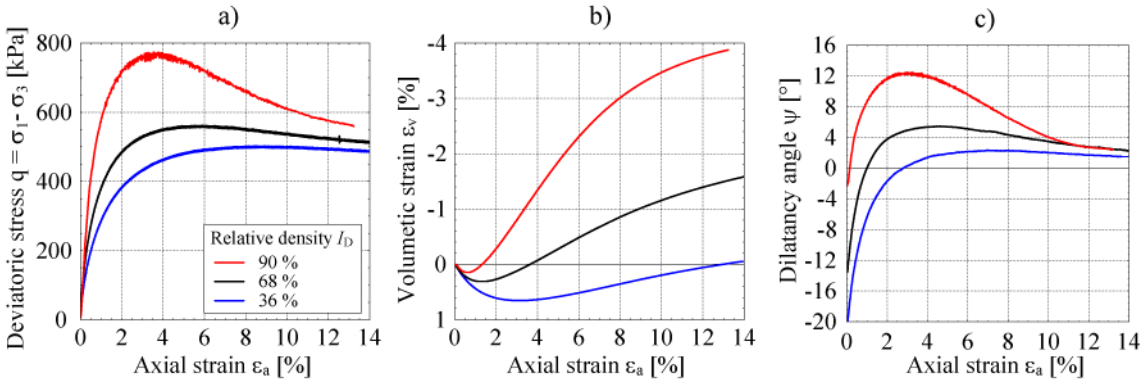

Fig. 3: Deviatoric stress (a) volumetric strain (b) and dilatancy angle (c) vs. axial strain plots for confining pressure σ_c=200 kPa and three relative densities $\boldsymbol{I_D}$

From these tests, a friction angle at critical state $\varphi_c = 31.5°$ was evaluated (average of all tests). This φ_c is independent on the density and the confining pressure. The mobilized friction angle at the peak φ_P depends primarily on the density. From the test results a function for the peak friction angle was defined with:

$$\varphi_P = 31.5 \cdot e^{0.42 \cdot {I_{D,P}}^{0.29}}$$

In which, $I_{D,P}$ is the relative density at peak condition ($0 \leq I_{D,P} \leq 1.0$). Test with dense sample experience a significant peak while in the loose sample, the development of the deviatoric stress do not shows a peak (Fig. 3a). In this case, the peak will be defined with the maximum value of the deviatoric stress, at critical state (according to Le (Le, 2015 (in German))).

Fig. 2c and Fig. 3c show the development of the dilatancy angles during the shearing. These dilatancy angles were evaluated with the following function according to Schanz & Vermeer (Schanz & Vermeer, 1996) :

$$\sin\psi = -\frac{\dot{\varepsilon}_v/\dot{\varepsilon}_1}{2 - \dot{\varepsilon}_v/\dot{\varepsilon}_1}$$

2.3 Cyclic drained triaxial tests

Stress-controlled cyclic loading tests are conducted with an isotropic confining pressure σ_c of 150 kPa and an initial relative density I_D of 60% (Tab. 1). After the consolidation phase, the axial stress is increased up to 300 kPa, which will

be referred to as the average axial stress $\sigma_{1,avr}$. Three cyclic loading amplitudes ($\sigma_{1,amp} = \sigma_{1,max} - \sigma_{1,avr}$) of 20, 40 and 60 kPa are considered.

Tab. 1: Summary of laboratory cyclic triaxial tests

Test #	$\boldsymbol{\sigma_c}$ [kPa]	$\boldsymbol{\sigma_{1,avr}}$ [kPa]	$\boldsymbol{\sigma_{1,amp}}$ [kPa]	$\boldsymbol{I_D}$ [%]	$\boldsymbol{\sigma_{1,avr}/\sigma_c}$	$\boldsymbol{\sigma_{1,amp}/\sigma_c}$
1	150	300	20	60	2	0.13
2	150	300	40	60	2	0.26
3	150	300	60	60	2	0.4

No pre-shearing is considered, and the stopping criterion is the completion of 10^5 cycles. The first cycle is executed with a low frequency of 0.01 Hz to avoid an excess of the pore pressure. The next 200 cycles are executed with a frequency of 0.25 Hz. The remaining cycles up to 10^5 are executed with a frequency of 0.5 Hz. This frequency is low enough to avoid the excess of pore pressure and high enough to speed up the tests. The strain rates of the tests with cyclic loading amplitudes of 40 kPa (Fig. 4) and 60 (Fig. 5) and for frequencies of 0.25 Hz (left figures) and 0.5 Hz (right figures) are plotted. According to the figures, the strain rate depends on the frequency and the cyclic amplitude. The selected frequencies and stress amplitudes are sufficiently low for guaranteeing quasi-static conditions (Achmus, et al., 2005); hence, the inertia effect is neglected and the dissipation of the pore water pressure is ensured. The maximum strain rate (without considering the fluctuations of the signal) for the cyclic loading amplitudes of 40 kPa and the frequency of 0.5 Hz is circa 0.06 %/s, while for the cyclic loading amplitudes of 60 kPa is circa 0.09 %/s.

The results of the cyclic tests will be presented in terms of the average components for the axial strain, the volumetric strain and the relative densities. The accumulated strains are calculated by averaging the maximum and the minimum values of each loading cycle and are zeroed at the beginning of the second cycle, as illustrated in Fig. 6. The first cycle is not considered because typically

features a high deformation due to the application of the first loading cycle.

The macroscopic deformation of the sand is subjected to 10^5 cyclic loads and the results are plotted in Fig. 7. The following graphs present the results of the test with a cyclic amplitude of 40 kPa and an initial relative density of 60%. The number of cycles on the x-axis is plotted on a logarithmic scale. The granular assembly is contracting (increasing in relative density), and the rate of accumulation of deformation is decreasing and leading towards a stable behaviour (shakedown (García-Rojo & Herrmann, 2005)) that is not yet fully reached after 10^5 cycles. An extensive test program with Berlin sand was carried out in a previous study. The influence of void ratio, amplitude, mean stress as well as stress ratio in cyclic triaxial test are presented in (Le, 2015 (in German)).

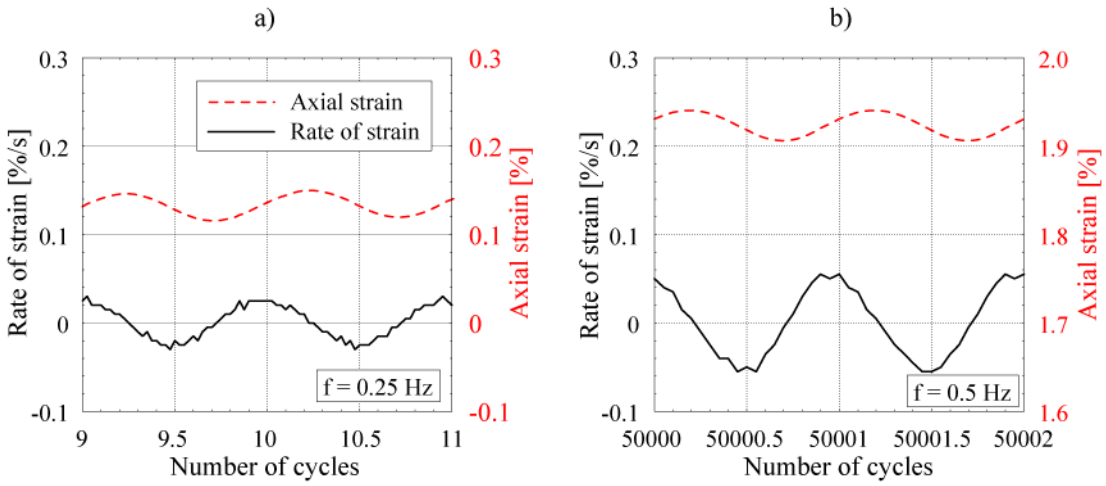

*Fig. 4: Axial strains and strain rates for $\sigma_{1,amp}$ = 40 kPa: **f** = 0.25 Hz (a) and **f** = 0.5 Hz (b)*

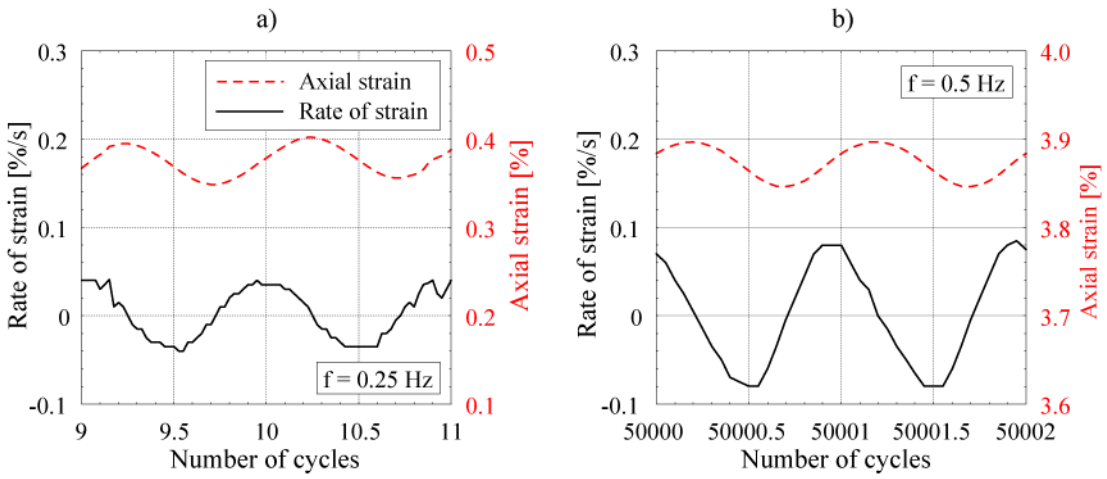

*Fig. 5: Axial strains and strain rates for $\sigma_{1,amp}$ = 60 kPa: **f** = 0.25 Hz (a) and **f** = 0.5 Hz (b)*

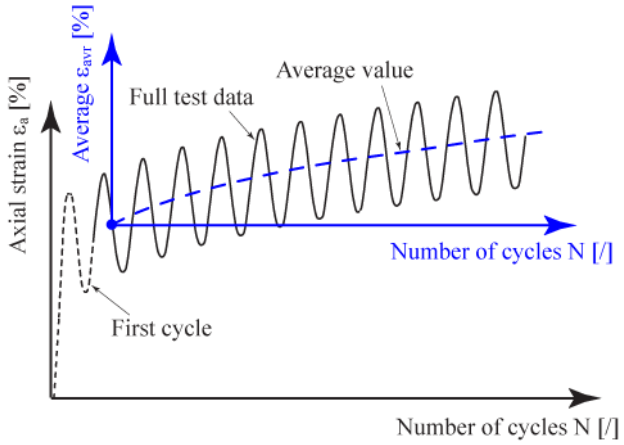

Fig. 6: Schematic diagram of the accumulated average axial strain

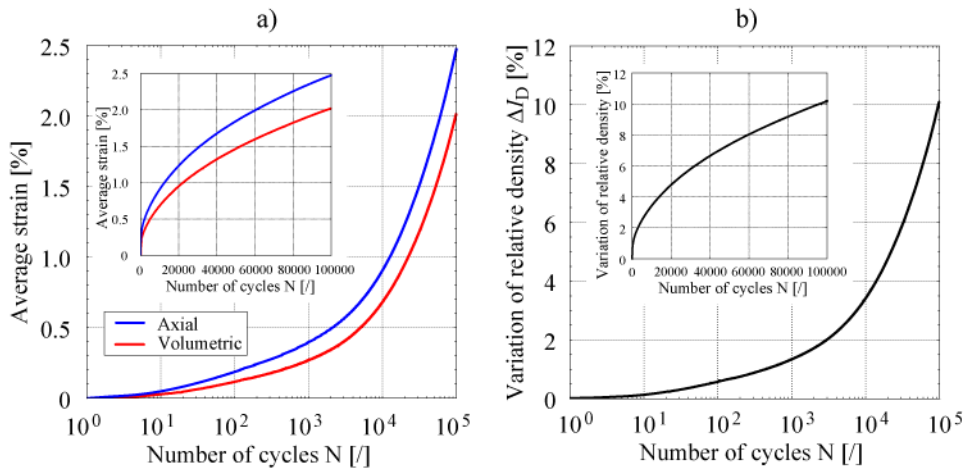

Fig. 7: Accumulated axial and volumetric strains (a) and accumulated relative density (b) for the test with $\boldsymbol{\sigma_{1,avr}}$*= 300 kPa,* $\boldsymbol{\sigma_{1,amp}}$*= 40 kPa,* $\boldsymbol{\sigma_c}$*=150 kPa and* $\boldsymbol{I_D = 60\%}$

3. DEM SIMULATIONS

Using DEM to simulate laboratory experiments requires the definition of a modelling strategy. In most cases, the exact conditions for realistic material properties and physical parameters (for example, the strain rate) of the experimental tests cannot be simulated due to low computational efficiency (Modenese, et al., 2012). In addition, the grain shape cannot be reproduced without a substantial increase in computational effort. Hence, spherical discrete elements are widely simulated with a resistance against particle rotation to mimic the effect of grain roughness when using DEM. Other strategies for reducing the computation time (and, thus, increasing the time step) are density scaling and approximated PSD. Once the modelling strategy has been selected, the contact parameters are calibrated to match the macroscopic behaviour of the idealized material with the behaviour of the real material. The following chapters thoroughly explain the modelling strategy, calibration and sensitivity analysis for the monotonic and cyclic triaxial tests that are simulated with DEM.

3.1 Simulation of monotonic triaxial tests

For replicating the mechanical behaviour of the soil that is obtained from our

laboratory campaigns of triaxial tests we used a cubic REV with periodic conditions. It represents the minimum volume (or minimum number of spheres) that statistically represents the behaviour of the whole material under a specified dispersion of the macroscopic response (namely, the minimum volume for which repeatability is realized). As pointed out by Kozicki et al. (Kozicki, et al., 2014), DEM triaxial tests can be performed with flexible membranes, periodic walls and rigid walls. Differences are generally observed for large strain values. The main advantage of using REV periodic boundary conditions is to avoid modelling the real boundary conditions of the test (plate and membrane) and, thus, the elimination of finite-size effects (Radjai & Dubois, 2011). Furthermore, for defining the REV, only a limited number of spheres are needed.

As the objective of this work is to use the DEM to execute many cycles in a short time, using a smaller REV with periodic boundary conditions is the most promising approach. The DEM simulations are conducted using an open-source code, namely, YADE (Šmilauer, 2015), which is based on a soft-particle approach. The granular material is modelled with spheres. Moreover, to accelerate the DEM calculation (by increasing the time step), the finer grain sizes are not considered in the model (see the red line in Fig. 8). The critical time step is based on the velocity of the P-wave propagation along the granular assembly (Šmilauer, 2015), which is directly proportional to the minimum radius, the rigidities (E) and the masses (ρ) of the spheres.

$$\Delta t_{cr} = \min R_i \sqrt{\frac{\rho_i}{E_i}}$$

The contact model that is utilized in this work is linearly elastic in the normal direction and linearly elastoplastic in the tangential direction. In addition, the rolling and twisting stiffnesses and their corresponding plastic limits are used to consider the little grain surface roughness (Šmilauer, 2015; Widuliński, et al., 2009). Using this model, 7 micromechanical parameters must be calibrated to control the contact law:

- the elastic modulus at contact E_c;
- Poisson's ratio at contact υ_c (ratio between shear and normal stiffness at

contact);

- the inter-particle friction angle φ_c;
- the dimensionless rolling stiffness coefficient β_r;
- the dimensionless twisting stiffness coefficient β_{tw};
- the plastic limit of the rolling behaviour α_r;
- the plastic limit of the twisting behaviour α_{tw}.

In the present calibration, the rolling and the twisting coefficients are assumed to have the same value; however, in practice, the rolling and twisting mechanisms are not the same (Zhang, et al., 2016). The reason is to avoid increasing the degree of difficulty during the calibration process.

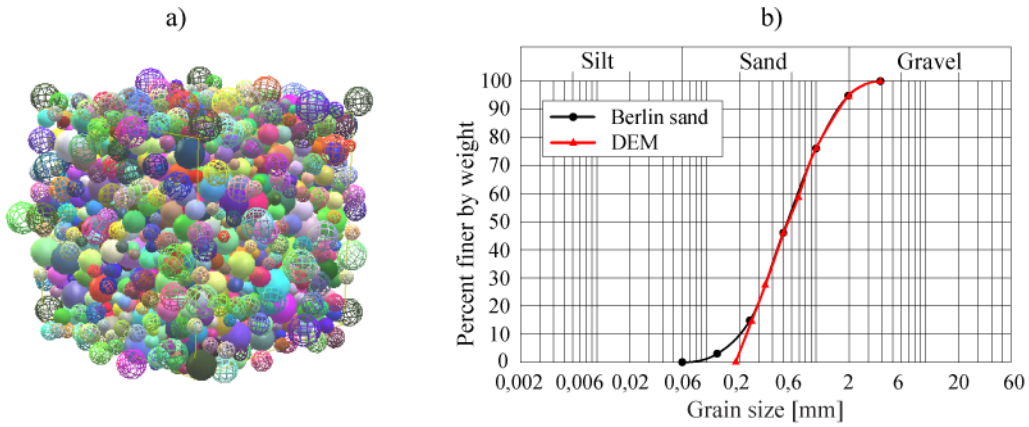

Fig. 8: Typical REV (a) and particle size distribution (b)

Due to the simplifying assumptions regarding the particle shape and the PSD, the real minimum and maximum void ratios of the Berlin Sand introduced earlier cannot be attained. Hence, in the calibration phase, only the relative densities of the triaxial experiments are matched.

In the numerical simulation, the minimum void ratio of e_{min}^{DEM} = 0.437 and the maximum void ratio of e_{max}^{DEM} = 0.788 are estimated for the DEM sample by setting the contact friction angle to 0° and 90°, respectively, and using a reference confining pressure of 100 kPa. Via the following expressions, the porosity of the

DEM sample is calculated based on the relative density I_D^{exp} that is used in the experimental test.

$$e = e_{max}^{DEM} - I_D^{exp}\left(e_{max}^{DEM} - e_{min}^{DEM}\right)$$

$$n = \frac{e}{1+e}$$

For the sample generation technique, a slightly modified version of the approach in (Aboul Hosn, et al., 2017) is used. An initially non-overlapping random cloud of spheres with a high contact friction angle ($\varphi_c = 90°$) is created in a larger cubic cell. Then, the spheres are shuffled by imposing random velocities. An isotropic confining pressure σ_c is applied until a stable sample is realized. Stability is considered to have been realized if the unbalanced force ratio is smaller than 10^{-3} (Aboul Hosn, et al., 2017). Via this approach, the maximum porosity of the sample is attained. Then, a steeper decrease of the contact friction angle is applied at each particle contact until the specified porosity has been reached. Then, the contact friction angle is set to the desired value. A strain rate of 10 %/s is used during the sample generation.

Once a stable periodic cell at the desired isotropic confining pressure and relative density has been created, the deviatoric phase begins. Hereafter, the term axial direction refers to the loading direction while the term lateral direction refers to the direction that is orthogonal to the previous one. The loading is conducted via a strain control mechanism by maintaining the axial rate at 7 %/s (which is higher than the experimental rate). The lateral stresses are kept constant at the prescribed confining pressure.

Preliminary numerical simulations that were conducted with glass beads (not presented here) demonstrate that a REV with 3000 spheres is sufficient for accurately modelling the mechanical behaviour (acceptable test repeatability and low computation time). In the next section, the uncertainty of the macroscopic behaviour will be investigated with respect to the sample size and the random distribution of spheres.

It is common practice to calibrate the contact parameters by fitting the macroscopic responses of a real triaxial test and a simulated triaxial test. The fitting is

conducted by tuning the contact parameters. The calibration should be performed under various boundary conditions. In the triaxial tests, various confining pressures must be considered. The calibration of only a single boundary condition could lead to a set of parameters that are not valid for other boundary conditions.

In the literature, various guidelines for calibrating the micromechanical parameters of a DEM sample have been proposed. Two main approaches can be followed: trial and error and a more automatic minimization strategy such as the use of an optimization approach, e.g., a surrogate model or a particle filter method (Cheng, et al., 2017). In the present study, the micromechanical parameters are tuned via trial and error and many numerical simulations with various combinations of the local parameters are conducted.

During the calibration, the same initial cloud of spheres is used to eliminate the possible effects on the macroscopic behaviour that are due to the random distribution of the spheres. The Young modulus and Poisson's ratio at the contact are related to the initial stiffness in the deviatoric plot and the initial contraction dilation behaviour in the volumetric plot and they are the first to be calibrated (Plassiard, et al., 2007).

Tab. 2: Calibrated DEM contact parameters for the Berlin Sand

Property	E_c [MPa]	υ_c [-]	β_r [-]	β_{tw} [-]	α_r [-]	α_{tw} [-]	φ_c [°]
Value	500	0.3	3.4	3.4	2.9	2.9	15.5

Tab. 2 lists the final contact parameters that were obtained via calibration and Fig. 9 plots the results of this calibration procedure. Satisfactory agreement between the experimental and numerical tests is realized according to the deviatoric graphs and the volumetric strain plots for up to 6% axial strain.

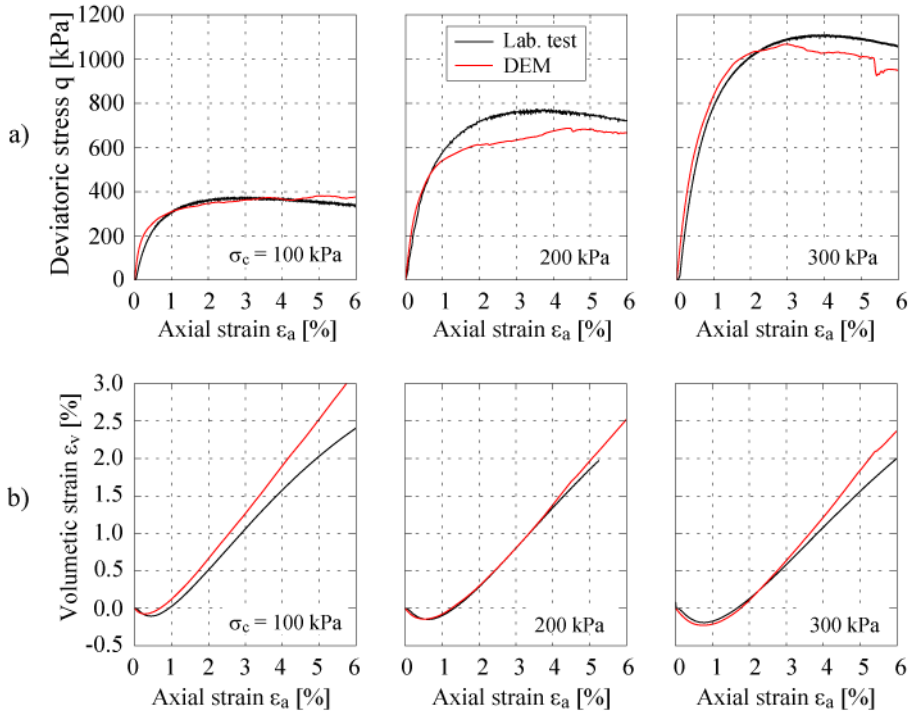

Fig. 9: Simulated (red lines) and experimental (black lines) monotonic triaxial test results for three confining pressures (100, 200 and 300 kPa) and I_D = 90%: deviatoric (a) and volumetric (b) plots

3.2 Effects of the sample size and the repeatability

Selecting the size of the REV and the test repeatability is always a dilemma. For granular material, due to the random distribution of the spheres that are obtained via the sample generation procedure, an REV is not unique. Due to the small number of spheres that are used in each generation of the periodic cell, the macroscopic response depends on the fabric. Moreover, the REV must be sufficiently large to exhibit a uniform distribution of the contact normal orientation and a homogeneous distribution of the force chain but sufficiently small for ensuring the computational efficiency (Guo, 2014).

Therefore, to investigate the effects of the REV size and the repeatability, the monotonic triaxial response is simulated with various numbers of spheres, namely, 500, 1000, 2000, 3000 and 4000, and three confining pressures, namely,

100, 200 and 300 kPa. For each combination of a confining pressure and a number of spheres, the Monte Carlo method is used to create 100 random spatial distributions of the granular assembly (100 fabrics). The same local parameters as in Tab.2 and a relative density of 90% are used in all the simulations. Hereafter, the size and repeatability of the REVs are analysed in terms of the macroscopic behaviour and properties.

To compare the tests with the three confining pressures, plots of the deviatoric ratio (deviatoric stress over the confining pressure) vs. the axial strain and the volumetric plots are presented in Fig. 10 and Fig. 11. For each number of spheres and confining pressure, the results of the 100 simulations are plotted together. The black line represents the experimental test response. Increasing the number of spheres reduces the influence of the sample size on the macroscopic response. Moreover, the dispersion of the curves is reduced by increasing the lateral confining pressure.

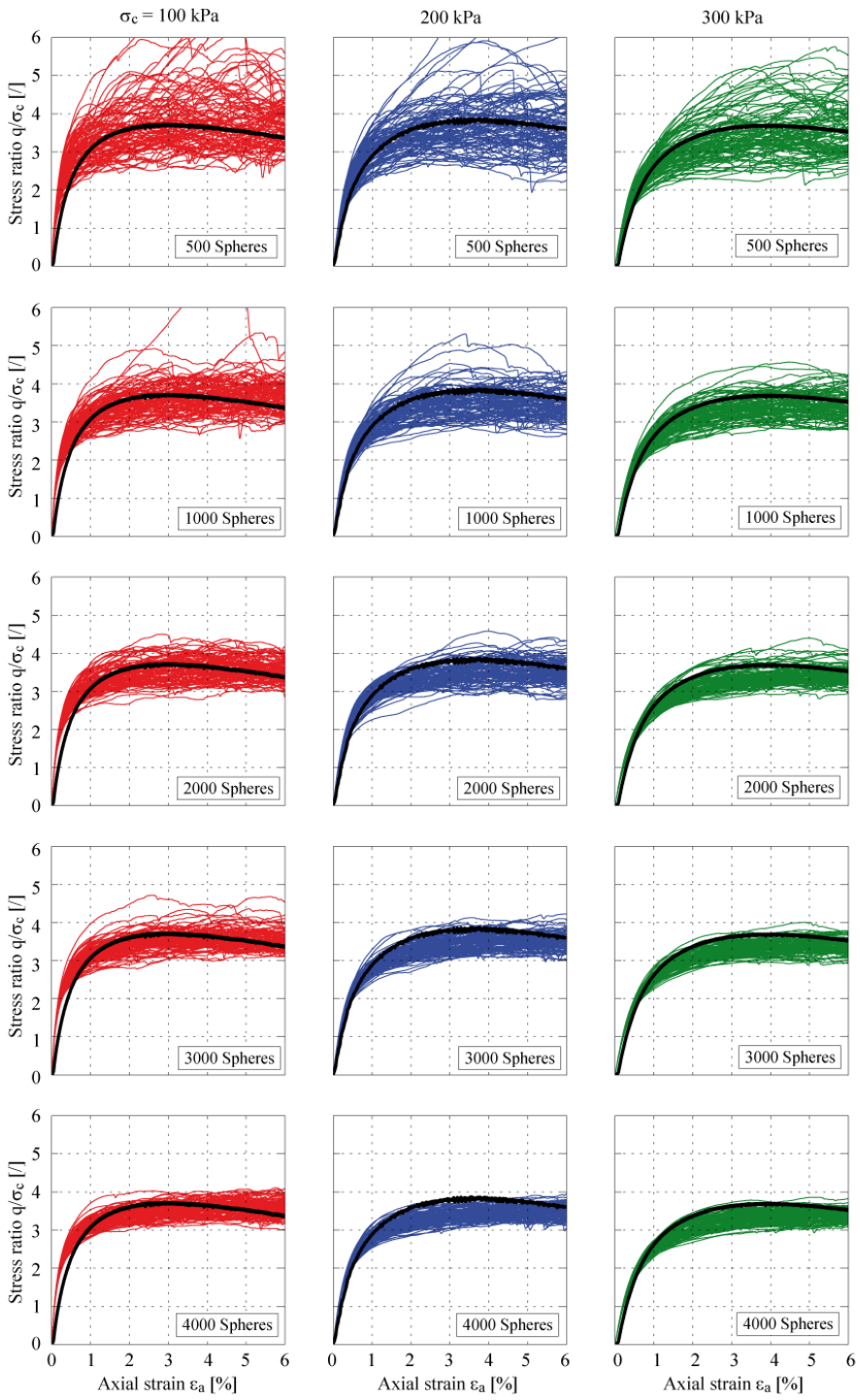

Fig. 10: Triaxial tests on periodic cells with various numbers of spheres and confining pressures: development of the deviatoric stress

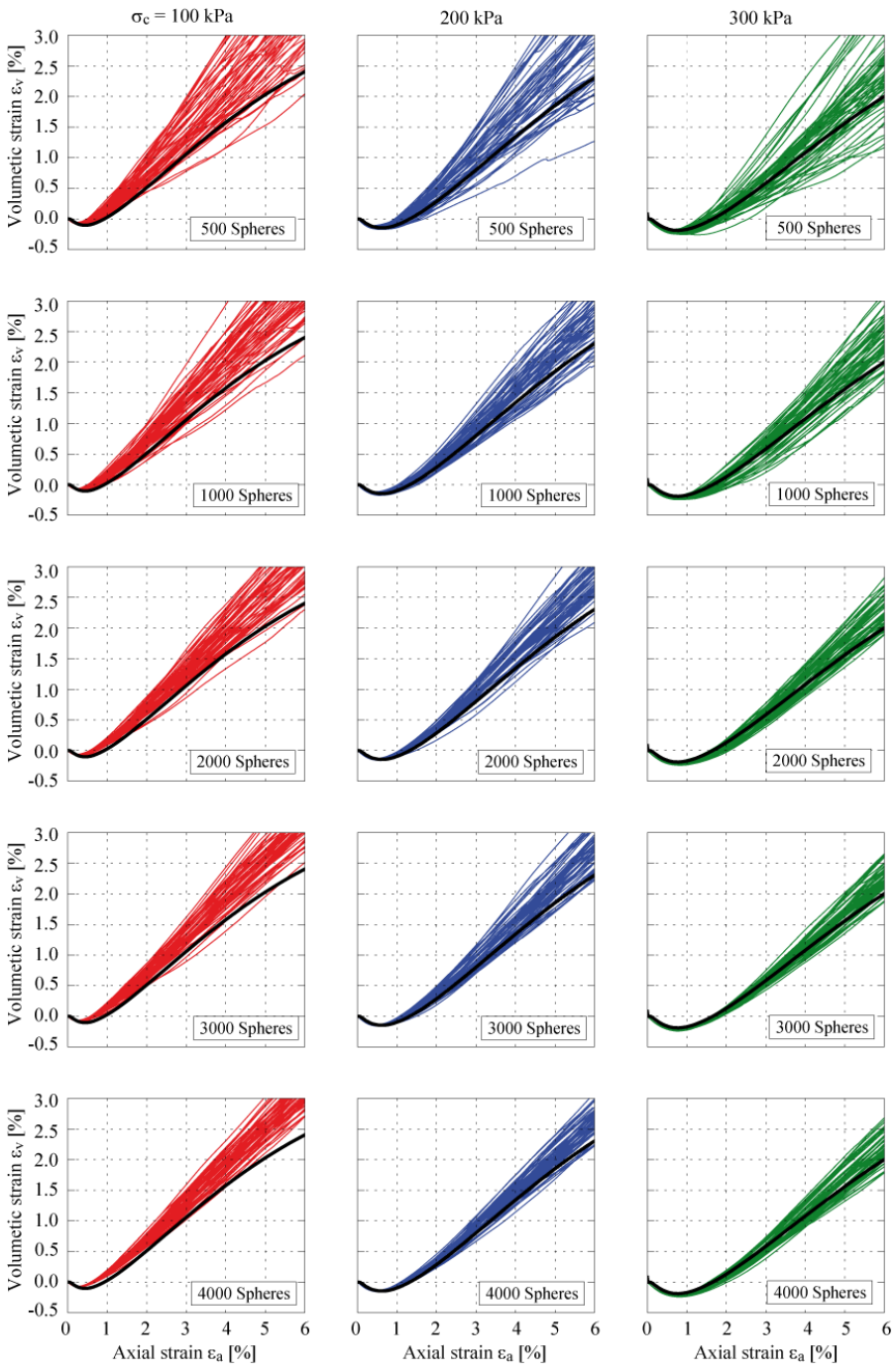

Fig. 11: Triaxial tests on periodic cells with various numbers of spheres and confining pressures: development of volumetric strain

Then, the effects of the sample size and the repeatability on the macroscopic properties are analysed. The Young's modulus E_{50} (measured at 50% of the peak stress), the Poisson's ratio ν, the dilatancy angle ψ and the peak η_{peak} and residual η_{res} deviatoric ratios are calculated for each simulation. To assess the uncertainty of these properties that is due to the initial random fabric distribution, the mean value and the coefficient of variation (CoV = the standard deviation over the mean value), which reflects the level of dispersion around the mean, are calculated using a set of 100 simulations for each number of spheres and confining pressure combination.

Tab. 3 summarizes the values. According to the CoVs for the various macroscopic quantities, increasing the number of spheres results in a decrease of the dispersion of the macroscopic response. Moreover, the higher the confining pressure, the higher the repeatability. The same trend with a lower standard deviation when increasing the number of spheres is identified in (Roux & Combeb, 2010). Fig. 12 is a visualization of Tab. 3 in which the CoV is plotted as a function of the number of spheres. For each confining pressure, the CoV curves stabilize at a plateau. The difference between 4000 and 3000 spheres is sufficiently small for 3000 spheres to yield acceptable repeatability in terms of accuracy. The minimal number of spheres is selected to minimize the computation time and is crucial for this type of study.

Tab. 3: Variation of the macroscopic mechanical parameters that were obtained from DEM triaxial simulations using various confining pressures and numbers of spheres

		500 Spheres		1000 Spheres		2000 Spheres		3000 Spheres		4000 Spheres	
σ_c	Values	Mean	CoV [%]	Mean	CoV [%]	Mean	CoV [%]	Mean	CoV [%]	Mean	CoV [%]
100 [kPa]	E_{50} [MPa]	89.1	29	92.9	17	97.8	10	99.6	9	99.7	8
	ψ [°]	15.7	16	15.2	13	14.4	11	14.4	9	14.4	7
	ν [-]	0.4	26	0.3	12	0.3	6	0.3	6	0.3	5
	η_{peak}	4.4	26	4.0	12	3.8	8	3.7	7	3.7	5
	η_{res}	3.9	29	3.7	13	3.5	8	3.5	7	3.6	5
200 [kPa]	E_{50} [MPa]	105.8	20	106.8	13	108.4	9	107.1	7	109.4	6
	ψ [°]	14.7	18	14.4	12	14.1	10	14.0	8	13.5	8
	ν [-]	0.3	15	0.3	9	0.3	7	0.3	5	0.3	4
	η_{peak}	4.1	19	3.7	11	3.7	8	3.6	6	3.6	4
	η_{res}	3.6	21	3.5	12	3.5	8	3.5	6	3.5	4
300 [kPa]	E_{50} [MPa]	112.4	16	113.9	11	114.2	7	115.0	6	115.0	6
	ψ [°]	14.0	21	13.5	15	13.3	9	13.1	8	12.7	9
	ν [-]	0.3	13	0.3	7	0.3	5	0.3	4	0.3	3
	η_{peak}	3.8	18	3.6	9	3.5	6	3.5	5	3.5	5
	η_{res}	3.6	19	3.4	10	3.4	7	3.4	5	3.4	5

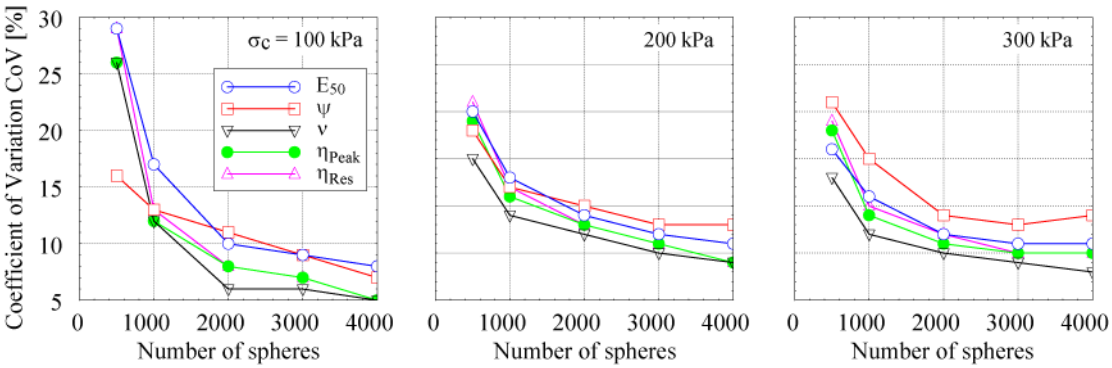

Fig. 12: CoV trends of the macroscopic mechanical parameters for each confining pressure and number of spheres

3.3 Performances of various relative densities

It would be desirable to obtain a unique set of contact parameters during the calibration phase that universally describes the behaviour of the granular material under various conditions (drained or undrained with varying confining pressures, relative densities and stress paths). The previous calibration is executed by considering various confining pressures but the same relative density of 90%. The experimental cyclic loading triaxial tests are conducted with a lower relative density, which is why it is important to ensure that the calibrated contact parameters can describe the monotonic responses of triaxial tests at lower relative densities. Moreover, a densification effect is expected during the cyclic loading phase.

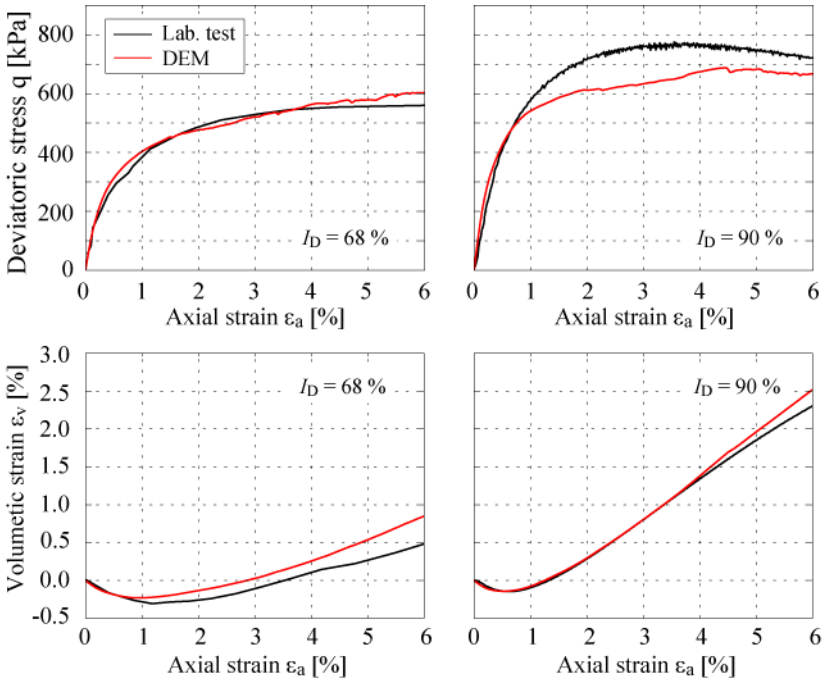

Fig. 13: Deviatoric and volumetric plots for two different relative densities with a confining pressure σ_c = 200 kPa

According to Fig. 13, for the medium dense sand of 68% relative density, the selected contact parameters describe the experimental macroscopic behaviour highly accurately. The red lines represent the DEM and the black lines the laboratory tests. The experimental and numerical confining pressure is maintained at 200 kPa.

4. CYCLIC LOADING SIMULATIONS

The DEM simulations of the cyclic triaxial tests consist of three phases: The first is the sample generation under an isotropic confining pressure, as in the experimental tests, of σ_c= 150 kPa using the same procedure as was described earlier (Chapter 2.1). The second phase is the application of the average load σ_{avr}. The sample is sheared monotonically by increasing the axial load up to $\sigma_{1,avr}$ =300 kPa, which corresponds to approximately $0.4 \cdot q_{max}$. This load is applied with a strain rate of 7 %/s.

The last phase is the regular cyclic load simulation. The cyclic simulations are

stress-controlled and the cyclic amplitude $\sigma_{1,amp}$ is defined as the difference between the maximum $\sigma_{1,max}$ (or minimum) stress and the average stress $\sigma_{1,avr}$. As in the experiments, the first cycle of the cyclic loading phase is applied sufficiently slowly (with a strain rate of 7 %/s) for avoiding a large deformation. Three tests with three cyclic loading amplitudes are performed with stress amplitudes $\sigma_{1,amp}$ of 20, 40 and 60 kPa. A periodic cell with 3000 spheres is used and as in the experimental tests a relative density of 60% are simulated.

The cyclic phase requires the selection of two inputs: the axial strain rate (v_z) and the non-local numerical damping. The experimental axial strain rate was presented previously and is a function of the cyclic amplitude and frequency. In DEM simulations, the objective is to execute many cycles in a reasonable amount of time. Therefore, a sufficiently high strain rate should be selected to accelerate the simulation. However, it should be sufficiently low for guaranteeing the quasi-static assumption (gradual sinusoidal change) to avoid inertial effects, which are expected if the loading is too fast. Hence, various strain rates are simulated from 10 %/s to 100 %/s (Fig. 14). It is interesting to see that there is a strain rate dependency to the accumulation of the deformation meaning that the different loading rate are influencing the contact chain distribution. To evaluate the quasi-static equilibrium in each time step, the dimensionless unbalanced force ratio is plotted (Fig. 15). The unbalanced force ratio is the ratio between the mean resultant particle unbalanced force and the mean contact force (Aboul Hosn, et al., 2017).

Therefore, in the following, the axial strain rate is selected as 50 %/s for the DEM simulations; this value is approximately 800 times the maximum experimental strain rate for the cyclic amplitude of 40 kPa and will ensure that results are obtained in a reasonable computation time and that a quasi-static behaviour is observed (the maximum unbalanced force ratio is approximately 3e-2, and its trend is not chaotic). In contrast to the experiments, in the DEM simulations the same axial strain rate is considered for all cyclic stress amplitudes.

As introduced previously, a numerical non-local numerical damping (Cundall & Strack, 1979; Šmilauer, 2015) is used, which aims at dissipating kinetic energy to decrease the dynamic forces between the spheres. Cyclic loading simulations

with samples that are composed of a few thousand spheres generate excessive chain buckling, thereby leading to a rapid increase in the deformation after a few hundred cycles. Increasing the numerical non-local numerical damping is beneficial for mitigating this problem. It is not clear if the need for a high damping is related to the small number of spheres that are used in the periodic cell. At this stage, it is not clear whether the calibration of the optimal axial strain rate and the damping value is a general approach or an approach that depends on the experimental set-up.

Fig. 16 compares the experimental and the simulated cyclic tests for the cyclic amplitudes of 20, 40 and 60 kPa. Satisfactory agreement regarding the accumulation of the average axial strain between the DEM and the experimental tests is realized with an axial strain rate of 50 %/s and a non-local numerical damping of 0.4. This relative high damping value is necessary to reach a high number of cycles and maintaining stability of the sample. This is necessary due to the small number of particles. The number of cycles that are executed is 10000. A periodic cell with only 3000 spheres can replicate the deformation behaviour of a cyclic triaxial test with millions of grains of sand in terms of monotonic behaviour (cf. Fig 9) and cyclic behaviour (cf. Fig 16). The rapid increase of deformation for the simulation with 40 kPa is due to buckling effect of large chain forces. The external load is carried out by few force chain and when the maximum strength is reached, then there is a sudden increase of deformation in the sample.

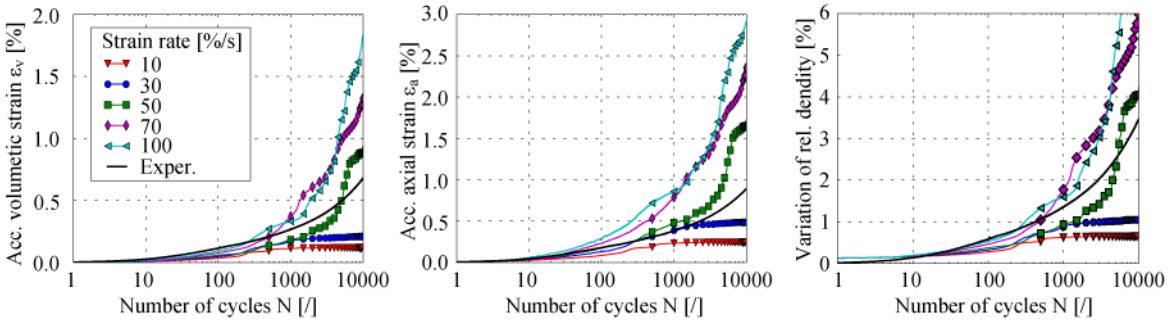

Fig. 14: Cyclic triaxial test results for various axial strain rates from 10 to 100 %/s (σ_c = 150 kPa, I_D = 60%, and $\sigma_{1,amp}$ = 40 kPa)

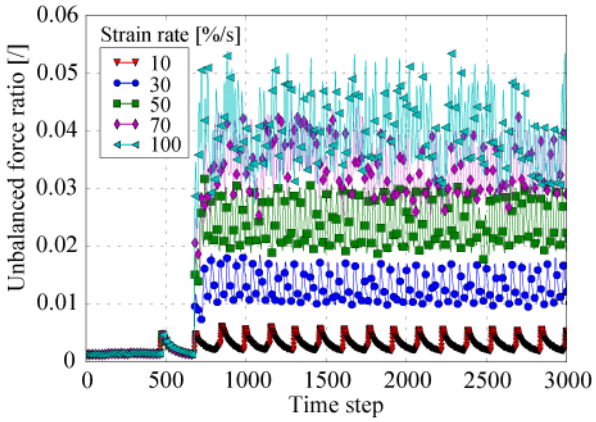

Fig. 15: Unbalanced force ratios for various axial strain rates from 10 to 100 %/s (σ_c = 150 kPa, I_D = 60%, and $\sigma_{1,amp}$ = 40 kPa)

The DEM curves show a higher variability regarding the macroscopic behaviour; this outcome is due to the small number of spheres that are used and the strong dependency on the force chain network. The DEM simulations slightly overestimate the accumulation of the axial strain. Regarding the volumetric strain, closer agreement is realized via underestimation of the radial strain by the DEM. Advantageously, the computation time is reduced to a few seconds per simulated cycle; hence, the DEM is a highly interesting tool for simulating many cycles.

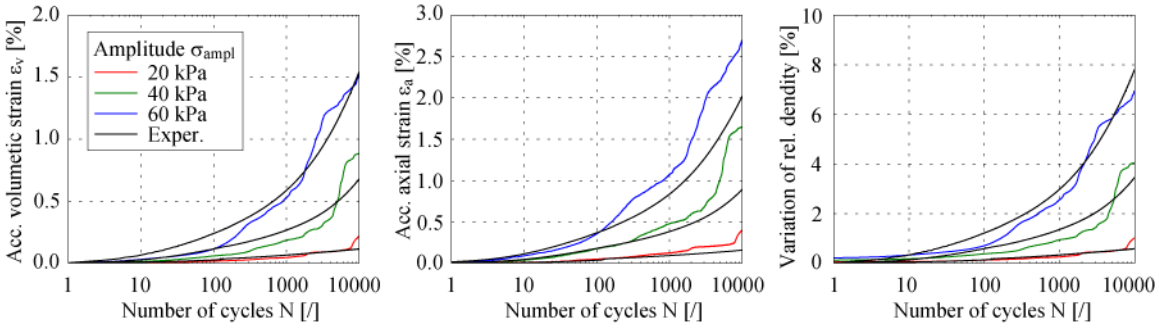

Fig. 16: Cyclic triaxial test results for various cyclic amplitudes (σ_c = 150 kPa, I_D = 60%, and $\sigma_{1,amp}$ = 20, 40, and 60 kPa)

5. ANALYSIS OF MICROSCOPIC CONTACT QUANTITIES

This chapter discusses the evolution of microscopic quantities such as the contact orientation and the force chain network and the results from post-cyclic monotonic behaviour. An REV with 30000 cycles and a cyclic amplitude of 40 kPa is considered. The REV has a confining pressure of σ_c= 150 kPa and a relative density of 60%. The computation time is a single day. The following figures compare the DEM simulation results with the experimental results. Overall, the DEM overestimates the accumulation of deformation in terms of the axial and volumetric strains (Fig. 17). At approximately 10000 and 30000 cycles, the accumulation of deformation reaches a very low rate of deformation (close to a plateau). This plateau is due to the stabilization of the force network in the sample, which can carry the external cyclic loading conditions elastically. Then, as the number of cycles is increased, a chain buckling occurs under a sudden increase of the accumulated deformation. Due to the simplifying assumptions regarding the spheres, the PSD difference and the small number of spheres, the chain buckling during cyclic loading is a highly important problem. The granular assembly is carrying the applied load by means of strong force chains propagating the stress through the sample. Due to the cyclic loading, the local failure of one of these chains can change the entire force distribution across the sample, which is accompanied by an increase in the permanent deformation (Hu , et al., 2010). Theoretically, larger samples will be less strongly influenced due to a higher redistribution of the force chains. Due to the small number of spheres, the use of non-local numerical damping to reduce the forces between the contacts can prevent a possible buckling of the chain.

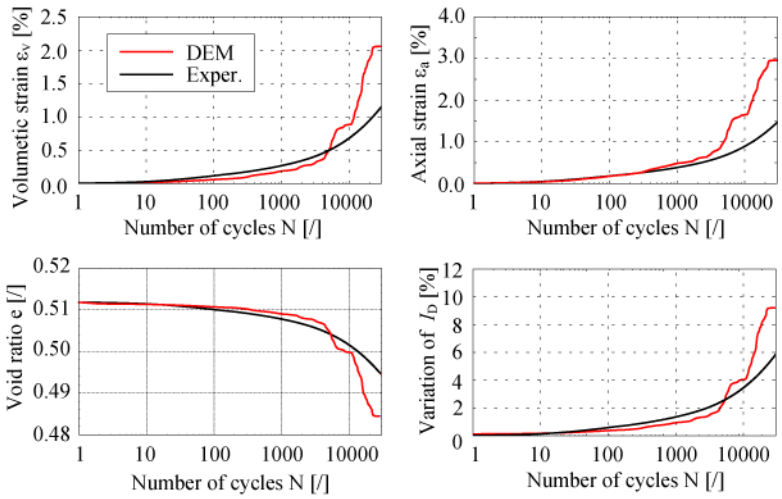

Fig. 17: Cyclic triaxial test results for $\sigma_{1,amp}$=40 kPa (σ_c= 150 kPa and I_D= 60%)

5.1 Contact orientation

To derive the distribution of the orientation of the contacts, a statistical analysis is conducted. During the cyclic loading test, various samples are saved at the minimum loading point and unloaded with a small strain rate until isotropic conditions are realized.

The contact points, the normal forces (perpendicular to the surface) and the shear forces (tangential to the surface) between each pair of spheres are saved in local coordinates. These contacts (their directions) are represented as projections on the surface of a unit sphere.

Then, the half-sphere is divided into a spherical grid and the number of contact points in each cell of the grid is counted. To account for the differences in dimension among the cells (smaller on the top and larger on the equator), the contact distribution function is calculated as follows:

$$P[\theta, \varphi] = \frac{N_c[\theta, \varphi]}{N_{max} * A[\theta, \varphi]}$$

where $N_c[\theta, \varphi]$ is the number of points in each spherical sector that is defined by $[\theta, \varphi]$, N_{max} is the total number of contact points and $A[\theta, \varphi]$ is the area of the spherical sector that is defined by $[\theta, \varphi]$. More contact points lead to a better

statistic of the distribution of the contacts. The contact distribution has been visualized by 2D spherical polar plots. The unit sphere is oriented along the Z-direction, which is the loading direction. Fig. 18 shows the density distribution of the contacts for the initial sample (prior cyclic loadings) and the isotropic unloaded sample after 30000 cycles. In triaxial loadings, the directions that are normal to the loading can be thought as a plane of isotropy. Therefore, no variation is expected by changing the polar coordinate (theta) and the variation of the contact density should be observable over the phi coordinate (from the equator to the pole). Hence, the density is an average between sectors with different values of theta and the same value of phi.

In the initial state (Fig. 18, upper left), a uniform variation of the contact distribution is observed. As expected, the isotropic consolidation leads to a uniform distribution of the normal contacts.

After 30000 cycles (Fig. 18, upper right), the density of the contacts is reduced at the pole (centre of the spherical plot) and increased at the equator (circumference of the spherical plot). For the pole and equator definition see Fig. 18, below.

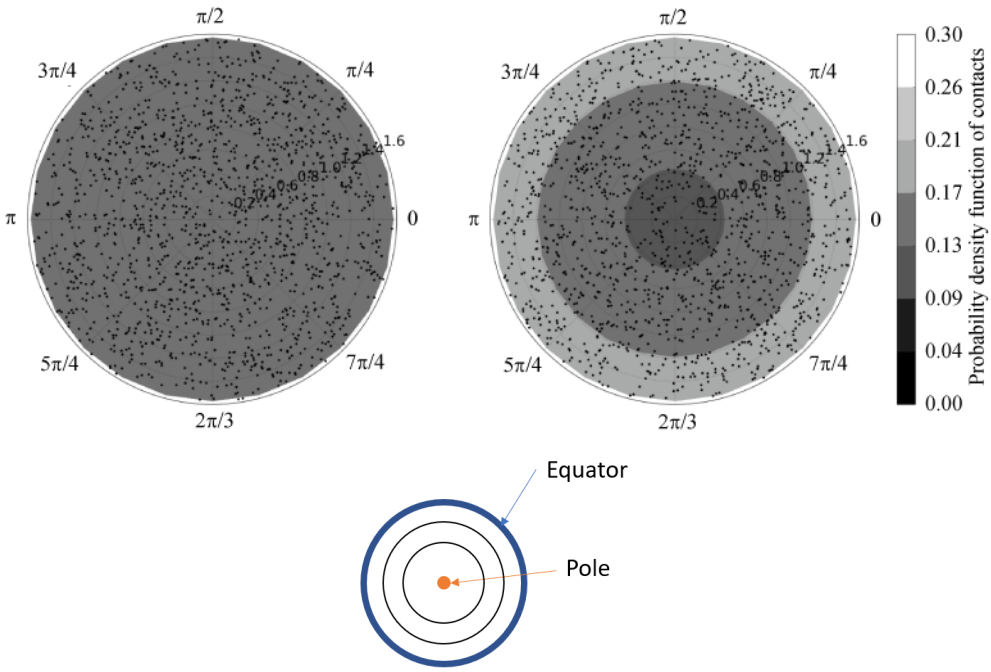

Fig. 18: Distributions of the normal forces at the initial state (upper left) and after 30000 cycles (upper right) (Z-oriented). Below, explanation of pole and equator.

5.2 Contact force Network

The magnitudes and the orientations of the normal forces at contact are plotted in Fig. 19. The normal forces are normalized by the maximum normal force that is experienced after 30000 cycles, interpolated over the spherical grid and plotted as a 2D spherical polar graph.

A uniform distribution of the normal forces is observed initially after the sample generation via isotropic compression (Fig. 19, left). The 30000 loading cycles lead to a concentration of forces at the pole and a decrease of the force magnitudes at the equator. Hence, large vertical chains are forming over the sample and aligning themselves with the loading direction, whereas smaller chains are horizontally distributed. Then, fewer contacts that are aligned along z are responsible for carrying the z-loading of the granular assembly (strong chain network). Most of the contacts are distributed along the equator but with a smaller normal force (weak network of forces), which is perpendicular to the loading direction. The weak network is also important since it supports the stronger

force chains. The same phenomenon is observed when plotting the shear forces at the contacts (Fig. 20). Initially, a uniform distribution is observed, whereas later the higher scalar values are concentrated around the pole.

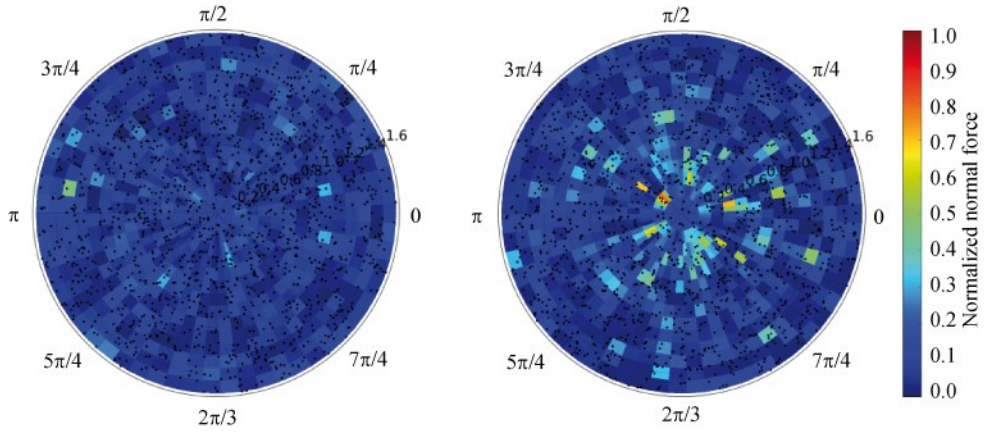

Fig. 19: Distributions of the normal forces at the initial state (left) and after 30000 cycles (right) (Z-oriented)

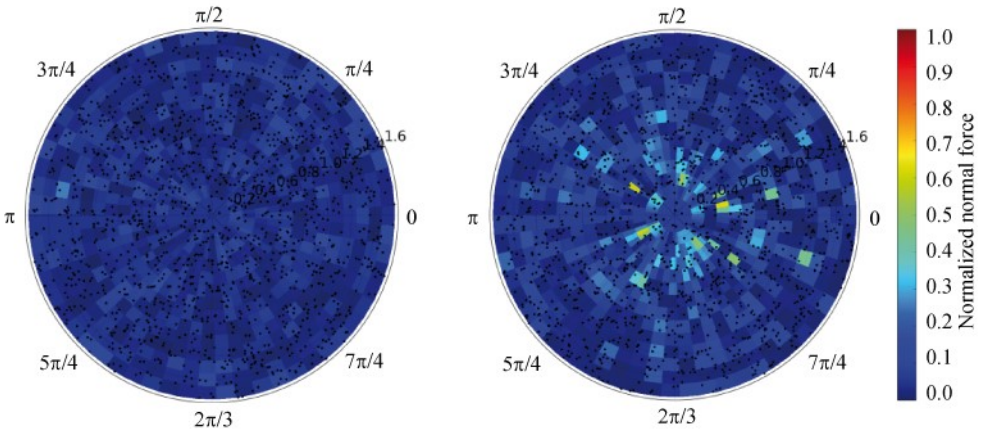

Fig. 20: Distributions of the shear forces at the initial state (left) and after 30000 cycles (right) (Z-oriented).

5.3 Post-cyclic behaviour

The drained monotonic response of post-cyclic loaded soil is important for geotechnical structures such as retaining walls, integral bridges and offshore structures. Here, a stiffening of the soil response may lead to substantially higher lateral stresses (which are important for integral bridges) or a stiffer foundation response, which may result in resonance problems. In this prospective, the use of DEM enables a post-cyclic assessment of the granular material. An REV with 30000 cycles and a cyclic amplitude of 40 kPa is considered. The REV has a confining pressure of σ_c= 150 kPa and a relative density of 60%. The DEM sample is saved at various cycles and unloaded at an isotropic state of 150 kPa. The post-cyclic behaviour is investigated by conducting monotonic triaxial tests. The deviatoric stress and volumetric strain plots are presented in Fig. 21. Due to the effects of the cyclic loading, the granular assembly is densifying and rearranging the contact network of spheres in terms of the contact orientation and the force chain distribution. Increasing the number of cycles leads to a stiffer response with a higher shear strength: a higher deviatoric peak is observed in Fig. 21 left and an increase in the dilatancy is observed in Fig. 21 right. The curve labelled "initial" is the monotonic shearing of the sample before the cyclic phase.

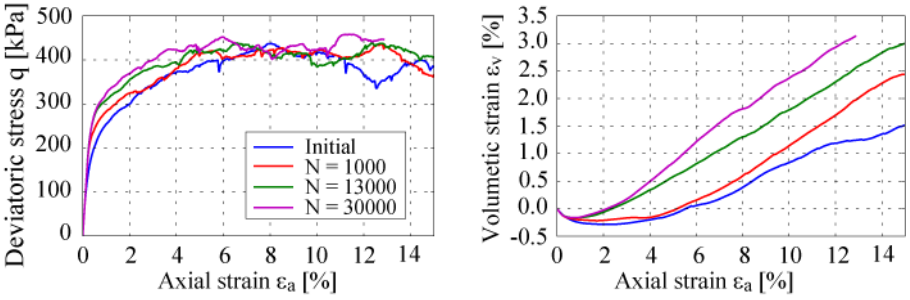

Fig. 21: Post-cyclic behaviour after various numbers of cycles: development of deviatoric stress and volumetric strain

6. EXPLICIT METHOD USING CONTOUR DIAGRAMS FOR CYCLIC LOADING

This section first shows the validation of the explicit method implemented to

predict the accumulation of permanent strain due to cyclic loads. The validation is carried out with a full-scale cyclic loading test on a gravity-based foundation. Secondly, a practical application of the DEM with the explicit method is shown. DEM is used to create the cyclic contour diagram for the Berlin sand and a prediction of the residual tilting of a typical gravity-based foundation subjected to a design storm event is presented.

6.1 Introduction to the innovative explicit method using contour diagrams

An innovative explicit method (Zorzi, et al., 2018) is developed to predict the accumulated foundation displacement that results from cyclic lateral loading. The explicit method integrates the cyclic contour diagram of the permanent strain, which is typically derived from a large quantity of cyclic laboratory test results, into the finite element (FE) software PLAXIS via a remote scripting interface. One of the advantages of this concept is that no sophisticated constitutive model for soil is required. An elasto-plastic model is sufficient for this purpose. The accumulated strain will be calculated in form of a degradation of the stiffness.

Three-dimensional FE modelling of foundations is used to assess a realistic stress distribution in the soil domain. The effect of cyclic degradation is considered by reducing the elastic shear modulus of the soil in a cluster-wise division in the finite element mesh. Each cluster in the FE model is subjected to an individual degradation of the soil stiffness, hence accumulation of permanent deformation is based on the local stress distribution. This stiffness degradation method (Achmus, et al., 2007) is based on the accumulated strain extracted from the cyclic contour diagram framework.

A cyclic contour diagram consists of a 3D interpolation of the permanent axial strain, which is typically obtained by conducting a few tests. The extraction of the accumulated strain, used for the degradation of the stiffness, is in function of the average stress ratio (ASR; the average stress divided by the confining pressure), the cyclic stress ratio (CSR; the cyclic stress amplitude divided by the confining pressure) and the number of cycles. The cyclic contour diagrams are relative density specific, each diagram represents the accumulation of

deformation at different stress levels for one void ratio. An example is presented in Fig. 24, where the colour points and their interpolations in the two slices represent the strain surfaces at two values of the average stress ratio (Zorzi, et al., 2019).

For the calibration of these diagrams, the results of the experimental or numerical tests can be used. Hereby, the results of the DEM simulations are a simple option in comparison to the expensive and time consuming laboratory tests. In case of using DEM, only some standard experimental results for the calibration of the material parameters are required. The contour diagrams based from DEM contains different uncertainties related to the numerical simulations. However, they can be seen as a simplified solution. For the comprehensive investigations, contour diagrams from laboratory tests are recommended. In the following calculations the contour diagram from the experimental test results will be used for the validation (full-scale cyclic test, section 6.2). In the second example, the diagram generated from the DEM results for Berlin sand will be used (section 6.3).

In this explicit method, a simple conventional soil model is necessary for implementing the soil stiffness degradation. In this study, the Mohr–Coulomb soil model will be used. This method is a simplification of the real behaviour of the soil and aims solely on predicting the accumulation of permanent strain after a certain number of load cycles.

6.2 Validation with a full-scale cyclic test

This section introduces the validation of the explicit method with a cyclic load full-scale test for a gravity-based foundation (GBF) developed by Ed. Züblin AG – STRABAG (Ed. Züblin AG, 2013). Most of the information are extracted from the final report of the research project (Ed. Züblin AG, 2013). The 3D model of the foundation is shown in Fig. 22. The dimensions of the foundation as well as the installation process are described by Sedlacek et al. (Sedlacek, et al., 2012).

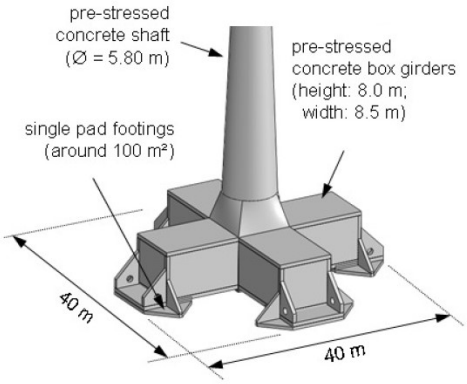

Fig. 22: 3D view of the foundation (Sedlacek, et al., 2012)

After the installation, the foundation is subjected to the cyclic load program shown in Fig. 23a (Zachert, et al., 2014). It consists of two phases: pre-loading and storm event. The first phase is characterized by different regular packages at relatively low stress cycles (packages green, blue and red). This initial phase has a total number of cycles of circa 312000 cycles. The second phase (grey shading packages Fig. 23a) is the storm event load which is characterized by regular loading packages with increasing magnitude of stress cycles. The total number of cycles considered in the storm event is circa 13500. In the FE simulations, the loading condition is reorganized and simplified as in Fig. 23. The pre-loading phase is reorganized in three parcels (named 1-2-3). The simulated storm is grouped in 4 parcels (from parcel 4 to 8).

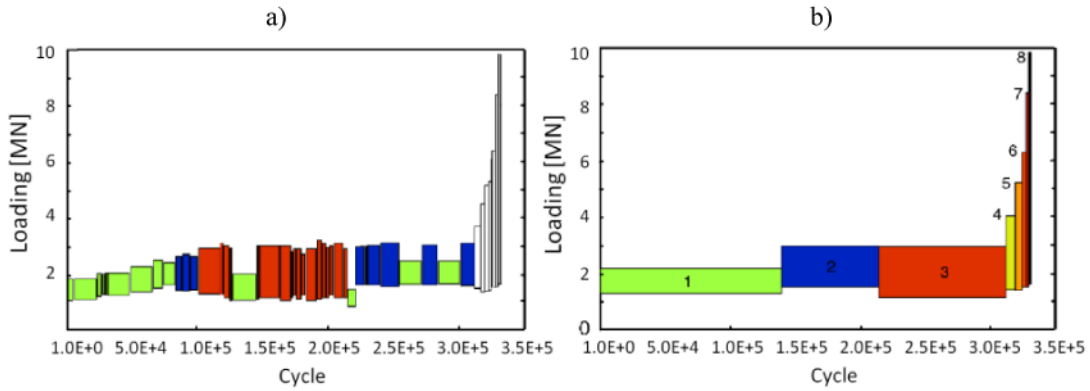

Fig. 23: Parcel organization: (a) tested parcel, (b) re-organized parcels, according to Zachert et al. (Zachert, et al., 2014)

The behaviour of the soil-structure interaction during the cyclic loading program was extensively monitored (pore pressure sensors, foundation settlement, stress distribution and structural tilting). For the validation of the innovative explicit method, the monitored structural tilt is considered and presented hereafter along with the FE results. The inclination of the structure was measured by means of an inclinometer chain installed on the wall of the concrete shaft.

For the numerical investigation, the soil profile was divided in to three layers based on the cone resistant obtained from the CPTs and the classification of the soil. The characteristic soil mechanical parameters of the layers are listed in the Tab. 4. The evaluation of the parameters in the table, the relative densities D_r, the friction angles φ, the reference stiffness modulus for unloading and reloading $E_{ref,ur}$, the increment of the stiffness E_{inc} and the Poisson ratio ν were presented in (Zorzi, submitted, 2020) in details. In the explicit calculation step, the accumulated strain will be considered only in the first two layers. For the third layer, it is assumed that the soil is deep enough to behave elastically and not accumulating deformation during cyclic loading.

Tab. 4: Summary of the soil design parameters for cyclic loading

Layer	**Depth [m]**	**Soil type**	$\boldsymbol{D_r}$ **[%]**	$\boldsymbol{\varphi}$ **[°]**	$\boldsymbol{E_{ref,ur}}$ $[\boldsymbol{MPa}]$	$\boldsymbol{E_{inc}}$ **[MPa/m]**	⚜ **[/]**
1	0 -19	Fine - medium sand	70	38	30	2	0.2
2	19 – 26	Sand - fine gravel	90	43	105	5	0.2
3	26 - ∞	Medium coarse sand	80	42	80	5	0.2

For the explicit calculation, two contour diagrams for the first two layers were created (Fig. 24). The dotted colour lines in Fig. 24 represent different slices of the 3D matrix for the layer 1 and 2. The diagrams were calibrated with the

undrained simple shear tests conducted with the two representative sands for layer 1 an 2. The colours are related to different strain surfaces of the permanent shear strain γ_N obtained from the initial interpolation. Details of this procedure are presented in (Zorzi, submitted, 2020).

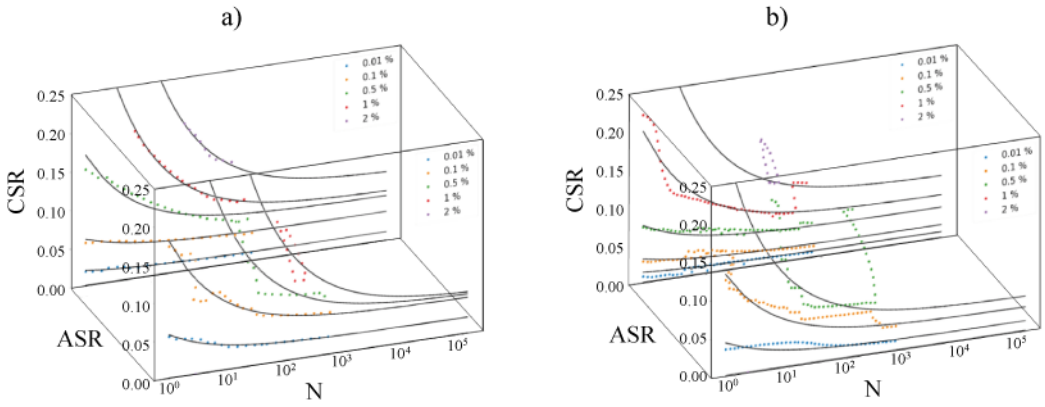

Fig. 24: Cyclic contour diagrams for permanent strain accumulation for layer 1 (a) and layer 2 (b)

Regarding the 3D FE model, the soil domain is modelled as three layers, as found at the ground investigation. The dimension of the soil domain is large enough to avoid the influence of the boundary. The soil domain is divided in different cylindrical sectors (soil clusters). The division is characterized by three discretization: vertical, radial and circular. The soil layers 1 and 2 are both vertically divided in three clusters. The radial and circular divisions are generated in order to fit the feet edges of the foundation and are shown in Fig. 25. No clusters are considered in the layer 3 assuming that most of the deformation due to cyclic loading occurs in the two upper layers.

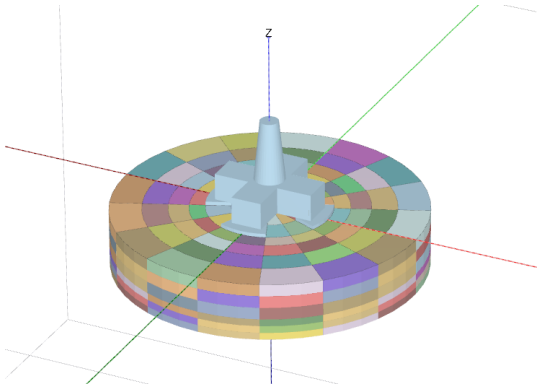

Fig. 25: Cluster division, centre part of the numerical model

In order to replicate the experimental conditions as close as possible, the foundation is modelled with the same dimensions as in the full-scale test. In the numerical model, the shape of the four feet is a cylindrical sector in order to fit with the circular cluster division. The foot area of 100 m^2 is kept the same. The foundation is modelled as a weightless rigid body. On each foot a surface load of 256 kN/m^2 is applied to account for the weight of the structure. The average and cyclic amplitude loads are applied by means of a point load at the top of the cone shaft at z = 30 m. The point load features a vertical and horizontal component which are derived from the decomposition of the experimental force applied at an angle of 60° from the vertical axis. In the numerical model, the water level is set 5 meters over the soil domain.

The predicted tilting in FE of the structure is evaluated as differential settlement between the opposite plates. Considering the drained assumption, a good agreement of the tilting is predicted with the explicit method (Fig. 26).

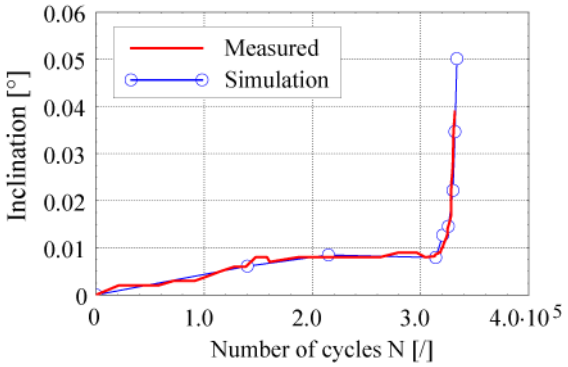

Fig. 26: Structural tilting: measured and predicted

6.3 A practical application of DEM for the contour diagrams

The previous section shows that the explicit method is a simple but reliable method which can be used for predicting the residual tilting of a structure subjected to regular cyclic loads. The key point is to obtain a reliable contour diagram. For this reason, various regular cyclic loading packages must be applied to the investigated soil at various stress levels (average and cyclic stress), various drainage conditions, various densities and sometimes a very high number of cycles. For these conditions, an extensive laboratory test campaign is required and not practical leading to the introduction of different source of uncertainties.

The DEM can be now used in place of the experimental cyclic laboratory tests to generate the cyclic contour diagram for the design of offshore structures that are subjected to cyclic lateral loads. Previously, the potential of the REV for simulating many cycles in a short computation time was demonstrated.

To construct the contour diagram, various drained cyclic triaxial tests are simulated with DEM under various stress averages and stress amplitudes. The stopping criterion is the completion of 5000 cycles (which is higher than the maximum number of cycles of the storm event). The same initial REV package is considered in all the simulations. A 60% relative density and a confining pressure of 150 kPa are adopted. Thirty-five simulations are performed with various combinations of the average stress ratio (ASR) and the cyclic stress ratio (CSR). The ASR is varied from 0.1 to 1, while the CSR is varied from 0.07 to 0.6. Considering all the cyclic simulations, the axial strains accumulated at the end of

each cycle are assembled and interpolated into a 3D matrix. Fig. 27 shows two slices (CSR vs. the number of cycles) of the matrix for the ASRs of 0.4 (a) and 0.8 (b). The coloured lines represent the permanent axial strain surfaces. The assembled 3D matrix properly represents the trends of the strain surfaces as the numbers of cycles and stress levels are varied. In the present case, the interpolation of a function for various strain levels is not considered (Zorzi, et al., 2019).

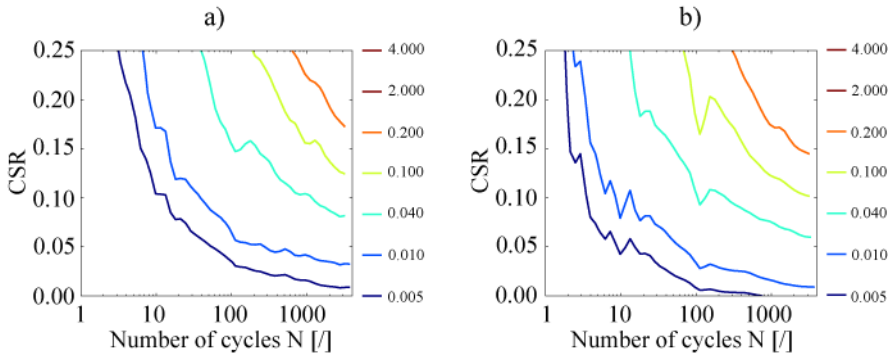

Fig. 27: Accumulated axial strain in two slices of the 3D cyclic contour diagram: a) ASR = 0.4 and b) ASR = 0.8

To demonstrate the applicability of the DEM in the aforementioned explicit method, the accumulated displacement of an offshore gravity-based foundation that is subjected to a substantial storm event is simulated.

In this case study, a uniform soil profile of Berlin sand with a relative density of 60% is employed in the analysis. The soil parameters that are used for the Mohr-Coulomb constitutive model in FEM are listed in Tab. 5 and are calibrated against a drained monotonic triaxial test that is performed with the DEM. In the monotonic test, a confining pressure of 150 kPa and a relative density of 60% are selected.

Tab. 5: Soil model parameters

Soil parameter	E [MN/m²]	ν [-]	φ [°]	ψ [°]	γ_{sat} [kN/m³]	γ_{Unsat} [kN/m³]

Value	42	0.3	35	0	19	9

The substructure consists of a conical section with a lower diameter of 50 m and a height of 23 m. A constant vertical force of 100 MN is applied to account for the weight of the foundation and the superstructure. The structure is modelled as a rigid body and the reference point for the load application (force and rotation) is the mudline.

The substantial storm event is composed of 5 regular loading packages with a horizontal force (average and maximum components), a moment (average and maximum components) and a specified number of cycles. The packages are applied in ascending order. The loading parcels are summarized in Tab. 6. H_{avr} is the average horizontal force at mudline, H_{max} is the maximum horizontal force at mudline and M_{avr} and M_{max} are the average and maximum overturning moment at mudline, respectively. The frequency of the cyclic loading does not have an effect on the FEM calculation.

Tab. 6: Loading parcel programme

Loading Parcel	$\mathbf{H_{avr}}$ [**kN**]	$\mathbf{H_{max}}$ [**kN**]	$\mathbf{M_{avr}}$ [**kNm**]	$\mathbf{M_{max}}$ [**kNm**]	Number of Cycles
1	3000	4500	90000	150000	4000
2	6000	9000	150000	255000	3100
3	9000	15000	210000	345000	2100
4	12000	21000	240000	390000	1120
5	15000	25500	270000	435000	250

The 3D matrix of the cyclic contour diagram is coupled with FEM. Regarding the cluster division in the soil domain, a large stress variation is likely to occur

close to the foundation; therefore, smaller clusters are considered. Then, the soil is divided into larger clusters that are further away from the structure to reduce the computation time. Fig. 28 shows the considered cluster division. A soil material is assigned to each cluster; hence, the clusters are represented with various colours. The total box of the soil model is a cube with an edge of 180 m. A mean water level of 30 m is assumed in the case study.

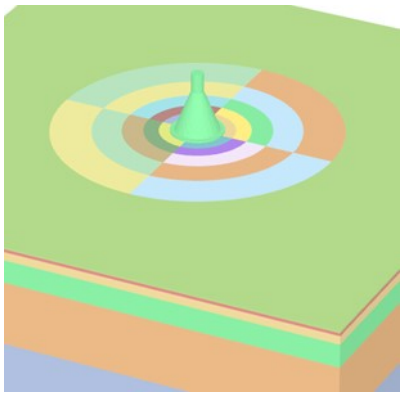

Fig. 28: Cluster division of the soil domain near the foundation

For each simulated parcel in Tab. 6, the accumulation of deformation in the soil is explicitly predicted by applying three different phases (Zorzi, et al., 2018). The first phase is characterized by the application of the average external loads (horizontal force and moment) and the calculation of the ASR for each cluster. In the next phase, the average loads are increased by adding the cyclic amplitude and the CSR is calculated for each cluster. Based on the ASRs, CSRs and number of cycles for the simulated parcel, the accumulated axial strains are extracted from the cyclic contour diagram shown in Fig. 27. The extracted strains are then used for degrading the stiffness in each cluster. The final phase is the application of the average external loads with the degraded stiffness in each cluster. The change in the stiffness modulus reflects the accumulated deformations at the end of the cyclic loading. The strain history resulting from the application of various parcels in Tab. 6 is taken into account by adopting the equivalent number of cycles method.

The following figures present the output of the explicit method. Fig. 29 shows the tilting of the foundation at the end of each loading parcel along the loading

direction. For this practical application, the considered foundation experiences a rotation of circa 0.055° for the simulated storm event. Fig. 30 shows the total displacement contour plots after the installation (left) and at the end of the last loading package (right). In the present case study, the accumulation of deformation after the simulated storm event is noticeable until a depth of approximately 0.2 times the diameter of the foundation.

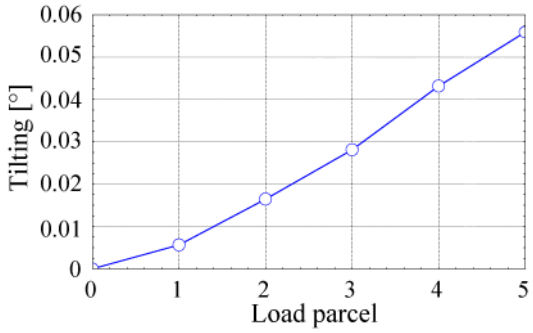

Fig. 29: Tilting of the foundation at the end of each parcel

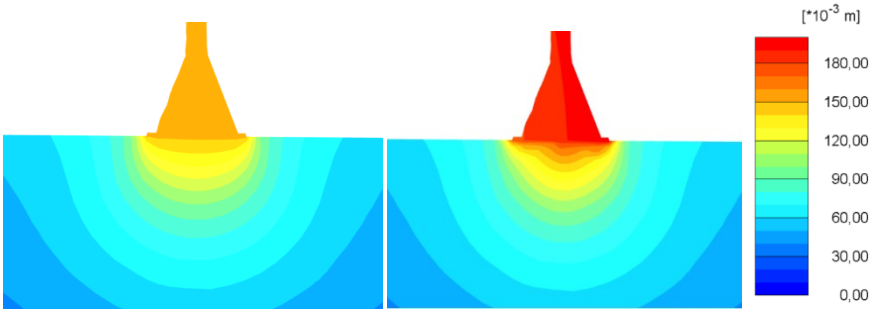

Fig. 30: Total displacement close to the foundation: after installation (left) and at the end of the last loading parcel (right)

7. CONCLUSION AND FUTURE DEVELOPMENTS

This research represents a first step towards a highly promising approach for integrating simple laboratory tests with DEM simulations into FEM modelling, which is used to predict the behaviour of soil-structure interactions under long-term cyclic loading. In the first part of the study, the possibility of using DEM

for modelling of the cyclic element test is investigated. The simulation of the triaxial test with DEM, the following knowledge can be observed:

- Simulations of Berlin sand on monotonic triaxial tests with different confining pressure and initial densities are carried out. The number of spheres has a significant effect on the repeatability of the simulations. Increasing the number of spheres reduces the influence of the sample size on the macroscopic response. The dispersion of the curves is reduced by increasing the lateral confining pressure.
- Variation of the macroscopic mechanical parameters depending on the number of spheres is investigated. A REV with 3000 spheres is sufficient for Berlin sand.
- The results of the cyclic test with for different cyclic amplitudes show a good agreement with the experimental tests.
- The strain rate and the non-local numerical damping have a significant influence on the behaviour on the cyclic test. An excessive buckling of the chain forces between the particles leads to a very large accumulation of defomration. A high damping parameter is needed due to the small number of particles used in the REV in order to reach a high number of cycles.
- The post cyclic behaviour is investigated. Increasing the number of cycles leads to a stiffer response with a higher shear strength. The soil behaves more dilatant.

In the second part, the explicit method for predicting the accumulation of permanent deformation of the soil due to cyclic loading is presented. Two practical applications are successfully demonstrated for the design of a cyclic lateral loaded offshore gravity-based foundation in which the cyclic contour diagrams are adopted. The following conclusions can be considered:

- The validation of the explicit method with a full-scale test is presented and a good agreement in the prediction of the permanent rotation is achieved.
- The contour diagram can be generated using the results of experimental

tests or DEM simulations.

- Several load packages with different amplitude, average values and number of cycles can be applied in form of loading parcels.

The study showed that DEM and FEM explicit calculation method using contour diagram has a high potential for simulation of boundary condition problem under long-term cyclic loading. However, several shortcomings remain in various aspects. For the improvement of the method further in-depth studies will be necessary in the future. A few points are listed below:

- Influence of different parameters such as confining pressure, initial void ratio, preloading must be investigated.
- The random distribution of the initial particle package has a significant influence on the repeatability of the simulation.
- The method should be investigated for different grain sizes.
- The roles of the strain rate and the non-local numerical damping must be further investigated.
- The contour diagram is density specific. For different initial densities, several diagrams are required.
- By the calculation with the contour diagram, the density is assumed as constant. During the cyclic loading, the density of soil can change. This must be considered in the calculation.
- The time loading history have an important role in the cyclic behaviour. For the boundary condition problem with different load packages, it must be considered by the generation of the contour diagram.
- The explicit method does not aim to predict the change in stiffness nor in relative density but just in the accumulation of deformation of the soil.

8. ACKNOWLEDGEMENTS

This research is part of the Innovation and Networking for Fatigue and Reliability Analysis of Structures - Training for Assessment of Risk (INFRASTAR)

project. This project has received funding from the European Union's Horizon 2020 research and innovation programme under the Marie Skłodowska-Curie grant agreement No. 676139.

REFERENCE

[1] A. Niemunis, T. Wichtmann and T. Triantafyllidis, "A high-cycle accumulation model for sand," Computers and Geotechnics, vol. 32, no. 4, pp. 245-263, 2005.

[2] N. Allotey and M. El Naggar, "Cyclic soil degradation/hardening models: a critique," in Proc. of 16th International Conference of Soil Mechanics and Geotechnical Engineering, Rotterdam, 2005.

[3] K. Andersen, "Cyclic soil parameters for offshore foundation design," in The 3rd McClelland Lecture. Frontiers in Offshore Geotechnics III, ISFOG'2015, London, 2015.

[4] G. Zorzi, T. Richter, F. Kirsch, A. Augustesen, M. Ostergaard and S. Sorensen, "Explicit Method to Account for Cyclic Degradation of Offshore Wind Turbine Foundations Using Cyclic Interaction Diagrams," in The 28th International Ocean and Polar Engineering Conference, International Society of Offshore and Polar Engineers, ISOPE, Sapporo, Japan, 2018.

[5] P. Cundall and O. Strack, "A discrete numerical model for granular assemblies," Géotechnique 29(1), pp. 47-65, 1979.

[6] C. O'Sullivan, L. Cui and S. O'Neil, "Discrete element analysis of the response of granular materials during cyclic loading," Soils and Foundations, 48(4), pp. 511-530, 2008.

[7] M. Jiang, A. Zhang and T. Li, "Distinct element analysis of the microstructure evolution in granular soils under cyclic loading.," Granular Matter (2019), 21: 39, https://doi.org/10.1007/s10035-019-0892-8, 2019.

[8] N. Hadda and R. Wan, "Micromechanical analysis of cyclic and asymptotic behaviors of a granular backfill," Acta Geotechica, vol. 15, p. 715–734, 2020.

[9] L. Cui and S. Bhattacharya, "Soil–monopile interactions for offshore wind turbines," in Proceedings of the Institution of Civil Engineers - Engineering and Computational Mechanics, 2016.

[10] G. Zorzi, M. Baeßler and F. Gabrieli, "Influence of Structural Stiffness on Ratcheting Convection Cells of Granular Soil under Cyclic Lateral Loading," in 1st International Conference on the Material Point Method, MPM 2017, doi: 10.1016/j.proeng.2017.01.046, 2017.

[11] G. Zorzi, F. Kirsch, F. Gabrieli and F. Rackwitz, "Long-term cyclic triaxial tests with DEM simulations," in Proceedings of Particles 2017, V International Conference on Particle-based Methods.Fundamentals and Applications, 2017.

[12] V. H. Le, Zum Verhalten von Sand unter zyklischer Beanspruchung mit Polarisationswechsel im Einfachscherversuch, PhD Thesis, Volume 66 of Publication of Soil Mechanics and Geotechnical Division, Technische Universität Berlin, Shaker Aachen, 2015 (in German).

[13] R. Glasenapp, Das Verhalten von Sand unter zyklischer irregulärer Belastung, PhD Thesis, Technische Universität Berlin, 2016, http://dx.doi.org/10.14279/depositonce-5402 (in German).

[14] A. Skempton, The Pore-Pressure Coefficients A and B, ICE Publishing. doi: 10.1680/geot.1954.4.4.143, 1954.

[15] T. Schanz and P. A. Vermeer, "Angles of friction and dilatancy of sand," Géotechnique, vol. 46, no. 1, pp. 145-151, 1996.

[16] M. Achmus, K. Abdel-Rahman and P. Peralta, On the design of monopile foundations with respect to static and quasi-static cyclic loading, Copenhagen Offshore Wind 2005, 2005.

[17] R. García-Rojo and H. Herrmann, "Shakedown of unbound granular material," Granular Matter 7(2-3), pp. 109-118, 2005.

[18] C. Modenese, S. Utili and G. Houlsby, "A Numerical Investigation of Quasi-static Conditions for Granular Media," in Discrete Element Modelling of Particulate Media. The Royal Society of Chemistry, 2012.

[19] J. Kozicki, J. Tejchman and H. B. Mühlhaus, "Discrete simulations of a triaxial compression test for sand by DEM," Numerical und Analytical Methods in Geotechnics, vol. 38, no. 18, pp. 1923-1952, 2014.

[20] F. Radjai and F. Dubois, Discrete-element modeling of granular materials, Wiley-Iste, 425 p., 2011.

[21] V. Šmilauer, Yade Documentation, 2nd ed. The Yade Project. doi: 10.5281/zenodo.34073, 2015.

[22] L. Widuliński, J. Kozicki and J. Tejchman, "Numerical Simulations of Triaxial Test with Sand Using DEM," Archives of Hydro-Engineering and Environmental Mechanics 56, nr. 3-4, pp. 149-172, 2009.

[23] L. Zhang, N. Nguyen, S. Lambert, F. Nicot and F. Prunier, "The role of force chains in granular materials: from statics to dynamics," European Journal of Environmental and Civil Engineering 21(7-8), pp. 874-895, 2016.

[24] R. Aboul Hosn, L. Sibille, N. Benahmed and B. Chareyre, "Discrete numerical modeling of loose soil with spherical particles and interparticle rolling friction," Granular Matter, Springer Verlag,19 (1), pp.4. 10.1007/s10035-016-0687-0, 2017.

[25] H. Cheng, T. Shuku, K. Thoeni and H. Yamamoto, "Calibration of micromechanical parameters for DEM simulations by using the particle filter," EPJ Web of Conferences 140:12011, 2017.

[26] J. Plassiard, N. Belheine and F. Donze, "Calibration procedure for spherical discrete elements using a local moment law," University Grenoble, 2007.

[27] N. Guo, Multiscale characterization of the shear behavior of granular media, Hong Kong: The Hong Kong University of Science and Technology, 2014.

[28] J. Roux and G. Combeb, "How granular materials deform in quasistatic conditions," in AIP Conference Proceedings. 1227, 260, 2010.

[29] M. Hu , C. O'Sullivan, R. Jardine and M. Jiang, "Stress-induced anisotropy in sand under cyclic loading," Granular Matter 12(5), pp. 469-476, 2010.

[30] M. Achmus, K. Abdel-Rahman and Y. Kuo, "Behavior of large diameter monopiles under cyclic horizontal loading," in Twelfth International Colloquium on Structural and Geotechnical Engineering, 2007.

[31] G. Zorzi, T. Richter, F. Kirsch, M. Ostergaard and S. Sorensen , "Validation of explicit method to predict accumulation of strain during single and multistage cyclic loading," in Proceedings of the XVII ECSMGE-2019, 2019.

[32] Ed. Züblin AG, "Final Report of the Research Project "Beschreibung des Bodenverhaltens bei zyklisch belasteten Flachgründungen für Offshore-Windenergieanlagen durch Versuche im Originalmaßstab (FKZ 0325175)," Technische Informationsbibliothek Hannover, 2013.

[33] G. Sedlacek, A. Miehe, A. Libreros and Y. Heider, "Geotechnical Stability of Gravity Base Foundations for Offshore Wind Turbines on Granular Soils," ASME 2012 31st International Conference on Ocean, Offshore and Arctic Engineering, 2012.

[34] H. Zachert, T. Wichtmann, P. Kudella, T. Triantafyllidis and U. Hartwig, "Validation of a high cycle accumulation model via FE-simulations of a full-scale test on a gravity base foundation for offshore wind turbines," International Wind Engineering Conference, IWEC, 2014.

[35] G. Zorzi, Cyclic loading design of offshore wind turbine foundations, Berlin: PhD Thesis, Technische Universität Berlin, submitted, 2020.

Appendix E

Comparison of cyclic simple shear tests for different types of sands

This paper was presented at the 2nd International Conference on Natural Hazards & Infrastructure (ICONHIC2019) held in Chania (Greece), 2019 (https://iconhic.com/2019/).

This is the post-print of the published version of the manuscript.

Original version: Zorzi, G., Kirsch, F., Richter, T., Østergaard, M., & Sørensen, S. (2019). Comparison of cyclic simple shear tests for different types of sands. 2nd International Conference on Natural Hazards & Infrastructure (ICONHIC2019)

Comparison of cyclic simple shear tests for different types of sands

G. Zorzi, F. Kirsch, T. Richter

GuD Geotechnik und Dynamik Consult GmbH, Berlin, Germany

M.U. Østergaard, S.P.H. Sørensen

COWI A/S, Aalborg, Denmark

ABSTRACT

To assess the cyclic behavior of soil a series of cyclic laboratory tests were carried out to investigate the soil resistance to strain accumulation, liquefaction etc. under different cyclic and average stress levels, relative densities and drainage conditions. The paper presents different comparisons which aim to study the factors that influence the undrained cyclic loading behavior of two different types of sands. The effect of different stress conditions, relative densities and granulometric curves are compared in terms of permanent shear strain accumulation. For certain cyclic loading conditions, the governing behavior of the soil is uncertain as it can be undrained, partially-drained or drained and different laboratory tests should be executed with different drainage conditions. In order to reduce time and costs, the last part of the paper proposes a formulation to scale the accumulated permanent shear strain from undrained to drained cyclic loading.

Keywords: cyclic loading, cyclic mobility, undrained, cyclic simple shear test

INTRODUCTION

Nowadays cyclic loading is one of the main design drivers for fatigue analysis of many civil engineering structures like transportation facilities, industrial plants, coastal structures, as well as offshore structures. These structures are subjected to cyclic action originating from environmental sources such as earthquakes, wind, waves, tides, and man-made loads such as traffic loads and loads from vibrational machinery.

The foundations of offshore wind turbines are a typical example of a structure which is subjected to millions of irregular cyclic loads throughout its lifetime which makes the prediction of its performance uncertain. For geotechnical engineers it is essential to adopt reliable tools to be able to predict the change in soil properties under cyclic loading as these could have an impact on the behavior of the structure in terms of settlement, loss of capacity or dynamic resonance problems.

The present authors have been developing an explicit method to optimize the foundation design of offshore structures under a design storm event or earthquake event. To predict the accumulated rotation of the foundation, a link between the cyclic contour diagram, derived from cyclic laboratory tests (*Andersen, 2015*), and the stiffness degradation method has been proposed. For a realistic assessment of the stress distribution in the soil domain under the foundation, the proposed link was integrated to the 3D finite element software PLAXIS by means of a remote scripting interface (Zorzi, et al., 2018).

Cyclic contour diagrams give the 3D variation of the investigated variable of interest (i.e. permanent shear strain, pore pressure etc.) based on the number of cycles as well as cyclic and average stress. However, due to the variability of the data, the interpolation entails imprecisions that are not compatible from the mechanical point of view. A mathematical formulation has to be fitted to make the data usable (*Zorzi, et al., 2019*).

A series of laboratory tests were done to develop a framework that allows to produce a reliable construction of cyclic contour diagrams. The paper presents selected results of this laboratory test campaign. Different comparisons will be shown which aim to study the factors that influence the undrained cyclic loading behavior of two different types of sand. The effect of different stress conditions, relative density and granulometric curves are compared in terms of permanent shear strain accumulation.

In the last part of the paper a preliminary formulation is explained to potentially scale the accumulated permanent shear strain from undrained to drained cyclic loading. For certain cyclic loading conditions, the governing behavior of the soil is uncertain as it can be undrained, partially-drained or drained. It is convenient

to carry out two analyses and have an upper bound of the accumulated displacement of the structure (undrained soil condition) and a lower bound displacement (drained soil condition). This will require two sets of cyclic contour diagrams: drained and undrained.

Due to time and budged constrains of a project, it might not be feasible to plan a large laboratory test campaign in order to assess the drained and undrained behavior of the soil under different cyclic stress loading conditions. Therefore it may be possible to scale the shear strain from undrained to drained in order to reduce the amount of laboratory tests. For example, undrained cyclic test can be carried out for different stresses and relative densities conditions in order to produce undrained cyclic contour diagrams for permanent shear strain. Then the accumulated permanent shear strain from the undrained tests can be scaled to the drained accumulated permanent shear strain and the drained cyclic contour diagrams can be prepared.

UNDRAINED CYCLIC BEHAVIOUR OF SOIL

Material

Two types of sand, named S1 and S2, are considered in this study. The granulometric curves are shown in Fig. 1. The sand S1 is characterized by a more uniform-graded particle size distribution than the S2 sand. The index properties of the two types of sand are listed in Table 1, where e_{min} and e_{max} are the minimum and maximum void ratio, D_{50} is the median grain size, U_c is the coefficient of uniformity and C_c is the coefficient of curvature.

Table 1. *Index properties*

Sand	e_{min}	e_{max}	D_{50}	U_c	C_c
S1	0.5	0.9	0.2	2	1.4
S2	0.4	0.7	0.5	3.2	1

Sample preparation and test procedure

A series of single stage one-way cyclic simple shear tests have been performed at the Soil Mechanics Laboratories of the Technical University of Berlin. The

tested soil specimens have dimensions of 90 mm in diameter and 20 mm in height. The tests have been performed on reconstituted soil samples for S1 and S2. The sample preparation method employed was air pluviation. Relative density I_D of 70% and 90 % and different vertical consolidation pressure σ'_v from 100 kPa to 200 kPa was considered. After consolidation, a monotonic shear stress has been applied under drained conditions. The applied monotonic shear stress is called the average shear stress, τ_{avg}. The Average Stress Ratio (ASR) is defined as the ratio between the average shear stress and the vertical consolidation pressure. Then the cyclic loading phase was performed under undrained conditions (constant volume) and as stress-controlled with constant loading amplitude and period. The Cyclic Stress Ratio (CSR) is defined as the ratio between the cyclic shear stress and vertical consolidation pressure. No pre-shearing was considered. The tests were stopped when reaching 1000 cycles or after the development of the "*cyclic mobility*" conditions.

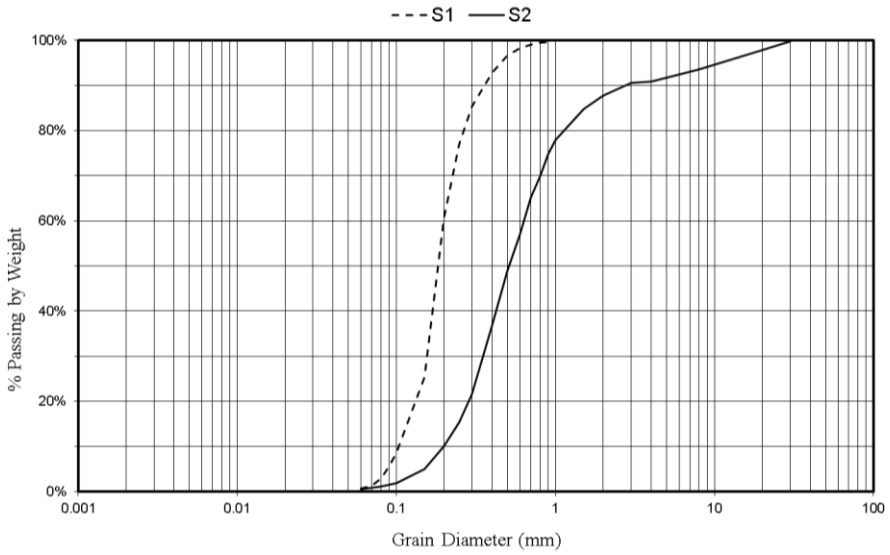

Figure 1. *Granulometric curves*

Typical undrained cyclic behavior using direct simple shear device

During undrained cyclic loading, the specimen tends to contract but no pore water can escape leading to an increase in excess pore pressure (positive pore water pressure). In order to maintain constant volume (undrained conditions), the vertical effective stress decreases. The change in vertical effective stresses is

equal to the accumulation of pore water pressure. Fig. 2 shows a typical stress path for a dense specimen under undrained conditions. In the presented test the vertical consolidation stress is 200 kPa with ASR = CSR = 0.05 and ID=90%. Point A is the start of the cyclic loading phase and due to undrained conditions, the stress path moves towards the state of zero effective stress. The dashed line signifies the drained failure envelope.

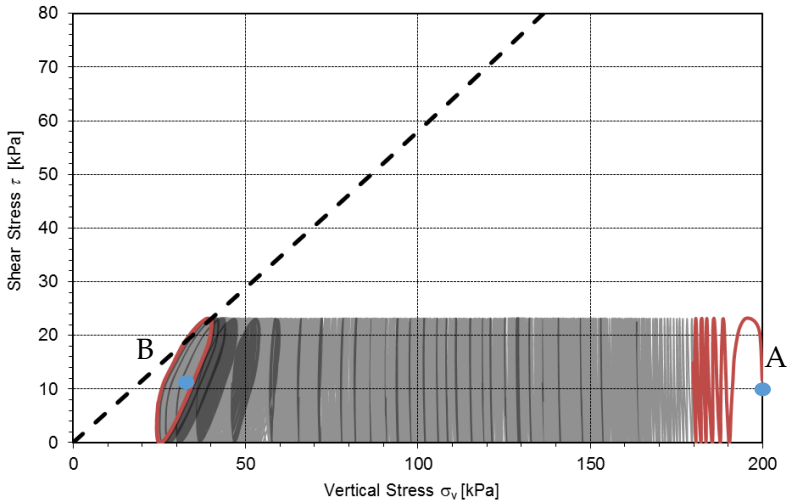

Figure 2. *Typical stress path for dense sand in undrained condition (ASR=CSR=0.05)*

Depending on the type of soil, relative density and the stress level, a stabilization of the accumulated pore pressure is occurring at a critical number of cycles. This phase, in which the plastic deformations suddenly increase (*"strain take-off"*), is called cyclic mobility (*Casagrande, 1971; Castro, 1975*). At the same time, there is an alternate generation of positive (compressive soil behavior: decrease of vertical stress) and negative (dilative soil behavior: increase of vertical stress) pore pressures, which neutralize each other leading to a stable behavior (no softening nor hardening). This state is also known as Cyclic Stable State (*Shajarati, et al., 2012*). Similar as in (*Lombardi, et al., 2014*), the data showing the accumulation of shear strain (Fig. 3) can be divided into a bi-linear model diagram in which the intersection of the two lines can be called "strain take-off", marking the start of the cyclic mobility phase.

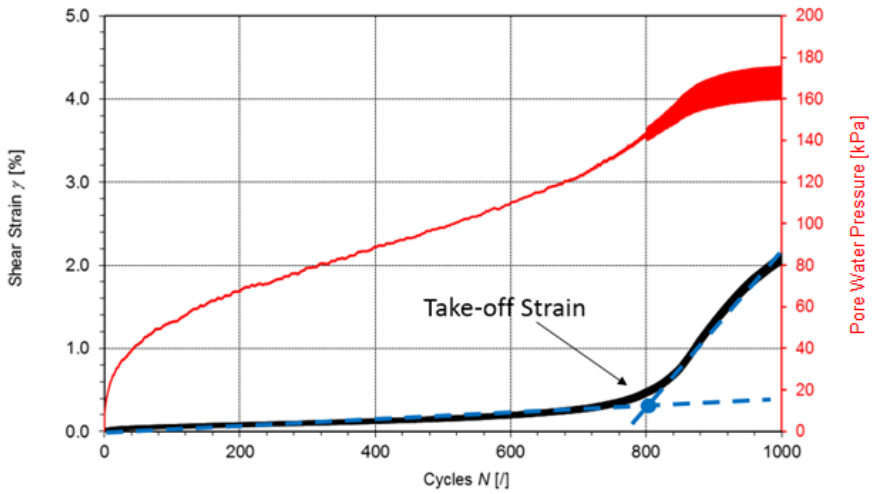

Figure 3. *Shear strain and pore water pressure accumulation*

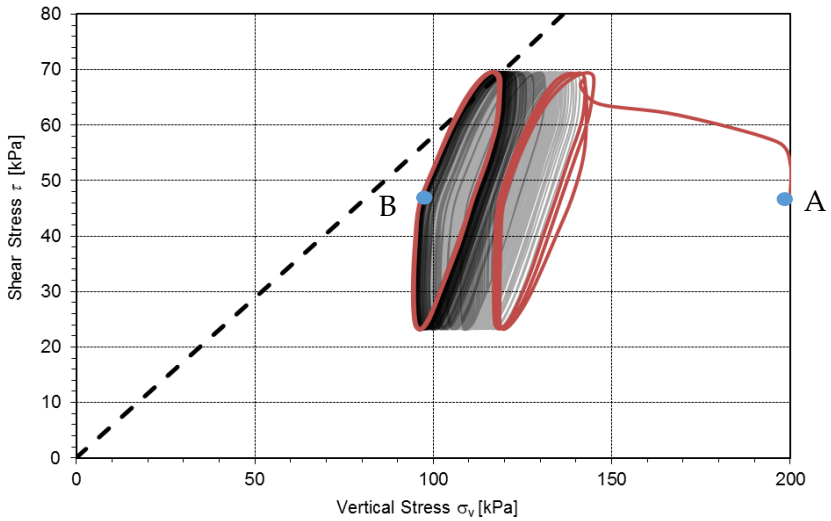

Figure 4. *Typical stress path for dense sand in undrained condition (ASR=0.21, CSR =0.11)*

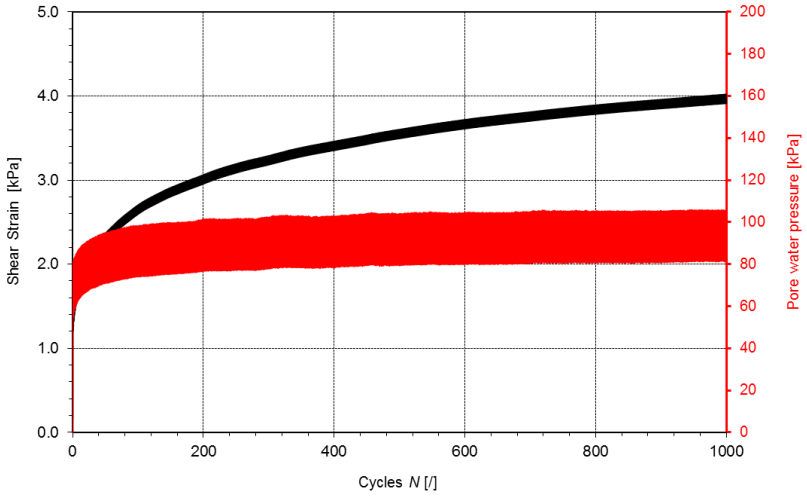

Figure 5. *Shear strain and pore water pressure accumulation*

Fig. 4 shows the stress path of an undrained test with an ASR=0.21, CSR =0.11 and ID=90%. The vertical consolidation stress is 200 kPa. Compared to the test in Fig. 2 the cyclic mobility is reached already in the very beginning of the test: significant shear strains are observed already at the first cycle. The accumulated pore pressure stabilizes after few cycles and alternating positive and negative pore pressures can be observed from the first loading cycle.

Comparison of Undrained cyclic simple shear tests

Comparison-1: Soil=S1; different ASR; CSR=0.05; σ'_v *= 200 kPa; ID=90%. (See Fig.6 and 7).*

In this comparison the undrained cyclic behavior of the sand S1 is investigated. Fig. 6 compares four tests with different ASR ranging from 0 to 0.17. The same relative density of 90%, CSR of 0.05 and initial vertical consolidation stress σ'_v = 200 kPa were applied in all tests. For this specific CSR, increasing the ASR from 0 to 0.11 leads to a decrease of the number of cycles before strain take-off (start of cyclic mobility phase). This is also shown in Fig. 7 where the permanent pore water pressure accumulation causes stable state conditions.

However, for an ASR of 0.17, the result shows a reduced amount of deformation. Under certain conditions of high relative density, high initial vertical stresses and a small cyclic amplitude the opportunity of the grains to unlock

and move relative to each other is reduced (*Kammerer, et al., 2001*). The test with an ASR of 0.17 does not show any cyclic mobility while the permanent pore water pressure is increasing steadily. After a higher number of cycles than tested a cyclic mobility condition may be reached.

The behavior of the test with ASR=0 is to be noted. Even though no significant accumulation of permanent deformation is shown in Fig. 6, a substantial increase in permanent pore water pressure is taking place (Fig. 7) which could rapidly lead to cyclic mobility as well as a fast increase of deformation.

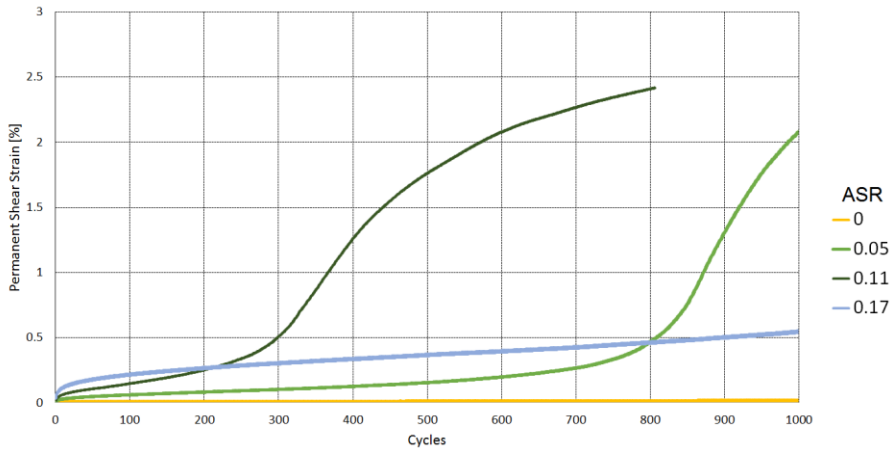

Figure 6. *Permanent shear strain accumulation for different ASR Soil=S1; CSR=0.05; σ'_v = 200 kPa; ID=90%.*

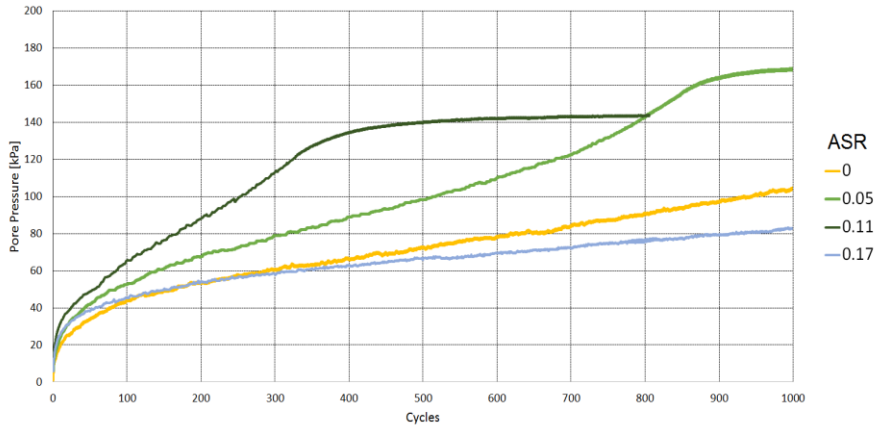

Figure 7*. Permanent pore water pressure accumulation for different ASR Soil=S1; CSR=0.05; σ'v = 200 kPa; ID=90%.*

Comparison-2: Soil=S1; different ASR; CSR=0.05; σ'_v = 200 kPa; ID=70%. (See Fig. 8)

In this comparison, the same soil S1 is considered. The Fig. 8 compares the tests with different ASR ranging from 0 to 0.17. A relative density of 70% is used. The CSR = 0.05 and σ'_v = 200 kPa are kept constant in all the tests. Increasing the ASR causes a shift on the take-off of the cyclic mobility to a lower number of cycles. Differently to *Comparison-1*, for the ASR = 0.17 a rapid increase of shear strain takes place at the first cycles (See Fig. 8). The accumulated pore pressure is quickly stabilizing in the first cycles, reaching Cyclic Stable State conditions. For the same number of cycles and stress conditions, decreasing the relative density of 20% leads to a significantly higher amount of accumulated deformation.

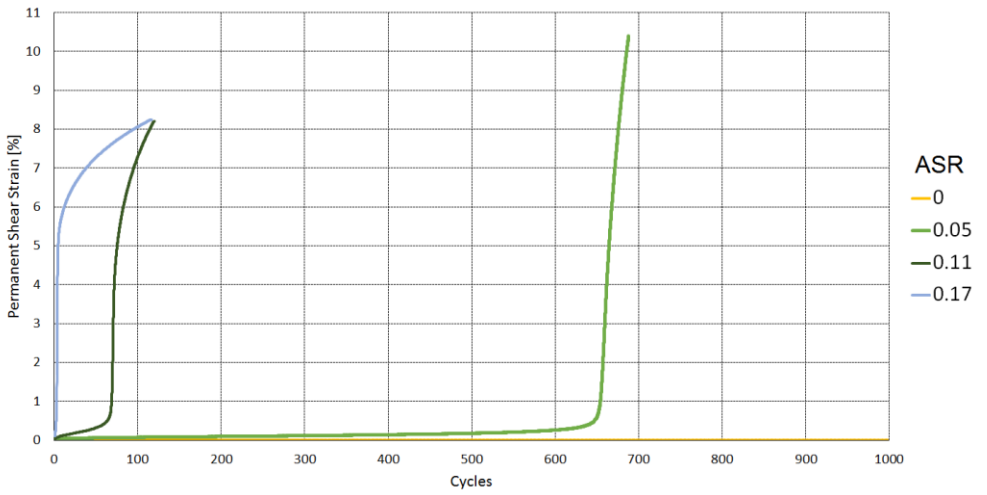

Figure 8. *Permanent shear strain accumulation for different ASR Soil=S1; CSR=0.05; σ'_v = 200 kPa; ID=70%.*

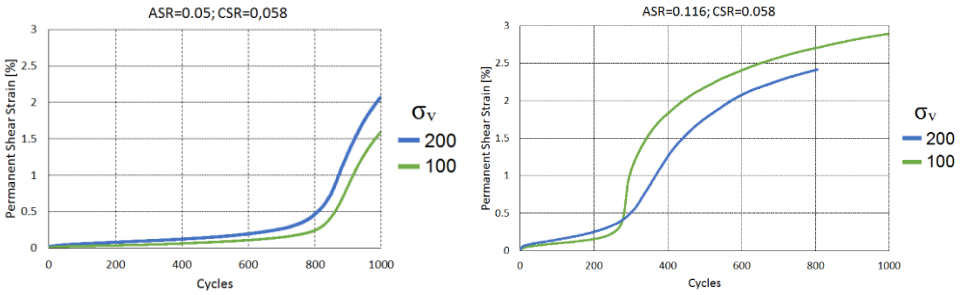

a) b)

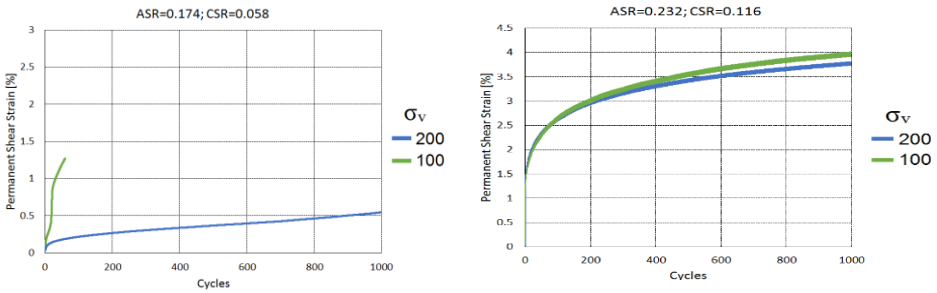

c) d)

Figure 9. *Permanent shear strain accumulation for different σ_v Soil=S1; ID=90%.*

Comparison-3: Soil=S1; different σ'_v; ID=90%. (See Fig. 9)

It is important to verify that the accumulation of deformation is similar for different tests with different initial vertical consolidation pressure. This means that the contour diagrams can be attached to the finite element (FE) model at different depths. The following figures show the comparison between the tests with two different consolidation pressures (100 vs 200 kPa) but the same ASR, CSR and relative density of 90%. The S1 type of sand S1 is considered. For the combination of ASR-CSR in Fig. 9.a, 9.b and 9.d the effect of varying consolidation stresses appears to be small. However, for the combination of ASR and CSR in Fig. 8.c, the vertical consolidation significantly alters the cyclic soil behavior.

Comparison-4: Soil=S2; different ASR; CSR=0.05; σ'_v = 200 kPa; ID=90%. (See Fig. 10)

Undrained cyclic tests executed on sand S2 are analyzed in the following. Fig. 10 compares the tests with different ASR ranging from 0.05 to 0.17. The same relative density of 90% and CSR of 0.05 with a σ_v of 200 kPa were applied. The same qualitative behavior as in *Comparison1* can be observed. For the considered CSR = 0.05, increasing the average stress from 0.05 to 0.116, leads to an earlier the take-off of strain. For the ASR = 0.17, the same effect was found for the sand S1: a gradual increase of average shear strain and the accumulation of pore water pressure.

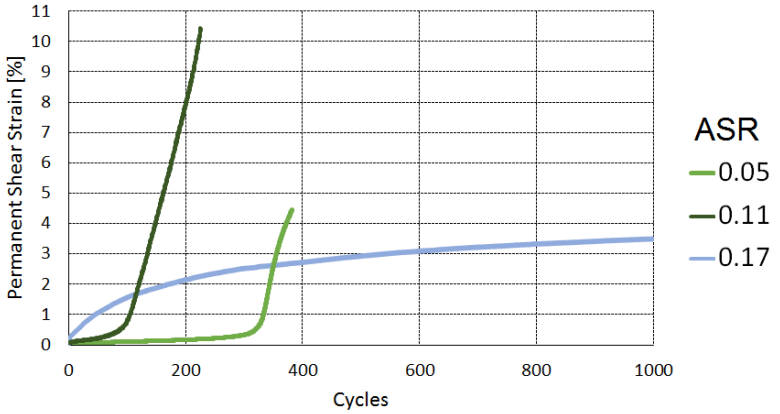

Figure 10. *Permanent shear strain accumulation for different ASR Soil=S2; CSR=0.05; σ'_v = 200 kPa; ID=90%.*

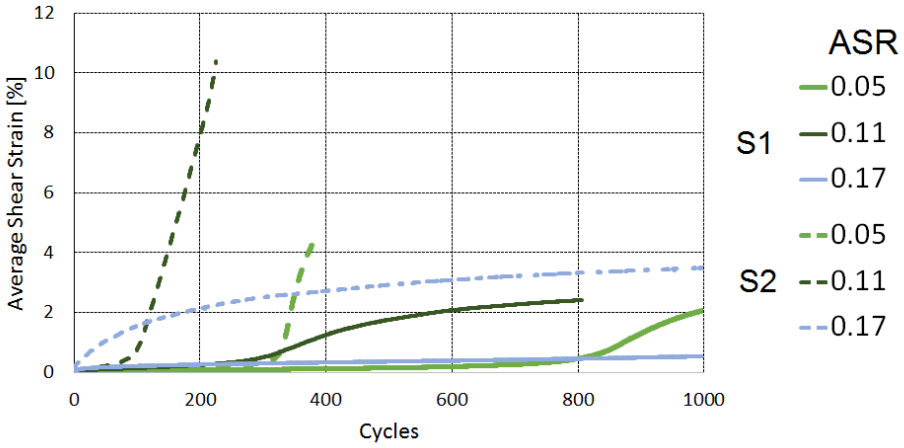

Figure 11. *Comparison of S1 and S2: permanent shear strain accumulation for different ASR CSR=0.05; σ'_v = 200 kPa; ID=90%.*

Comparison-5: Different types of sands and ASR; CSR=0.05; σ'_v = 200 kPa; ID=90%. (See Fig. 11)

To analyze the effect of particle size distribution on the accumulation of shear strain, a final comparison between the two types of sands is shown in Figure 10. For constant relative density of 90% and the initial vertical consolidation of 200 kPa, a remarkable increase of permanent deformation with increasing the uniformity coefficient and d_{50} is found. The sand S2 that has more a graded

granulometric curve shows an earlier take-off of deformation, hence an earlier start of the cyclic mobility phase. (Wichtmann, 2016), found the same behavior for different granulometric curves on undrained cyclic triaxial tests. This results is in line with the common practice of using well graded material for soil compaction methods.

Relationship between permanent shear strain between undrained and drained tests

A formula which transform the permanent shear strain between the drained and undrained behavior is proposed to potentially reduce the amount of laboratory tests. Considering a saturated sample subjected to drained cyclic loading under a certain ASR-CSR, it will show a decrease of volume and increase of shear strain due to densification of the grains. If the same sample with the same stress level is tested in undrained conditions, the magnitude of the accumulated shear strain is amplified by the increase of the pore water pressure. Therefore, a formula can be proposed to reduce the permanent shear strain developed under undrained conditions in each cycle $\gamma_{N,ud}$ to the permanent drained shear strain $\gamma_{N,d}$ theoretically developed with the same test configuration but in drained conditions. The reduction factor should be a function of the residual pore pressure build up u_N at the end of each cycle and the initial vertical consolidation stress σ'_v, elevated by a factor p.

$$\gamma_{N,d} = \gamma_{N,ud} * \left(\frac{\sigma'_{v,0} - u_N}{\sigma'_v}\right)^p \quad (1)$$

From the theoretical point of view, the limits of the formulation can be verified. When the pore water pressure u_N tends to zero (no pore water pressure), then the undrained shear strain are equal to the drained one. If the u_N tends to $\sigma'_{v,0}$ (cyclic mobility), the reduction factor tends to zero which means that the undrained shear strain tends to a very high number.

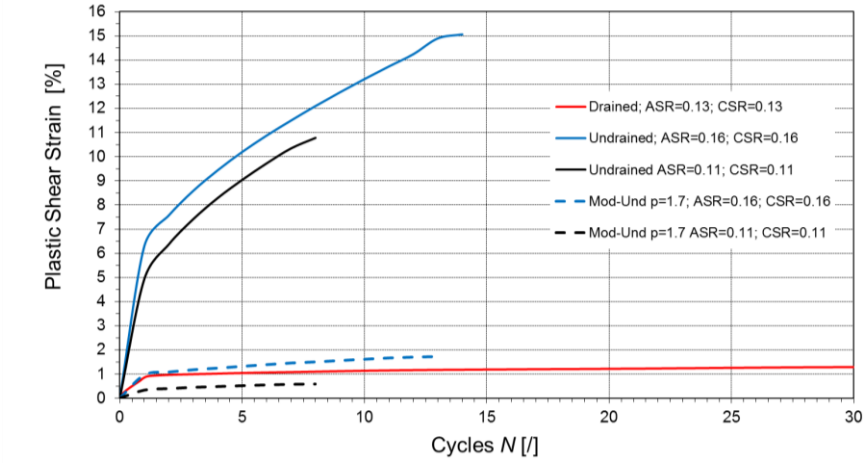

Figure 12. *Transformation of permanent shear strain from undrained to drained*

To test this relation and calibrate the factor p a cyclic simple shear test under drained conditions was considered for the sand S2. The test has an ASR = CSR = 0.13, a relative density of 90% and an initial vertical consolidation stress of 150 kPa. The red line in Fig. 11 is the permanent shear strain measured in the test. Two undrained tests with similar ASR and CSR (relative density of 70% and vertical consolidation stress of 200 kPa), are plotted as a blue and a black line. The dashed and dotted lines are the reduced shear strain by applying the formula (1). For p equal to 1.7, a good match is achieved. However, this is a preliminary result and the relation should be thoroughly investigated to confirm its validity. It should be noted that in the literature other relationships between the volume reductions during drained cyclic loading and the corresponding pore-water pressure generation under undrained conditions are found such as in (Martin, et al., 1975) and will be compared in further studies with the presented one.

CONCLUSION

A series of cyclic direct simple shear tests have been performed assessing the influence of a range of parameters on the shear strain accumulation, pore pressure build up and on the number of cycles at which cyclic mobility is reached. For this assessment the following parameters have been varied: average stress

ratio, cyclic stress ratio, consolidation stress, drained versus undrained testing conditions.

A relation between the permanent shear strains obtained during undrained and drained conditions is proposed. For one set of average stress ratio, cyclic stress ratio, consolidation stress and sand type the relation is validated. Extensive laboratory testing will be performed to assess the validity of the expression further under different conditions such as different relative densities and for different ASR-CSR values.

ACKNOWLEDGEMENTS

This research is part of the Innovation and Networking for Fatigue and Reliability Analysis of Structures Training for Assessment of Risk (INFRASTAR) project. This project has received funding from the European Union's Horizon 2020 research and innovation program under the Marie Skłodowska-Curie grant agreement No. 676139. The laboratory tests are provided by the Chair of Soil Mechanics and Geotechnical Engineering of the Technical University of Berlin. The authors are grateful for the kind permission to use those test results.

REFERENCES

Andersen, K. (2015). Cyclic soil parameters for offshore foundation design. The 3rd McClelland Lecture. Frontiers in Offshore Geotechnics III, ISFOG'2015, (pp. 5-82).

Casagrande, A. (1971). On Liquefaction Phenomena. Géotechnique, pp. 21(3):197–202.

Castro, G. (1975). Liquefaction and Cyclic Mobility of Saturated Sands. Journal of the Geotechnical Engineering Division, pp. 101(6):551–569.

Jostad, H., Grimstad, G., Andersen, K., M., S., Shin, Y., & D., Y. (2014). A FE Procedure for Foundation Design of Offshore Structures – Applied to Study a Potential OWT Monopile Foundation in the Korean Western Sea. Geotechnical Engineering Journal of the SEAGS & AGSSEA, p. 45(4).

Kammerer, A. M., Wu, J., M.Riemer, J.M.Pestana, & R.B.Seed. (2001). Use of Cyclic Simple Shear Testing in Evaluation of the Deformation Potential of Liquefiable Soils. International Conferences on Recent Advances in Geotechnical Earthquake Engineering and Soil Dynamics, (p. 16).

Lombardi, D., Bhattacharya, S., Hyodo, M., & Kaneko, T. (2014). Undrained behaviour of two silica sands and practical implications for modelling SSI in liquefiable soils. Soil Dynamics and Earthquake Engineering, pp. 293-304.

Martin, G., Finn, W., & Seed, H. (1975). Foundamentals of liquefaction under cyclic loading. Journal of the Geotechnical engineering division, pp. 101(5):423-438.

Shajarati, A., Sørensen, K. W., Nielsen, S. K., & Ibsen, L. B. (2012). Behaviour of Cohesionless Soils During Cyclic Loading. Aalborg: Department of Civil Engineering, Aalborg University. DCE Technical Memorandum, No. 14.

Wichtmann, T. (2016). Soil behaviour under cyclic loading - experimental observations, constitutive description and applications. In Habilitation thesis.

Zorzi, G., Kirsch, F., Richter, T., Østergaard, M., & Sørensen, S. (2019). Validation of explicit method to predict accumulation of strain during single and multistage cyclic loading. Proceedings of the XVII ECSMGE-2019, Geotechnical Engineering foundation of the future, (pp. -).

Zorzi, G., Richter, T., Kirsch, F., Augustesen, A. H., Østergaard, M. U., & Sørensen, S. P. (2018). Explicit Method to Account for Cyclic Degradation of Offshore Wind Turbine Foundations Using Cyclic Inter-action Diagrams. International Society of Offshore and Polar Engineers. Sapporo, Japan.

Appendix F

Validation of the explicit method to predict accumulation of strain during single and multistage cyclic loading

This paper was presented at the XVII European Conference on Soil Mechanics and Geotechnical Engineering held in Reykjavik (Iceland), 2019 (https://www.ecsmge-2019.com/).

This is the post-print of the published version of the manuscript.

Original version: Zorzi, G., Kirsch, F., Richter, T., Østergaard, M., & Sørensen, S. (2019). Validation of explicit method to predict accumulation of strain during single and multistage cyclic loading. ECSMGE 2019 - The XVII European Conference on Soil Mechanics and Geotechnical Engineering

The additional remarks in red to the original paper have been made for this thesis.

Validation of explicit method to predict accumulation of strain during single and multistage cyclic loading

Validation d'une méthode explicite pour prédire l'accumulation de déformation lors d'un chargement cyclique à une ou plusieurs étapes

G. Zorzi, F. Kirsch, T. Richter

GuD Geotechnik und Dynamik Consult GmbH, Berlin, Germany

M.U. Østergaard, S.P.H. Sørensen

COWI A/S, Aalborg, Denmark

ABSTRACT

The present paper validates an innovative explicit method to predict the accumulation of soil deformation during cyclic loading condition. The accumulation of strains is produced by reducing a fictive elastic shear modulus of the soil based on cyclic contour diagrams. This connection is integrated into the finite element software PLAXIS 3D by means of a remote scripting interface. The paper will provide an insight into how to interpolate the permanent shear strain in 3D cyclic contour diagrams from single-stage cyclic tests with a sand, which is typical for the North Sea. A mathematical framework is proposed which helps to ease the interpolation. After this, the validation of the link between the stiffness degradation method and the 3D cyclic contour diagram is provided by modeling single stage tests in PLAXIS 3D. Further, the explicit method is compared against multistage tests to understand the link between the stress history of cyclic stress parcels.

RESUME

Le présent article valide une méthode explicite innovante permettant de prédire l'accumulation de déformations du sol sans des conditions de chargement cycliques. L'effet de l'accumulation de déformation est pris en compte en réduisant un module de cisaillement élastique fictif du sol sur la base de diagrammes de déformation cycliques. Cette connexion est intégrée au logiciel de calcul par éléments finis PLAXIS 3D au moyen d'une interface de script à distance.

L’article explique comment interpoler la déformation plastique moyenne sur des diagrammes de déformation cycliques 3D à partir d'essais cycliques à une étape pour un sable typique de la mer du Nord. Un cadre mathématique est proposé pour faciliter l’interpolation. La validation du lien entre la méthode de dégradation de la rigidité et le diagramme de déformation cyclique 3D est fournie par la modélisation des tests à une étape dans PLAXIS 3D. En outre, la méthode explicite est comparée à un test à plusieurs étapes pour comprendre le lien entre l'historique des contraintes de parcelles de contraintes cycliques.

Keywords: Finite element modelling; cyclic loading; strain accumulation; explicit method

1. INTRODUCTION

The design of foundation structures for offshore wind turbines requires assessment of the soil-structure-interaction (SSI) subjected to cyclic loading conditions (DNV-GL, 2017). It must be ensured that the rotational accumulation does not exceed the limit prescribed by the wind turbine manufacturer and that a possible pore pressure build up is not affecting the stability of the foundation. Being able to accurately verify these requirements leads to an improved risk assessment of the foundation structure and an optimization of the design of offshore foundations.

It is common practice to gather information about the cyclic behavior of soil by means of cyclic laboratory tests. Mainly stress-controlled cyclic direct simple shear tests or cyclic triaxial tests are performed. Often the response of the soil is tested under undrained conditions (constant volume). Different regular cyclic loading packages with varying average and cyclic stresses are tested in relation to the possible stress variation, which the soil will be exposed to during the design storm event. Engineering judgement, experience from previous projects, simplified models and three-dimensional finite element models (3D FEM) can help to extract the stress conditions appropriate for the laboratory test campaign.

Reliable methods are needed to make use of the obtained information from the laboratory test campaign to predict the behavior of the soil under the design

load scenario (i.e. significant storm event or earthquake event). Occasionally a "soil fatigue model" is used in geotechnical engineering projects. One model of this type, also recommended by DNV-GL, is the cyclic contour diagram established with laboratory testing of the investigated soil material.

Different cyclic contour diagrams can be established for different “fatigue variables” such as:

- Average and cyclic plastic strain
- Average and cyclic pore pressure
- Damping
- Dynamic stiffness
- Post-cyclic stiffness

Based on the considered geotechnical verification, e.g. verification of permanent rotations/displacements, liquefaction analysis or dynamic analysis, different assumptions can be made for the final assessment of the SSI under cyclic loading.

The construction of the cyclic contour diagrams is a challenge because it is derived from a three-dimensional interpolation of data from usually only a few cyclic laboratory tests. Moreover, those diagrams must be integrated in a 3D FEM domain to quantify a realistic stress level distribution and hence allow for a better assessment of the foundation behavior under cyclic loading conditions.

Finally, the irregular load series of the selected storm event is broken down to a series of ascending parcels with constant mean and amplitude loads and number of cycles. This stress history is usually considered by utilizing the "equivalent number of cycles"-procedure.

This paper validates the method explained in Zorzi et al. (2018) which predicts the strain and displacement accumulation for a severe storm event. It is based on 3D cyclic contour diagrams in which the fatigue variable is the permanent shear strain. The integration in the 3D FEM model is done by means of a stiffness degradation of the soil in a cluster-wise division. The software PLAXIS 3D 2017 was used for this integration because it allows the use of a remote scripting interface.

This method has shown different advantages, such as, flexibility for automating the design and the application on different types of offshore foundations (Zorzi et al., 2018). The present paper will explore the behavior of the method closely for single and multistage cyclic laboratory tests.

The creation of cyclic contour diagrams from single stage tests is presented for a sand, which is typical for the North Sea environment. A mathematical framework is proposed, which can help to reduce the uncertainty and ease the interpolation procedure. The link between the stiffness degradation method and the strain contour diagrams is validated based on the single stage cyclic laboratory tests. Lastly, the explicit method is compared to multistage cyclic laboratory tests test to investigate the link between the stress history of the parcels.

2.FATIGUE CONTOUR DIAGRAMS

A series of single and multiple stage two-way cyclic simple shear tests have been performed at the Soil Mechanics Laboratories of the Technical University of Berlin. The tests have been performed on a soil reconstituted to a relative density of 90% and with a granulometric curve of $d_{0\%}$ = 0.06 mm, $d_{50\%}$ = 0.2 mm and $d_{100\%}$ = 2 mm.

The tests were carried out undrained (constant volume) with different average and amplitude stresses. Prior to cyclic loading the soil was consolidated to a vertical consolidation pressure of 200 kPa. No pre-shearing was done prior to the cyclic loading. The average stress was applied under drained condition. Table 1 presents an overview of the test campaign. The Average Stress Ratio (ASR), which is defined as the ratio between the average shear stress and the vertical effective stress in the tests, ranges from 0.00 to 0.26, while the Cyclic Stress Ratio (CSR), which is the ratio between the cyclic shear stress and vertical effective stress in the tests, ranges from 0.02 to 0.26. The present methodology is focused on the prediction of the strain accumulation. Therefore, the fatigue variable extracted from the tests was the *accumulated permanent shear strain*, γ_p, at the end of each stress cycle.

Table 1. Summary of the test campaign.

# Test	ASR	CSR

1	0.000	0.029
2	0.029	0.029
3	0.058	0.029
4	0.087	0.029
5	0.000	0.058
6	0.058	0.058
7	0.116	0.058
8	0.174	0.058
9	0.000	0.116
10	0.116	0.116
11	0.232	0.116
12	0.000	0.232
13	0.232	0.232

All data was assembled in a three-dimensional matrix (ASR, CSR, number of cycles N) and a three-dimensional interpolation of γ_p was done to map the entire 3D space. Due to the variability of the data, a mathematical formulation had to be fitted. Different two-dimensional slices at different ASR were extracted. In each slice a power law function for different strain levels was calibrated. The power law function is in the form of Equation (1).

$$CSR = a * N^b + c \quad (1)$$

The parameter b represents the shape of the curve, a is a scaling factor and c is the intersection with the CSR axis. The fitting of a mathematical formulation provides smooth diagrams avoiding the test uncertainties to cause an unrealistic shape of the cyclic contour diagrams. During the fitting procedure, the shape parameter b has been kept constant at -0.35 for the different strain levels and different ASR.

Figure 1 and Figure 2 show a satisfactory agreement between the power law fit and the laboratory measurements.

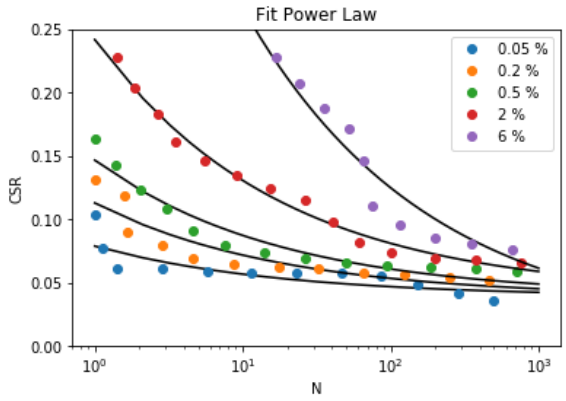

Figure 1. Two-dimensional slice showing curves of average shear strain versus the number of cycles and CSR. ASR=0.06.

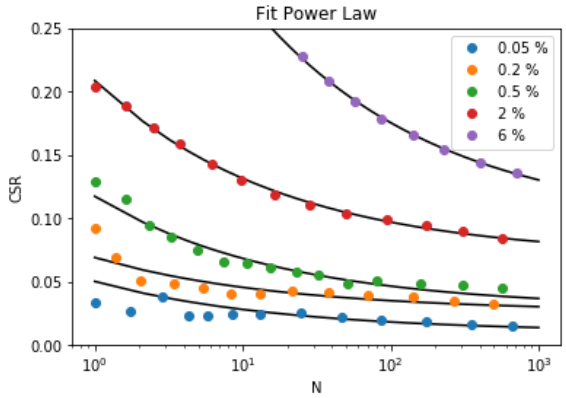

Figure 2. Two-dimensional slice showing curves of average shear strain versus the number of cycles and CSR. ASR=0.22.

Boukpeti et al. (2014) also adopted a power law function to approximate the strain contour diagrams of carbonate silt sediments. In this case the shape factor *b* was calibrated for different strain surfaces as well, and the values for the different strain contours were found to vary from -0.40 to -0.37. This is supporting the assumption that keeping the shape factor constant and further the chosen value of -0.35 is in good agreement with Boukpeti et al. (2014). Finally, the functions for each slice are grouped together and interpolated between each other to establish a smooth final 3D matrix.

3. VALIDATION WITH SINGLE STAGE TESTS

The first validation is done against the single stage tests used in Table 1. The link of the stiffness degradation approach with the 3D cyclic contour diagram is validated by modelling different simple shear tests in PLAXIS 3D and comparing the predictions to the laboratory test results.

3.1 3D FEM model of simple shear test

The simple shear tests used in section 2, are modelled as a cube with sides of 1 m in length. A coarse mesh is used to speed up the computation. The linear elastic perfectly plastic Mohr-Coulomb model, cf. PLAXIS (2017), is used. The soil parameters (Table 2) are calibrated against monotonic simple shear tests with the same relative density and vertical effective stress as used for the cyclic tests.

Table 2. Soil model parameters.

Soil Parameters	**Values**
G [MN/m²]	30.0
ν [-]	0.2
φ [°]	36.0
ψ [°]	0.0
γ_{sat} [kN/m³]	18.0
γ_{unsat} [kN/m³]	9.0

The modelling of the shear tests in finite element calculation was carried out in three steps:

1. Initialization of a unit soil cube
2. Application of the vertical load (200 kPa) to reach the K0-consolidation. The bottom of the cube is fixed in all directions, the sides of the cube are fixed in the normal direction and the top of the cube is not fixed.
3. Application of surface displacement along X-axis (red axis in Figure 3). At the top of the model, a uniform displacement is applied and at the sides, the displacement varies linearly from zero at the bottom to the maximum value at the top.

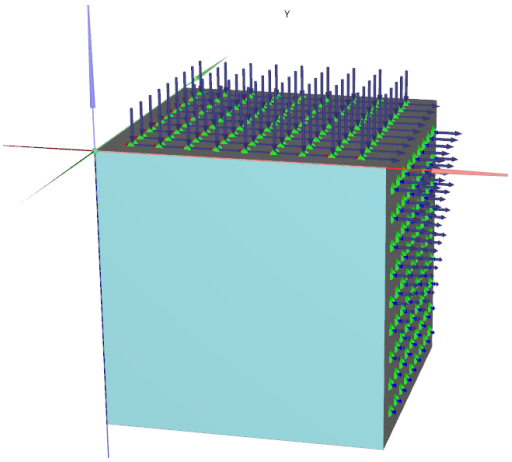

Figure 3. FE model of cyclic direct simple shear test.

Due to the presence of stress concentrations along the boundaries on the FEM model, a small soil volume in the center has been considered, which ensures a uniform stress and strain distribution. The inner soil volume is a cube with side lengths of 0.5 m as shown in Figure 4.

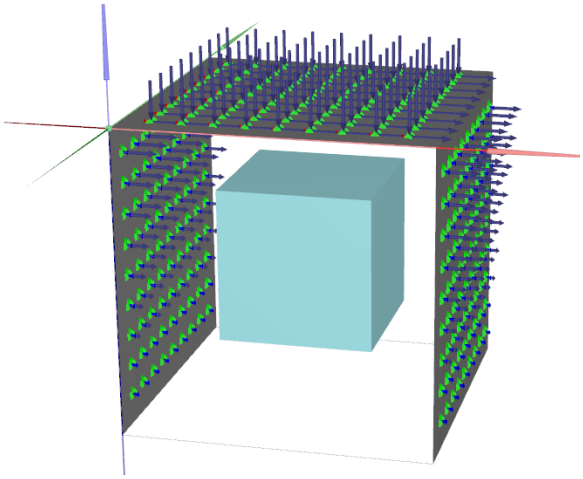

Figure 4. Illustration of inner soil volume in FE model.

3.2 Validation of the method

The concept of the stiffness degradation method is to degrade the initial stiffness based on the accumulated plastic strain extrapolated from the contour diagrams at a certain stress level. This procedure is shown in Figure 5. The blue line represents an idealization of the cyclic test, the thick black line with an

initial shear stiffness of G_{ini} is the assumed linear elastic behavior. G_N is the degraded fictive stiffness which leads to an accumulation of strain of $\gamma_{ini} + \gamma_n$.

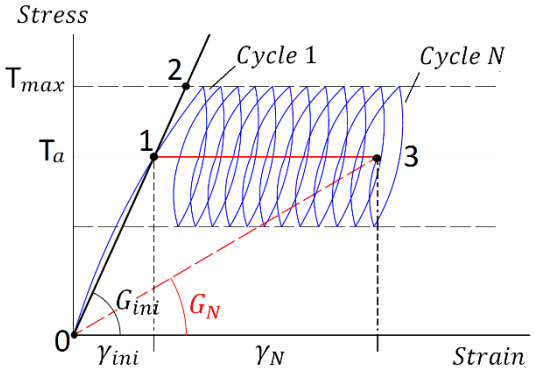

Figure 5. Stiffness degradation concept.

The following procedure has been applied in the numerical model:

0. Initialization of the sample and K0-consolidation
    a. Average of the cartesian stress and strain tensor in the inner soil volume ($\boldsymbol{\sigma}_{ini}$, $\boldsymbol{\varepsilon}_{ini}$).
    b. Average of the vertical effective stress σ_v.
1. Shearing of the sample until T_a (from phase 0).
    a. Average of the cartesian stress and strain tensor in the inner soil volume ($\boldsymbol{\sigma}_{avr}$, $\boldsymbol{\varepsilon}_{avr}$).
    b. Subtraction of the initial stress and strain (from 0.a).
    c. Principal stress transformation in which $\tau_a = \tau_{max}$, $\gamma_{ini} = \gamma_{max}$.
2. Shearing of the sample until T_{max} (from phase 1).
    a. Average of the cartesian stress tensor in the inner soil volume ($\boldsymbol{\sigma}_{max}$).
    b. Subtraction of the average stress (from 1.b).
    c. Principal stress transformation in which $\tau_{cly} = \tau_{max}$,

d. Extrapolation of γ_N from the contour diagram based on τ_a, τ_{cly}, σ_v and N.

3. Degradation of the initial stiffness and shearing of the sample until T_a (from phase 0).

Figure 6, Figure 7 and Figure 8 show the cyclic loading test results in blue for different stress levels. The FEM monotonic behavior with G_{ini} = 30 MPa is shown in black. The dashed red line is the FEM monotonic behavior with the degraded fictive stiffness. The yellow square is the predicted strain.

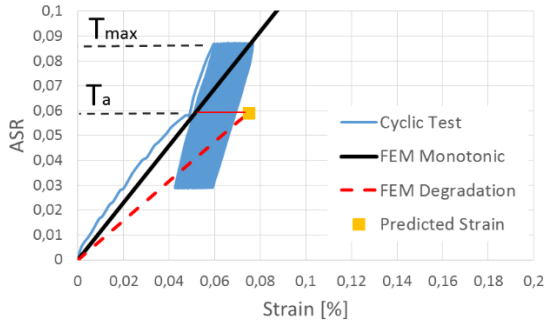

Figure 6. Comparison between FE predictions and laboratory tests for single-stage test with ASR=0.058, CSR=0.029 and N=800.

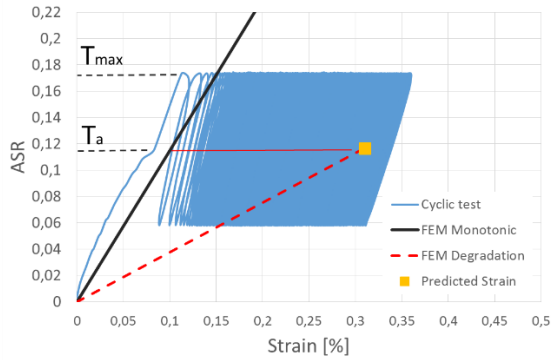

Figure 7. Comparison between FE predictions and laboratory tests for single-stage test with ASR=0.11, CSR=0.058 and N=200.

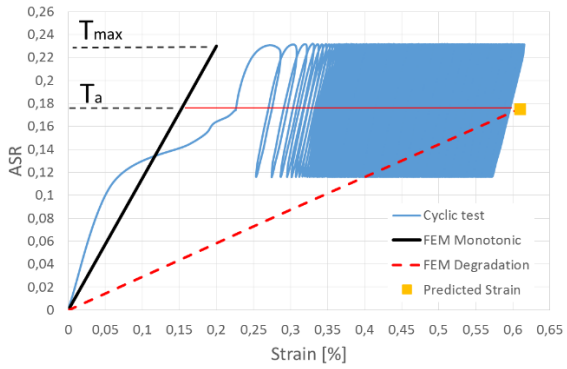

Figure 8. Comparison between FE predictions and laboratory tests for single-stage test with ASR=0.17, CSR=0.058 and N=500.

The FE model utilizing the explicit degradation method provides satisfactory results as a good agreement with the laboratory tests are obtained.

4. VALIDATION AGAINST MULTISTAGE TESTS

A validation of the explicit method against two multistage cyclic direct simple shear tests have been performed. This validation is relevant to elucidate the methods capability to simulate load events with varying magnitude such as a design storm event. The multistage cyclic tests consist of three identical stages (in terms of stress level and number of cycles).

For one multistage test, the pore water pressure was allowed to dissipate after the application of each load parcel. This test can be related to the behavior of the foundation during the lifetime for which it is likely that pore pressure can dissipate between storm events.

The second test was done without re-consolidation between each parcel. This case can be related to the behavior of soil during a single design storm event in which the soil condition can be assumed (close to) undrained.

Table 3 summarizes the test conditions for the two tests.

Table 3. Summary of the cyclic stages for the two multi-stage tests. Similar stress levels and number of cycles was adopted for the two tests.

Stage no.	ASR/CSR	N	σ'_v	ID
1	0.029/0.029	500	200	90
2	0.058/0.058	500	200	90
3	0.116/0.116	100	200	90

The explicit method considers the accumulation procedure denoted as "Method 2" in Zorzi et al. (2018). For this method, the stress history is modelled by means of the number of equivalent load cycles. This value is extracted independently from the cyclic contour diagram based on the actual stress level and the previous strain that the soil has already experienced. For example, the equivalent number of load cycles for load parcel 2 shall be determined such that the permanent strains accumulated for load cycles with stresses corresponding to load parcel 2 equals the permanent strains of all the previous load parcels.

Inter-parcel with consolidation

Figure 9 shows the accumulation of strain versus the number of cycles. The equivalent number of cycles from the accumulation procedure is predicted to 1 for load parcel 2 and 3. This means that the stress level of the following parcel is reaching the accumulated deformation in the first cycle. This low number of equivalent load cycles is predicted due to the significant difference in cyclic stresses between the three considered stages.

For parcel 2 a higher predicted strain is obtained which likely due to the uncertainties in the contour diagram. Very few tests were available at small CSR.

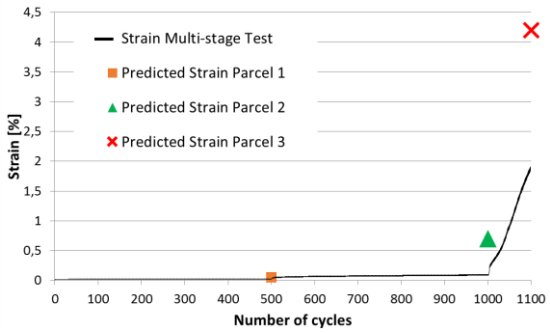

Figure 9. Strain accumulation: Multistage test vs predicted strain.

It is observed that the explicit method over-predicts the accumulated cyclic strain. This is caused by the changes in soil fabric due to the pore water pressure dissipation between cyclic stages. The explicit method does not account for this effect.

Inter-parcel without consolidation

The second cyclic test was performed without consolidation between cyclic stages. For this test a better agreement is found between the predictions of the explicit method and the laboratory results, cf. Figure 10.

For parcel 2 a higher predicted strain is obtained which likely due to the uncertainties in the contour diagram. Very few tests were available at small CSR.

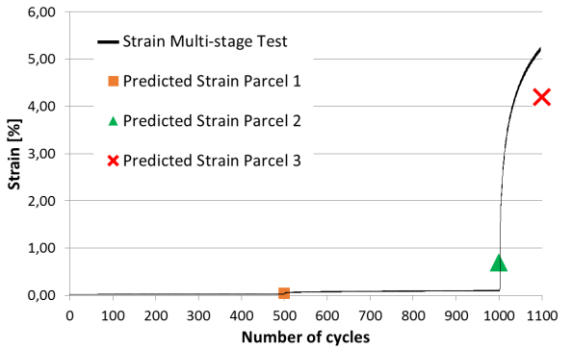

Figure 10. Strain accumulation: Multistage test vs predicted strain

5. CONCLUSION AND FUTURE RESEARCH

The paper shows that the linking between the stiffness degradation method and the 3D cyclic contour diagrams is a valid and simple method to predict the soil deformation under regular one-staged cyclic loading conditions.

The explicit method has also been compared to multistage cyclic tests. Here, the method in its current form is not applicable for cyclic laboratory tests allowing pore-pressure dissipation between cyclic stages. However, the method has shown to provide a reasonable match with a multistage laboratory test which does not allow pore-pressure dissipation between cyclic stages. As pore-pressure will likely not dissipate during a design storm event, whilst it will likely dissipate between significant storm events, the explicit method is expected to provide accurate predictions for single storm events.

It is noted that the method has only been validated against two multistage tests and that these tests were performed with a significant variation in stress conditions between the cyclic stages. To further validate the explicit method, additional multistage cyclic laboratory tests will be performed and compared against the explicit method.

ACKNOWLEDGMENT

This research is part of the Innovation and Networking for Fatigue and Reliability Analysis of Structures - Training for Assessment of Risk (INFRASTAR) project. This project has received funding from the European Union's Horizon 2020 research and innovation program under the Marie Skłodowska-Curie grant agreement No. 676139. The laboratory tests are provided by the Chair of Soil Mechanics and Geotechnical Engineering of the Technical University of Berlin. The authors are grateful for the kind permission to use those test results.

REFERENCES

Boukpeti N, Lehane B, Carraro JH. 2014. Strain Accumulation Procedure During Staged Cyclic Loading of Carbonate Sediments. ASME. International

Conference on Offshore Mechanics and Arctic Engineering, Volume 3: Offshore Geotechnics OMAE2014.

DNV GL AS. 2017. Offshore soil mechanics and geotechnical engineering, Offshore Standard DNVGL-RP-C212, Edition August 2017.

PLAXIS. 2017. Plaxis 3D, Reference Manual, Edited by Brinkgreve, R.B.J., Kumarswamy, S., Swolfs, W.M., and Foria F.

Zorzi, G., Richter, T., Kirsch, F., Augustesen, A. H., Østergaard, M. U., & Sørensen, S. P. H. 2018. Explicit Method to Account for Cyclic Degradation of Offshore Wind Turbine Foundations Using Cyclic Interaction Diagrams. International Society of Offshore and Polar Engineers.

Zorzi, G., Richter, T., Kirsch, F., Østergaard, M. U., & Sørensen, S. P. H. 2018. Lifetime tilting prediction of offshore wind turbine foundations due to soil strain accumulation. 14th EAWE PhD Seminar on Wind Energy. Brussel, Belgium

Appendix G

Application of the Soil Cluster Degradation method to simulate a full-scale test of a gravity-based foundation.

This paper is a draft ready to be submitted to a journal.

An application of the Soil-Cluster-Degradation method to a full-scale gravity-based foundation test

Gianluca Zorzi[1], Thomas Richter[1], Fabian Kirsch[1], Martin Underlin Østergaard[2], Søren Peder Hyldal Sørensen[2]

[1] GuD Geotechnik und Dynamik Consult GmbH, Berlin, Germany

[2] COWI A/S, Aalborg, Denmark

ABSTRACT

In most offshore wind turbine projects, the cyclic behaviour of the soil-structure-interaction (SSI) is not sufficiently considered due to the lack of generally accepted methods and guidelines. Consequently, the present work aims to evaluate the accuracy and credibility of an advanced numerical method, called soil cluster degradation (SCD) method, by simulating a full-scale cyclic loading test of a gravity-based foundation. The paper goes through all the steps necessary for the application of the SCD method: the investigation of the in-situ soil conditions to obtain the engineering soil properties, the development of the cyclic contour diagram and the modelling assumptions. Lastly, a comparison with the measurement data in terms of foundation settlement, tilting and stress redistribution is presented. The good agreement with the measurement data suggests that the SCD method is a reliable and simple method to provide a fairly accurate cyclic loading behaviour for a SSI problem.

Notation

ASR	Average stress ratio
CSR	Cyclic stress ratio
$\boldsymbol{F_a}$	Average load
$\boldsymbol{F_{cly}}$	Cyclic amplitude load
FE	Finite Element
$\boldsymbol{G_{ini}}$	Initial shear stiffness
$\boldsymbol{G_N}$	Fictious stiffness at cycle N
LCOF	Levelized cost of energy
$\boldsymbol{N}$	Number of cycles

SCD	Soil cluster degradation
SLS	Serviceability Limit State
SSI	Soil structure interaction
RNA	Rotor nacelle assembly
$\boldsymbol{\gamma_N}$	Permanent shear strain at cycle N
$\boldsymbol{\gamma_{ini}}$	Initial shear strain at the application of $\boldsymbol{\tau_a}$
$\boldsymbol{\tau_a}$	Average stress
$\boldsymbol{\tau_{cly}}$	Cyclic amplitude stress
$\boldsymbol{\sigma'_v}$	Effective vertical stress

INTRODUCTION

Offshore wind turbines are very slender structures continuously swing due to the action of environmental (e.g. winds, waves, currents) and accidental (e.g. typhoons, earthquakes) loads. The foundation component is receiving large cyclic moments which are transmitted to the surrounding soil in form of cyclic stresses. The cyclic behaviour of the soil supporting the wind turbine is a very important aspect that offshore geotechnical engineers have to analyse. Saturated soil subjected to repeated cyclic stresses develops an accumulation of permanent deformations and stress redistribution along the soil-structure interface leading to an irreversible rotation of the foundation. Due to operational reasons, wind turbine manufactures provide a maximum allowed tilting throughout the planned lifetime of the wind turbine, e.g. 0.25° (DNV-GL, 2017). This strict verticality requirement originates from different possible problems (Bhattacharya, 2019): different stresses in the nacelle bearing, difficulties in the motor capacity for yawing, blade tower collision and increase loads in the foundation (P-δ effect).

Offshore geotechnical engineers are challenged to employ numerical tools to predict the accumulation of permanent deformation in the soil and the related rotation of the foundation. To date, there is no developed cyclic constitutive model which can accurately simulate in time domain all the key characteristic of the soil response when subjected to a high number of cyclic loads. Common

soil constitutive models employed for investigating the soil behaviour when subjected to static load cannot be implemented in modelling the response in time domain for a high number of cyclic loads due to an inevitable accumulation of numerical errors (Niemunis, 2005). Therefore, for practical purpose the accumulation of permanent strain is explicitly predicted over N number of cycles. This explicit prediction is relying on cyclic laboratory tests which provides the permanent strain in relation to the number of cycles and the stress level. Different methods exist to insert the permanent strain field to the FE soil domain (Niemunis, 2005; Zorzi, et al., 2018; Jostad, et al., 2014). In this paper, the advanced numerical tool which predict explicitly the accumulation of rotation of a foundation subjected to a cyclic load design event is the soil cluster degradation (SCD) method (Zorzi, et al., 2018). The SCD method is based on 3D finite element (FE) simulations in which the effect of the cyclic accumulation of permanent strain in the soil is taken into account through the modification of a fictional elastic shear modulus in a clustered division of the soil domain. In each cluster, the reduction of the soil modulus is based on the local stress level and the interpolated permanent strain extracted from cyclic contour diagrams (Andersen, 2015). The Mohr-Coulomb model is used as soil constitutive model. The loading input for the model must be a design storm event simplified in a series of regular parcels. For each cluster, the number of equivalent load cycles is calculated to account for the damage accumulation between load parcels.

The verification and validation of the SCD method is ultimately fundamental when implemented for real projects to carry out cost-effective and reliable design. Therefore, this paper aims to evaluate the accuracy and credibility of the SCD method by simulating a full-scale cyclic loading test of an innovative gravity-based foundation (Ed. Züblin AG, 2013). This test was developed by Ed. Züblin AG in the city of Cuxhaven (Germany) where the soil conditions are similar to those in the North Sea. Several regular cyclic load parcels, were applied to the gravity-based foundation. Soil and structure were subjected to a large monitoring campaign in order to investigate the behaviour of the soil-structure interaction.

This paper introduces the full scale test in term of prototype dimension, installation, the cyclic load program and the behaviour in terms of settlement, power

water pressure and stress redistribution measured during the test. Then a detail application of the SCD method to simulate the full scale test is given: assessment of the soil properties, developing of the cyclic contour diagrams, FE modelling and final comparison with the measurement data in terms of foundation settlement, tilting and stress redistribution.

DESCRIPTION OF THE FULL SCALE TEST

This chapter introduces the cyclic load full-scale test for a gravity-based foundation developed by Ed. Züblin AG – STRABAG. Location of the test and dimension of the prototype is first explained. The chapter then provides information regarding the experimental set up, installation, cyclic load program and the results from the monitoring campaign. The information is obtained from the final report of the test (Ed. Züblin AG, 2013).

Test set-up and installation

In the past years Ed. Züblin AG, developed a new type of gravity-based foundation for offshore wind turbine which can be used for 5+ MW turbine and at a water depth of approximately 50 meters. Before starting production, the prototype in original size was built in order to investigate the behaviour of the foundation under cyclic loads. The full scale test was carried out in Cuxhaven, Germany, in the vicinity of the Elbe estuary (cf. Figure 1). The test site is in proximity of the German North Sea coast since the soil conditions are similar.

Figure 1. Test site location (from Google Maps)

The 3D model of the foundation is shown in Figure 2 (Sedlacek, et al., 2012). The foundation is in contact with the soil by means if four independent feet of

approximately 100 m² (8m x 12m) each. These feet are connected by two hollow crossed pre-stresses concrete box girders. The length of these boxes is approximately 32 meters and with a cross-sectional area of 68 m². At the intersection of the boxes there is a conical pre-stressed concrete shaft built up 30 meter above the foundation level.

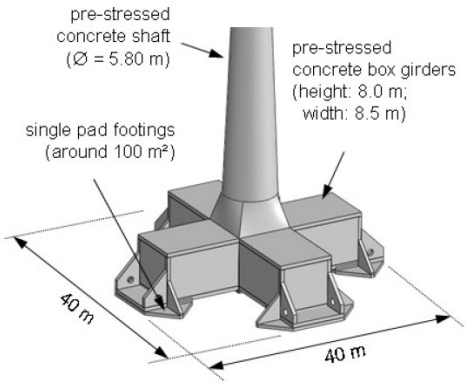

Figure 2. 3D view of the foundation (Sedlacek, et al., 2012)

In order to simulate offshore conditions, the GBF was installed 7 meter below ground in a foundation pit (cf. Figure). The water level inside the pit was 5 meters which corresponds to the ground water level outside the pit. Sheet piles were used to support the foundation pit and are embedded until 5 meter under the foundation level. The installation of the foundation was done in different steps, namely, construction of the feet and boxes, removal of the temporary sand layer, construction of the shaft, ballasting of the foundation and flooding of the pit. The final vertical displacement after the installation was circa 70 mm. The total dead weight under buoyancy including foundation, ballast and the shaft is 80 MN. The uplifting force of the submerged part is calculated and results in 23 MN. Therefore, the total weight is 103 MN.

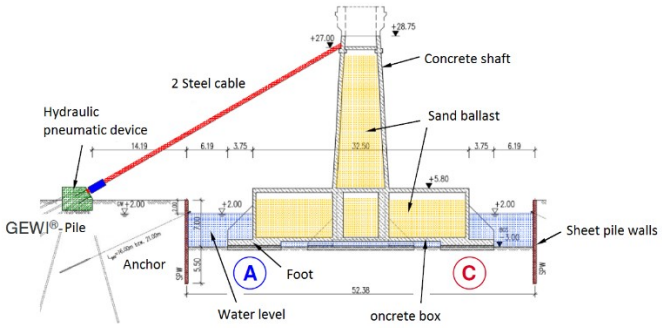

Figure 3. Section of the foundation along the loading direction (Ed. Züblin AG, 2013)

Two hauling steel cables with 55 strands were attached to the shaft at 30 meter from the foundation level and at an angle of 60° from the vertical direction (cf. Figure). In order to accurately measure the applied pulling force in the two cables, load cells were installed at the anchorage point at the foundation shaft. A hydraulic pneumatic device was used to pull the cable. The box girder was directed at an angle of 0° and 90° to the loading direction which is the most critical condition and transfers the highest stresses in the ground. In this configuration the front plate A is subjected to the highest load while the back plate C is in unloading conditions. The stresses in the lateral plates are predominately resulting from the self-weight of the structure and the vertical component of the cyclic test.

Cyclic loading behaviour

After the installation, the foundation is subjected to the cyclic load program shown in Figure .a. It consists of two phases: pre-loading and storm event. The first phase is characterized by different regular packages at relatively low stress cycles (light blue parcels). This initial phase has a total number of cycles of circa 312000 cycles. The second phase (cf. Figure 4, yellow parcels) is the storm event load which is characterized by regular loading packages with increasing magnitude of stress cycles. The total number of cycles considered in the storm event is circa 13500.

The behaviour of the soil-structure interaction during the cyclic loading program was monitored by measuring settlement and structural tilting of the structure, pore water pressure in the soil and contact stress distribution between the

soil and the plates. The vertical settlements were measured along the loading direction by means of a vertical extensimeter. The sensors were mounted at the top of the box and anchored by rigid steel bars at a depth of 30 meter below the feet. The inclination of the structure was measured by means of an inclinometer chain installed on the wall of the concrete shaft.

Figure 4.b-c-d show the measured vertical settlement for the feet and tilting of the structure along the loading direction (plates A-C). The low stress cycles provide a progressive accumulation of settlement/inclination while the storm is responsible for the highest accumulation of deformation of approximately 25 mm in the front plate A.

Pore water pressure is also monitored by means of piezoresistive piezometer sensors placed at different depths below the foundation. The pore water presure measurements below the foundation feet show no accumulation of pore water pressure during the all the cyclic events (Sedlacek, et al., 2012). Therefore the drainage condition of the test is considered drained.

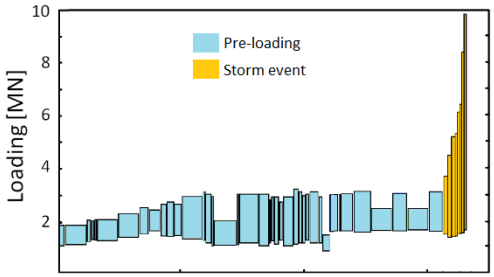

a)

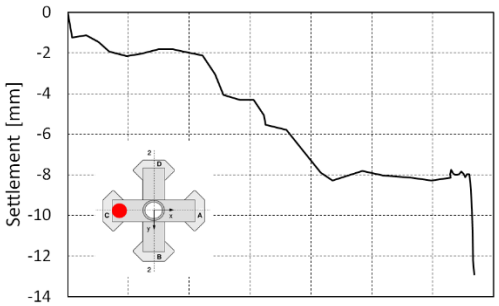

b)

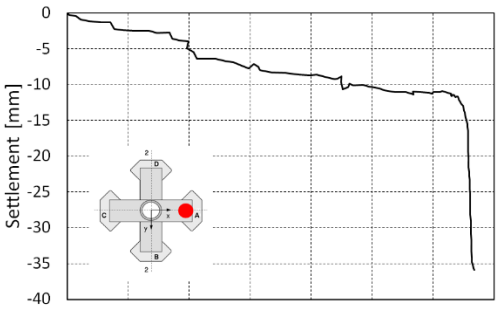

c)

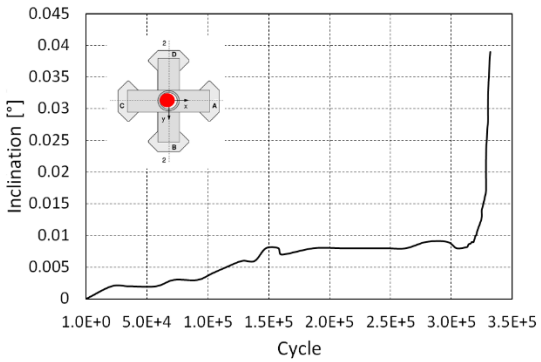

d)

Figure 4. Measured foundation settlement and inclination

In order to investigate the contact stress distribution, different total stress sensors where installed under each plate at different depths. Figure 5 shows the contour plot of the measured total stresses at the depth of -0.5 m below the bottom of the foot plates before and after the first storm event. Before the storm event (Figure 5.a) an irregular distribution of the stresses is already visible which most likely occurs due to the application of the 312000 cycles prior to the first storm (Zachert, et al., 2016). Theoretically, after the installation a uniform stress distribution of circa 256 kPa should be visible (light green colour) due to the weight of the foundation.

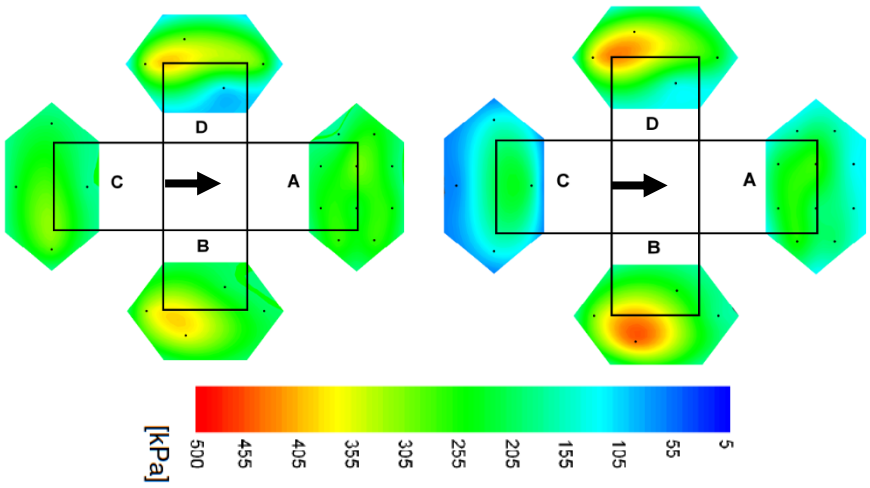

(a) (b)

Figure 5. Contact stress distribution: (a) before the storm, (b) after the storm

The cyclic loads induced a contact stress redistribution under the 4 plates. There is a stress relaxation along the loading direction (plates A-C) especially on the borders of the plates. Due to this stress relaxation, the external stresses are then transferred to plate B and D perpendicular to the loading direction. Figure 5.b shows that the two plates experience an increase of the stresses which is almost double in magnitude compared to the plates A and C.

APPLICATION OF THE SCD METHOD

The application of the SCD method requires different steps summarize in Figure 6. First, the assessment of the in situ soil conditions: layering and the derivation of the unloading-reloading young soil modulus for the Mohr-coulomb model. The second step is the definition of the design event. The load is divided in regular parcels with constant average and cyclic amplitude and N number of cycles. The FEM modelling is the division of the soil domain into clusters. The cluster division has to agree with the soil layering and the geometry of the foundation. The 3D local stress assessment phase is fundamental to understand the magnitude of the local stresses in each cluster which assist the planning of the load program (average and cyclic stresses) for the laboratory test campaign. The next step is conducting the cyclic laboratory tests and interpolating the cyclic contour diagrams. The final step is running the program and extract the foundation tilting.

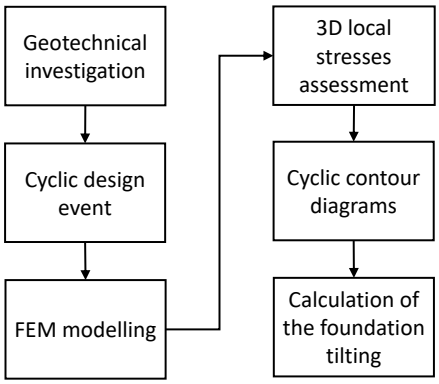

Figure 6. Necessary steps for the application of the SCD method

Assessment of the soil properties

Before the installation of the gravity-based foundation, a geotechnical ground survey was conducted by means of Cone Penetration Tests (CPTs) and boreholes under the four feet (Ed. Züblin AG, 2013). A preliminary judgment of the boreholes and CPTs suggests that the soil can be divided in 3 different layers. The characterization of the soil samples extracted from the boreholes, show that the first layer S1 is predominantly composed of fine sand, the second layer S2 is a well graded sand with fine gravels and the third layer S3 is a medium coarse sand. Figure 7 shows the tip resistance of the 4 CPTs under the four feet. The tip resistance is starting at a depth of z=-7 which is the foundation level inside the pit. As shown in Figure 7 and in line with the borehole results, the four CPTs feature an increase of the tip resistance with depth, which is typical for dense sand. The three different layers are marking by colours (S1: blue, S2: red, S3: green). Regarding the spatial variability between the four feet, the first layer S1 is quite uniform in terms of magnitude of the tip resistance and depth. Contrary to that, the thickness of the second layer S2 is varying from 5 to 10 meters under the foundation. Moreover, a higher scattering of the CPTs is visible due to the variability of the grain size.

In order to estimate the design profile, a linear model of the tip resistance is fitted to the data for each layer. Hereafter it is assumed that the size of the foundation feet are large enough in order to globally describe the soil behaviour by means of linear models and the local variabilities of the tip resistances can be ignored. Figure 7 shows the linear model as a dashed black line over the original

tip resistance. The linear equations are also included (z is the depth and *t* is the tip resistance).

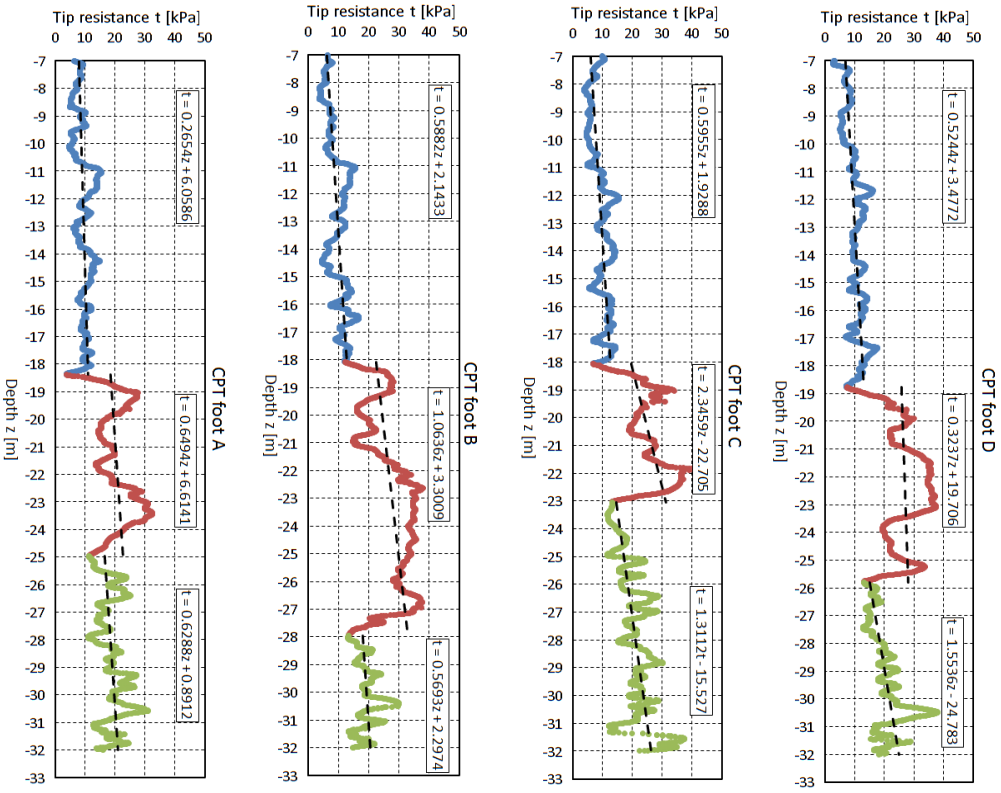

Figure 7. Tip resistance from CPT under the 4 feet

For modelling reasons, one soil design profile is calculated by averaging the best-fit lines of the 4 CPTs. Regarding the thickness of the layers, a mean value is chosen. Figure 8.a visualizes the linear models of the 4 CPTs and the soil design profile in soil black line. The final soil profile is summarized in table 1.

Layer	Depth	Type	Design profile
	m	-	Linear equation
S1	-7;-19	Fine-medium sand	$t = 0.49z + 3.40$
S2	-19;-26	Sand-fine gravel	$t = 1.01z - 9.26$
S3	-26;	Medium coarse sand	$t = 1.09z + 1.26$

Table 1. Soil design profile

In order to perform the cyclic laboratory tests campaign, the relative density of the soil must be assessed. The relative density D_r is calculated adopting the empirical formula from Baldi et al (Baldi, et al., 1986):

$$D_r = \frac{1}{C_2}\, ln\left[\frac{q_c}{C_0(\sigma')^{C_1}}\right], \quad (1)$$

Where C_0, C_1 and C_2 are soil constant, σ' is the effective stress (vertical σ'_{v0} or mean p'_0 effective stress) in kPa and q_c is the tip restistance in kPa.

During the earlier phases (Saale and Elster) of the ice age (or quaternary glaciation), glaciers were advancing on land in the northern part of Europe (Quinteros, et al., 2018). This ice-cover generated a very high stress in the ground leaving the sand in an overconsolidation state when the glaciers retrieved.

Taking this overconsolidation into account, the coefficients $C_0 = 157$, $C_1 = 0.55$ and $C_2 = 2.41$ and the vertical effective stress is used in Equation 1. It is noted that the calculation of the relative density is affected by uncertainties. The coefficients are based on an extensive calibration testing on Ticino sand (Baldi, et al., 1986) which is a clean uniform silica sand with subangular grains and modest compressibility. Cuxhaven sand has a higher content of quartz than the Ticino sand used for the calibration of the coefficients (Quinteros, et al., 2018; Lunne, et al., 1997). Sand with higher quartz content has a lower compressibility and hence a higher cone resistance (Lunne, et al., 1997).

Figure 8.b shows the comparison of the relative density calculated from the design tip resistance and the design relative density used for the laboratory tests campaign. A constant value of relative density for each layer is assumed.

The friction angle of the soil is then estimated based on the relative density and the soil gradation characteristic using the relation from Schmertmann (Schmertmann, 1978). The values are shown in Tables 2. It is noted that this relation is valid until an overburden pressure of 150 kPa. Using this relation for soil at lower depth slightly overestimates the friction angle.

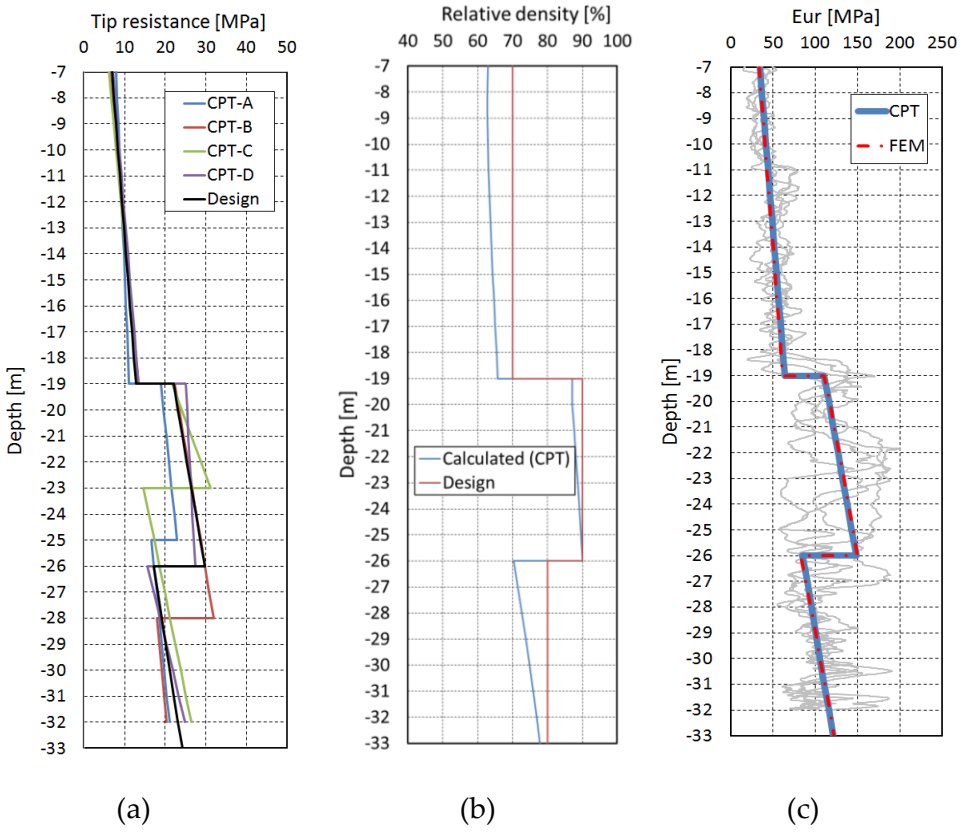

Figure 8. (a) Design tip resistance; (b) Relative density; (c) Unloading/reloading Stiffness Modulus

The soil stiffness employed in the in the SCD method for the Mohr-Coulomb soil model is calculated from the soil design profile of the tip resistance. The drained constrained modulus in unloading/reloading $E(z)_s$ is derived using a linear empirical relationship with the tip resistance (Lunne, et al., 1997). This relation is valid for overconsolidated sand.

$$E(z)_s = \alpha * q(z)_c \,, \qquad (2)$$

However there is no unique relation between the stiffness modulus and the tip resistance because the α value is highly dependent on the soil, stress history, relative density, effective stress level and other factors (Lunne, et al., 1997; Bellotti, et al., 1989; Jamiolkowski, et al., 1988). In this analysis $\alpha = 5$ is chosen (Lunne, et al., 1997).

Assuming an elastic behaviour of the soil during unloading/reloading the soil stiffness modulus for unloading/reloading $E(z)_{ur}$ can be related with the oedometric modulus $E(z)_s$ by means of

$$E(z)_s = \frac{(1-\upsilon_{ur})}{(1+\upsilon_{ur})*(1-2*\upsilon_{ur})} E(z)_{ur} \,, \tag{3}$$

where υ_{ur} is the elastic Poisson ratio for unloading/reloading . In this elastic range, the υ_{ur} can be set equal to 0.2 (Mayne, et al., 2009).

The soil stiffness is stress depended, i.e. increasing with depth. In the Mohr-Coulomb model a linear increase of stiffness with depth is accounted using the following formula (PLAXIS, 2017):

$$E(z)_{ur} = E(z_{ref})_{ur} + \left(z_{ref} - z\right) * E_{inc} \,, \tag{4}$$

where $E(z)_{ur}$ is the Young's modulo for unloading/reloading at a depth z, $E(z_{ref})_{ur}$ is the Young's modulo for unloading/reloading at a reference depth z_{ref} and E_{inc} is the increment of the Young's modulo over depth.

Using these equations for a given input value of $E(z_{ref})_{ur}$ and the increment E_{inc} , the $E(z)_{ur}$ in unloading/reloading employed in the Mohr-Coulomb model can be derived at a specific depth below surface and compared to $E(z)_s$ as specified in the design soil profile derived from CPT. The Young's moduli and z_{ref} values are listed in Table 2. Figure 8.c shows the stiffness derived directly from the raw tip resistance (grey lines), the one calculated from the design tip resistance (in blue) and the fitted stiffness employed in the FE (dashed-red line).

Layer	$\boldsymbol{D_r}$	$\boldsymbol{\varphi}$	$\boldsymbol{z_{ref}}$	$\mathbf{E(z_{ref})_{ur}}$	$\boldsymbol{E_{inc}}$	$\boldsymbol{\nu}$
-	%	°	m	MPa	MPa/m	-
S1	70	38	0	30	2	0.2

S2	90	43	-19	105	5	0.2
S3	80	42	-26	80	5	0.2

Table 2. Summary of the soil design parameters for cyclic loading

FEM modelling

The soil domain is modelled as three layers, as found at the ground investigation (see chapter 3). The dimension of the soil domain is large enough to avoid the influence of the boundary. The soil domain is divided in different cylindrical sectors (soil clusters). The division is characterized by three discretization: vertical, radial and circular. The layers S1 and S2 are both vertically divided in three clusters. The radial and circular divisions are generated in order to fit the feet edges of the foundation and are shown in Figure 9. No clusters are considered in the deeper layer assuming that most of the deformation due to cyclic loading occurs in the two upper layers.

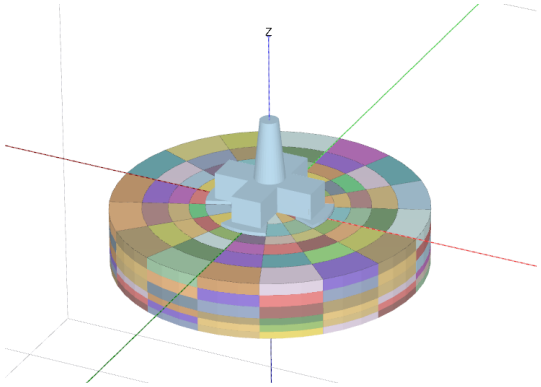

Figure 9. Cluster division and application of the external loads

In order to replicate the experimental conditions as close as possible, the foundation is modelled with the same dimension as in the full scale test. In the numerical model, the shape of the four feet is a cylindrical sector in order to fit with the circular cluster division. The foot area of 100 m^2 is kept the same. Figure 10 shows the comparison between the FE model (Figure 10.a) and the full-scale model (Figure 10.b). No interface, i.e. reduction of shear strength between the feet and the soil is considered.

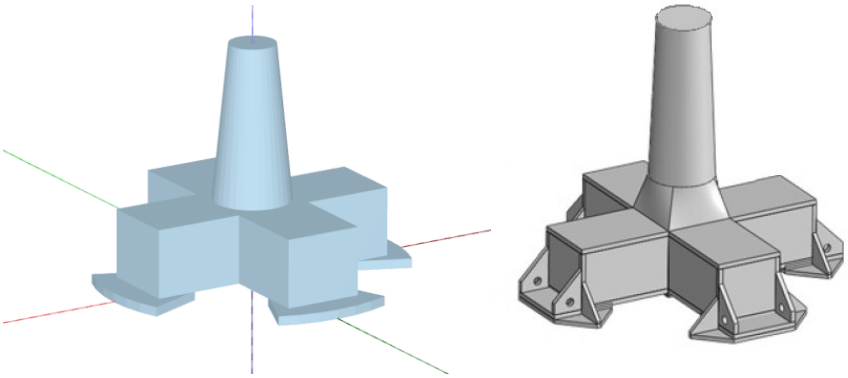

(a) (b)

Figure 10. (a) 3D FE modelling, (b) tested design

The foundation is modelled as a weightless rigid body. On each foot a surface load is applied to account for the weight of the structure. A surface load of 256 kN/m² is applied.

The average and cyclic amplitude loads are applied by means of a point load at the top of the cone shaft at z = 30 meter. The point load features a vertical and horizontal component which are derived from the decomposition of the experimental force applied at an angle of 60° from the vertical axis.

The excavation pit and the embedded pile sheets are not modelled assuming to not have a significant influence on the foundation behaviour. In the numerical model, the water level is set 5 meters over the soil domain.

Cyclic design event

The loading conditions are reorganized and simplified as in Figure 11 and listed in Table 3 (Zachert, et al., 2014). The pre-loading phase is reorganized in three parcels. The simulated storm is grouped in 4 parcels (from parcel 4 to 8).

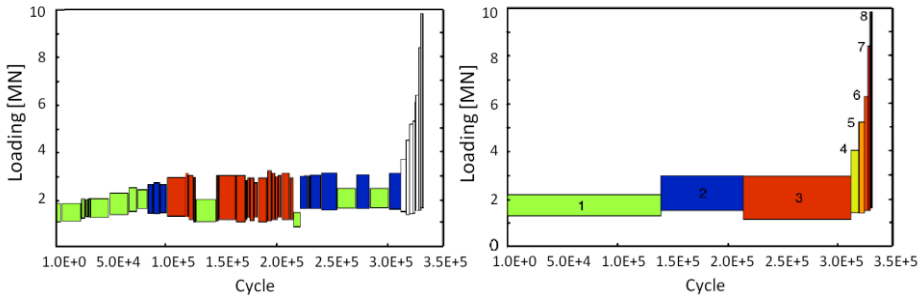

(a) (b)

Figure 11. Parcel organization (Zachert, et al., 2014)*: (a) tested parcel, (b) re-organized parcels*

Parcel	**N**	**F_{min} [kN]**	**F_{max} [kN]**	**F_{avr} [kN]**	**F_{cly} [kN]**
1	140000	1250	2136	1693	443
2	75000	1471.8	2947.8	2209.8	738
3	99000	1085.2	2919.2	2002.2	917
4	6600	1310	4430	2870	1560
5	5200	1340	5260	3300	1960
6	4200	1540	6340	3940	2400
7	1849	1468	8402	4935	3467
8	1849	1592	9860	5726	4134

Table 3. Summary of the loading parcel

Assessment of the 3D local stresses

The accumulation of deformation of cyclic loaded soil is linked to the 3D stress variation around the foundation in terms of average and cyclic amplitude stresses. When planning the laboratory test campaign, different combinations between the average and cyclic amplitude stresses are tested in order to reflect the stress distribution around the foundation. In this regard, the FE model can be used to assess the local distribution of the stresses in the soil clusters which helps to design the cyclic laboratory test campaign.

The FE model in chapter 4.2 is used in combination with the soil parameters for unloading/reloading listed in Table 2. The 3D stress variation in terms of ASR and CSR is found by applying the largest average load of 5.7 MN at the top of the cone shaft and then the maximum load (average plus cyclic amplitude) of 9.8 MN which correspond to the peak of the storm (cf. Table 3). The point load is applied after the installation of the foundation.

Figure 12 illustrates the interpolation of the ASR under the foundation at different depth z. The loading direction is along the plates A-C. The highest stress ratio of 0.5 is forming under the plate A. A ASR=0.25 is visible on the back plate which is in unloading condition.

Looking at the CSR (cf. Figure 13), the magnitude of the ratio is 5 times smaller than the maximum ASR value. This is expected because the gravity based foundation is characterized by a very high vertical load compared to the magnitude of the cyclic loads.

Orthogonal to the loading direction (feet B-D), the magnitude of CSR is lower compared to the feet along the loading direction. The feet B and D are then characterized by a high average stress and a lower cyclic amplitude stress.

At lower depth of z=-17 m both the ASR and CSR ratio are decreasing significantly. It can be concluded that most of the deformations due to cyclic loading actions are appearing on the first two layers (from z=0 to z= -19m) while on the third layer the soil behaviour is assumed to be elastic (no accumulation of permanent strain).

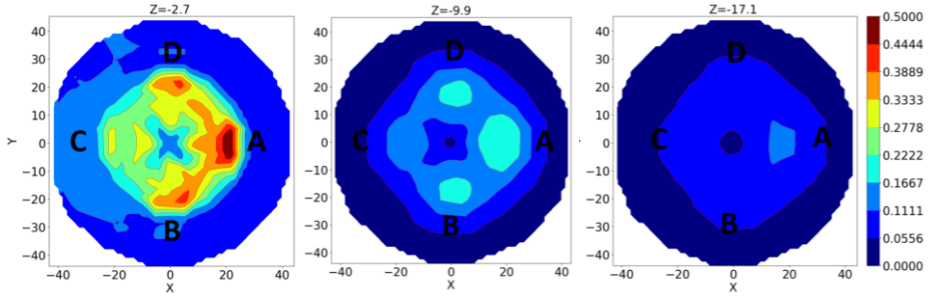

Figure 12. Average stress ratio contour plot at different depth

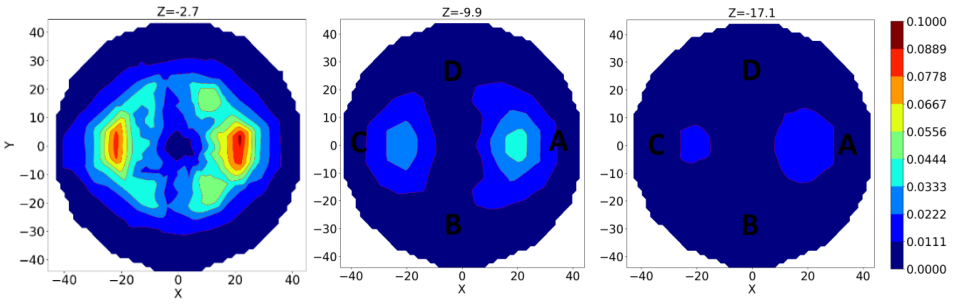

Figure 13. Cyclic stress ratio at different depth

Drained cyclic contour diagrams

Figure 14 shows the granulometric curves of the sands tested in the laboratory. The blue line is the particle size distribution curve assumed for the first layer S1 which is a fine-medium sand. The second layer S2 is adopted by the red curve which is a medium-coarse sand. Due to the variability of the granulometric curves for each layer, these curves can be considered representative for the Cuxhaven sand.

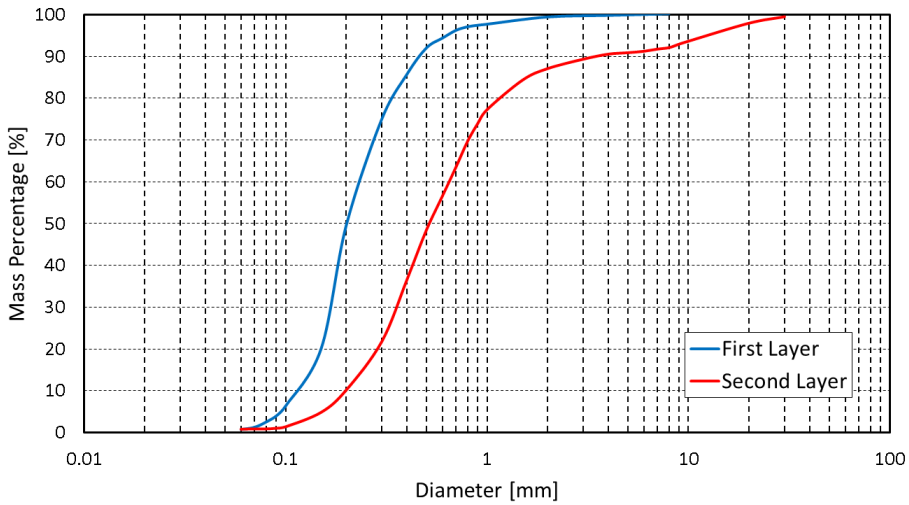

Figure 14. Assumed particle size distribution for the first layer (Sand S1) and second layer (Sand S2)

Undrianed cyclic simple shear tests are available for the two types of sands (cf Figure 14). The simple shear test apparatus is assumed to be representative of the stress path under the gravity-based foundation. The tested soil specimens have dimensions of 90 mm in diameter and 20 mm in height. The tests have

been performed on reconstituted soil samples and the preparation method employed was air pluviation. The sand S1 was tested with a relative density I_D of 70% and an initial vertical confining pressure σ_v' of 200 kPa. The sand S2 was tested with I_D of 90% and σ_v' of 200 kPa. After consolidation, the monotonic shear stress τ_{avg} is applied under drained conditions. The cyclic loading phase is performed under undrained conditions (constant volume) with constant loading amplitude and period. The tests were stopped when reaching 1000 cycles or after the development of the "cyclic mobility" condition which is marked by an increase in shear strain and stabilization of the pore water pressure. Different combinations of ASR and CSR are tested and the ranges for each ratio are summarized in Table 3. For each sand 10 tests are considered sufficient for the construction of the contour diagrams.

Sand	**ASR**	**CSR**
S1	From 0 to 0.35	From 0.04 to 0.16
S2	From 0 to 0.22	From 0.03 to 0.22

Table 4. Ranges of ASR and CSR tested in the laboratory

The drainage condition during the cyclic loading test is found to be drained. Therefore, the undrained shear strains of all the tests are converted to the drained shear strain using the following relation called Undrained2drained (the degree of drainage $u_c = 1$):

$$\gamma_{d_i} = \gamma_{u_i}\left(1 - \frac{u_i\, u_c}{\sigma_v'}\right)^p \quad for\ i = 1, \ldots, N, \tag{7}$$

where, for each cycle i, γ_{d_i} is the calculated permanent drained shear strain, $\gamma_{u_i}$is the undrained permanent shear strain obtained from the test, σ_v' is the initial vertical effective stress, u_i is the residual pore pressure build up u_i at the end of each cycle i. In Appendix A the derivation of the formula is explained. A value of p = 1.7 is used.

All the calculated drained permanent shear strains were assembled in a three-dimensional matrix (ASR, CSR, log(N)) and a three-dimensional linear interpolation was run to map the entire 3D space.

The dotted colour lines in Figures 15 and 16 represent different slices of the 3D matrix for the sands S1 and S2. The colours are related to different strain surfaces of the permanent shear strain γ_N obtained from the initial interpolation. Cyclic simple shear tests have a low test-repeatability which can be attributed to the relatively small specimen size used for testing (Vanden Bergen, 2001). This makes the cyclic tests sensitive to sample preparation such as different initially measured relative density, soil fabric and void ratio non-uniformity.

The raw interpolation of data and the uncertainty related to low sample repeatability of the tests cause an unrealistic non-smooth shape of the strain surfaces. Due to this variability of the tests, a mathematical formulation needs to be fitted to the initial raw interpolation (black lines in Figure 15 and 16). The strain surfaces are then substituted by power law functions and interpolated again together to create the final smooth 3D contour diagram. In the loading program (cf. Table 3) the number of cycles for each load package is larger than the tested in the laboratory. The power law functions can be used to extrapolate the accumulation of permanent strain at high number of cycles. This extrapolation carries as well a degree of uncertainty.

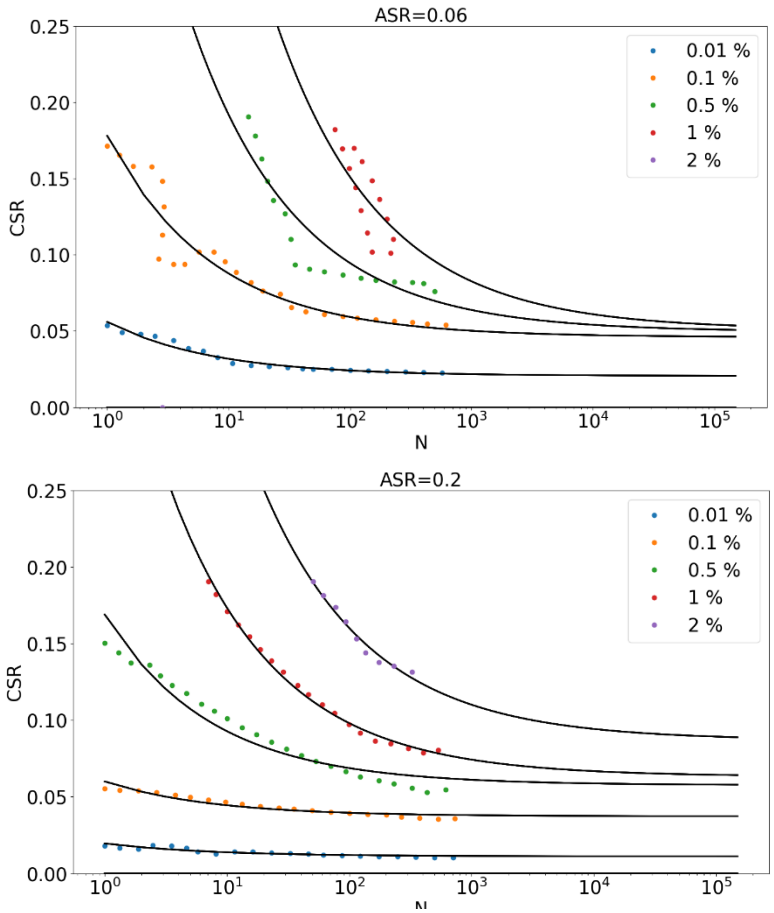

Figure 15. Contour diagrams for permanent shear of sand S1 under drained conditions

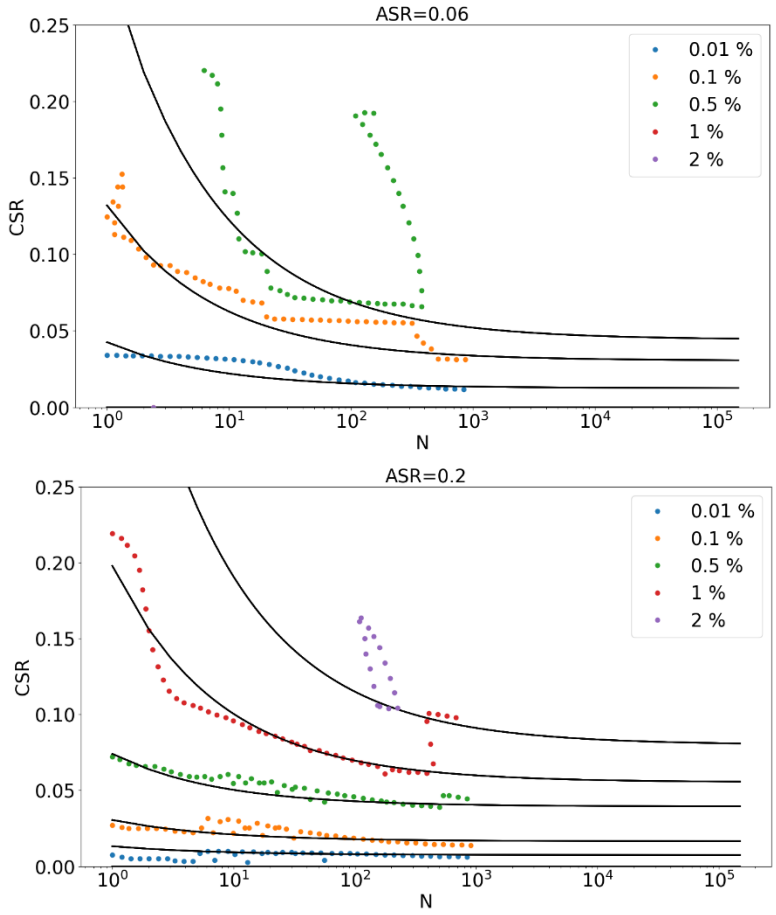

Figure 16. Contour diagrams for permanent shear strain of sand S2 under drained conditions

It is noted that from the numerical assessment of the ASR distribution (cf. Figure 12) in the first layer, some clusters have a value of $ASR_{max} = 0.5$ which is higher than the maximum ASR tested in the laboratory ($ASR_{max} = 0.35$) for the sand S1. Hereafter, a threshold is set at ASR = 0.35. From the contour diagrams it can be seen that increasing the ASR, a higher accumulation of permanent shear strain is developed. The same behaviour was found for a similar sand tested in drained cyclic simple shear test at different average shear stresses (Glasenapp, 2016). Therefore, it is expected an under estimation of the settlement in the numerical model prediction.

Comparison of FE prediction and measurement

This chapter compares the measurements and predictions in terms of foundation settlement, tilting and contact distribution of the soil-structure-interaction developed with the cyclic load program.

First the vertical settlement of the plates along the loading direction is investigated (cf Figure 17). Analysing the settlement under the plate A, a slightly under estimation is obtained at the end of the simulated peak storm. A lower settlement is predicted for the initial 3 pre-loading packages. This is likely due to the uncertainty in extrapolating the permanent shear strain at a high amount of cycles.

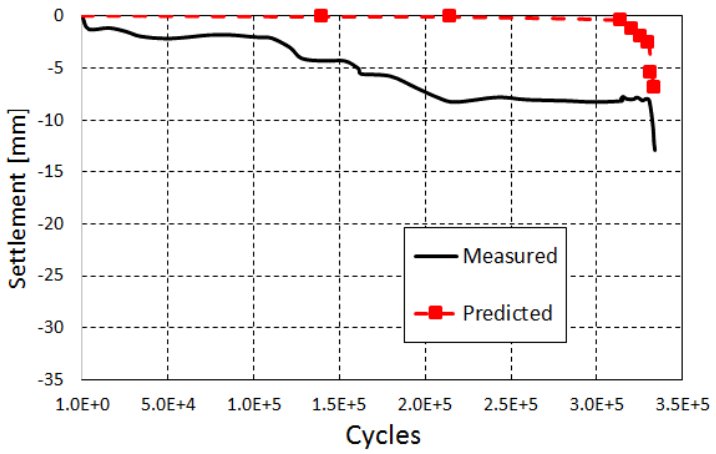

Figure 17. Settlement of Plate C: measured and predicted

Looking at the back plate C (cf. Figure 18), an underestimation of the numerical prediction is visible under drained conditions. A possible reason is in the high uncertainty when the shear stresses are extrapolated from the contour diagrams at a high number of cycles.

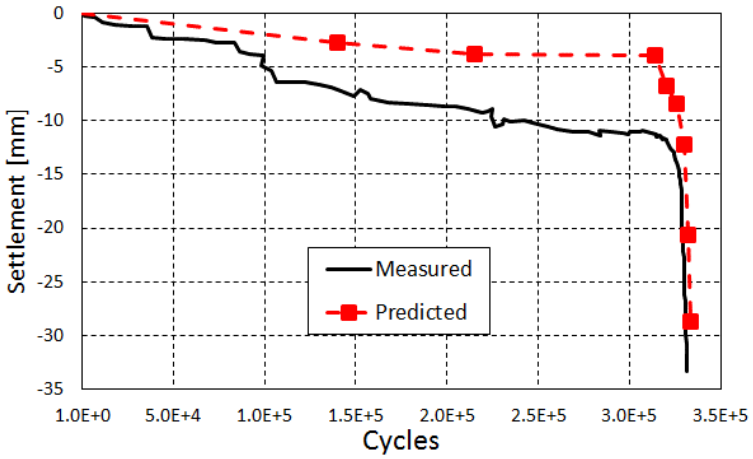

Figure 18. Settlement of Plate A: measured and predicted

The predicted tilting of the structure is evaluated as differential settlement between the plates A and C. Considering the drained assumption, a good agreement of the tilting is predicted with the SCD method (cf. Figure 19).

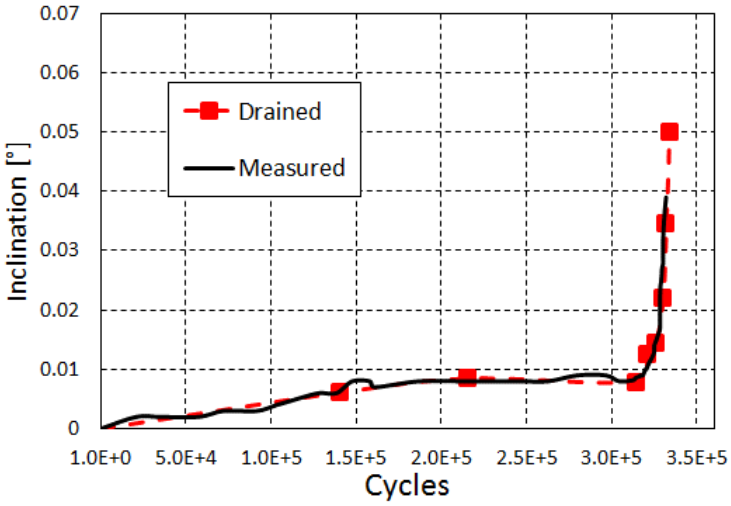

Figure 19. Structural tilting: measured and predicted

Under drained conditions, the soil experiences an improvement of its mechanical properties when subjected to low-frequency cyclic loading. Phenomena such as grain rearrangement (densification) and orientation is decreasing the ability of the soil to deform (resulting in higher stiffness) and is increasing the strength of the soil. At the present state, the SCD method does not consider the possible soil densification during the cyclic loading.

The accumulation of deformation is based on the degradation of the soil stiffness in the different soil clusters. A higher degradation of the stiffness reflects an increase in the accumulation of permanent shear strain. The figure 20 represents a section of the foundation-soil domain along the loading direction (plates A-C). Figure 20.a shows the original stress-dependent stiffness of the soil. The reduction of the stiffness under the foundation at the end of the pre-loading phase (parcel 3) is visualized in Figure 20.b while the reduction at end of the peak of the storm is in Figure 20.b. Higher degradations of the clusters are in the vicinity of the plates where the local stresses are higher. The plate A transfers the higher loads to the soil, hence a deeper degradation of the stiffness is visible.

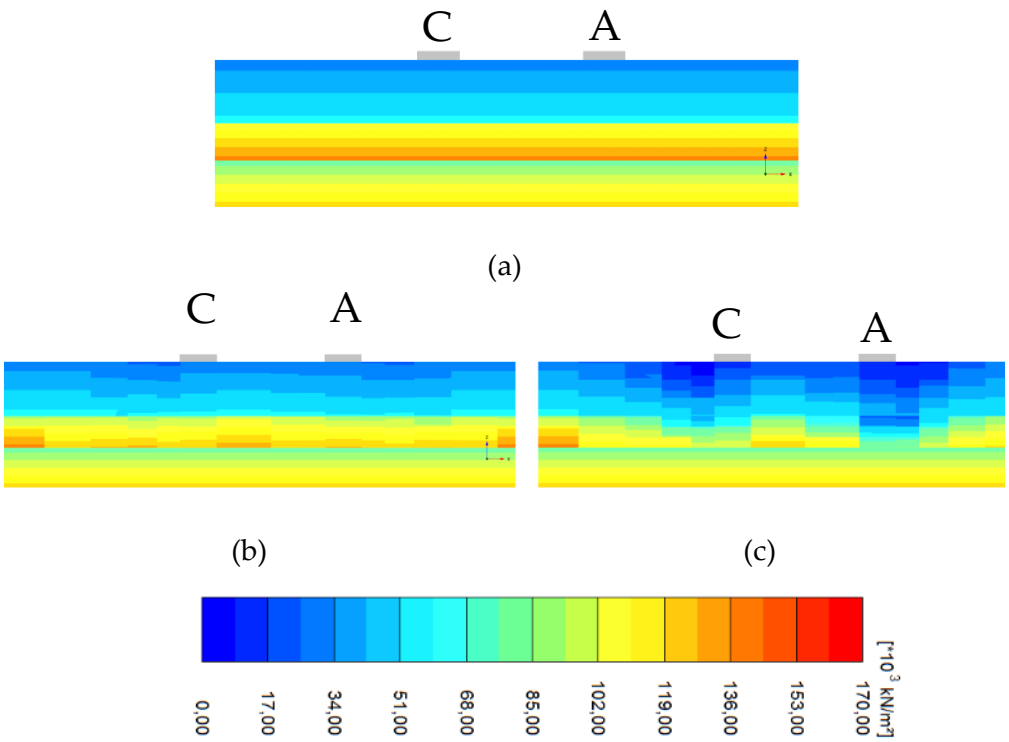

Figure 20. Stiffness degradation: (a) initial soil stiffness, (b) stiffness degradation after parcel 3, (c) stiffness degradation after parcel 8(peak of the storm)

Figure 21 and 22 shows the total contact stress distribution under the four foundation feet at -0.5 m from foundation level. Figure 21 is the predicted (extracted from FE) total stresses distribution after the foundation installation. It

is visible an uniform distribution due to the equal vertical application of the foundation weight. Figure 22 shows the total contact stress distribution after the application of the storm event for the measured and the predicted one (FE simulation). It is visible that the SCD method can successfully predict the stress redistribution on the soil structure interaction due to the cyclic loading.

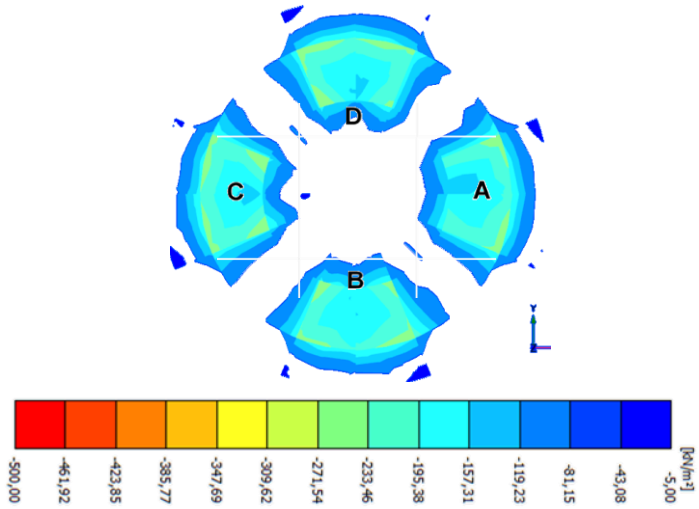

Figure 21. Contact stress distribution after installation (from FE simulation)

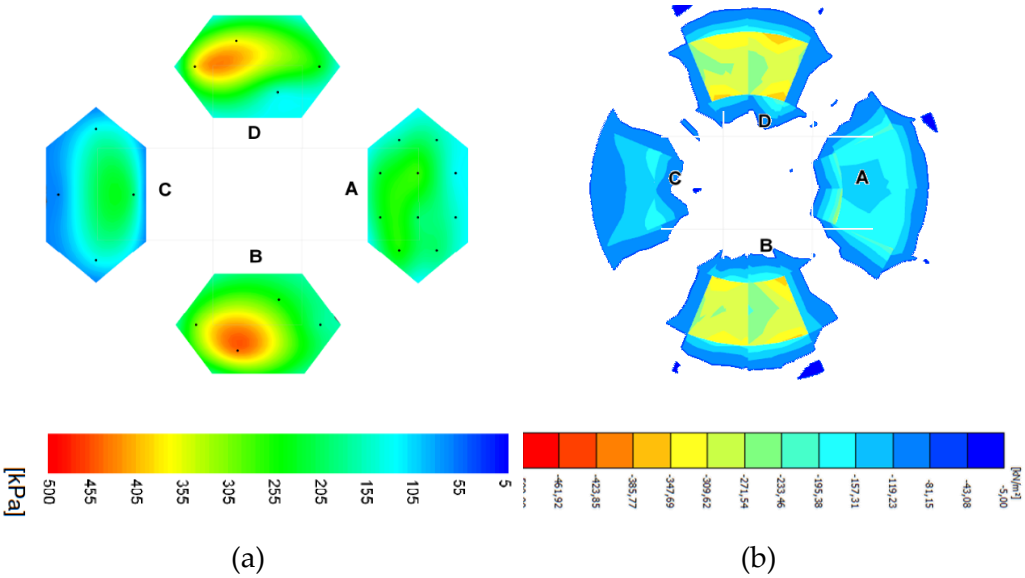

Figure 22. Contact stress distribution after the storm peak: a) measured, (b) FE simulation

CONCLUSION

This paper demonstrates the application of the SCD method for predicting the tilting of a full-scale cyclic load test developed for a gravity-based foundation. The following findings are summarized:

- The SCD method is a reliable and simple method to provide a fairly accurate cyclic loading behaviour for a SSI problem in terms of accumulation of deformation and stress redistribution.
- The satisfactory prediction of the tilting marked the validation of the drained cyclic contour diagrams calculated using the relating Undrained2drained.
- The simulation of the full-scale test is developed automatically by developing a python script. Future development is sensitivity analysis of the final prediction accounting for uncertainty in the soil stiffness calculation, cluster discretization and cyclic contour diagrams

ACKNOWLEDGEMENT

This research is part of the Innovation and Networking for Fatigue and Reliability Analysis of Structures - Training for Assessment of Risk (INFRASTAR) project. This project has received funding from the European Union's Horizon 2020 research and innovation program under the Marie Skłodowska-Curie grant agreement No. 676139. The laboratory tests are provided by the Chair of Soil Mechanics and Geotechnical Engineering of the Technical University of Berlin. The authors are grateful for the kind permission to use those test results.

REFERENCES

Andersen, K. H., 2015. Cyclic soil parameters for offshore foundation design. The 3rd McClelland Lecture, Frontiers in Offshore Geotechnics III, ISFOG'2015, pp. 5-82.

Baldi, G. et al., 1986. Interpretation of CPTs and CPTUs; 2nd part: drained penetration of sands. Proc. 4th Int. Geotech. Seminar, pp. 143-156.

Bellotti, R., Ghionna, V., Jamiolkowski, M. & Robertson, P., 1989. Design parameters of cohesionless soils from in situ tests. Transportation Research Record.

Bhattacharya, S., 2019. Design of foundations for offshore wind turbines. s.l.:Wiley.

DNV-GL, 2017. DNVGL-RP-C212 - Offshore soil mechanics and geotechnical engineering.

Ed. Züblin AG, 2013. Final Report of the Research Project "Beschreibung des Bodenverhaltens bei zyklisch belasteten Flachgründungen für Offshore-Windenergieanlagen durch Versuche im Originalmaßstab (FKZ 0325175). Technische Informationsbibliothek Hannover.

Glasenapp, R., 2016. Das Verhalten von Sand unter zyklischer irregulärer Belastung. Ph.D thesis, Technical University of Berlin.

Jamiolkowski, M., Ghionna, V., Lancellotta, R. & Pasqualini, E., 1988. New correlations of penetration tests for design practice. International Journal Of Rock Mechanics And Mining Sciences & Geomechanics.

Jostad, H. P. et al., 2014. FE Procedure for Foundation Design of Offshore Structures – Applied to Study a Potential OWT Monopile Foundation in the Korean Western Sea. Geotechnical Engineering Journal of the SEAGS & AGS-SEA, p. 45(4).

Lunne, T., Robertson, P. & Powell, J., 1997. Cone Penetration Testing in Geotechnical Practice. CRC Press, London.

Mayne, P. W. et al., 2009. State-of-the-art paper (SOA-1): geomaterial behavior and testing. 17th International Conference on Soil Mechanics and Geotechnical Engineering.

Niemunis, A. W. T. a. T. T., 2005. A high cycle accumulation model for sand. Computers and Geotechnics, p. 245–263.

PLAXIS, 2017. Plaxis 3D Reference Manual. Edited by Brinkgreve, R.B.J., Kumarswamy, S., Swolfs, W.M., and Foria F., .

Quinteros, V. et al., 2018. Shallow depth characterisation and stress history assessment. of an over-consolidated sand in Cuxhaven, Germany. Proceedings of the 4th International Symposium on Cone Penetration Testing (CPT'18).

Schmertmann, J. H., 1978. Guidlines for cone penetration test, performance and design. US Federal Highway Administration, Washington DC, Report FHWA-TS-78-209.

Sedlacek, G., Miehe, A., Libreros, A. & Heider, Y., 2012. Geotechnical Stability of Gravity Base Foundations for Offshore Wind Turbines on Granular Soils. ASME 2012 31st International Conference on Ocean, Offshore and Arctic Engineering.

Vanden Bergen, J., 2001. Sand Strength Degradation within the Framework of Vibratory Pile Driving. PhD thesis, University Catholique de Louvain, Faculty of Applied Science Civil and Environmental Engineering Division.

Zachert, H. et al., 2014. Validation of a high cycle accumulation model via FE-simulations of a full-scale test on a gravity base foundation for offshore wind turbines. International Wind Engineering Conference, IWEC 2014.

Zachert, H., Wichtmann, T. & Triantafyllidis, T., 2016. Soil Structure Interaction of Foundations for Offshore Wind Turbines. International Society of Offshore and Polar Engineers ISOPE.

Zorzi, G. et al., 2018. Explicit Method to Account for Cyclic Degradation of Offshore Wind Turbine Foundations Using Cyclic Inter-action Diagrams. International Society of Offshore and Polar Engineers, pp. ISOPE-I-18-271.

APPENDIX

From the slices of the cyclic contour diagram in Figure 12-13, it can be inferred that the relation between the CSR and the strain surface is not linear but it can be assumed to follow an exponential relation.

$$\gamma_i = (CSR_i)^p \quad for\ i = 1, \dots, N\ , \tag{6}$$

This means that doubling the CSR value is not directly resulting in a double permanent shear strain at the certain number of cycles. Considering an

undrained simple shear test, this exponential relation can be defined in terms of total stresses at each cycle (the apex * stands for total stress)

$$\gamma_{u_i} = (CSR_i{}^*)^p = \left(\frac{\tau_{cyl}}{\sigma'_{v,0}-u_i}\right)^p \quad for\ i = 1,\dots,N, \tag{7}$$

It is assumed that the same exponential variation between the shear strain and the CSR is occurring as well in the drained tests

$$\gamma_{d_i} = (CSR_i{}^*)^p = \left(\frac{\tau_{cyl}}{\sigma'_{v,0}}\right)^p, \tag{8}$$

Now comparing the tests run with the same cyclic stress amplitude in drained and undrained conditions, the following relationship can be formulated

$$\tau_{cly}^p = \gamma_{d_i}\,(\sigma'_{v,0})^p = \gamma_{u_i}\left(\sigma'_{v,0} - u_i\right)^p \quad for\ i = 1,\dots,N, \tag{9}$$

Which leads to

$$\gamma_{d_i} = \gamma_{u_i}\left(\frac{\sigma'_{v,0}-u_i}{\sigma'_{v,0}}\right)^p \quad for\ i = 1,\dots,N, \tag{10}$$

Therefore, the undrained permanent shear strain can be multiplied by a reduction factor based on the residual pore pressure build up u_i at the end of each cycle i and the initial vertical consolidation stress $\sigma'_{v,0}$, elevated by a factor p. This allows the calculation of the permanent drained shear strain γ_{d_i} theoretically developed in drained conditions.

The equation (10) can be modified to account for the intermediate partially drainage conditions. A degree of drainage term u_c is multiplied to the pore water pressure and the new relation is:

$$\gamma_{d_i} = \gamma_{u_i}\left(1 - \frac{u_i\,u_c}{\sigma'_{v,0}}\right)^p \quad for\ i = 1,\dots,N, \tag{11}$$

u_c varies from 0 to 1. Looking at the limits of this value, when $u_c = 1$ the drained shear strains are derived (Equation 10). On the other extreme, $u_c = 0$, i.e. no drainage assumed, the shear strains are equal to the undrained one ($\gamma_{d_i} = \gamma_{u_i}$). If $0 < u_c < 1$ then different shear strain with partially drainage conditions can be theoretically obtained.

The value p is then calibrated by means of comparing two simple shear tests executed under undrained conditions with two under drained conditions. The sand utilized is similar to the S1 (Glasenapp, 2016) and the samples are prepared to have a relative density of 60% and an initial vertical pressure of 200 kPa.

An ASR of 0.1 is applied for all the tests. Two different CSR values of 0.05 and 0.1 are investigated. Figure 1 compares the undrained, drained and the permanent drained shear tests obtained from the Equation 10. A value of p = 1.7 gives a satisfactory agreement. From the plots it can be inferred that the proposed relation is valid before the cyclic mobility phase ("strain take off"). It should be stressed that further research is necessary in order to validate this empirical formulation and to learn under which assumptions it is valid.

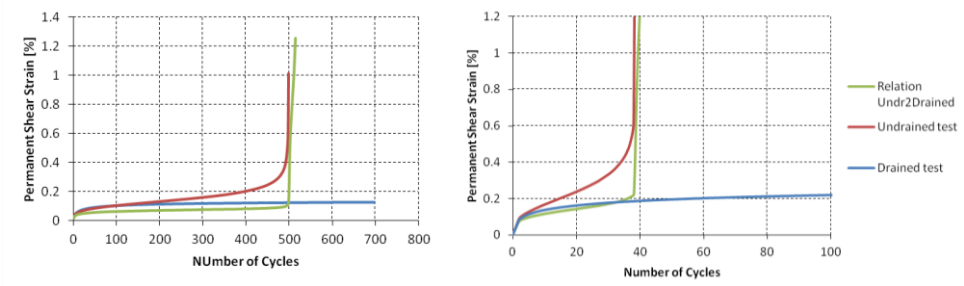

(a) (b)

Figure 1. Comparison of permanent shear strain under drained and undrained conditions: a) I_D=60%, ASR=1, CSR=0.05, σ'_v=200 kPa; b) I_D=60%, ASR=1, CSR=0.1, σ'_v=200 kPa.

Appendix H

Reliability analysis of offshore wind turbine foundations under lateral cyclic loading

This paper has been published in the Wind Energy Science journal. The review and the open discussion is available here: https://www.wind-energ-sci-discuss.net/wes-2019-57/.

This is the post-print of the accepted manuscript of the article. The original article can be found here WES - Reliability analysis of offshore wind turbine foundations under lateral cyclic loading (copernicus.org)

Original version: Zorzi, G., Mankar, A., Velarde, J., Sørensen, J. D., Arnold, P., and Kirsch, F.: Reliability analysis of offshore wind turbine foundations under lateral cyclic loading, Wind Energ. Sci., 5, 1521–1535, https://doi.org/10.5194/wes-5-1521-2020, 2020.

Reliability analysis of offshore wind turbine foundations under lateral cyclic loading

Gianluca Zorzi[1], Amol Mankar[2], Joey Velarde[3], John D. Sørensen[2], Patrick Arnold[1], Fabian Kirsch[1]

[1] GuD Geotechnik und Dynamik Consult GmbH, Berlin, 10589, Germany

[2]Aalborg University, Aalborg, 9100, Denmark

[3] COWI A/S, Aarhus, 8000, Denmark

Correspondence to: Gianluca Zorzi (zorzi@gudconsult.de)

Abstract.

The design of foundations for offshore wind turbines (OWT) requires the assessment of long-term performance of the soil–structure-interaction (SSI), which is subjected to many cyclic loadings. In terms of serviceability limit state (SLS), it has to be ensured that the load on the foundation does not exceed the operational tolerance prescribed by the wind turbine manufacturer throughout its lifetime. This work aims at developing a probabilistic approach along with a reliability framework with emphasis on verifying the SLS criterion in terms of maximum allowable rotation during an extreme cyclic loading event. This reliability framework allows the quantification of uncertainties in soil properties and the constitutive soil model for cyclic loadings and extreme environmental conditions and verifies that the foundation design meets a specific target reliability level. A 3D finite element (FE) model is used to predict the long-term response of the SSI, accounting for the accumulation of permanent cyclic strain experienced by the soil. The proposed framework was employed for the design of a large diameter monopile supporting a 10 MW offshore wind turbine.

1 Introduction

Offshore wind turbines are slender and flexible structures which have to withstand diverse sources of irregular cyclic loads (e.g., winds, waves, and typhoons). The foundation, which has the function to transfer the external loads to the soil must resist this repeated structural movement by minimising the deformations.

The geotechnical design of foundation for an OWT has to follow two main design steps named static load design (or pre-design) and cyclic load design. A design step is mainly governed by limit states: i.e. the ultimate limit state (ULS), the serviceability limit state (SLS) and the fatigue limit state (FLS). The design of an offshore structure mostly starts with the static load design step in which a loop between the geotechnical and structural engineers is required to converge to a set of optimal design dimensions (pile dimeter, pile length and can thickness). This phase is governed by the ULS in which it must be ensured that the soil's bearing capacity withstands the lateral loading of the pile within the allowable deformations (i.e. pile deflection/pile rotation at the mudline).

Subsequently, the pre-design is checked for the cyclic load. The verification of the pre-design for the cyclic load design step regards three limit states: ULS, SLS and FLS. The cyclic stresses transferred to the soil can reduce the lateral resistance by means of liquefaction (ULS), can change the soil stiffness which can cause resonance problems (FLS) and can progressively accumulate deformation into the soil leading to an inclination of the structure (SLS). If one of these limit states is not fulfilled, cyclic loads are driving the design and the foundation dimensions should be updated.

Performing the checks for the cyclic load design step is very challenging due to the following: (i) a high number of cycles is usually involved; (ii) soil subjected to cyclic stresses may develop non linearity of the soil response, pore water pressure, changing in stiffness and damping and accumulation of soil deformation (Pisanò, 2019).; (iii) the load characteristic such as frequency, amplitude and orientation are continually varying during the lifetime; (iv) characteristic of the soil such as type of material, porosity, drainage condition can lead to different soil response; (iv) the relevant codes (BSH, 2015; DNV-GL, 2017) do not recommend specific cyclic load methods for predicting the cyclic load behaviour of structures which lead to the development of various empirical formulations (Cuéllar et al., 2012; Hettler, 1981; LeBlanc et al., 2009) or numerical based models (Zorzi et al., 2018; Niemunis et al., 2005; Jostad et al., 2014; Achmus et al, 2007). Despite the different techniques used in these models, they all predict the soil behaviour "explicitly", based on the number of cycles instead of a time domain analysis (Wichtmann, 2016). Time domain analysis for a large number of

cycles is not convenient due to the accumulation of numerical errors (Niemunis et al., 2005).

In common practice due to the non-trivial task faced by the engineers, simplifications and hence introduction of uncertainties and model errors, are often seen. The application of probabilistic-based methods for designing offshore foundations is not a new topic (Velarde et al., 2019a; Velarde et al., 2019b; Carswell et al., 2014); and it is mainly related to the static design stage. Very limited research has been developed regarding the probabilistic design related to the cyclic load design stage.

This current work focuses on the cyclic loading design stage and the verification of the serviceability limit state. During the design phase, the wind turbine manufacturers provide a tilting restriction for operational reasons. The recommended practice DNV-GL-RP-C212 (DNV-GL, 2017) provides the order of magnitude for the maximum allowed tilting of 0.25° throughout the planned lifetime. This strict verticality requirement may have originated from different design criteria, which however, are mainly rooted within the onshore wind turbine sector and are given below (extracted from Bhattacharya, 2019):

- Blade–tower collision: owing to an initial deflection of the blades, a possible tilting of the tower may reduce the blade–tower clearances.
- Reduced energy production: change in the attack angle (wind-blades) may reduce the total energy production.
- Yaw motors and yaw breaks: reducing motor capacity for yawing into the wind.
- Nacelle bearing: a tilted nacelle may experience different loadings in the bearing, causing a reduction of their fatigue life or restrict their movements.
- Variation in fluid levels and cooling fluid movement.
- P-δ effect: the mass of the rotor-nacelle-assembly is not aligned with the vertical axis and this creates an additional overturning moment in the tower, foundation, grouted connection, and the soil surrounding the foundation.
- Aesthetic reasons.

In SLS designs, extreme as well as relevant accidental loads, such as typhoons and earthquakes, should be accounted for as they can be design-driving loads. A very strict tilting requirement, i.e., 0.25°, in conjunction with these accidental conditions can increase the foundation dimensions and significantly raise the cost of the foundation.

An advanced numerical method called soil cluster degradation (SCD) method was developed (Zorzi et al., 2018). This method explicitly predicts the cyclic response of the SSI in terms of the foundation rotation. The main objective of this study is to use the SCD method within a probabilistic approach. The probabilistic approach along with the reliability framework was used to quantify the main uncertainties (aleatoric and epistemic), explore which uncertainty the response is most sensitive to, and de-sign the long-term behaviour of the foundation for a specific target reliability level. In this paper first the developed reliability-based design (RBD) frame-work is outlined in detail. Finally, an application of the proposed RBD frame-work is presented for a large diameter monopile supporting a 10 MW offshore wind turbine.

2 Development of the RBD framework

2.1 Limit state function for SLS

The rotation experienced by the foundation structure subjected to cyclic loading is considered partially irreversible (irreversible serviceability limit states) because the soil develops an accumulation of irreversible deformation due to the cyclic loading action. For this reason, it is noted that the accidental and environmental load cases for the SLS design are the extreme loads that give the highest rotation. As for a deterministic analysis, the first step in the reliability-based analysis is to define the structural failure condition(s). The term failure signifies the infringement of the serviceability limit state criterion, which is here set to a tilting of more than 0.25°. The limit state function $g(\boldsymbol{X})$ can then be written as

$$g(\boldsymbol{X}) = \theta_{max} - \theta_{calc}(\boldsymbol{X}) \,, \tag{1}$$

where $\theta_{max} = 0.25°$ is the maximum allowed rotation and $\theta_{calc}(\boldsymbol{X})$ is the predicted rotation (i.e. the model response) based on a set of input stochastic variables $\boldsymbol{X}$.

2.2 Estimation of the probability of failure

The design has to be evaluated in terms of the probability of failure. The probability of failure is defined as the probability of the calculated value of rotation $\theta_{calc}(\boldsymbol{X})$ exceeding the maximum allowed rotation θ_{max} as it does when the limit state function $g(\boldsymbol{X})$ becomes negative, i.e.:

$$P_f = \mathrm{P}[g(\boldsymbol{X}) \leq 0] = P[\theta_{max} \leq \theta_{calc}(\boldsymbol{X})] \quad (2)$$

Once the probability of failure is calculated, the reliability index β is estimated by taking the negative inverse standard normal distribution of the probability of failure:

$$\beta = \Phi^{-1}(P_f) \quad (3)$$

where $\Phi(\,)$ is the standard normal distribution function. The probability of failure in this work is estimated using the Monte-Carlo (MC) simulation. For each realisation, the MC simulation randomly picks a sequence of random input variables, calculates the model response $\theta_{calc}(\boldsymbol{X})$, and checks if $g(\boldsymbol{X})$ is negative (Fenton and Griffiths, 2008). Thus, for a total of n realisations the probability of failure can be computed as:

$$P_f = \frac{n_f}{n}\ , \quad (4)$$

with n_f being the number of realisations for which the limit state function is negative (rotation higher than 0.25°).

IEC 61400-1 (IEC, 2019) sets as a requirement with regard to the safety of wind turbine structures, an annual probability of failure equal to 5×10^{-4} (ULS target reliability level). This reliability level is lower than the reliability level indicated in the Eurocodes EN1990 for building structures where an annual reliability index equal to 4.7 is recommended. Usually, in the Eurocodes, for the geotechnical failure mode considered in this paper the irreversible SLS is used. In

EN1990 Annex B, an annual target reliability index for irreversible SLS equal to 2.9 is indicated, corresponding to an annual probability of failure of 2×10^{-3}.

IEC61400-1 does not specify the target reliability levels for the SLS condition. Therefore, it can be argued that the target for SLS in this paper should be in the range of $5 \times 10^{-4} - 2 \times 10^{-3}$. In this work, the same reliability target for ULS of 5×10^{-4} is also considered for the irreversible SLS as a conservative choice.

2.3 Derivation of the model response θ_{calc}

The calculation of the model response θ_{calc} is based on the soil cluster degradation (SCD) model. The SCD method explicitly predicts the long-term response of an offshore foundation accounting for the cyclic accumulation of permanent strain in the soil. The SCD model is based on 3D finite element (FE) simulations, in which the effect of the cyclic accumulation of permanent strain in the soil is considered through the modification of a fictional elastic shear modulus in a cluster-wise division of the soil domain. A similar approach of reducing the stiffness in order to predict the soil deformation can be found in Achmus (Achmus et al, 2007). The degradation of the fictional stiffness is implemented using a linear-elastic Mohr Coulomb model. Reduction of the soil stiffness is based on the cyclic contour diagram framework (Andersen, 2015). The cyclic contour diagrams are derived from a laboratory campaign using cyclic test equipment. The tests are performed with different combinations of cyclic amplitude and average load for N number of cycles. These diagrams provide a 3D relation between the stress level and number of cycles for an investigated variable: accumulation of strain, pore pressure, soil stiffness or damping. The cyclic contour diagrams have been applied successfully for many years for the design of several offshore foundations (Jostad et al., 2014; Andersen, 2015), however careful engineering judgment is required for the construction and interpretation.

The loading input for the model must be a design storm event simplified in a series of regular parcels. This loading assumption is also recommended by DNV-GL-RP-C212 (DNV-GL, 2017) and the BSH standard (BSH, 2015). The method is implemented in the commercial code PLAXIS 3D (PLAXIS, 2017).

Three stochastic input variables ($\boldsymbol{X} = [\boldsymbol{X_1}, \boldsymbol{X_2}, \boldsymbol{X_3}]$) are necessary for the SCD model:

- $\boldsymbol{X_1}$ = soil stiffness that is derived from the Cone Penetration Test (CPT);
- $\boldsymbol{X_2}$ = cyclic contour diagram that is derived from the cyclic laboratory tests;
- $\boldsymbol{X_3}$ = extreme environmental loads that are derived from metocean data and a fully coupled aero-hydro-servo-elastic model.

These inputs have to be quantified in terms of their point statistics (e.g., the mean, standard deviation, and probability distribution type) representing the uncertainties. When using the MC simulation, $100/p_f$ realisations are needed to estimate an accurate probability of failure, which makes it challenging to apply it in combination with the FE simulations. Since the SCD model is based on 3D FE simulations, it is computationally intensive and hence, expensive to complete a large number of realisations. One FE simulation takes approximately 30–40 min. For this reason, a response surface (RS) is trained in such a way that it yields the same model response θ_{calc} as the SCD model for the studied range of the input variables $\boldsymbol{X}$. The response surface is a function (usually first or second order polynomial form) which approximate the physical or FE models but allow the reliability assessment of the investigated problem with resealable computational effort.

The design of experiment (DoE) procedure is used to explore the most significant combinations of the input variables $\boldsymbol{X}$. Based on the developed FE simulation plan, the obtained outputs θ_{calc} are used to fit the response function.

Figure 1 summarises the methodology for the reliability analysis design for lateral cyclic loading. The framework starts with the uncertainty quantification from the available data (CPT, cyclic laboratory tests of the soil and metocean & aero-hydro-servo-elastic model) and the derivation of the stochastic input variables (soil stiffness, cyclic contour diagram, and storm event). The chosen stochastic variables are the inputs of the SCD model. Based on the stochastic input variables, a response surface is then trained to yield the same output (in terms of structural tilting) of the 3D FE simulations. The response surface is then used

to calculate the probability of failure passing through the formulation of the limit state equation and the MC simulation. If the calculated probability of failure does not meet the target probability, then the foundation geometry has to be changed and the methodology is repeated to check whether the new design is safe.

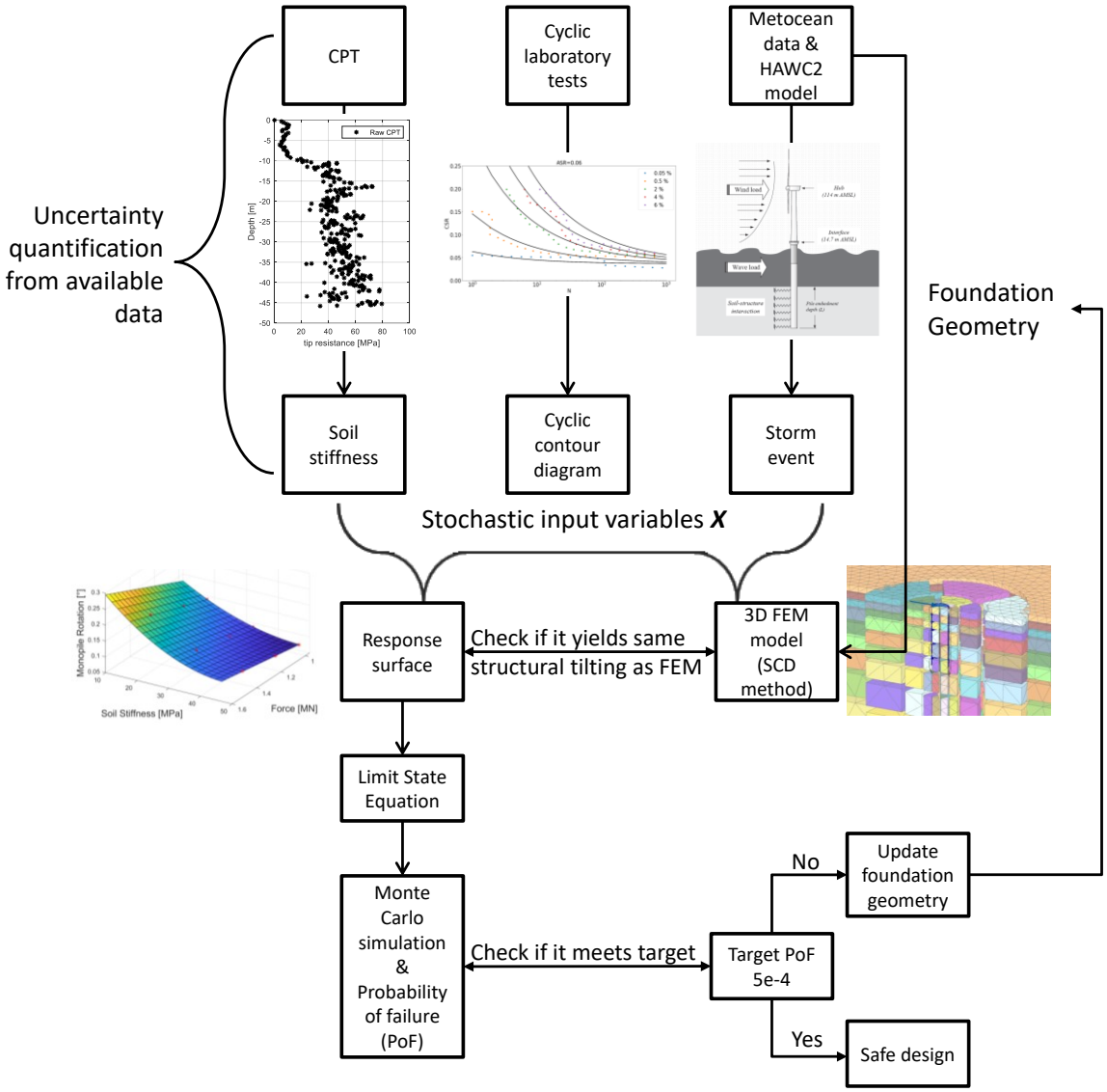

Figure 131: Methodology of reliability analysis.

3. CASE STUDY: RELIABILITY DESIGN FOR A MONOPILE SUPPORTING A 10MW WIND TURBINE

In this section, firstly, the monopile pre-design (static load design step) is carried out in which the subsoil conditions of the case study and the ULS design of the monopile geometry supporting a 10 MW wind turbine are explained. The pre-design of the monopile is developed using the Hardening Soil model in finite element to predict the static response of the monopile.

Then the reliability framework for the cyclic load design shown in Figure 1 is applied to the monopile to check if the pre-design satisfies the SLS criteria. The following subsections discuss the derivation of input uncertainties for the SCD method, derivation of the response surface and probability of failure, and reliability index calculation.

3.1 Monopile pre-design: subsoil condition and pile geometry

For the present case study, a tip resistance from the cone penetration test (CPT) and the boring profile are used to determine the geotechnical properties and soil stratigraphy at the site, where the monopile is assumingly installed. A CPT is basically a steel cone which is pushed into the ground and the tip resistance is recorded. Base on the recorded tip resistance, soil stratigraphy and soil properties can be empirically derived.

The CPT, shown in Figure 2, features an increase in the tip resistance with increasing depth, which is typical for sand. In combination with the borehole profile, the tip resistance from the CPT suggests that the soil can be divided into two different layers. At approximately –10 m there is a jump in the tip resistance marking a transition to another layer with a higher magnitude visible, leading to the conclusion that denser sand is present. The characterisation of the soil extracted from the boreholes, shows the first layer (from 0 to –10 m) consisting of fine to medium sand and the second layer (from –10 m) of well-graded sand with fine gravel.

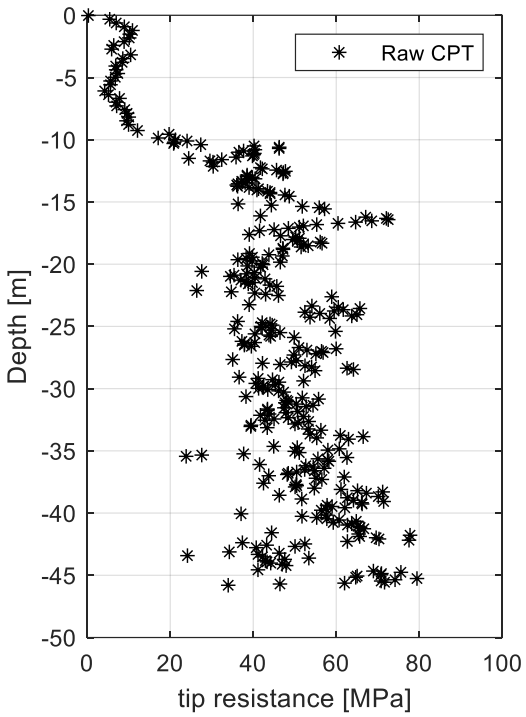

Figure 2: CPT profile.

To accurately predict the soil–structure-interaction and incorporate the rigid behaviour of the large diameter monopile, the ULS geotechnical verification of the preliminary design of the monopile is carried out, using the finite element method in PLAXIS 3D.

The monopile is modelled in PLAXIS as a hollow steel cylinder using plate elements. For the steel, a linear elastic material is assumed with a Young's modulus of 200 GPa and a Poisson coefficient of 0.3. The interface elements are used to account for the reduced shear strength at the pile's surface.

The soil model used is the Hardening Soil model with small-strain stiffness (HSsmall) (PLAXIS, 2017). The hardening soil model with small strain stiffness can predict the non-linear stress-strain behaviour of the soil. It considers a stress and strain stiffness dependency, can predict the higher stiffness of the soil at small strain which is relevant for cyclic loading condition and it distinguishes between loading and unloading stiffness.

On the other hand, the Mohr-Coulomb model approximates the complex non-linear behaviour of the soil by a linear-elastic perfectly plastic constitutive law.

The soil model parameters for the two layers are derived from the tip resistance (Figure 2) and listed in Table 1. The relative density (which is related to the soil porosity) of the two layers is calculated using the formula from Baldi et al. (Baldi et al., 1986) with the over-consolidated parameters (typical for offshore conditions) leading to a mean value of 70% and 90% for the first and second layers, respectively.

Soil	Parameter	Value	Soil	Parameter	Value
	E_{50} [MPa]	33.3	Medium-coarse sand	E_{50} [MPa]	98.3
Fine-medium sand	E_{oed} [MPa]	33.3		E_{oed} [MPa]	98.3
	E_{ur} [MPa]	99.9		E_{ur} [MPa]	295
	m [-]	0.5		m [-]	0.5
	c [kN/m2]	0.1		c [kN/m2]	0.1
Depth: from 0 to -10 m	φ [°]	39	Depth: from -10 m	φ [°]	42
	ψ [°]	9		ψ [°]	12
	G_0 [MPa]	116		G_0 [MPa]	196.6
Relative density: 70%	$\gamma_{0.7}$ [−]	0.0001	Relative density: 90%	$\gamma_{0.7}$ [−]	0.0001

Table 1: Soil model parameters.

The monopile design requires a loop between the structural and geotechnical engineers to update the soil stiffness and loads at the mudline level. A fully coupled aero-hydro-servo-elastic model using HAWC2 (Larsen and Hansen, 2015) is developed to perform the time-domain wind turbine load simulations (Velarde et al., 2019b). The soil structure interaction model is based on the Winkler-type approach, which features a series of uncoupled nonlinear soil springs (so called p-y curves) distributed at every 1 m. The force (p) – deformation (y)

relations are extracted from the PLAXIS 3D model. At each meter section, the calculation of the force (p) is carried out by integrating the stresses along the loading direction over the surface. The displacement (y) is taken as the plate's displacement. The PISA project (Byrne et al. 2019) highlights that additional soil reaction curves components (distributed moment, horizontal base force and base moment) are needed in conjunction with the p-y curves in order to have a more accurate soil structure interaction behaviour. For the sake of simplicity, only the p-y curves extracted from FE are considered.

The final pile design consists of an outer pile diameter at the mudline level of 8 m, a pile thickness of 0.11 m, and a pile embedment length of 29 m. The natural frequency of the monopile is 0.20 Hz and is designed to be within the soft-stiff region. Fatigue analysis of the designed monopile is also carried out (Velarde et al., 2019b). Figure 3.a shows the horizontal displacement contour plot at 3.5 MN horizontal force, while Figure 3.b shows the horizontal load-rotation curve at the mudline.

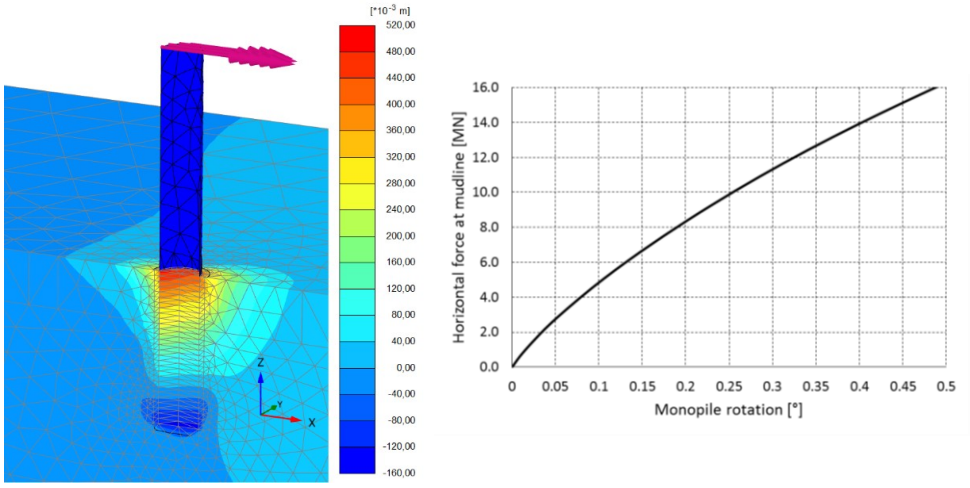

a b

Figure 3: (a) Horizontal displacement contour plot at 3.5 MN horizontal load; (b) Monopile rotation.

3.2 Input uncertainties for the SCD model

The application of the SCD model requires three inputs — soil stiffness (for the Mohr-Coulomb soil model), cyclic contour diagrams, and a design storm event. The laboratory testing and field measurements are used to estimate the inputs for the model. In this estimation process, different sources of uncertainty of unknown magnitude are introduced (Wu et al., 1989). These parameters then have to be modelled as stochastic variables with a certain statistical distribution.

3.2.1 Soil Stiffness

The uncertainties of the soil stiffness used in the SCD model is analysed. The soil model employed in the SCD method is the Mohr–Coulomb model, with a stress-dependent stiffness (i.e., the stiffness increases with depth). For cyclic loading problems, the unloading–reloading Young's modulus E_{ur} is used. This soil modulus is obtained from the tip resistance from the CPT test (Figure 2). The layering of the soil domain is assumed to be deterministic as explained in section 3.1.

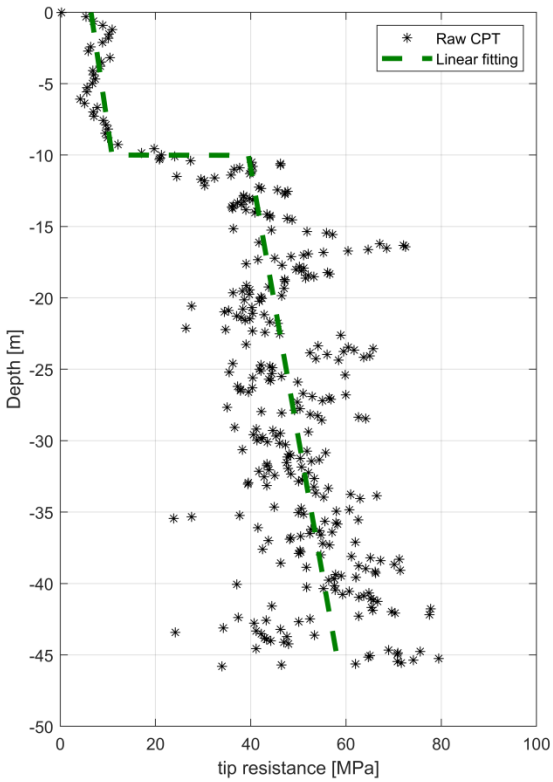

Figure 4: Average tip resistance.

The design tip resistance is established by means of the best-fit line in the data. A linear model is fitted to the data for each layer (Figure 4, green line). The maximum likelihood estimation (MLE) is used for estimating the parameters of the linear model along with the fitting error (assumed to be normally distributed and un-biased). From the MLE method, the standard deviations and correlations of the estimated parameters (Sørensen, 2011) are obtained. The linear model is expressed by means of Eq. (5) as below:

$$q_c = \boldsymbol{X}_a \, z + \boldsymbol{X}_b + \varepsilon \,, \tag{5}$$

where $\boldsymbol{X}_a$, $\boldsymbol{X}_b$ are stochastic variables modelling parameter uncertainty related to the parameters a and b, respectively; ε is the fitting error; and z is the depth (m). Table 2 shows a summary of the fitting parameters.

The residuals are then plotted to check the assumption of the normality of the model error. For the first layer (Figure 5.a), the distribution of the residual is slightly skewed to the right. This means that the trend line underrepresents the tip resistance due to the presence of high peeks at the boundary layer. For the second layer (Figure 5.b), a normal distribution about the zero mean is visible, implying that a better fit is achieved.

Parameter	Distribution	Mean	Standard Deviation
$\boldsymbol{X_a}$ (1st layer)	Normal	-0.42	0.049
$\boldsymbol{X_a}$ (2st layer)	Normal	-0.53	0.024
$\boldsymbol{X_b}$ (1st layer)	Normal	6.35	0.28
$\boldsymbol{X_b}$ (2st layer)	Normal	34.05	0.72
$\boldsymbol{\varepsilon}$ (1st layer)	Normal	0	3.14
$\boldsymbol{\varepsilon}$ (2st layer)	Normal	0	16.06 [MPa]
$\boldsymbol{\rho_{X_a,X_b}}$ (1st layer)	-	0.86	-
$\boldsymbol{\rho_{X_a,X_b}}$ (2st layer)	-	0.98	-

Table 2: Stochastic input variable for tip resistance.

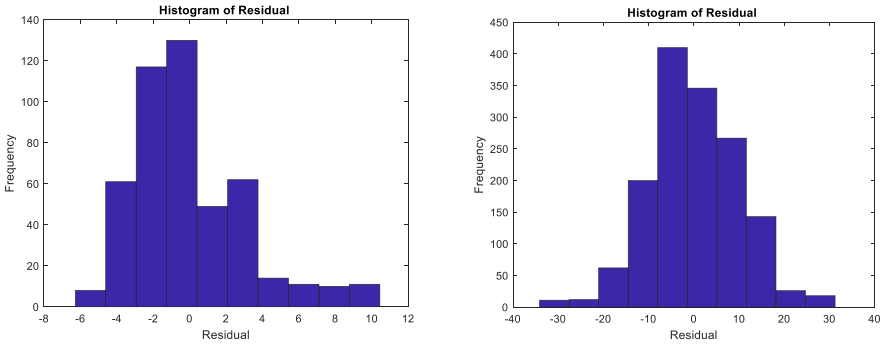

a b

Figure 5: Histogram of residual for layer 1 (a) and layer 2 (b).

An empirical linear relationship is used to calculate the drained constraint modulus in unloading/reloading E_s (Lunne et al., 1997, Lunne and Christoffersen, 1983):

$$E_s = \boldsymbol{X}_\alpha \; q_c \,, \tag{6}$$

where $\boldsymbol{X}_\alpha$ is a unit-less stochastic variable. For over-consolidated sand, which is typical of offshore conditions, a value of $\alpha = 5$ is recommended (Lunne and Christoffersen, 1983). However, there is no unique relation between the stiffness modulus and the tip resistance because the α value is highly dependent on the soil, stress history, relative density, effective stress level, and other factors (Lunne et al., 1997; Bellotti et al. 1989; Jamiolkowski et al. 1988).

To understand the uncertainty in the stiffness modulus, α is treated as a stochastic normal variable varying from $\alpha_{min} = 3$ to $\alpha_{max} = 8$ with a mean $\mu = 5.5$ and standard deviation $\sigma = 1.25$. The standard deviation is calculated by $(\alpha_{min} - \alpha_{max})/4$, assuming that 95.4% of the values are enclosed between the α values of 3 and 8.

Thus, the calculation of the drained constraint modulus in unloading/reloading, covering all possible uncertainties is summarised as follows:

$$E_s = \boldsymbol{X}_\alpha \, [\boldsymbol{X}_a \, z + \boldsymbol{X}_b + \varepsilon] \,, \tag{7}$$

Depending on the size of the foundation, the local fluctuation (physical uncertainty) of the tip resistance can have a significant impact on the structural behaviour. If the size of the foundation is large enough, the soil behaviour is governed by the average of the global variability of the tip resistance (mean trend value). For a smaller foundation, the local effect, i.e., the local physical variability of the tip resistance governs the soil behaviour. If the local variability of the tip resistance does not affect the foundation behaviour compared to the fitted linear model, it can be neglected. Moreover, the uncertainty related to the empirical formulation for calculating the soil stiffness ($\boldsymbol{X}_\alpha$), has a higher influence compared to the one used to approximate the tip resistance with a linear model ($\boldsymbol{X}_a, \boldsymbol{X}_b, \varepsilon$). The preliminary results show that the uncertainty associated with approximating the tip resistance with the mean trend line is negligible due to

the size of the monopile. For this reason, $\boldsymbol{X}_a, \boldsymbol{X}_b, \varepsilon$ are considered deterministic at their mean value.

Figure 6 shows the variability of the soil modulus E_s over depth. The red lines are the realisations, using the MC simulation by performing random sampling on the stochastic variable $\boldsymbol{X}_\alpha$. The black points are the deterministic multiplication of the tip resistance with a mean value of $\alpha = 5.5$.

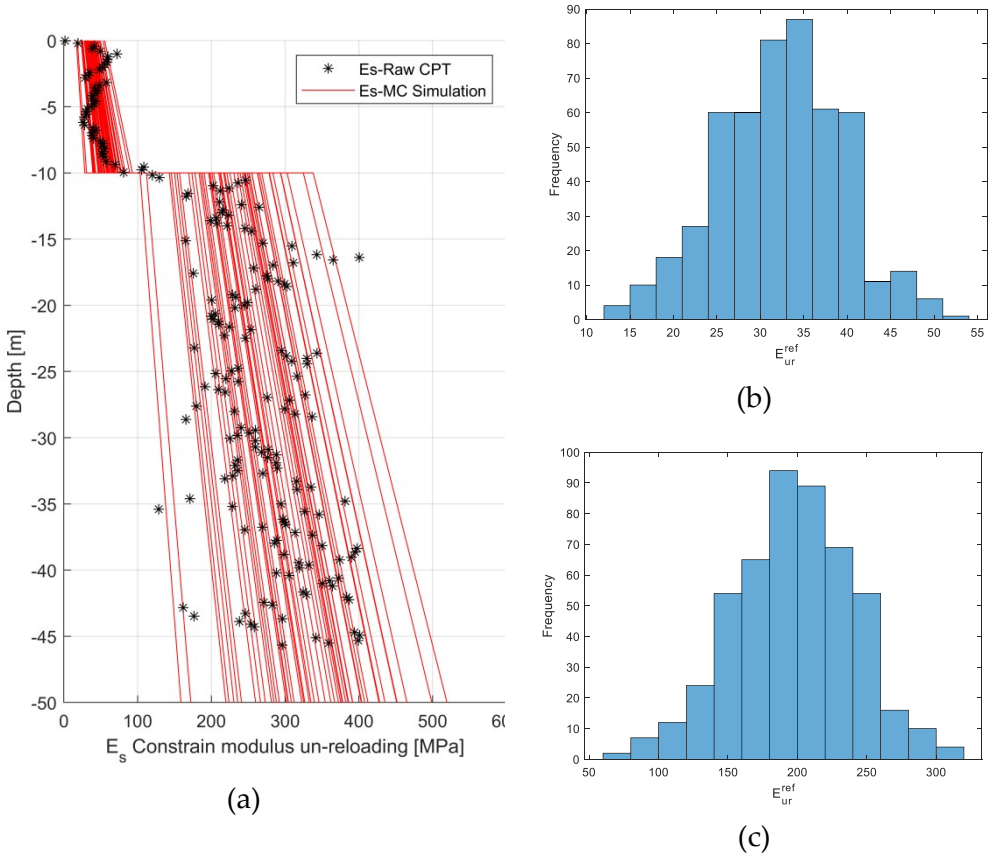

Figure 6: (a) Variability of the soil modulus $\boldsymbol{E_s}$ over depth; (b) Histogram of the soil stiffness at $\boldsymbol{z_{ref} = 0\ m}$; (c) Histogram of the soil stiffness at $\boldsymbol{z_{ref} = -10\ m}$;

The drained constraint modulus in unloading/reloading E_s is then converted to the drained triaxial Young's modulus in unloading/reloading E_{ur} used in the Mohr–Coulomb soil model in PLAXIS. Assuming an elastic behaviour of the soil during unloading/reloading, E_s and E_{ur} can be related as:

$$E_s = \frac{(1-\upsilon_{ur})}{(1+\upsilon_{ur})*(1-2*\upsilon_{ur})} E_{ur} \, , \quad (8)$$

where υ_{ur} is the Poisson ratio (= 0.2).

The soil stiffness depends on the depth. In the Mohr–Coulomb model, a linear increase in the stiffness with depth is accounted for using the following formula:

$$E(\mathrm{z})_{ur} = E(z)_{ur}^{ref} + \left(z_{ref} - z\right) E_{inc} \, , \quad (9)$$

where $E(\mathrm{z})_{ur}$ is the Young's modulus for unloading/reloading at a depth z; $E(z)_{ur}^{ref}$ is the Young's modulus for unloading/reloading at a reference depth z_{ref}; and E_{inc} is the increment of the Young's modulus. Using this equation for a given input value of E_{ur}^{ref} and the increment E_{inc}, E_{ur} can be derived at a specific depth below the surface and compared to E_s, as specified in the design soil profile. For all realisations of different soil stiffnesses (Figure 6 red lines), E_{ur}^{ref} and the increment E_{inc} are calculated:

- For the first layer at $z_{ref} = 0$ (Figure 6.b): $\mu_{E_{ur}^{ref}} = 32.25\ MPa$ and $\sigma_{E_{ur}^{ref}} = 7.06\ MPa$
- For the second layer at $z_{ref} = -10\ m$ (Figure 6.c): $\mu_{E_{ur}^{ref}} = 196.90\ MPa$ and $\sigma_{E_{ur}^{ref}} = 43.14\ MPa$

Other soil properties, such as specific weight, friction angle, and relative density are considered to be deterministic. A full positive correlation between the two soil layer stiffness is assumed.

3.2.2 Cyclic contour diagrams

The aim of the contour diagrams is to provide a 3D variation of the accumulated permanent strain in the average stress ratio (ASR), which is the ratio of the average shear stress to the initial vertical pressure or confining pressure, the cyclic stress ratio (CSR), which is the ratio of the cyclic shear stress to the initial vertical pressure or confining pressure, and the number of cycles (N). An extensive laboratory test campaign is needed to have an accurate 3D contour diagram. The laboratory campaign generally consists of carrying out different regular

cyclic load tests with different average and cyclic amplitude stresses for a certain number of cycles.

For this work, a series of undrained single-stage two-way cyclic simple shear tests were performed at the Soil Mechanics Laboratories of the Technical University of Berlin. The tests were carried out on reconstituted soil samples. The samples were prepared by means of air pluviation method. The initial vertical pressure was 200 kPa and no pre-shearing was considered.

The cyclic behaviour of the upper layer of sand was evaluated with samples prepared at a relative density of 70%. For the lower layer sand, a 90% relative density was used. Two-way cyclic loading tests were carried out, testing different combinations of ASR and CSR. All the tests were stopped at 1000 cycles or at the start of the cyclic mobility phase. For the results on the cyclic behaviour of various tests and relative densities, refer to Zorzi et al. (Zorzi et al., 2019.b).

All the data extracted from the laboratory tests were assembled in a 3D matrix (ASR, CSR, N) and a 3D interpolation of the permanent shear strain (γ_P) was created to map the entire 3D space. The repeatability of the cyclic simple shear tests is an important aspect to consider in evaluating the uncertainties in the cyclic contour diagram. Cyclic simple shear tests feature a low repeatability for dense sand, which can be attributed to the relatively small specimen size used for testing (Vanden Bergen, 2001). This makes the cyclic tests sensitive to sample preparation, this resulting in, for example, different initially measured relative densities, soil fabric, and void ratio non-uniformities.

Owing to this variability of the test, a mathematical formulation was fitted to the raw interpolation. For this reason, different two-dimensional slices (CSR vs. N) at different ASR values were extracted. Figure 7 represents a slice of ASR equal to 0.06. The different coloured points represent the strain surfaces γ_P for different levels of deformation. The raw interpolation of data and the uncertainty related to the low sample repeatability of the tests cause an unrealistic non-smooth shape of the strain surfaces. Therefore, each slice is assumed to follow a power law function (variation of CSR as power of N) for different strain levels and then calibrated to fit the data. Finally, the calibrated strain surfaces

are interpolated to create the final smooth 3D contour diagram. This procedure and its validation are explained in Zorzi et al. (Zorzi et al., 2019a).

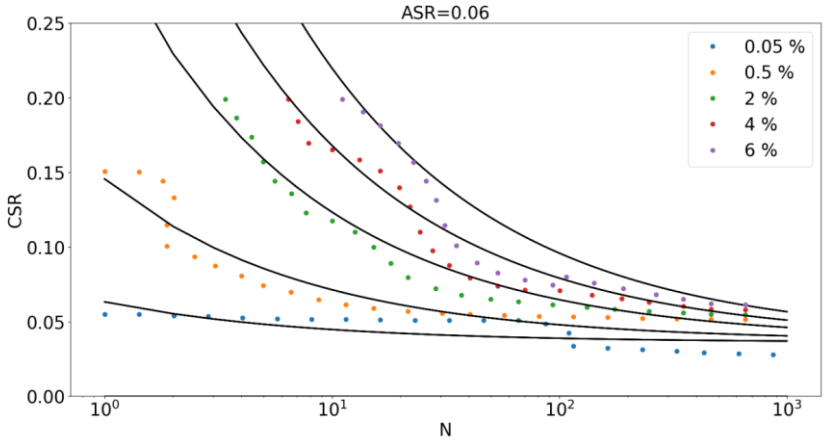

Figure 7: Slice of the cyclic contour diagram.

The power law function can be written in the form of Equation (1).

$$CSR = \mathbf{X}_c \, N^{\boldsymbol{X}_d} + \boldsymbol{X}_e + \varepsilon \,, \qquad (10)$$

where $\boldsymbol{X}_d$ represents the shape of the curve; $\mathbf{X}_c$ is a scaling factor; $\boldsymbol{X}_e$ is the intersection with the CSR axis, and ε is the fitting error. Using the maximum likelihood method (MLM) it is possible to fit the mathematical model and estimate the standard deviation of the fitting error and the standard deviation of the parameters c and e. During the fitting procedure, the shape parameter d is assumed fixed at –0.35 for the lower layer and –0.50 for the upper layer.

Based on the results of the fitting procedure, a standard deviation of the fitting error of 0.008 is chosen for the two diagrams for the two soils. The parameters c and e are considered deterministic, as the standard deviation associated is very low. Preliminary simulations show that the uncertainty of a and c derived from the MLM has less influence than the uncertainty in the fitting error.

It has to be noted that the fitting error, to some extent, reflects the uncertainties of repeatability of the tests. Moreover, the relative density of the soil samples is

based on the empirical relation applied to the tip resistance (section 3.1). To account for the uncertainty in the relative density, different sets of contour diagrams should have been derived from several tests performed with soil samples at different relative densities.

The contour diagrams for two different ASR slices are presented in Figures 8 and 9 for the upper and lower layers, respectively.

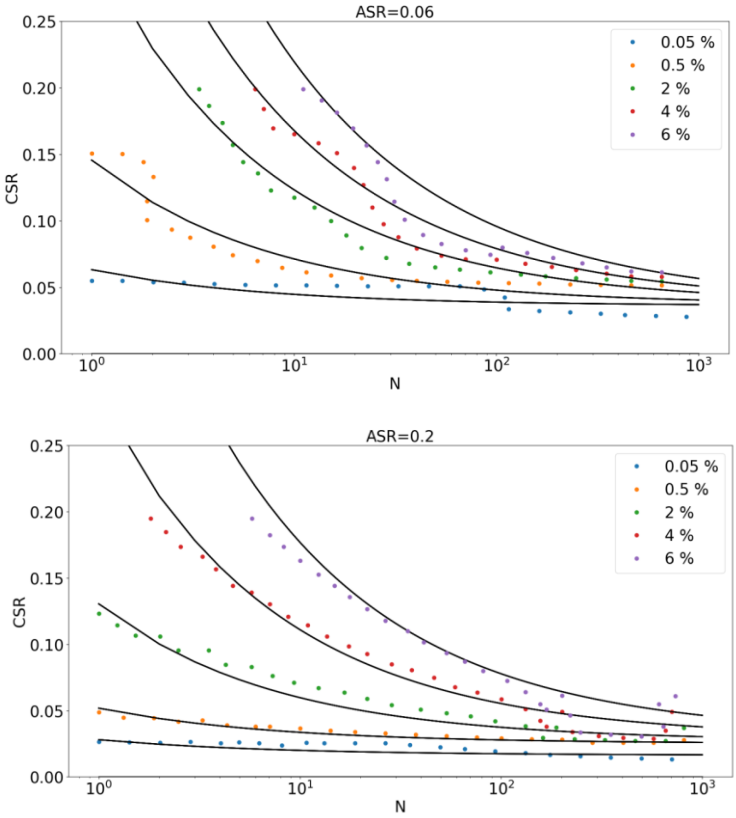

Figure 8: Cyclic contour diagram for the first layer.

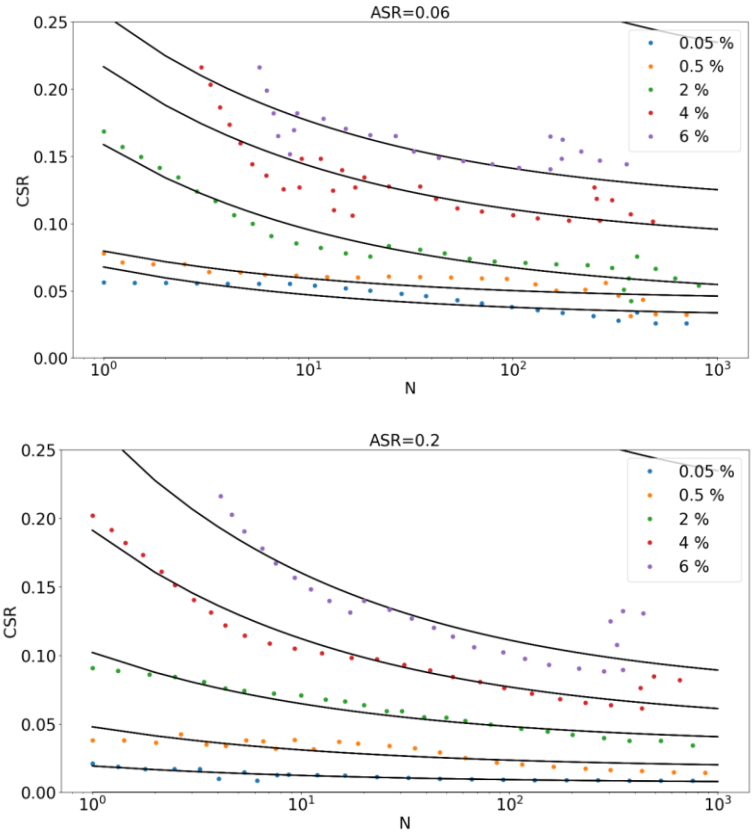

Figure 9: Cyclic contour diagram for the second layer.

3.2.3 Load uncertainty

The load input parameter for the SCD model is characterised by a regular loading package with a mean and cyclic amplitude load, and an equivalent number of cycles (hereafter, called "load inputs" for simplicity). In common practice, the structural engineer provides the irregular history at mudline level by means of the aero-hydro-servo-elastic model. Therefore, a procedure is needed to transform the irregular design storm event to one single regular loading parcel. The environmental load used for the cyclic loading design relies on the chosen return period for the load. The statistical distribution of the environmental loads is then based on different return periods.

The design storm event is here defined as a six hour duration of the extreme load (also called the peak of the storm) (DNV-GL, 2017). The underlying assumption in considering only the peak is that most of the deformations, which the soil experiences, happen at the peak of the storm. The considered design load case is DLC 6.1 (IEC, 2009; BSH, 2015), i.e., when the wind turbine is parked and yaw is out of the wind. The ULS loads are considered for the cyclic load design.

To derive the irregular load history at the mudline level, the fully coupled aero-hydro-servo-elastic model is developed in the wind turbine simulation tool, HAWC2. Based on 5-year in-situ metocean data from the North Sea, the environmental contours for different return periods are derived as shown in Figure 10 (Velarde et al, 2019a). The marginal extreme wind distribution is derived using the peak-over-the-threshold method for wind speed above 25 m/s. Furthermore, it is assumed that maximum responses are given by the maximum mean wind speed and conditional wave height for each return period (red point in Figure 10).

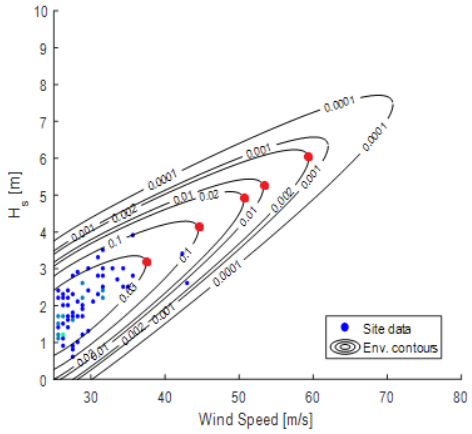

Figure 10: Environmental contour plot for extreme sea states (Velarde et al, 2019a).

The five design sea states for maximum wind speed are summarised in Table 3. To account for short-term variability in the responses, 16 independent realisations are considered for each design sea state.

Annual Exceedance Probability (q)	Return period [year]	Wind speed Uw [m/s]	Wave height Hs [m]	Wave period Tp [s]
0.63	1	37.4	3.17	7.95
0.10	10	44.5	4.10	8.84
0.02	50	50.6	4.90	9.54
0.01	100	53.3	5.24	9.83
0.002	500	59.4	6.04	10.44

Table 3: Design sea state for maximum wind speed.

Time-domain simulations provide an irregular force history of 10 min at the mudline. To transform the 10 min irregular loading to a 6-h storm, each 10-min interval is repeated 36 times.

The irregular load histories have to be simplified to one equivalent regular package with a specific mean and cyclic load amplitude and an equivalent number of cycles that lead to the same damage accumulation (accumulation of soil deformation) as that of the irregular load series.

The following procedure is used (Andersen, 2015):

- The rainflow counting method is utilised to break down the irregular history into a set of regular packages with different combination of mean force F_a and cyclic amplitude force F_{cly} and number of cycles N. Figure 11 shows an example of the output from the rainflow counting.

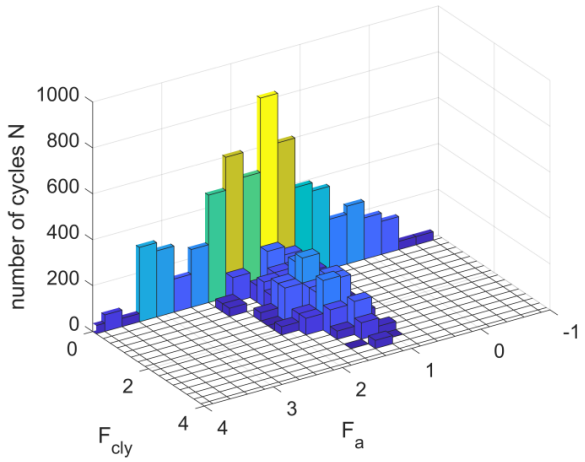

Figure 11: Rainflow matrix for 100 year return period wind speed.

- All the bins are ordered with increasing maximum force F_{max} obtained from the sum of the mean and the cyclic amplitude ($F_{max} = F_a + F_{cly}$).
- 3D contour diagrams in conjunction with the strain accumulation method are then used to calculate the accumulation of deformation. After scaling the loads to shear stresses, the result of this procedure gives the equivalent number of cycles for the highest maximum force F_{max}^{max}, which in turn gives the same accumulation of deformation of the irregular load history.

This procedure is applied for all simulations with different return periods.

To obtain a statistical distribution, the mean force, cyclic amplitude force, and the equivalent number of cycles are plotted versus the probability of non-exceedance for each return period.

The black points in the three following figures are, respectively, the mean load, cyclic amplitude and number of cycles of the regular packages obtained from the previous procedure and plotted vs. the probability of not exceedance for each return period. Assuming that for each return period the black points have

a normal distribution, the 0.50 fractile (red circles) and the 0.95 fractile (blue circles) are obtained.

The statistical distributions for the loads are derived by fitting a Gumbel distribution to the 0.95 fractile values (NORSOK, 2007). The MLM is employed to fit the cumulative Gumbel distribution to the extreme response (blue circles). The cumulative density function distribution is defined as:

$$CDF(x) = \exp(-\exp(-(\mathrm{x} - \alpha) / \beta)) \,, \tag{11}$$

$$\mu = \alpha + \beta\ 0.5772 \,, \tag{12}$$

$$\sigma = \frac{\pi}{2.44}\ \beta \,, \tag{13}$$

The Table 4 summarises the parameters of distribution for the three load inputs. The standard deviation of the fitting error is small, marking a good fitting of the distribution function.

Load	$\boldsymbol{\alpha}$	$\boldsymbol{\beta}$	$\boldsymbol{\mu}$	$\boldsymbol{\sigma}$	$\boldsymbol{\sigma_\varepsilon}$
F_a	1.092	0,113	1.158 [MN]	0.382 [MN]	0.0040
F_{cly}	3.66	0.093	3.71 [MN]	0.347 [MN]	0.011
N_{eq}	329.75	70.08	370.2 [Cycles]	9.49 [Cycles]	0.024

Table 4: Gumbel parameters of the distribution for the load inputs.

Looking at the distribution of Figure 12 a-b-c, larger 0.50 fractiles (red circles) are present when increasing the return period. This is more pronounced for the mean force and is expected because the higher the return period, the higher is the mean pressure on the wind turbine tower.

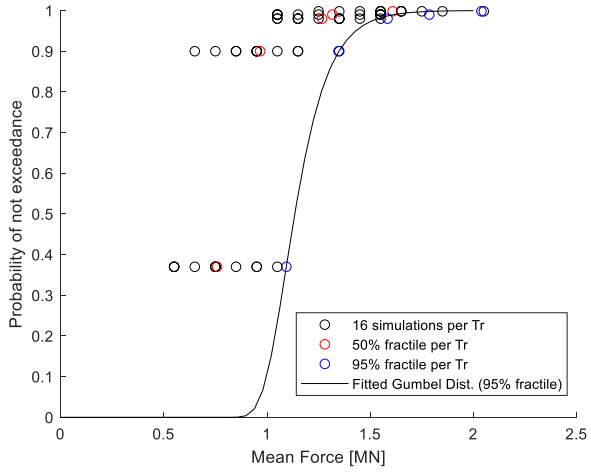
Probability of not exceedance
Mean Force [MN]
16 simulations per Tr
50% fractile per Tr
95% fractile per Tr
Fitted Gumbel Dist. (95% fractile)

(a)

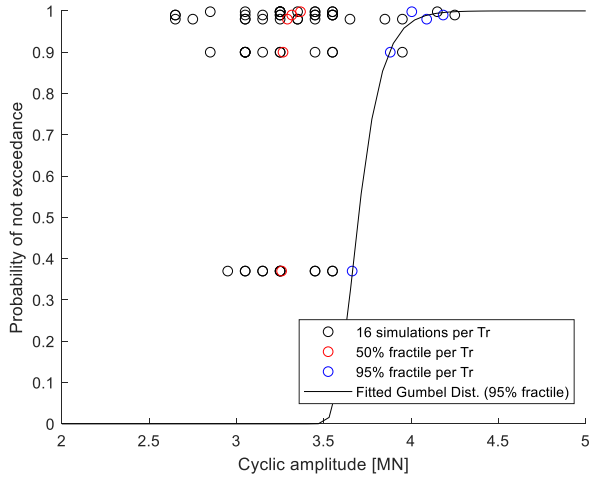
Probability of not exceedance
Cyclic amplitude [MN]
16 simulations per Tr
50% fractile per Tr
95% fractile per Tr
Fitted Gumbel Dist. (95% fractile)

(b)

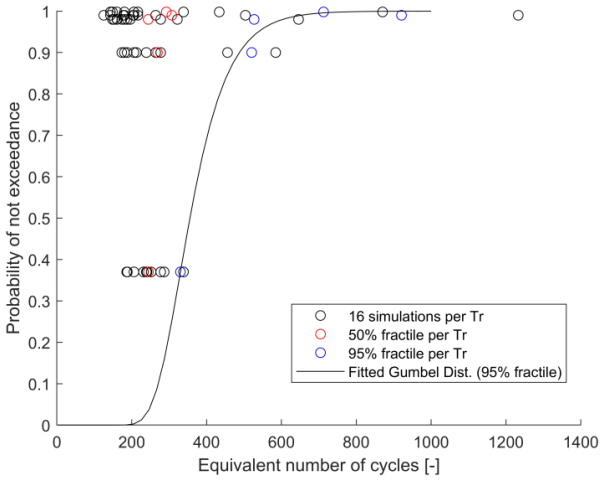

(c)

Figure 12: Distribution of the load inputs.

The scatter for each return period is more significant when the return period increases. This can have different reasons, for example, the "rare" storms with a lower probability of occurrence could give more non-linearity problems varying the wave and wind speeds in the aero-hydro-servo-elastic model. It could also depend on the model uncertainty in the time domain simulations.

The correlation coefficients ϱ for the 0.95 fractile values between the mean and cyclic loads and the equivalent number of cycles are: $\rho_{F_a-F_{cly}} = 0.77$, $\rho_{N_{eq}-F_{cly}} = 0.81$, and $\rho_{N_{eq}-F_a} = 0.85$. The three coefficients mark a strong positive correlation between the three load inputs.

3.2.4 Model error

This type of error is difficult to estimate because it requires the validation of the numerical error against different model tests. In the case of the SCD model, this error is arising due to the simplification of the model for a much more complex behaviour of the soil-structure-interaction under cyclic loading. The model error ε_{model} is estimated as a random variable and multiplied to predict the structural tilting (Eq. 14). The model error is assumed to be normally distributed with

a unitary mean and a coefficient of variation of 10%. Ideally, this model uncertainty should be quantified comparing the results from the SCD model with several different test results. However, such a large number of tests is not feasible.

$$g(\boldsymbol{X}) = \theta_{max} - \varepsilon_{model}\,\theta_{calc}(\boldsymbol{X})\,, \tag{14}$$

3.3 Derivation of the response surface

The stochastic variables are summarized in Table 5. For simplicity, a full correlation between the soil stiffness of the two layers and the loads is assumed.

$\boldsymbol{X}$	Unit	PDF	$\boldsymbol{\mu}$	$\boldsymbol{\sigma}$	CoV [%]	ϱ
Soil stiffness Layer 1 $\boldsymbol{E_{ur}^{ref}}$	MPa	Normal	32.25	7.06	21.9	1
Soil stiffness Layer 2 $\boldsymbol{E_{ur}^{ref}}$	MPa	Normal	196.90	43.14	21.9	
Cyclic contour diagrams fitting error $\boldsymbol{CCD_{err}}$	-	Normal	0	0.008	-	-
Input load $\boldsymbol{F_a}$	MN	Gumbel	1.158	0.382	32.9	1
Input load $\boldsymbol{F_{cly}}$	MN	Gumbel	3.71	0.347	9.3	
Input load $\boldsymbol{N_{eq}}$	Cycles	Gumbel	370.2	9.49	2.5	

Table 5: Summary of the stochastic variables.

Once the stochastic variables are defined, the 3D FEM model has to be substituted by a response surface.

The DoE is used to obtain the training point from the FE simulation. As most of the variables are correlated, three stochastic variables are considered: (i) the stiffness of the upper soil layer E_{ur}, (ii) the fitting error of the cyclic contour diagram CCD_{err}, and (iii) the mean load F_a. The independent input stochastic variables have the statistical distribution shown in Table 5. For each factor, three different levels are assumed: minimum value $\mu - 2 * \sigma$, average value μ and

maximum value $\mu + 2 * \sigma$. A full factorial design in three levels is implemented. Therefore, a total of 33 simulations are needed to explore all possible combinations.

Based on visual inspection of the output from the 3D FEM model, a second-order polynomial function is fitted to the sample data. The linear regression method is used to estimate regression coefficients of the polynomial function. The following function is the outcome of the linear regression analysis:

$$\theta_{calc} = 0.248\, F_a - 0.007\, E_{ur}\, F_a - 0.144\, F_a\, CCD_{err} + 0.0000746\, {E_{ur}}^2\, F_a + \varepsilon_{fit} \quad , \tag{15}$$

An un-biased fitting error (ε) with normal distribution is assumed and the estimate of residual standard deviation ($\sigma_{\varepsilon_{fit}}$) is 0.0013. R-squared is a statistical measure of how close the data is to the fitted regression line. For the fitted function, the R-squared value is 0.9984 underlining a good fit of the function to the data and hence the choice of the initial choice of the second-order polynomial function.

Figure 13.a shows the function at the $CCD_{err} = 0$ (the mean value). The surface shows that at a lower soil stiffness and a high force, a higher rotation of the monopile is reached. Values higher than 0.25 are considered as failures. The red points are from the numerical simulations. The 3D plot (Figure 13.b) shows the response surface for the mean value of the force $F_a = 1.158$ MN. It is apparent that the fitting error for the contour diagram is small and thus, does not have a significant influence on the results.

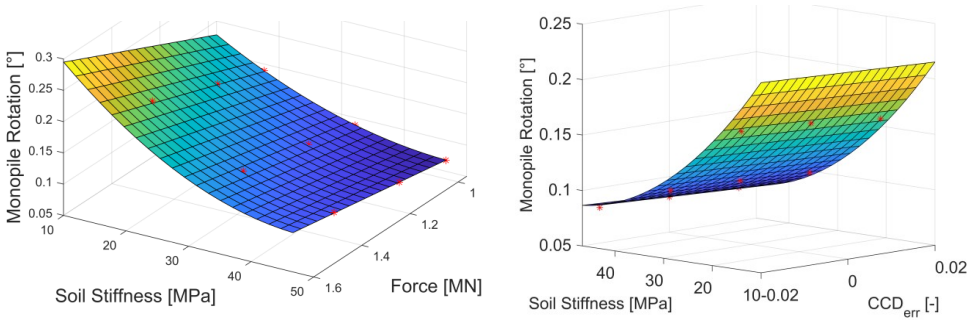

a) b)

Figure 13: Response surfaces.

3.4 Reliability analysis

The limit state function is written as:

$$g(\boldsymbol{X}) = 0.25° - (0.248\, F_a - 0.007\, E_{ur}\, F_a - 0.144\, F_a\, CCD_{err} + 0.0000746\, {E_{ur}}^2\, F_a + \varepsilon_{fit})\, \varepsilon_{model}\,, \quad (16)$$

10^7 MC simulations were performed by random sampling of the input stochastic variables. This number was the minimum required to keep the relative error of the reliability index lower than 1%. The stochastic variables and their probability distribution functions are given in Table 5. The derivation of the design mean, and standard deviation are explained in section 3.2.

With the analysed monopile design, the annual probability of failure is 2.7000e-05 and the corresponding annual reliability index is 4.03. This means, that the monopile meets the target reliability index of 2.9–3.3 and is considered safe for long-term behaviour in terms of rotation accumulation for the design storm event.

3.5 Sensitivity analysis

The sensitivity analysis of the stochastic input variables on the reliability index is conducted by varying the coefficient of variation one at a time for each input (0.5 CoV and 2 CoV). The inclination of dashed lines in Figure 14 marks the sensitivity of the stochastic variable. Mean force F_a and the soil stiffness E_{ur} are

both influencing the reliability index significantly more than the fitting error and numerical model error do.

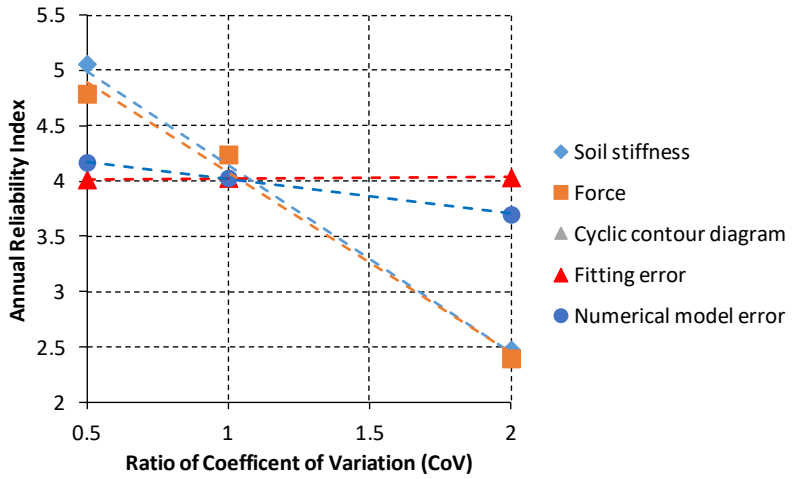

Figure 14: Sensitivity plot.

4. CONCLUSION

During the lifetime of wind turbines, storms, typhoons, or seismic action are likely to cause permanent deformation of the structure owing to the accumulation of plastic strain in the soil surrounding the foundation. The serviceability limit state criteria require that the long-term structural tilting does not exceed the operational tolerance prescribed by the wind turbine manufacturer (usually less than 1°) with a specific target reliability level. In this study, the SLS design for long-term structural tilting is addressed within a reliability framework. This framework is developed based on the 3D FE models for the prediction of the SSI under cyclic loading. For the case study of a large monopile installed on a typical North Sea environment, a reliability index of 4.03 was obtained. Sensitivity analysis also shows that uncertainties related to the soil stiffness and the environmental loads significantly affect the reliability of the structure. For regions where assessment against accidental loads due to typhoons are necessary, uncertainty of the extreme environmental loads can increase by up to 80%. Such load scenarios can significantly reduce the reliability index, and therefore become the governing limit state.

A discussion has to be started in the offshore community regarding the very strict tilting requirement (i.e., 0.25°). This very small operational restriction can lead to foundations of excessively large dimensions, which are unfeasible from an economic point of view. On the other hand, a less strict verticality requirement (which could be a function of the dimension and type of the installed wind turbine), for example an angle of rotation of 1–3°, could lead to a smaller foundation size and still meet the safety requirements. For this reason, by means of aero-elastic analyses, the investigation of the position of the natural frequency of the whole system and fatigue analysis should be carried out when a wind turbine is tilted at 1–3°. Allowing a less stringent tilting of the foundation can also be beneficial during the monopile installation. A small foundation dimension saves vessel and equipment cost, which contributes significantly to the overall cost reduction of the foundation.

In this paper, a simplified model to calculate the permanent rotation (the SCD method) is implemented. It is noted that other models of varying complexity can also be used in the proposed probabilistic framework. If new inputs are introduced, the respective uncertainties should be considered in the reliability calculation and the function for the response surface should be adjusted accordingly.

CODE AND DATA AVAILABILITY

The codes can be made available by contacting the corresponding author.

AUTHOR CONTRIBUTION

Zorzi, Mankar, Velarde and Sørensen designed the proposed methodology. Zorzi prepared the manuscript with the contributions from all co-authors.

COMPETING INTERESTS

The authors declare that they have no conflict of interest.

ACKNOWLEDGEMENT

This research is part of the Innovation and Networking for Fatigue and Reliability Analysis of Structures - Training for Assessment of Risk (INFRASTAR) project. This project has received funding from the European Union's Horizon

2020 research and innovation program under the Marie Skłodowska-Curie grant agreement No. 676139. The laboratory tests are provided by the Chair of Soil Mechanics and Geotechnical Engineering of the Technical University of Berlin. The authors are grateful for the kind permission to use those test results.

REFERENCES

Achmus, M., Abdel-Rahman, K, and Kuo, Y.: Behaviour of large diameter monopiles under cyclic horizontal loading, Twelfth International Colloquium on Structural and Geotechnical Engineering, 2007.

Andersen, K.H.: Cyclic soil parameters for offshore foundation design, Frontiers in Offshore Geotechnics III, ISFOG'2015, Oslo, Norway, 10-12 June 2015, 5-82, doi: 10.1201/b18442-4, 2015.

Baldi, G., Bellotti, R., Ghionna, V., Jamiolkowski, M., and Pasqualini, E.: Interpretation of CPTs and CPTUs; 2nd part: drained penetration of sands, Proc. 4th Int. Geotech. Seminar, Singapore, 143-156, 1986

Bellotti, R., Ghionna, V.N., Jamiolkowski, M., and Robertson, P.K.: Design parameters of cohesionless soils from in situ tests, Transportation Research Record, 1235, 0361-1981, 1989.

Bhattacharya, S.: Challenges in Design of Foundations for Offshore Wind Turbines, Engineering & Technology Reference, 9, doi: 10.1049/etr.2014.0041, 2014.

Bhattacharya, S.: Design of foundations for offshore wind turbines, Wiley, doi: 10.1002/9781119128137, 2018.

BSH: Standard Design - minimum requirements concerning the constructive design of offshore structures within the Exclusive Economic Zone (EEZ), Federal Maritime and Hydrographic Agency (BSH), 2015.

Byrne, B. W., Burd, H. J., Zdravkovic, L., Abadie, C. N., Houlsby, G. T., Jardine, R. J. and Taborda, D. M. G.: PISA Design Methods for Offshore

Wind Turbine Monopiles, Offshore Technology Conference, doi:10.4043/29373-MS, 2019.

Carswell, W. Arwade, S., DeGroot, D., Lackner, M.: Soil–structure reliability of offshore wind turbine monopile foundations, Wind Energy, 2014.

Cuéllar, P., Georgi, S., Baeßler, M. and Rücker, W.: On the quasi-static granular convective flow and sand densification around pile foundations under cyclic lateral loading, Granular Matter, Band 141, 2012.

DNV-GL: DNVGL-RP-C212 - Offshore soil mechanics and geotechnical engineering, 2017.

Fenton, G. and Griffiths, D.: Risk assessment in geotechnical engineering, John Wiley & Sons, doi: 10.1002/9780470284704, 2008.

Hettler, A.: Verschiebungen starrer und elastischer Gründungskörper in Sand bei monotoner und zyklischer Belastung, Institut für Bodenmechanik und Felsmechanik der Universität Fridericiana, 1981.

IEC: IEC 61400-3 - Wind turbines Part 3: Design requirements for offshore wind turbines, International Electrotechnical Commission, 2009.

Jamiolkowski, M., Ghionna, V., Lancellotta, R., and Pasqualini, E.: New correlations of penetration tests for design practice, International Journal Of Rock Mechanics And Mining Sciences & Geomechanics, 27(2), A91, doi: 10.1016/0148-9062(90)95078-f, 1988.

Jostad, H.P., Grimstad, G., Andersen, K.H., Saue, M., Shin, Y., & You, D.: A FE Procedure for Foundation Design of Offshore Structures – Applied to Study a Potential OWT Monopile Foundation in the Korean Western Sea. Geotechnical Engineering Journal of the SEAGS & AGSSEA, 45(4), 2014.

Larsen T. J. and Hansen A. M.: How 2 HAWC2, the user's manual, Risø National Laboratory, 2015.

LeBlanc, C., Houlsby, G. and Byrne, B.: Response of stiff piles in sand to long-term cyclic lateral loading, Geotechnique, Band 602, 2009.

Lunne, T. and Christoffersen, H. P.: Interpretation of Cone Penetrometer Data for Offshore Sands, Offshore Technology Conference, Houston, Texas, 2-5 May 1983, doi:10.4043/4464-MS, 1983.

Lunne, T., Robertson, P.K. and Powell, J.J.M.: Cone Penetration Testing in Geotechnical Practice, CRC Press, London, doi: https://doi.org/10.1201/9781482295047, 1997.

Niemunis, A., Wichtmann, T. and Triantafyllidis, T.: A high-cycle accumulation model for sand, Computers and Geotechnics, 32(4), 2005.

NORSOK : NORSOK Standard N-003, Actions and action effects, 2007.

Pisanò, F.: Input of advanced geotechnical modelling to the design of offshore wind turbine foundations, Proceedings of the XVII ECSMGE-2019: Geotechnical Engineering foundation of the future, Reykjavik, Iceland, 01-06 September 2019, https://doi.org/10.32075/17ECSMGE-2019-1099, 2019.

PLAXIS :. Plaxis 3D Reference Manual, Edited by Brinkgreve, R.B.J., Kumarswamy, S., Swolfs, W.M., and Foria F., 2017.

Sørensen J. D.: Notes in Structural Reliability Theory and Risk Analysis, Aalborg University, 2011.

Vanden Bergen J.F.: Sand Strength Degradation within the Framework of Vibratory Pile Driving, PhD thesis, University Catholique de Louvain, Faculty of Applied Science Civil and Environmental Engineering Division, 2001.

Velarde J., Kramhøft C. and Sørensen JD.: Reliability-based Design Optimization of Offshore Wind Turbine Concrete Structures, 13th International Conference on Applications of Statistics and Probability in Civil Engineering,

Seoul, Korea, 26-30 May 2019, doi: https://doi.org/10.22725/ICASP13.185, 2019a.

Velarde, J., Sørensen, J. D., Kramhøft, C., and Zorzi, G.: Fatigue reliability of large monopiles for offshore wind turbines, Submitted to International Journal of Fatigue, 2019b.

Wichtmann, T.; Soil behaviour under cyclic loading - experimental observations, constitutive description and applications, Habilitation thesis, 2016.

Wu, T., Tang, W., Sangrey, D., and Baecher, G.: Reliability of Offshore Foundations-State of the Art, Journal of Geotechnical Engineering, 115, 157-178. doi: 10.1061/(asce)0733-9410(1989)115:2(157), 1989.

Zorzi, G., Richter, T., Kirsch, F., Augustesen, A. H., Østergaard, M. U., and Sørensen, S. P.: Explicit Method to Account for Cyclic Degradation of Offshore Wind Turbine Foundations Using Cyclic Inter-action Diagrams, International Society of Offshore and Polar Engineers, Sapporo, Japan, 10-15 June 2018, ISOPE-I-18-271, 2018.

Zorzi, G., Kirsch, F., Richter, T., Østergaard, M., and Sørensen, S.: Validation of explicit method to predict accumulation of strain during single and multistage cyclic loading, Proceedings of the XVII ECSMGE-2019 - Geotechnical Engineering foundation of the future, Reykjavik, Iceland, 1-6 September 2019, 2019a.

Zorzi, G., Kirsch, F., Richter, T., Østergaard, M., and Sørensen, S.: Comparison of cyclic simple shear tests for different types of sands, 2nd International Conference on Natural Hazards & Infrastructure, Chania, Greece, 23-26 June 2019, 2019b.

Scientific contribution of the PhD student to each paper

Paper in appendix A	
Paper title	Explicit method to account for cyclic degradation of offshore wind turbine foundations using cyclic interaction diagrams.
List of authors	Zorzi G., Richter T., Kirsch F., Augustesen A.H., Østergaard M.U., Sørensen S.P.H.
Percentage of the scientific contribution of the PhD student	70%

Paper in appendix B	
Paper title	Lifetime tilting prediction of offshore wind turbine foundations due to soil strain accumulation.
List of authors	Zorzi G., Kirsch F., Richter T., Østergaard M.U., Sørensen S.P.H.
Percentage of the scientific contribution of the PhD student	85%

Paper in appendix C	
Paper title	Long-term cyclic triaxial tests with DEM simulations.
List of authors	Zorzi G., Kirsch F., Gabrieli F., Rackwitz F.
Percentage of the scientific contribution of the PhD student	75%

Paper in appendix D

Paper title	DEM modelling of high cyclic triaxial tests: calibration, sensitivity analysis and practical application.
List of authors	Zorzi G., Gabrieli F., Le H.V., Rackwitz F., Kirsch F.
Percentage of the scientific contribution of the PhD student	70%

Paper in appendix E

Paper title	Comparison of cyclic simple shear tests for different types of sands.
List of authors	Zorzi G., Kirsch F., Richter T., Østergaard M.U., Sørensen S.P.H.
Percentage of the scientific contribution of the PhD student	95%

Paper in appendix F

Paper title	Validation of the explicit method to predict accumulation of strain during single and multistage cyclic loading.
List of authors	Zorzi G., Kirsch F., Richter T., Østergaard M.U., Sørensen S.P.H.
Percentage of the scientific contribution of the PhD student	80%

Paper in appendix G

Paper title	Application of the Soil Cluster Degradation method to simulate a full-scale test of a gravity-based foundation.

List of authors	Zorzi G., Kirsch F., Richter T., Østergaard M.U., Sørensen S.P.H.
Percentage of the scientific contribution of the PhD student	80%

Paper in appendix H

Paper title	Reliability analysis of offshore wind turbine foundations under lateral cyclic loading
List of authors	Zorzi G., Kirsch F., Richter T., Østergaard M.U., Sørensen S.P.H.
Percentage of the scientific contribution of the PhD student	60%